ANALYSIS OF THE WAVE SCATTERING FROM TURBULENT PREMIXED FLAME

A Dissertation
Presented to
The Academic Faculty

by

Ju Hyeong Cho

In Partial Fulfillment
of the Requirements for the Degree
Doctor of Philosophy in
Aerospace Engineering

Georgia Institute of Technology
August 2006

ANALYSIS OF THE WAVE SCATTERING FROM TURBULENT PREMIXED FLAME

Approved By:

Dr. Tim Lieuwen, Advisor
School of Aerospace Engineering
Georgia Institute of Technology

Dr. Suresh Menon
School of Aerospace Engineering
Georgia Institute of Technology

Dr. Ben T. Zinn
School of Aerospace Engineering
Georgia Institute of Technology

Dr. Peter Rogers
School of Mechanical Engineering
Georgia Institute of Technology

Dr. Massimo Ruzzene
School of Aerospace Engineering
Georgia Institute of Technology

Date Approved: 6 May 2006

DEDICATION

To my parents and family

"God, let our souls awake and remember our spiritual selves."

ACKNOWLEDGEMENTS

I would like to express my deepest gratitude to my advisor, Dr. Tim Lieuwen, for his support and many valuable discussions with encouragement throughout my studies. I would also like to express my deep appreciation to Dr. Ben T. Zinn, Dr. Massimo Ruzzene, Dr. Suresh Menon, and Dr. Peter Rogers for their helpful comments and many pieces of advice as my thesis committee. Though I can not thank them each by name, I would like to thank all the combustion lab members for their helpful assistance and memorable time.

Finally, I would like to give my warmest thanks to my parents and family for their constant love with sincere concern and encouragement, which gave me strength and endurance at every moment in my life.

TABLE OF CONTENTS

LIST OF FIGURES

NOMENCLATURE

c	speed of sound
D	transmission coefficient
D_T	thermal diffusivity ($=\lambda_r/(\rho_r c_{pr})$)
$\vec{e}_x, \vec{e}_y, \vec{e}_z$	unit vectors in Cartesian coordinates
E	normalized acoustic energy flux
ΔE	net acoustic energy flux
f	frequency
$\tilde{f}_0$	dimensionless frequency of an incident wave ($=\omega_0 t_c/(2\pi)$)
f_c	frequency of flame surface oscillation ($=1/t_c$)
G	Green's function or a variable in G-equation
h	flame front position
I	acoustic intensity
$\boldsymbol{k}$	horizontal components of wave number vector ($=k_x\vec{e}_x + k_y\vec{e}_y$)
$\vec{K}$	wave number vector ($=(k_x,k_y,k_z)=k_x\vec{e}_x + k_y\vec{e}_y + k_z\vec{e}_z$)
l_c	correlation length of flame front
$\tilde{l}_c$	dimensionless correlation length of flame front ($= K_0 l_c$)
Le	Lewis number
m	mass burning rate per unit area ($=\rho S_L$)
M_S	mean flame speed mach number ($=\overline{S}_L^{(1)}/c_1$)

M_r reference mass flux per unit area

$\vec{\boldsymbol{n}}$ vector normal to the flame surface

p acoustic pressure

P_I incident acoustic pressure

q_k vertical component of wave number vector

Q acoustic source

$\boldsymbol{r}$ horizontal coordinates (= (x, y))

R reflection coefficient

$\vec{\boldsymbol{R}}$ 3 dimensional coordinates (= (x, y, z))

$S^{N_1N_2}$ scattering amplitude (from medium N_2 into medium N_1)

S_L laminar flame speed for unburned gas

t time

t_c correlation time of flame front

t_r reference time for diffusion of flame (= $\rho_r \lambda_r / c_{pr} M_r^2$)

<T> mean transmission coefficient

u,v,w velocity component in x,y,z direction, respectively

$\vec{\boldsymbol{v}}$ acoustic velocity

$\vec{\boldsymbol{V}}$ flow velocity vector

$\boldsymbol{V}_{\mathrm{H}}$ horizontal components of velocity vector

<V> mean reflection coefficient

w vertical component of velocity vector

W power spectral density, see Eq. (4.15)

$\breve{W}$ correlation function, see Eq. (4.16)

x,y,z Cartesian coordinates

$< >$ ensemble average

Greeks

β jump factor in acoustic velocity

$\delta( )$ dirac delta function

$\delta_{( )}$ kronecker delta function

ε dimensionless magnitude of linearized incident pressure $(=\left|P_1\right|/(\rho_1 c_1^2))$

ϕ polar angle or equivalence ratio

γ specific heat ratio

λ thermal conductivity

Λ temperature ratio $(=T_2/T_1)$

Δ laplacian $(=\partial_{xx}+\partial_{yy}+\partial_{zz})$

∇ horizontal gradient $(=(\partial_x,\partial_y)=\vec{\boldsymbol{e}}_{\boldsymbol{x}}\partial_x+\vec{\boldsymbol{e}}_{\boldsymbol{y}}\partial_y)$

$\vec{\nabla}$ three-dimensional gradient $(=(\partial_x,\partial_y,\partial_z)=\vec{\boldsymbol{e}}_{\boldsymbol{x}}\partial_x+\vec{\boldsymbol{e}}_{\boldsymbol{y}}\partial_y+\vec{\boldsymbol{e}}_{\boldsymbol{z}}\partial_z)$

θ dimensionless activation energy

ρ density

σ rms height or scattering cross section

$\tilde{\sigma}$ dimensionless rms height of flame front $(=K_0\sigma)$

τ the ratio of diffusion time to correlation time of flame $(=t_r/t_c)$

ω angular frequency

ψ velocity potential

Superscripts

$\bar{(\ )}$ time average

$(\ )'$ fluctuating value or integral variable

$\tilde{(\ )}$ normalized value

$\vec{(\ )}$ three-dimensional vector

(1),(2) medium (1) and (2), respectively

Subscripts

0 incident wave or zero-th order term

1,2 medium (1) and (2) or 1st and 2nd order perturbation terms

av average value

c complex value

co coherent energy flux

I incident wave or medium containing it

inc incoherent energy flux

J jump effect

n n-th order perturbation term

r reference value

R reflection

T transmission

total	total acoustic energy flux
ω	wrinkling effect

SUMMARY

The purpose of this study is to lay a foundation for theoretical investigation of acoustic wave interactions with turbulent premixed flames. Such interactions affect the characteristic unsteadiness of combustion processes, e.g., combustion instabilities. Scattered acoustic waves are generated by the interaction with a wrinkled, moving flame front while the shape of flame front is also distorted by the scattered wave fields.

The significance of this work is that, although a great deal of studies have been reported for acoustic wave–flame interactions, no analysis has been performed to analytically evaluate the coherent and incoherent energy amplification / damping due to the transient interaction of acoustic waves and turbulent flames in three-dimensional space. In this thesis the small perturbation method (SPM) was utilized to evaluate the scattered fields as a result of the flame-wave interaction at the instantaneous wrinkling surface of a randomly moving turbulent flame. Stochastic analysis of ensemble-averaged net acoustic energy was conducted to examine coherent and incoherent acoustic energy amplification /damping by the interaction. Net acoustic energy flux out of the flame is due to two factors: the acoustic velocity jump due to unsteady heat release from flame. The other is the flame's unsteady motion. Five(5) dimensionless parameters that govern this net acoustic energy were determined: rms height of flame front, $\tilde{\sigma} = K_0\sigma$, correlation length of flame front, $\tilde{l}_c = K_0 l_c$, incident wave frequency, $\tilde{f}_0 = f_0 t_c$, the ratio of flame's diffusion time to flame front's correlation time, $\tau = t_r / t_c$, and incidence angle. The dependence of net

acoustic energy upon these dimensionless parameters is illustrated by numerical simulations in case of Gaussian statistics of flame front. The major factors that determine amplification /damping of the total net energy are $\tilde{f}_0$ and incidence angle; Amplification occurs when $\tilde{f}_0 \geq 1$ or at near-critical anlges. τ and $\tilde{l}_c$ have a significant effect on the total energy balance only for a large value (>>1) of $\tilde{f}_0$. Coherent (incoherent) energy is damped (amplified) with the square of rms height.

The flame response to equivalence ratio perturbations was also examined, showing that the overall heat release response is controlled by the superposition of three disturbances: heat of reaction, flame speed, and flame area. Heat of reaction disturbances dominate the flame response at low Strouhal numbers, roughly defined as (frequency x flame length)/(axial flow velocity). All three disturbances play equal roles at Strouhal numbers of O(1). In addition, the mean equivalence ratio exerts little effect upon this transfer function at low Strouhal numbers. At O(1) Strouhal numbers, the flame response increases with decreasing values of the mean equivalence ratio. Thus, this result is in partial agreement with heuristic arguments made in prior studies that the flame response to equivalence ratio oscillations increases as the mixture becomes leaner.

CHAPTER 1 INTRODUCTION

1.1 Motivation

This thesis deals with the analysis of acoustic wave interactions with turbulent premixed flames. Such interactions play an important role in many fundamental and practical problems in various combustion and propulsion systems. For instance, those interactions affect the characteristic unsteadiness of combustion processes and play a crucial role in the problem of combustion instabilities, which have been known to arise from the interactions between acoustic waves and combustion processes which occur in a self-exciting manner at lean premixed conditions.[1,2]

Figure 1 Illustration of detrimental effects caused by combustion instabilities

1.2 Background

A number of studies have been reported to examine combustion instabilities using analytical modelings associated with acoustic perturbations. [3,4,5,6,7,8] McManus et al.[3] reviewed instability mechanisms with active control. They presented a simple model for an acoustically coupled instability and analysed the frequency of

thermoacoustic oscillation and its growth rate via dispersion relations (by zero-determinant condition) using an n-τ model. Hubbard and Dowling[4] performed a stability analysis of a simplified combustor geometry and considered the influence of entropy waves generated by density inhomogeneities in ref.[6,7] This analysis was extended to 3-D cylindrical and annular combustors by Dowling and Stow.[8] Recently Lipatnikov and Sathiah[9] demonstrated the effects of turbulent flame speed development on thermoacoustic instabilities. Using a flame speed expression based on classic turbulent diffusion theory, they showed a marked influence of flame speed upon thermoacoustic instabilities. The aforementioned analyses incorporate the flame's unsteady heat release, which has an influence on frequency and stability of oscillations. The flame's unsteadiness, however, is also coupled with the acoustic flow field and, accordingly, the interaction of acoustic waves with flames should be examined. Some of other mechanisms which have been identified as potentially significant are large scale, convected coherent structures [10, 11], unsteady flame extinction and re-ignition, flame-wall interactions [12], and reactive mixture composition perturbations (i.e., equivalence ratio oscillations) [13, 14, 15, 16, 17]. The latter mechanism, equivalence ratio oscillations excited by pressure and/or velocity oscillations in the premixer, is known to be particularly important in lean, premixed combustors. It will be discussed in section 1.2.2.

1.2.1 Acoustic wave–flame interactions

Acoustic wave–flame interactions have been considered in a large number of theoretical and experimental studies so far. Theoretical treatment of the acoustic wave-flame interaction phenomena was initiated by Chu [18], who regarded the flame front as

a temperature discontinuity that separates the unburned reactants from the burned products. Markstein[19] also analyzed the effects of unsteady small perturbations upon a steady-state planar flame by treating the flame front as a surface of discontinuity and applying first order perturbation methods to linearize the conservation equations of mass, momentum and energy, and flame kinematic equations. These works have been extended in several recent analyses, such as those of McIntosh and coworkers [20,21,22,23], Peters and Ludford [24], and Ledder and Kapila [25], which assessed the effects of pressure perturbations on the unsteady inner flame structure. Other analyses incorporating the coupling effects between the acoustic wave and the burning-rate fluctuations have also been reported by Lieuwen [26], Clavin et al. [27], Poinsot and Candel [28] and others. Another important process in these interactions, i.e., the periodic acceleration and/or convection of the flame front by the oscillatory flow field, has been discussed by Markstein [19], Searby and Rochwerger [29], and Fleifil et al. [30].

There are three canonical modes of disturbances, i.e., acoustic, entropy and vorticity modes which become strongly coupled at the flame front.[31] The acoustic wave-flame interactions are manifested by amplification or damping of acoustic waves via energy transfer among these three disturbance modes. Theoretical investigations were reported by Poinsot and Candel [28], McIntosh[23], Lieuwen[26] and others. McIntosh[23] reported that the low frequency acoustic wave amplification is sensitive to the impedance at the burner surface. More recently, Lieuwen[26] reported two-dimensional analysis by considering acoustic waves that are obliquely incident upon the planar flame front. He demonstrated that net acoustic energy flux out of the flame is controlled by competition between acoustic energy production and dissipation processes.

Energy addition is due to unsteady heat release through fluctuations in flame speed or density while energy damping is due to baroclinic production of vorticity. He reported that such amplification/damping of acoustic energy is more complicated processes which result from the combined effects of refraction, temperature jump across the flame, vorticity production and flame speed modulation, and so on. Other researchers, for instance, McManus *et al*.[3], Bloxsidge *et al*.[32], Poinsot *et al*.[33], and others, reported estimations of amplification or damping of acoustic waves by utilizing Rayleigh's criterion to evaluate local or global instability associated with combustion-acoustic wave interactions. Rayleigh's criterion states that acoustic waves will be locally amplified (damped) if acoustic pressure are in phase (out of phase) with flame's heat release oscillations. Nicoud and Poinsot [34] recently proposed an extended Rayleigh's criterion which includes entropy fluctuation term that may have a significant effect when mean entropy gradient exists.

The primary emphasis of the theoretical work mentioned above is to model the laminar flame–acoustic wave interaction problems. Searby and Clavin[35] performed theoretical analysis to examine the dynamic behavior of a wrinkled flame front propagating downwards in a weakly turbulent flow. Coupled linearized forms of continuity, momentum, and flame's kinematics equations are solved to evaluate the mutual interactions between wrinkled flame and turbulent flow field in terms of Froude number (gravity effect) and Markstein number (flames curvature effect). They applied jump conditions of pressure and velocity across the mean flame surface to calculate amplification / damping of flow velocity and flame position. However, fluctuation quantities of flame front position, pressure, and velocity are assumed to follow harmonic

oscillation and, therefore, stochastic analysis associated with random effect of turbulent flames are not actually incorporated. Furthermore, the boundary conditions are applied to the mean flame surface, not its instantaneous position. Several more recent studies have extended the developed analysis based on the laminar flame to the problems of acoustic wave interaction with turbulent flame [36, 37, 38] and non-reacting random rough surface [39] by applying stochastic analysis to account for randomly wrinkling turbulent flame. References 36-38 analyzed the scattering of high-frequency acoustic waves from single-connected, wrinkled flame fronts by modeling the flame as a dynamically evolving, wrinkled temperature discontinuity. Their results suggest that several qualitative differences exist between the characteristics of scattering waves from laminar and turbulent flames. Most significance of these results is the fact that a coherent, harmonically oscillating acoustic wave incident upon a turbulent flame generates both coherent and incoherent scattered waves. This is due to the characteristics of the wrinkled turbulent flame that transmits a coherent acoustic energy into diffuse, incoherent energy. Moreover, with increasing roughness σ/λ (σ = standard deviation of roughness, λ = acoustic wavelength), the power of the coherent field decreases and, subsequently, the power of the incoherent field increases, at least for small σ/λ. The above mentioned studies about acoustic-turbulent flame interaction are based on the assumption of high frequency acoustic waves whose wavelength is much shorter compared to the characteristic length of flame fronts. However, the flame interactions with long-wavelength (low-frequency) acoustic waves have been known to be consequential in the context of combustion instabilities. The previous work also assumed that the flame front position is prescribed; i.e., flame's response to perturbations in flow fields, e.g., acoustic

perturbations, was not accounted for. Such response of flame front, however, may not be negligible since the flame front's fluctuation is coupled with perturbations in flow fields, as is described by the flame kinematics. Such coupled problems have not yet been tackled analytically, which motivates the present study.

1.2.2 Mixture composition effect on heat release

A number of studies have provided strong experimental support for the significance of this mechanism by either directly measuring equivalence ratio oscillations during an instability [40 , 41], or by comparing the dependence of instability characteristics upon geometry and operating conditions with correlations developed from theoretical analyses [14, 15]. Predicting the conditions under which this mechanism is self-exciting requires models of all processes involved in the feedback loop; in particular, the response of the heat release to an equivalence ratio perturbation. As noted above, simple phenomenological models have been quite successful in correlating instability characteristics. However, these models often treat the flame as a concentrated source of heat release and, consequently, lack the fidelity to handle "distributed flame effects"; e.g., the effect of changes in local flame position (such as induced by changes in swirler configuration [42] or fuel composition) upon stability characteristics. As will be shown below, the magnitude of the Strouhal number, roughly given by the product of angular frequency of oscillations, ω, and flame length, L_F, divided by axial flow velocity, $\overline{u}$, determines whether it is appropriate to treat the flame as a concentrated ($St \ll 1$) or a distributed source of heat release ($St \sim O(1)$).

Since flame Strouhal numbers are often of order unity in practical systems, accurately predicting their response requires models with sufficient fidelity to incorporate

the spatial distribution of the heat release region. Putnam presented a model that predicted the response of a conical flame to equivalence ratio perturbations as a function of the mean flame position [1]. This model was generalized by Lieuwen *et al*. [15] for arbitrary flame shapes. A similar phenomenological approach was used by Krebs *et al*. [43]. However, these models essentially only account for the effects of the fluctuating heat of reaction of the incoming mixture upon the flame's response. They do not account for two other effects which are also significant: 1) Fluctuations in flame speed which effect the rate of local heat release per unit surface area of mean flame front, 2) Disturbances in flame surface area generated by the flame speed fluctuations. As will be shown below, the effects included by Putnam [1] and Lieuwen *et al*. [15] are sufficient to model the flame's response at low Strouhal numbers. However, since the purpose of these models is to capture distributed flame effects (i.e., $St \sim O(1)$), this limitation severely restricts their utility.

Models incorporating all three of these processes (heat of reaction, flame speed, and flame area) were developed by Hubbard and Dowling [5], Dowling and Hubbard [6], and Prasanth *et al*. [44]. These models treat the flame front as a surface of discontinuity dividing reactants and products. The flame front dynamics are modeled using a front tracking equation. These studies introduced these models as part of a larger model of the dynamics of unstable combustors and, therefore, did not discuss the characteristics of the equivalence ratio-heat release transfer function and the role of the processes affecting the dynamics of the interaction.

1.3 The scope of the present study

The objectives of this study are two fold. The first part is to address acoustic wave-flame interaction. CHAPTER 2 describes the problem statement, basic assumptions and revisits the linear wave equation solution to introduce scattering amplitudes. CHAPTER 3 presents a second-order small perturbation analysis to evaluate reflected/ transmitted scattering amplitudes. First, matching conditions in acoustic pressure and velocity are applied across a transient flame front as a boundary condition. Reciprocity theorem is proved by direct substitution and manipulation of scattering amplitudes up to second order. Jump condition in acoustic velocity due to flame's unsteady heat release is also applied across a transient flame front to evaluate scattering amplitudes with jump effect. Reciprocity theorem is analytically proved to hold even for locally reacting wrinkling surface, in Appendix A. Bragg scattering and Doppler frequency shift effects are illustrated using a periodically moving surface. CHAPTER 4 performs stochastic analysis of scattered fields to evaluate ensemble-averaged acousic energy flux of reflected / transmitted fields. Using factors that are found to cause energy amplification/damping, detailed net energy fluxes are examined. Net acoustic energy fluxes are formulated assuming Gaussian statistics for the flame front, and the key dimensionless parameters are identified that govern net energy fluxes. Then, associated results using numerical calculation are illustrated and discussed in CHAPTER 5. CHAPTER 6 characterizes the transient response of flame fronts to scattered acoustic fields. Flame front kinematics is incorporated into scattered acoustic fields using first-order small perturbation analysis to describe dynamically and temporally evolving interactions between low-frequency acoustic waves and premixed flame fronts.

0 models the response of laminar, premixed flames to perturbations in reactive mixture equivalence ratio. It utilizes the same approaches used in Refs. [5, 6, 44, 45] to develop this model, which is generalized for an arbitrary mean flame shape. It presents the results and detailed discussion of the dependence of the equivalence ratio-heat release transfer function upon Strouhal number and flame characteristics. In addition, it derives a result for the sensitivity of this transfer function to uncertainties in the mean flame position.

CHAPTER 8 draws conclusions and recommends future works.

CHAPTER 2 BACKGROUND ANALYSIS

2.1 Problem statement and basic assumptions

Figure 2 illustrates the problem of interest, where plane incident waves impinge obliquely upon a randomly moving, wrinkling flame surface and, subsequently, scattered waves are reflected and transmitted by the flame.

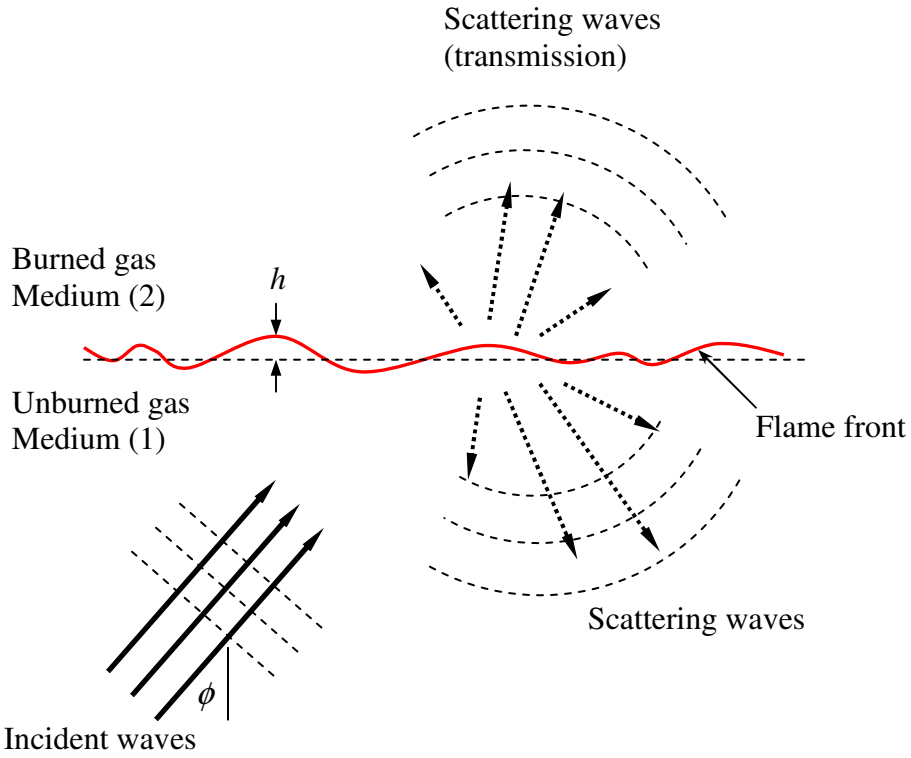

Figure 2 Schematic of flame surface and acoustic fields

The problems of interest are associated with:

1) how the scattered, i.e., reflected and transmitted, acoustic fields are characterized in terms of the incident field and the flame's kinematics quantities,

2) how the acoustic energy is amplified / damped after scattering, and how the net energy flux of the scattered fields can be obtained quantitatively,

3) what key factors influence the net coherent / incoherent energy fluxes of scattered wave fields.

Several assumptions are made to render the theoretical approach tractable.

1) The height and slope of a wrinkled flame surface are small, see Eqs. (3.13) and (3.14).

2) The flame extends without boundary. This assumption is equivalent to neglecting edge effects, such as diffraction from the flame edges.

3) Multiple scattering is not considered, i.e., all scattering is assumed to be single scattering. For instance, all the reflected scattering waves propagate downward and all the transmitted scattering waves propagate upward when incident waves propagate upward. This assumption, called Rayleigh's hypothesis, is known to yield the same result as the exact solution as long as the slope of the rough surface is sufficiently small; e.g., if the maximum slope of surface is not greater than 0.448 for the Dirichlet problem.[50] The assumption of single scattering implies that the present analysis applies to wrinkled flamelets, not to corrugated flamelets where multiple scattering will be present, see Borghi diagram in Figure 3.

4) The flame front is temperature discontinuity that separates the unburned reactants and burned products.

5) Vorticity and entropy modes are neglected in the present analysis.

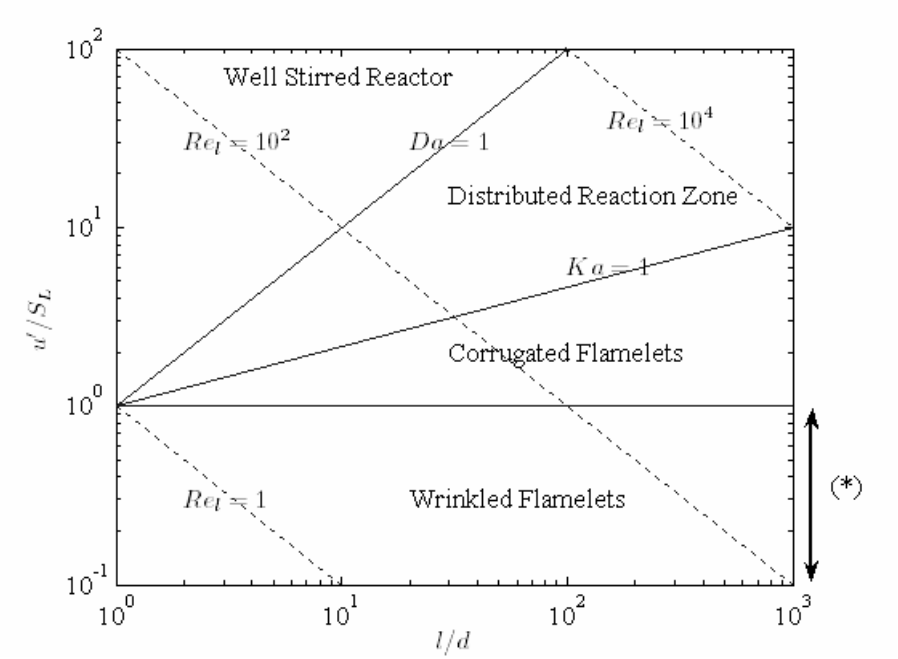

Figure 3 Borghi diagram illustrating region, (*), where the analysis applies

2.2 Linearized wave equations

The time-dependent acoustic wave fields are described by the linearized wave equation:

$$\left(\Delta - \frac{1}{c_0^2}\frac{\partial^2}{\partial t^2}\right) p(\vec{\boldsymbol{R}},t) = -\rho_0 \frac{\partial Q(\vec{\boldsymbol{R}},t)}{\partial t} \tag{2.1}$$

where $\Delta = \partial_{xx} + \partial_{yy} + \partial_{zz}$. We define ψ as the velocity potential:

$$\vec{v} = \vec{\nabla}\psi(\vec{\boldsymbol{R}},t) \tag{2.2}$$

where $\vec{\nabla} = (\partial_x, \partial_y, \partial_z)$. It follows from linearized Euler's equation, $\rho_0 \partial \vec{v} / \partial t = -\vec{\nabla} p$, that the acoustic pressure is also expressed in terms of ψ :

$$p = -\rho_0 \frac{\partial \psi(\vec{\boldsymbol{R}},t)}{\partial t} \tag{2.3}$$

Hereafter we use ψ instead of p to describe acoustic wave fields. Then Eq. (2.1) has the form in terms of ψ :

$$\left(\Delta - \frac{1}{c_0^2}\frac{\partial^2}{\partial t^2}\right)\psi(\vec{\boldsymbol{R}},t) = Q(\vec{\boldsymbol{R}},t) \tag{2.4}$$

ψ in Eq. (2.4) represents the acoustic wave field in free space caused by arbitrary distribution of sound sources, Q. The solution of Eq. (2.4) can be written in the following integral form. (E.g., see p. 38 in ref.[46], p. 230 in ref.[47], or p. 319 in ref.[48].)

$$\psi(\vec{\boldsymbol{R}},t) = -\frac{1}{4\pi}\int\int\int_{\vec{R}'=-\infty}^{\infty}\int_{t'=-\infty}^{\infty} Q(\vec{\boldsymbol{R}}',t')\frac{\delta(t-t'-|\vec{\boldsymbol{R}}-\vec{\boldsymbol{R}}'|/c_0)}{|\vec{\boldsymbol{R}}-\vec{\boldsymbol{R}}'|}dt'd\vec{\boldsymbol{R}}'$$

$$= -\frac{1}{4\pi}\iiint_{\frac{|\vec{\boldsymbol{R}}-\vec{\boldsymbol{R}}'|}{c_0}\le t}\frac{Q(\vec{\boldsymbol{R}}',t-|\vec{\boldsymbol{R}}-\vec{\boldsymbol{R}}'|/c_0)}{|\vec{\boldsymbol{R}}-\vec{\boldsymbol{R}}'|}d\vec{\boldsymbol{R}}' \tag{2.5}$$

The integral range, $|\vec{\boldsymbol{R}}-\vec{\boldsymbol{R}}'|/c_0 \le t$, results from the assumption that $Q(\vec{\boldsymbol{R}},t)$ vanishes for $t < 0$ (Causality condition). Actually the solution of Eq. (2.4) can also be expressed in terms of superposition of plane waves. To derive the solution in forms of superposition of plane waves, it is useful to summarize the procedure for obtaining the above solution in Eq. (2.5). Taking Fourier transform of (2.4) with respect to time yields:

$$\left(\Delta + \frac{\omega^2}{c_0^2}\right)\psi(\vec{\boldsymbol{R}},\omega) = Q(\vec{\boldsymbol{R}},\omega) \tag{2.6}$$

where $F(\vec{\boldsymbol{R}},\omega) = \frac{1}{2\pi}\int_{-\infty}^{\infty} F(\vec{\boldsymbol{R}},t)e^{i\omega t}dt$ for $F = \psi, Q$

Eq. (2.6) is the reduced wave equation or Helmholtz equation. Define G as the Green's function for the Helmholtz equation.

$$\left(\Delta + \frac{\omega^2}{c_0^2}\right)G(\vec{\boldsymbol{R}}) = \delta(\vec{\boldsymbol{R}}) \tag{2.7}$$

G represents a solution of an acoustic field in free space with a point source at the origin. Applying the spatial Fourier transform gives:

$$\left(\frac{\omega^2}{c_0^2} - K^2\right) G(\vec{K}) = \frac{1}{(2\pi)^3} \tag{2.8}$$

where $G(\vec{K}) = \frac{1}{(2\pi)^3} \iiint G(\vec{R}) e^{-i\vec{K}\cdot\vec{R}} d\vec{R}$, $\quad \vec{K} = (k_x, k_y, k_z)$, $\quad K = \left|\vec{K}\right|$

Note that $d\vec{R}$ is a short hand notation for a volume element, i.e., $d\vec{R} = dx\,dy\,dz$. Applying inverse Fourier transform in Eq. (2.8) leads to the following integral form.

$$G(\vec{R}) = \iiint G(\vec{K}) e^{i\vec{K}\cdot\vec{R}} d\vec{K} = \frac{1}{(2\pi)^3} \iiint \left(\frac{\omega^2}{c_0^2} - K^2\right)^{-1} e^{i\vec{K}\cdot\vec{R}} d\vec{K} \tag{2.9}$$

whose solution is: [49]

$$G(\vec{R}) = -\frac{\exp(i\omega |\vec{R}| / c_0)}{4\pi |\vec{R}|} \tag{2.10}$$

We chose $+i\omega$ as an outgoing wave, given our $\exp(-i\omega t)$ convention. Now, the solution of Eq. (2.6) has the following form.

$$\psi(\vec{R}, \omega) = \iiint G(\vec{R} - \vec{R}') Q(\vec{R}', \omega) d\vec{R}' \tag{2.11}$$

The solution of the wave equation in Eq. (2.4) is obtained by applying inverse Fourier transform to Eq. (2.11).

$$\psi(\vec{R}, t) = \int_{-\infty}^{\infty} \psi(\vec{R}, \omega) e^{-i\omega t} d\omega = \int_{-\infty}^{\infty} \left(\iiint_{-\infty}^{\infty} G(\vec{R} - \vec{R}') Q(\vec{R}', \omega) d\vec{R}' \right) e^{-i\omega t} d\omega$$

$$= -\int_{-\infty}^{\infty} \iiint_{-\infty}^{\infty} \frac{\exp(i\omega |\vec{R} - \vec{R}'| / c_0)}{4\pi |\vec{R} - \vec{R}'|} \left(\frac{1}{2\pi} \int_{-\infty}^{\infty} Q(\vec{R}', t') e^{i\omega t'} dt' \right) d\vec{R}' e^{-i\omega t} d\omega$$

$$= -\frac{1}{4\pi} \iiint_{-\infty}^{\infty} \int_{-\infty}^{\infty} Q(\vec{R}', t') \frac{\delta(t - t' - |\vec{R} - \vec{R}'| / c_0)}{|\vec{R} - \vec{R}'|} dt' d\vec{R}' \tag{2.12}$$

which is equivalent to Eq.(2.5). The last equality in (2.12) was obtained by means of the following property of delta function.

$$\frac{1}{2\pi}\int \exp(\pm i\omega t)\, d\omega = \delta(t) \tag{2.13}$$

Generally, the multidimensional version of the delta function has the form:

$$(2\pi)^{-n}\int\cdots\int \exp(\pm i\vec{\boldsymbol{\xi}}\cdot\vec{\boldsymbol{R}})\, d\vec{\boldsymbol{\xi}} = \delta(\vec{\boldsymbol{R}}) \tag{2.14}$$

Since the objective here is to represent the wave equation solution as a superposition of plane waves, the next step is taken by performing the integration in Eq. (2.9) over the z-component of wave number vector, i.e., $k_z = (-\infty, \infty)$, using the residue theorem of contour integrals. [49, 50]

$$G(\vec{\boldsymbol{R}}) = -\frac{i}{8\pi^2}\iint q_k^{-1} \exp(i\boldsymbol{k}\cdot\boldsymbol{r} + iq_k|z|)d\boldsymbol{k} \tag{2.15}$$

where $\boldsymbol{k} = (k_x, k_y)$, $d\boldsymbol{k} = dk_x dk_y$, $q_k = \left((\omega/c_0)^2 - k^2\right)^{1/2}$, $k = |\boldsymbol{k}|$, $\boldsymbol{r} = (x, y)$

Note that radiation condition requires that $\mathrm{Im}(q_k) \geq 0$ when $k > \omega/c_0$; i.e., the wave decays exponentially when going away from the source location. Substitution of Eq. (2.15) into the second equation in Eq. (2.12) yields:

$$\psi(\vec{\boldsymbol{R}}, t) = -\frac{i}{8\pi^2}\int_{\omega}\iint_{\boldsymbol{k}}\iiint_{\vec{\boldsymbol{R}}'} q_k^{-1}\, \mathrm{e}^{i[\boldsymbol{k}\cdot(\boldsymbol{r}-\boldsymbol{r}')+q_k|z-z'|-\omega t]}\, Q(\vec{\boldsymbol{R}}', \omega) d\vec{\boldsymbol{R}}' d\boldsymbol{k} d\omega$$

$$= \int_{\omega}\iint_{\boldsymbol{k}} q_k^{-1}\left[a_+(\boldsymbol{k}, \omega)\,\mathrm{e}^{i(\boldsymbol{k}\cdot\boldsymbol{r}+q_k z-\omega t)} + a_-(\boldsymbol{k}, \omega)\,\mathrm{e}^{i(\boldsymbol{k}\cdot\boldsymbol{r}-q_k z-\omega t)}\right] d\boldsymbol{k} d\omega \tag{2.16}$$

where

$$a_+(\boldsymbol{k}, \omega) = -\frac{i}{8\pi^2}\iiint_{z'<z} Q(\vec{\boldsymbol{R}}', \omega)\,\mathrm{e}^{-i(\boldsymbol{k}\cdot\boldsymbol{r}'+q_k z')}\, d\vec{\boldsymbol{R}}' \quad , \quad a_-(\boldsymbol{k}, \omega) = -\frac{i}{8\pi^2}\iiint_{z'>z} Q(\vec{\boldsymbol{R}}', \omega)\,\mathrm{e}^{-i(\boldsymbol{k}\cdot\boldsymbol{r}'-q_k z')}\, d\vec{\boldsymbol{R}}'$$

Equation (2.16) implies that acoustic wave fields in free space can be represented by superposition of elementary plane waves in a domain of horizontal wave number and frequency. The first term on the right hand side in Eq. (2.16) represents the waves propagating upward and the second term represents the waves propagating downward. Now consider media (1) and (2) that are separated by a (flame front) boundary as shown in

Figure 2. Let the incident wave be a plane wave that is propagating in medium (1) with a horizontal component of wave vector $\boldsymbol{k_0}$ and frequency ω_0 and impinging upward upon the (flame front) boundary. Then the total acoustic fields in each media can be described by the following forms considering reflected and transmitted waves:

In medium (1),

$$\psi^{(1)}(\vec{\boldsymbol{R}},t) = \mathrm{Re}[\psi_c^{(1)}] \tag{2.17}$$

where

$$\frac{\psi_c^{(1)}}{A_1} = (\rho_1 q_0^{(1)})^{-1/2}\, \mathrm{e}^{i(\boldsymbol{k_0}\cdot\boldsymbol{r}+q_0^{(1)}z-\omega_0 t)} + \int_{\omega}\iint_{\boldsymbol{k}} S^{11}(\boldsymbol{k},\boldsymbol{k_0},\omega,\omega_0)(\rho_1 q_k^{(1)})^{-1/2}\, \mathrm{e}^{i(\boldsymbol{k}\cdot\boldsymbol{r}-q_k^{(1)}z-\omega t)}\, d\boldsymbol{k}d\omega \tag{2.18}$$

$$A_1 = \frac{|P_1|}{\omega_0}\left(\frac{q_0^{(1)}}{\rho_1}\right)^{1/2},\ q_0^{(1)} = [(\omega_0/c_1)^2 - k_0^2]^{1/2},\ q_k^{(1)} = [(\omega/c_1)^2 - k^2]^{1/2},\ k = |\boldsymbol{k}|$$

In medium (2),

$$\psi^{(2)}(\vec{\boldsymbol{R}},t) = \mathrm{Re}[\psi_c^{(2)}] \tag{2.19}$$

where

$$\frac{\psi_c^{(2)}}{A_1} = \int_{\omega}\iint_{\boldsymbol{k}} S^{21}(\boldsymbol{k},\boldsymbol{k_0},\omega,\omega_0)(\rho_2 q_k^{(2)})^{-1/2}\, \mathrm{e}^{i(\boldsymbol{k}\cdot\boldsymbol{r}+q_k^{(2)}z-\omega t)}\, d\boldsymbol{k}d\omega \tag{2.20}$$

$$q_k^{(2)} = [(\omega/c_2)^2 - k^2]^{1/2}$$

In Eq.(2.18), P_I is a complex amplitude of an incident wave pressure and A_0 is a scaling factor, see Eq.(2.3). The term $(\rho_1 q_k^{(1)})^{-1/2}$ in the integral in Eq. (2.18) or $(\rho_2 q_k^{(2)})^{-1/2}$ in the integral in Eq.(2.20) results from rendering the energy flux in the waves along the z-axis to be constant and $\boldsymbol{k}$-independent.[50] The terms $q_0^{(1)}$, $q_k^{(1)}$ and $q_k^{(2)}$ denote the vertical wave number components of the incident and scattered waves in each medium. These can be complex when $\omega/c < k$, representing exponentially decaying waves. Actually the scattered field of our interest is the one far from a rough surface in which case only non-attenuating waves, for which q is real, are significant. The first term in the right hand side of Eq. (2.18) is an incident plane wave propagating upward towards the flame front. The second term is a scattered wave generated by reflection of the incident wave from the flame front and is expressed by the superposition of plane waves as discussed below Eq. (2.16). This second term, however, has only downward propagating waves, due to assumption (1). Its amplitude is S^{11}, instead of a_-, which will be evaluated so that it safisifies the boundary conditions on the flame fronts. Similarly, the integral in Eq.(2.20) represents a scattered wave field in forms of superposition of upward propagating plane waves of amplitude S^{21} that are generated by transmission of the incident wave through the flame front. (Note that $S^{N_1N_2}$ denotes the scattering amplitude of waves that are scattered into medium N_1 by incident waves from medium N_2. Therefore, S^{11} denotes reflected waves and S^{21} denotes transmitted waves.)

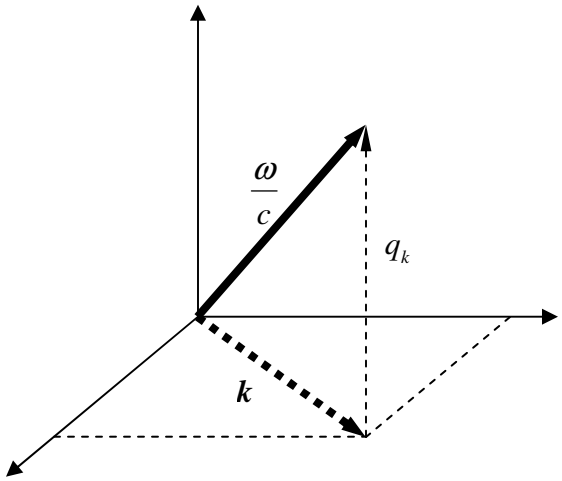

Figure 4 Notation used for horizontal / vertical wave number

CHAPTER 3 EVALUATION OF SCATTERING AMPLITUDES

3.1 Evaluation of scattering amplitudes with matching conditions

The boundary conditions at the flame front, $z = h(\boldsymbol{r},t)$, are the continuity of acoustic pressure and normal velocity. (Acoustic velocity jump condition due to unsteady heat release will be considered in section 3.3.) Both matching conditions can be expressed in terms of velocity potential from Eqs. (2.2) and (2.3).

$$\text{Pressure continuity : } \rho_1 \frac{\partial \psi_c^{(1)}(\vec{\boldsymbol{R}},t)}{\partial t}\bigg|_{z=h(\boldsymbol{r},t)} = \rho_2 \frac{\partial \psi_c^{(2)}(\vec{\boldsymbol{R}},t)}{\partial t}\bigg|_{z=h(\boldsymbol{r},t)} \tag{3.1}$$

$$\text{Normal velocity continuity : } \frac{\partial \psi_c^{(1)}(\vec{\boldsymbol{R}},t)}{\partial \boldsymbol{n}}\bigg|_{z=h(\boldsymbol{r},t)} = \frac{\partial \psi_c^{(2)}(\vec{\boldsymbol{R}},t)}{\partial \boldsymbol{n}}\bigg|_{z=h(\boldsymbol{r},t)} \tag{3.2}$$

Note that the above matching conditions use complex value of velocity potential, ψ_c, which also holds for real part, ψ, and also provides enough conditions to solve for complex values of scattering amplitudes. Substituting Eqs. (2.18) and (2.20) into Eq. (3.1) yields:

$$\rho_1\left[\omega_0(\rho_1 q_0^{(1)})^{-1/2}\,\mathrm{e}^{i(\boldsymbol{k_0}\cdot\boldsymbol{r}+q_0^{(1)}h(\boldsymbol{r},t)-\omega_0 t)} + \int_{\omega}\iint_{\boldsymbol{k}} \omega S^{11}(\boldsymbol{k},\boldsymbol{k_0},\omega,\omega_0)(\rho_1 q_k^{(1)})^{-1/2}\,\mathrm{e}^{i(\boldsymbol{k}\cdot\boldsymbol{r}-q_k^{(1)}h(\boldsymbol{r},t)-\omega t)}\,d\boldsymbol{k}d\omega\right]$$

$$= \rho_2 \int_{\omega}\iint_{\boldsymbol{k}} \omega S^{21}(\boldsymbol{k},\boldsymbol{k_0},\omega,\omega_0)(\rho_2 q_k^{(2)})^{-1/2}\,\mathrm{e}^{i(\boldsymbol{k}\cdot\boldsymbol{r}+q_k^{(2)}h(\boldsymbol{r},t)-\omega t)}\,d\boldsymbol{k}d\omega \tag{3.3}$$

The direction $\vec{\boldsymbol{n}}$ is normal to the flame surface, $G = z - h(\boldsymbol{r},t) = 0$, and has the form

$$\vec{\boldsymbol{n}} = \frac{\vec{\nabla} G}{\left|\vec{\nabla} G\right|} = \left(1+\left|\nabla h\right|^2\right)^{-1/2}(\vec{\boldsymbol{e}}_z - \nabla h) \tag{3.4}$$

where $\nabla = (\partial_x, \partial_y)$ is a horizontal gradient. Since the normal velocity has the following form

$$\frac{\partial \psi}{\partial \boldsymbol{n}} = \vec{\boldsymbol{n}} \cdot \vec{\nabla} \psi = \left(1 + \left|\nabla h\right|^2\right)^{-1/2} \left(\frac{\partial \psi}{\partial z} - \nabla h \cdot \nabla \psi\right), \tag{3.5}$$

the normal velocity continuity in Eq. (3.2) can be rewritten

$$\left(\frac{\partial}{\partial z} - \nabla h \cdot \nabla\right) \psi_c^{(1)}\Big|_{z=h(\boldsymbol{r},t)} = \left(\frac{\partial}{\partial z} - \nabla h \cdot \nabla\right) \psi_c^{(2)}\Big|_{z=h(\boldsymbol{r},t)} \tag{3.6}$$

Substituting Eqs. (2.18) and (2.20) into Eq. (3.6) yields

$$\begin{aligned}
&(\rho_1 q_0^{(1)})^{-1/2} \left(q_0^{(1)} - \nabla h(\boldsymbol{r},t) \cdot \boldsymbol{k_0}\right) \mathrm{e}^{i(\boldsymbol{k_0} \cdot \boldsymbol{r} + q_0^{(1)} h(\boldsymbol{r},t) - \omega_0 t)} \\
&- \int_{\omega} \iint_{\boldsymbol{k}} S^{11}(\boldsymbol{k}, \boldsymbol{k_0}, \omega, \omega_0) (\rho_1 q_k^{(1)})^{-1/2} \left(q_k^{(1)} + \nabla h(\boldsymbol{r},t) \cdot \boldsymbol{k}\right) \mathrm{e}^{i(\boldsymbol{k} \cdot \boldsymbol{r} - q_k^{(1)} h(\boldsymbol{r},t) - \omega t)} \, d\boldsymbol{k} d\omega \\
&= \int_{\omega} \iint_{\boldsymbol{k}} S^{21}(\boldsymbol{k}, \boldsymbol{k_0}, \omega, \omega_0) (\rho_2 q_k^{(2)})^{-1/2} \left(q_k^{(2)} - \nabla h(\boldsymbol{r},t) \cdot \boldsymbol{k}\right) \mathrm{e}^{i(\boldsymbol{k} \cdot \boldsymbol{r} + q_k^{(2)} h(\boldsymbol{r},t) - \omega t)} \, d\boldsymbol{k} d\omega
\end{aligned} \tag{3.7}$$

An approximate solution for scattering amplitude S^{11} and S^{21} in Eqs. (3.3) and (3.7) can be obtained by using perturbation method, i.e., expanding the scattering amplitudes in powers of h.

$$S^{N_1 N_2} = S_0^{N_1 N_2} + S_1^{N_1 N_2} + \cdots \tag{3.8}$$

where $S_n^{N_1 N_2} \sim O(h^n)$. Substituting Eq. (3.8) into Eqs. (3.3) and (3.7) yields

$$\begin{aligned}
&\rho_1 \Big[\omega_0 (\rho_1 q_0^{(1)})^{-1/2} \, \mathrm{e}^{i(\boldsymbol{k_0} \cdot \boldsymbol{r} - \omega_0 t)} \left\{1 + i q_0^{(1)} h(\boldsymbol{r},t) - \frac{1}{2} (q_0^{(1)} h(\boldsymbol{r},t))^2 + \cdots\right\} \\
&+ \int_{\omega} \iint_{\boldsymbol{k}} \omega \left(S_0^{11} + S_1^{11} + S_2^{11} + \cdots\right) (\rho_1 q_k^{(1)})^{-1/2} \, \mathrm{e}^{i(\boldsymbol{k} \cdot \boldsymbol{r} - \omega t)} \left\{1 - i q_k^{(1)} h(\boldsymbol{r},t) - \frac{1}{2} (q_k^{(1)} h(\boldsymbol{r},t))^2 + \cdots\right\} d\boldsymbol{k} d\omega \Big] \\
&= \rho_2 \int_{\omega} \iint_{\boldsymbol{k}} \omega \left(S_0^{21} + S_1^{21} + S_2^{21} + \cdots\right) (\rho_2 q_k^{(2)})^{-1/2} \, \mathrm{e}^{i(\boldsymbol{k} \cdot \boldsymbol{r} - \omega t)} \left\{1 + i q_k^{(2)} h(\boldsymbol{r},t) - \frac{1}{2} (q_k^{(2)} h(\boldsymbol{r},t))^2 + \cdots\right\} d\boldsymbol{k} d\omega
\end{aligned} \tag{3.9}$$

$$
\begin{aligned}
&(\rho_1 q_0^{(1)})^{-1/2} q_0^{(1)} \left(1-\frac{\nabla h(\boldsymbol{r},t)\cdot\boldsymbol{k_0}}{q_0^{(1)}}\right) e^{i(\boldsymbol{k_0}\cdot\boldsymbol{r}-\omega_0 t)} \left\{1+iq_0^{(1)}h(\boldsymbol{r},t)-\frac{1}{2}(q_0^{(1)}h(\boldsymbol{r},t))^2+\cdots\right\} \\
&-\int_{\omega}\iint_{\boldsymbol{k}} \frac{\left(S_0^{11}+S_1^{11}+S_2^{11}+\cdots\right)(\rho_1 q_k^{(1)})^{-1/2} q_k^{(1)} \left(1+\frac{\nabla h(\boldsymbol{r},t)\cdot\boldsymbol{k}}{q_k^{(1)}}\right) e^{i(\boldsymbol{k}\cdot\boldsymbol{r}-\omega t)}}{\times\left\{1-iq_k^{(1)}h(\boldsymbol{r},t)-\frac{1}{2}(q_k^{(1)}h(\boldsymbol{r},t))^2+\cdots\right\}} d\boldsymbol{k}d\omega \\
&=\int_{\omega}\iint_{\boldsymbol{k}} \frac{\left(S_0^{21}+S_1^{21}+S_2^{21}+\cdots\right)(\rho_2 q_k^{(2)})^{-1/2} q_k^{(2)} \left(1-\frac{\nabla h(\boldsymbol{r},t)\cdot\boldsymbol{k}}{q_k^{(2)}}\right) e^{i(\boldsymbol{k}\cdot\boldsymbol{r}-\omega t)}}{\left\{1+iq_k^{(2)}h(\boldsymbol{r},t)-\frac{1}{2}(q_k^{(2)}h(\boldsymbol{r},t))^2+\cdots\right\}} d\boldsymbol{k}d\omega \qquad (3.10)
\end{aligned}
$$

where $\exp(iq_k h(\boldsymbol{r},t))$ terms are expanded in a Taylor series by assuming:

$$q_k h(\boldsymbol{r},t) = Kh\cos\phi << 1 \qquad (K=\omega/c) \qquad (3.11)$$

which is called the Rayleigh parameter. It is also assumed in Eq. (3.10) that ∇h terms in brackets are of the same order as $q_k h$, hence much smaller than unity:

$$\frac{\nabla h(\boldsymbol{r},t)\cdot\boldsymbol{k}}{q_k} << 1 \qquad (3.12)$$

which imposes the condition that the slope of surface roughness be much smaller than the grazing angle of all incident and scattered waves. Eqs. (3.11) and (3.12) can have statistical forms in case of random oscillation.

Small rms height : $\tilde{\sigma}\cos\phi << 1$ (3.13)

Small slope : $\tilde{\sigma}_\Delta \tan\phi << 1$ (3.14)

where $\tilde{\sigma} := K\sigma = K\left\langle h^2\right\rangle^{1/2}$ and $\tilde{\sigma}_\Delta = \sqrt{2}\,\tilde{\sigma}/\tilde{l}_c$ (Ogilvy, [51], p. 22)). Assuming a maximum allowable value of $\tilde{\sigma}\cos\phi$ to be 0.3 in Eq. (3.13) yields a maximum allowable frequency $f_{\max} = Kc/2\pi \approx 540$ Hz for normal incidence ($\phi = 0$ deg) with $\sigma = 3$ cm, c = 340 m/s.

Equating the terms of $O(h^0)$ in Eqs. (3.9) and (3.10) gives

$$\rho_1\left[\omega_0(\rho_1 q_0^{(1)})^{-1/2}\,\mathrm{e}^{i(\boldsymbol{k_0}\cdot\boldsymbol{r}-\omega_0 t)}+\int_{\omega}\iint_{\boldsymbol{k}}\omega S_0^{11}(\boldsymbol{k},\boldsymbol{k_0},\omega,\omega_0)(\rho_1 q_k^{(1)})^{-1/2}\,\mathrm{e}^{i(\boldsymbol{k}\cdot\boldsymbol{r}-\omega t)}\,d\boldsymbol{k}d\omega\right]$$
$$=\rho_2\int_{\omega}\iint_{\boldsymbol{k}}\omega S_0^{21}(\boldsymbol{k},\boldsymbol{k_0},\omega,\omega_0)(\rho_2 q_k^{(2)})^{-1/2}\,\mathrm{e}^{i(\boldsymbol{k}\cdot\boldsymbol{r}-\omega t)}\,d\boldsymbol{k}d\omega \tag{3.15}$$

$$q_0^{(1)}(\rho_1 q_0^{(1)})^{-1/2}\,\mathrm{e}^{i(\boldsymbol{k_0}\cdot\boldsymbol{r}-\omega_0 t)}-\int_{\omega}\iint_{\boldsymbol{k}}S_0^{11}(\boldsymbol{k},\boldsymbol{k_0},\omega,\omega_0)q_k^{(1)}(\rho_1 q_k^{(1)})^{-1/2}\,\mathrm{e}^{i(\boldsymbol{k}\cdot\boldsymbol{r}-\omega t)}\,d\boldsymbol{k}d\omega$$
$$=\int_{\omega}\iint_{\boldsymbol{k}}S_0^{21}(\boldsymbol{k},\boldsymbol{k_0},\omega,\omega_0)q_k^{(2)}(\rho_2 q_k^{(2)})^{-1/2}\,\mathrm{e}^{i(\boldsymbol{k}\cdot\boldsymbol{r}-\omega t)}\,d\boldsymbol{k}d\omega \tag{3.16}$$

The explicit solution for the zeroth-order scattering amplitudes, S_0^{11} and S_0^{21}, follows from multiplying $\exp[-i(\boldsymbol{k}'\cdot\boldsymbol{r}-\omega' t)]/(2\pi)^3$ in (3.15) and (3.16) and integrating with respect to $\boldsymbol{r}$ and t.

$$\rho_1\left[\omega_0(\rho_1 q_0^{(1)})^{-1/2}\delta(\boldsymbol{k_0}-\boldsymbol{k}')\delta(\omega_0-\omega')+\omega' S_0^{11}(\boldsymbol{k}',\boldsymbol{k_0},\omega',\omega_0)(\rho_1 q_{k'}^{(1)})^{-1/2}\right]$$
$$=\rho_2\omega' S_0^{21}(\boldsymbol{k}',\boldsymbol{k_0},\omega',\omega_0)(\rho_2 q_{k'}^{(2)})^{-1/2} \tag{3.17}$$

$$q_0^{(1)}(\rho_1 q_0^{(1)})^{-1/2}\delta(\boldsymbol{k_0}-\boldsymbol{k}')\delta(\omega_0-\omega')-S_0^{11}(\boldsymbol{k}',\boldsymbol{k_0},\omega',\omega_0)q_{k'}^{(1)}(\rho_1 q_{k'}^{(1)})^{-1/2}$$
$$=S_0^{21}(\boldsymbol{k}',\boldsymbol{k_0},\omega',\omega_0)q_{k'}^{(2)}(\rho_2 q_{k'}^{(2)})^{-1/2} \tag{3.18}$$

where the integral variables were interchanged and the following were used.

$$\iint\exp[-i(\boldsymbol{k}'-\boldsymbol{k})\cdot\boldsymbol{r}]d\boldsymbol{r}/(2\pi)^2=\delta(\boldsymbol{k}'-\boldsymbol{k}),\quad\int\exp[-i(\omega-\omega')t]dt/(2\pi)=\delta(\omega-\omega') \tag{3.19}$$

Eqs. (3.17) and (3.18) yield an explicit solution for S_0^{11} and S_0^{21}.

$$S_0^{11}(\boldsymbol{k},\boldsymbol{k_0},\omega,\omega_0)=R(\boldsymbol{k})\delta(\boldsymbol{k}-\boldsymbol{k_0})\delta(\omega-\omega_0)\ \text{ with }\ R(\boldsymbol{k})\equiv\frac{\rho_2 q_k^{(1)}-\rho_1 q_k^{(2)}}{\rho_2 q_k^{(1)}+\rho_1 q_k^{(2)}} \tag{3.20}$$

$$S_0^{21}(\boldsymbol{k},\boldsymbol{k_0},\omega,\omega_0)=D(\boldsymbol{k})\delta(\boldsymbol{k}-\boldsymbol{k_0})\delta(\omega-\omega_0)\ \text{ with }\ D(\boldsymbol{k})\equiv\frac{2(\rho_1\rho_2 q_k^{(1)}q_k^{(2)})^{1/2}}{\rho_2 q_k^{(1)}+\rho_1 q_k^{(2)}} \tag{3.21}$$

R and D in the above equations denote reflection and transmission coefficients, respectively, associated with the mean (flat) surface. They are related by the relationship,

$R^2 + D^2 = 1$, which implies energy conservation; i.e., the sum of the reflected and the transmitted energy fluxes from the mean surface is equal to the incident energy flux.

First order approximation, $S_1^{N_1 N_2}$, can be obtained by equating the terms of $O(h^1)$ in Eqs. (3.9) and (3.10).

$$\rho_1 \left[(\rho_1 q_0^{(1)})^{-1/2} q_0^{(1)} \, \mathrm{e}^{i(\boldsymbol{k}_0 \cdot \boldsymbol{r} - \omega_0 t)} \, i\omega_0 h(\boldsymbol{r},t) + \int_{\omega} \iint_{\boldsymbol{k}} (\rho_1 q_k^{(1)})^{-1/2} \, \mathrm{e}^{i(\boldsymbol{k}\cdot\boldsymbol{r} - \omega t)} \left(-i\omega h(\boldsymbol{r},t) q_k^{(1)} S_0^{11} + \omega S_1^{11} \right) d\boldsymbol{k} d\omega \right]$$
$$= \rho_2 \int_{\omega} \iint_{\boldsymbol{k}} (\rho_2 q_k^{(2)})^{-1/2} \, \mathrm{e}^{i(\boldsymbol{k}\cdot\boldsymbol{r} - \omega t)} \left(i\omega h(\boldsymbol{r},t) q_k^{(2)} S_0^{21} + \omega S_1^{21} \right) d\boldsymbol{k} d\omega \qquad (3.22)$$

$$(\rho_1 q_0^{(1)})^{-1/2} \, \mathrm{e}^{i(\boldsymbol{k}_0 \cdot \boldsymbol{r} - \omega_0 t)} \left[i \left(q_0^{(1)} \right)^2 h(\boldsymbol{r},t) - \nabla h(\boldsymbol{r},t) \cdot \boldsymbol{k}_0 \right]$$
$$+ \int_{\omega} \iint_{\boldsymbol{k}} (\rho_1 q_k^{(1)})^{-1/2} \, \mathrm{e}^{i(\boldsymbol{k}\cdot\boldsymbol{r} - \omega t)} \left[S_0^{11} \left\{ i \left(q_k^{(1)} \right)^2 h(\boldsymbol{r},t) - \nabla h(\boldsymbol{r},t) \cdot \boldsymbol{k} \right\} - q_k^{(1)} S_1^{11} \right] d\boldsymbol{k} d\omega$$
$$= \int_{\omega} \iint_{\boldsymbol{k}} (\rho_2 q_k^{(2)})^{-1/2} \, \mathrm{e}^{i(\boldsymbol{k}\cdot\boldsymbol{r} - \omega t)} \left[S_0^{21} \left\{ i \left(q_k^{(2)} \right)^2 h(\boldsymbol{r},t) - \nabla h(\boldsymbol{r},t) \cdot \boldsymbol{k} \right\} + q_k^{(2)} S_1^{21} \right] d\boldsymbol{k} d\omega \qquad (3.23)$$

Multiplying $\exp[-i(\boldsymbol{k}' \cdot \boldsymbol{r} - \omega' t)]/(2\pi)^3$ in Eqs. (3.22) and (3.23), integrating with respect to $\boldsymbol{r}$ and t, and using S_0^{11}, S_0^{21} from Eqs. (3.20) and (3.21), it follows that

$$\rho_1 \left[i\omega_0 \left(1 - R(\boldsymbol{k}_0) \right) \left(\frac{q_0^{(1)}}{\rho_1} \right)^{1/2} h(\boldsymbol{k}' - \boldsymbol{k}_0, \omega' - \omega_0) + \omega' (\rho_1 q_{k'}^{(1)})^{-1/2} S_1^{11}(\boldsymbol{k}', \boldsymbol{k}_0, \omega', \omega_0) \right]$$
$$= \rho_2 \left[i\omega_0 D(\boldsymbol{k}_0) \left(\frac{q_0^{(2)}}{\rho_2} \right)^{1/2} h(\boldsymbol{k}' - \boldsymbol{k}_0, \omega' - \omega_0) + \omega' (\rho_2 q_{k'}^{(2)})^{-1/2} S_1^{21}(\boldsymbol{k}', \boldsymbol{k}_0, \omega', \omega_0) \right] \qquad (3.24)$$

$$i \left(1 + R(\boldsymbol{k}_0) \right) (\rho_1 q_0^{(1)})^{-1/2} \left[\left(q_0^{(1)} \right)^2 - (\boldsymbol{k}' - \boldsymbol{k}_0) \cdot \boldsymbol{k}_0 \right] h(\boldsymbol{k}' - \boldsymbol{k}_0, \omega' - \omega_0)$$
$$- (\rho_1 q_{k'}^{(1)})^{-1/2} q_{k'}^{(1)} S_1^{11}(\boldsymbol{k}', \boldsymbol{k}_0, \omega', \omega_0) =$$
$$i D(\boldsymbol{k}_0) (\rho_2 q_0^{(2)})^{-1/2} \left[\left(q_0^{(2)} \right)^2 - (\boldsymbol{k}' - \boldsymbol{k}_0) \cdot \boldsymbol{k}_0 \right] h(\boldsymbol{k}' - \boldsymbol{k}_0, \omega' - \omega_0)$$
$$+ (\rho_2 q_{k'}^{(2)})^{-1/2} q_{k'}^{(2)} S_1^{21}(\boldsymbol{k}', \boldsymbol{k}_0, \omega', \omega_0) \qquad (3.25)$$

where $h(\boldsymbol{k}' - \boldsymbol{k}_0, \omega' - \omega_0) = \dfrac{1}{(2\pi)^3} \iint_{\boldsymbol{r}} \int_{t} h(\boldsymbol{r},t) e^{-i[(\boldsymbol{k}' - \boldsymbol{k}_0)\cdot\boldsymbol{r} - (\omega' - \omega_0)t]} dt d\boldsymbol{r}$ (3.26)

Note that $\nabla h(\boldsymbol{r},t)$ in Eq. (3.23) was replaced by $i(\boldsymbol{k}'-\boldsymbol{k}_0)h(\boldsymbol{r},t)$ to obtain Eq. (3.25). This is justified as below with $\boldsymbol{a}=(a_1,a_2)=\mathrm{e}^{-i(\boldsymbol{k}'-\boldsymbol{k}_0)\cdot\boldsymbol{r}}\,\boldsymbol{k}_0$.

$$\iint \boldsymbol{a}\cdot\nabla h\,d\boldsymbol{r}=\iint\nabla\cdot(h\boldsymbol{a})\,d\boldsymbol{r}-\iint h\nabla\cdot\boldsymbol{a}\,d\boldsymbol{r}$$

$$=\int h(-a_2,a_1)\cdot d\boldsymbol{l}-\iint h\nabla\cdot\boldsymbol{a}\,d\boldsymbol{r} \qquad \text{by Green's theorem}$$

$$=-\iint h\nabla\cdot\boldsymbol{a}\,d\boldsymbol{r} \qquad \text{if } h(\boldsymbol{r})<|\boldsymbol{r}|^{-n}\ (n>1)\ \text{ as } |\boldsymbol{r}|\to\infty \tag{3.27}$$

Solving for S_1^{11} and S_1^{21} in Eqs. (3.24) and (3.25), it is found that

$$S_1^{11}(\boldsymbol{k},\boldsymbol{k}_0,\omega,\omega_0)=A(\boldsymbol{k},\boldsymbol{k}_0,\omega,\omega_0)h(\boldsymbol{k}-\boldsymbol{k}_0,\omega-\omega_0) \tag{3.28}$$

$$S_1^{21}(\boldsymbol{k},\boldsymbol{k}_0,\omega,\omega_0)=B(\boldsymbol{k},\boldsymbol{k}_0,\omega,\omega_0)h(\boldsymbol{k}-\boldsymbol{k}_0,\omega-\omega_0) \tag{3.29}$$

where

$$A(\boldsymbol{k},\boldsymbol{k}_0,\omega,\omega_0)=\frac{2i(q_0^{(1)}q_k^{(1)})^{1/2}\left[\dfrac{\omega_0}{\omega}\rho_1\left(\rho_2-\rho_1\right)q_0^{(2)}q_k^{(2)}+\rho_2\alpha(\boldsymbol{k},\boldsymbol{k}_0,\omega_0)\right]}{\left(\rho_2q_0^{(1)}+\rho_1q_0^{(2)}\right)\left(\rho_2q_k^{(1)}+\rho_1q_k^{(2)}\right)} \tag{3.30}$$

$$B(\boldsymbol{k},\boldsymbol{k}_0,\omega,\omega_0)=\frac{2i\left(\rho_1\rho_2q_0^{(1)}q_k^{(2)}\right)^{1/2}\left[-\dfrac{\omega_0}{\omega}\left(\rho_2-\rho_1\right)q_k^{(1)}q_0^{(2)}+\alpha(\boldsymbol{k},\boldsymbol{k}_0,\omega_0)\right]}{\left(\rho_2q_0^{(1)}+\rho_1q_0^{(2)}\right)\left(\rho_2q_k^{(1)}+\rho_1q_k^{(2)}\right)} \tag{3.31}$$

$$\alpha(\boldsymbol{k},\boldsymbol{k}_0,\omega_0)=\rho_2\left\{\left(\frac{\omega_0}{c_1}\right)^2-\boldsymbol{k}\cdot\boldsymbol{k}_0\right\}-\rho_1\left\{\left(\frac{\omega_0}{c_2}\right)^2-\boldsymbol{k}\cdot\boldsymbol{k}_0\right\} \tag{3.32}$$

Equations (3.28) and (3.29) coincide with the formulae of scattering amplitudes for a stationary surface as those derived by Voronovich[50], except that the above are more general versions allowing for arbitrary surface movement. When the incident wave originates from medium (2), the acoustic fields have the following forms:

In medium (1),

$$\frac{\psi_c^{(1)}}{A_2} = \int_{\omega}\iint_{\boldsymbol{k}} S^{12}(\boldsymbol{k},\boldsymbol{k_0},\omega,\omega_0)(\rho_1 q_k^{(1)})^{-1/2}\, \mathrm{e}^{i(\boldsymbol{k}\cdot\boldsymbol{r}-q_k^{(1)}z-\omega t)}\, d\boldsymbol{k}d\omega \qquad ;\ A_2 = \frac{P_I}{\omega_0}\left(\frac{q_0^{(2)}}{\rho_2}\right)^{1/2} \tag{3.33}$$

In medium (2),

$$\frac{\psi_c^{(2)}}{A_2} = (\rho_2 q_0^{(2)})^{-1/2}\, \mathrm{e}^{i(\boldsymbol{k_0}\cdot\boldsymbol{r}-q_0^{(2)}z-\omega_0 t)} + \int_{\omega}\iint_{\boldsymbol{k}} S^{22}(\boldsymbol{k},\boldsymbol{k_0},\omega,\omega_0)(\rho_2 q_k^{(2)})^{-1/2}\, \mathrm{e}^{i(\boldsymbol{k}\cdot\boldsymbol{r}+q_k^{(2)}z-\omega t)}\, d\boldsymbol{k}d\omega \tag{3.34}$$

Note that the above equations can be obtained from Eqs. (2.18) and (2.20) by exchanging $1 \leftrightarrow 2$ for media and by changing the sign of vertical coordinate, z. This means that S^{22} and S^{12} can be simply evaluated from Eqs. (3.20), (3.21), (3.28), and (3.29) to obtain:

$$S_0^{22}(\boldsymbol{k},\boldsymbol{k_0},\omega,\omega_0) = -R(\boldsymbol{k})\delta(\boldsymbol{k}-\boldsymbol{k_0})\delta(\omega-\omega_0) = -S_0^{11}(\boldsymbol{k},\boldsymbol{k_0},\omega,\omega_0) \tag{3.35}$$

$$S_0^{12}(\boldsymbol{k},\boldsymbol{k_0},\omega,\omega_0) = D(\boldsymbol{k})\delta(\boldsymbol{k}-\boldsymbol{k_0})\delta(\omega-\omega_0) = S_0^{21}(\boldsymbol{k},\boldsymbol{k_0},\omega,\omega_0) \tag{3.36}$$

$$\begin{aligned} S_1^{22}(\boldsymbol{k},\boldsymbol{k_0},\omega,\omega_0) &= A(\boldsymbol{k},\boldsymbol{k_0},\omega,\omega_0)\big|_{1\leftrightarrow 2}(-h)(\boldsymbol{k}-\boldsymbol{k_0},\omega-\omega_0) \\ &= \frac{2i(q_0^{(2)}q_k^{(2)})^{1/2}\left[\frac{\omega_0}{\omega}\rho_2(\rho_2-\rho_1)q_0^{(1)}q_k^{(1)} + \rho_1\alpha(\boldsymbol{k},\boldsymbol{k_0},\omega_0)\right]}{\left(\rho_2 q_0^{(1)} + \rho_1 q_0^{(2)}\right)\left(\rho_2 q_k^{(1)} + \rho_1 q_k^{(2)}\right)} h(\boldsymbol{k}-\boldsymbol{k_0},\omega-\omega_0) \end{aligned} \tag{3.37}$$

where $\alpha(\boldsymbol{k},\boldsymbol{k_0},\omega_0)\big|_{1\leftrightarrow 2} = -\alpha(\boldsymbol{k},\boldsymbol{k_0},\omega_0)$ was used.

$$\begin{aligned} S_1^{12}(\boldsymbol{k},\boldsymbol{k_0},\omega,\omega_0) &= B(\boldsymbol{k},\boldsymbol{k_0},\omega,\omega_0)\big|_{1\leftrightarrow 2}(-h)(\boldsymbol{k}-\boldsymbol{k_0},\omega-\omega_0) \\ &= \frac{2i\left(\rho_1\rho_2 q_k^{(1)}q_0^{(2)}\right)^{1/2}\left[-\frac{\omega_0}{\omega}(\rho_2-\rho_1)q_0^{(1)}q_k^{(2)} + \alpha(\boldsymbol{k},\boldsymbol{k_0},\omega_0)\right]}{\left(\rho_2 q_0^{(1)} + \rho_1 q_0^{(2)}\right)\left(\rho_2 q_k^{(1)} + \rho_1 q_k^{(2)}\right)} h(\boldsymbol{k}-\boldsymbol{k_0},\omega-\omega_0) \end{aligned} \tag{3.38}$$

Second order approximation, $S_2^{N_1N_2}$, can be obtained by collecting the terms of $O(h^2)$ in Eqs. (3.9) and (3.10).

<u>pressure continuity</u>:

$$\rho_1\Bigg[-\frac{1}{2}\omega_0(\rho_1 q_0^{(1)})^{-1/2}\,\mathrm{e}^{i(\boldsymbol{k_0}\cdot\boldsymbol{r}-\omega_0 t)}(q_0^{(1)}h(\boldsymbol{r},t))^2$$
$$+\int_{\omega}\iint_{\boldsymbol{k}}\omega(\rho_1 q_k^{(1)})^{-1/2}\,\mathrm{e}^{i(\boldsymbol{k}\cdot\boldsymbol{r}-\omega t)}\left\{-\frac{1}{2}\left(q_k^{(1)}h(\boldsymbol{r},t)\right)^2 S_0^{11}-iq_k^{(1)}h(\boldsymbol{r},t)S_1^{11}+S_2^{11}\right\}d\boldsymbol{k}d\omega\Bigg]$$
$$=\rho_2\int_{\omega}\iint_{\boldsymbol{k}}\omega(\rho_2 q_k^{(2)})^{-1/2}\,\mathrm{e}^{i(\boldsymbol{k}\cdot\boldsymbol{r}-\omega t)}\left\{-\frac{1}{2}\left(q_k^{(2)}h(\boldsymbol{r},t)\right)^2 S_0^{21}+iq_k^{(2)}h(\boldsymbol{r},t)S_1^{21}+S_2^{21}\right\}d\boldsymbol{k}d\omega \qquad (3.39)$$

<u>normal velocity continuity</u>:

$$(q_0^{(1)}/\rho_1)^{1/2}\,\mathrm{e}^{i(\boldsymbol{k_0}\cdot\boldsymbol{r}-\omega_0 t)}\left[-\frac{1}{2}\left(q_0^{(1)}h(\boldsymbol{r},t)\right)^2-ih(\boldsymbol{r},t)\nabla h(\boldsymbol{r},t)\cdot\boldsymbol{k_0}\right]$$
$$-\int_{\omega}\iint_{\boldsymbol{k}}(q_k^{(1)}/\rho_1)^{1/2}\,\mathrm{e}^{i(\boldsymbol{k}\cdot\boldsymbol{r}-\omega t)}\begin{bmatrix}S_0^{11}\left\{-\frac{1}{2}\left(q_k^{(1)}h(\boldsymbol{r},t)\right)^2-ih(\boldsymbol{r},t)\nabla h(\boldsymbol{r},t)\cdot\boldsymbol{k}\right\}\\+S_1^{11}\left\{-iq_k^{(1)}h(\boldsymbol{r},t)+\frac{\nabla h(\boldsymbol{r},t)\cdot\boldsymbol{k}}{q_k^{(1)}}\right\}+S_2^{11}\end{bmatrix}d\boldsymbol{k}d\omega$$
$$=\int_{\omega}\iint_{\boldsymbol{k}}(q_k^{(2)}/\rho_2)^{1/2}\,\mathrm{e}^{i(\boldsymbol{k}\cdot\boldsymbol{r}-\omega t)}\begin{bmatrix}S_0^{21}\left\{-\frac{1}{2}\left(q_k^{(2)}h(\boldsymbol{r},t)\right)^2-ih(\boldsymbol{r},t)\nabla h(\boldsymbol{r},t)\cdot\boldsymbol{k}\right\}\\+S_1^{21}\left\{iq_k^{(2)}h(\boldsymbol{r},t)-\frac{\nabla h(\boldsymbol{r},t)\cdot\boldsymbol{k}}{q_k^{(2)}}\right\}+S_2^{21}\end{bmatrix}d\boldsymbol{k}d\omega \qquad (3.40)$$

Multiplying $\exp[-i(\boldsymbol{k}'\cdot\boldsymbol{r}-\omega' t)]/(2\pi)^3$ in Eqs. (3.22) and (3.23), integrating with respect to $\boldsymbol{r}$ and t, and using Eqs. (3.20) and (3.21) for S_0^{11} and S_0^{21} yields

$$\rho_1\Bigg[-\frac{1}{(2\pi)^3}\iint_{\boldsymbol{r}}\int_{t}\frac{1}{2}\omega_0\left(1+R(\boldsymbol{k_0})\right)(\rho_1 q_0^{(1)})^{-1/2}\,\mathrm{e}^{-i[(\boldsymbol{k}'-\boldsymbol{k_0})\cdot\boldsymbol{r}-(\omega'-\omega_0)t]}\left(q_0^{(1)}h(\boldsymbol{r},t)\right)^2 dtd\boldsymbol{r}$$
$$+\frac{1}{(2\pi)^3}\iint_{\boldsymbol{r}}\int_{t}\int_{\omega}\iint_{\boldsymbol{k}}\omega(\rho_1 q_k^{(1)})^{-1/2}\,\mathrm{e}^{-i[(\boldsymbol{k}'-\boldsymbol{k})\cdot\boldsymbol{r}-(\omega'-\omega)t]}\left\{-iq_k^{(1)}h(\boldsymbol{r},t)S_1^{11}+S_2^{11}\right\}d\boldsymbol{k}d\omega dtd\boldsymbol{r}\Bigg]$$
$$=\rho_2\Bigg[-\frac{1}{(2\pi)^3}\iint_{\boldsymbol{r}}\int_{t}\frac{1}{2}\omega_0 D(\boldsymbol{k_0})(\rho_2 q_0^{(2)})^{-1/2}\,\mathrm{e}^{-i[(\boldsymbol{k}'-\boldsymbol{k_0})\cdot\boldsymbol{r}-(\omega'-\omega_0)t]}\left(q_0^{(2)}h(\boldsymbol{r},t)\right)^2 dtd\boldsymbol{r}$$
$$+\frac{1}{(2\pi)^3}\iint_{\boldsymbol{r}}\int_{t}\int_{\omega}\iint_{\boldsymbol{k}}\omega(\rho_2 q_k^{(2)})^{-1/2}\,\mathrm{e}^{-i[(\boldsymbol{k}'-\boldsymbol{k})\cdot\boldsymbol{r}-(\omega'-\omega)t]}\left\{iq_k^{(2)}h(\boldsymbol{r},t)S_1^{21}+S_2^{21}\right\}d\boldsymbol{k}d\omega dtd\boldsymbol{r}\Bigg] \qquad (3.41)$$

$$
\begin{aligned}
&-\frac{1}{(2\pi)^3}\iiint_{\boldsymbol{r}\,t}\left(1-R(\boldsymbol{k_0})\right)(\rho_1 q_0^{(1)})^{-1/2}\,q_0^{(1)}\,\mathrm{e}^{-i[(\boldsymbol{k'}-\boldsymbol{k_0})\cdot\boldsymbol{r}-(\omega'-\omega_0)t]}\left[\frac{1}{2}\left(q_0^{(1)}h(\boldsymbol{r},t)\right)^2+\frac{i}{2}\nabla h^2(\boldsymbol{r},t)\cdot\boldsymbol{k_0}\right]dtd\boldsymbol{r}\\
&-\frac{1}{(2\pi)^3}\iiint_{\boldsymbol{r}\,t}\iint_{\omega}\iint_{\boldsymbol{k}}(\rho_1 q_k^{(1)})^{-1/2}\,q_k^{(1)}\,\mathrm{e}^{-i[(\boldsymbol{k'}-\boldsymbol{k})\cdot\boldsymbol{r}-(\omega'-\omega)t]}\left[S_1^{11}\left\{-iq_k^{(1)}h(\boldsymbol{r},t)+\frac{\nabla h(\boldsymbol{r},t)\cdot\boldsymbol{k}}{q_k^{(1)}}\right\}+S_2^{11}\right]d\boldsymbol{k}d\omega dtd\boldsymbol{r}\\
&=-\frac{1}{(2\pi)^3}\iiint_{\boldsymbol{r}\,t}D(\boldsymbol{k_0})(\rho_2 q_0^{(2)})^{-1/2}\,q_0^{(2)}\,\mathrm{e}^{-i[(\boldsymbol{k'}-\boldsymbol{k_0})\cdot\boldsymbol{r}-(\omega'-\omega_0)t]}\left[\frac{1}{2}\left(q_0^{(2)}h(\boldsymbol{r},t)\right)^2+\frac{i}{2}\nabla h^2(\boldsymbol{r},t)\cdot\boldsymbol{k_0}\right]dtd\boldsymbol{r}\\
&+\frac{1}{(2\pi)^3}\iiint_{\boldsymbol{r}\,t}\iint_{\omega}\iint_{\boldsymbol{k}}(\rho_2 q_k^{(2)})^{-1/2}\,q_k^{(2)}\,\mathrm{e}^{-i[(\boldsymbol{k'}-\boldsymbol{k})\cdot\boldsymbol{r}-(\omega'-\omega)t]}\left[S_1^{21}\left\{iq_k^{(2)}h(\boldsymbol{r},t)-\frac{\nabla h(\boldsymbol{r},t)\cdot\boldsymbol{k}}{q_k^{(2)}}\right\}+S_2^{21}\right]d\boldsymbol{k}d\omega dtd\boldsymbol{r}
\end{aligned}
\tag{3.42}
$$

where ∇ in the first and third integral in Eq. (3.42) can be replaced by $i(\boldsymbol{k'}-\boldsymbol{k_0})$ using Eq. (3.27) with $\boldsymbol{a}=\mathrm{e}^{-i(\boldsymbol{k'}-\boldsymbol{k_0})\cdot\boldsymbol{r}}\,\boldsymbol{k_0}$. Similarly ∇ in the second and fourth integral can be replaced by $i(\boldsymbol{k'}-\boldsymbol{k})$ with $\boldsymbol{a}=\mathrm{e}^{-i(\boldsymbol{k'}-\boldsymbol{k})\cdot\boldsymbol{r}}\,\boldsymbol{k}$. Then Eq. (3.42) has the form:

$$
\begin{aligned}
&-\frac{1}{(2\pi)^3}\iiint_{\boldsymbol{r}\,t}\left(1-R(\boldsymbol{k_0})\right)(\rho_1 q_0^{(1)})^{-1/2}\,q_0^{(1)}\,\mathrm{e}^{-i[(\boldsymbol{k'}-\boldsymbol{k_0})\cdot\boldsymbol{r}-(\omega'-\omega_0)t]}\,\frac{h^2(\boldsymbol{r},t)}{2}\left[\left(q_0^{(1)}\right)^2-(\boldsymbol{k'}-\boldsymbol{k_0})\cdot\boldsymbol{k_0}\right]dtd\boldsymbol{r}\\
&+\frac{1}{(2\pi)^3}\iiint_{\boldsymbol{r}\,t}\iint_{\omega}\iint_{\boldsymbol{k}}(\rho_1 q_k^{(1)})^{-1/2}\,q_k^{(1)}\,\mathrm{e}^{-i[(\boldsymbol{k'}-\boldsymbol{k})\cdot\boldsymbol{r}-(\omega'-\omega)t]}\,iS_1^{11}h(\boldsymbol{r},t)\left\{q_k^{(1)}-\frac{(\boldsymbol{k'}-\boldsymbol{k})\cdot\boldsymbol{k}}{q_k^{(1)}}\right\}d\boldsymbol{k}d\omega dtd\boldsymbol{r}\\
&-(\rho_1 q_{k'}^{(1)})^{-1/2}\,q_{k'}^{(1)}S_2^{11}(\boldsymbol{k'},\boldsymbol{k_0},\omega',\omega_0)\\
&=-\frac{1}{(2\pi)^3}\iiint_{\boldsymbol{r}\,t}D(\boldsymbol{k_0})(\rho_2 q_0^{(2)})^{-1/2}\,q_0^{(2)}\,\mathrm{e}^{-i[(\boldsymbol{k'}-\boldsymbol{k_0})\cdot\boldsymbol{r}-(\omega'-\omega_0)t]}\,\frac{h^2(\boldsymbol{r},t)}{2}\left[\left(q_0^{(2)}\right)^2-(\boldsymbol{k'}-\boldsymbol{k_0})\cdot\boldsymbol{k_0}\right]dtd\boldsymbol{r}\\
&+\frac{1}{(2\pi)^3}\iiint_{\boldsymbol{r}\,t}\iint_{\omega}\iint_{\boldsymbol{k}}(\rho_2 q_k^{(2)})^{-1/2}\,q_k^{(2)}\,\mathrm{e}^{-i[(\boldsymbol{k'}-\boldsymbol{k})\cdot\boldsymbol{r}-(\omega'-\omega)t]}\,iS_1^{21}h(\boldsymbol{r},t)\left\{q_k^{(2)}-\frac{(\boldsymbol{k'}-\boldsymbol{k})\cdot\boldsymbol{k}}{q_k^{(2)}}\right\}d\boldsymbol{k}d\omega dtd\boldsymbol{r}\\
&+(\rho_2 q_{k'}^{(2)})^{-1/2}\,q_{k'}^{(2)}S_2^{21}(\boldsymbol{k'},\boldsymbol{k_0},\omega',\omega_0)
\end{aligned}
\tag{3.43}
$$

The terms including $h^2(\boldsymbol{r},t)$ can be rewritten in terms of the spectrum of surface height, $h(\boldsymbol{k},\omega)$, using

$$
h(\boldsymbol{r},t)=\iint_{\boldsymbol{k}}\int_{\omega}h(\boldsymbol{k},\omega)\,\mathrm{e}^{i(\boldsymbol{k}\cdot\boldsymbol{r}-\omega t)}\,d\omega d\boldsymbol{k} \tag{3.44}
$$

Hence

$$\iint_{\boldsymbol{r}}\int_{t} h^2(\boldsymbol{r},t)\,\mathrm{e}^{-i[(\boldsymbol{k}'-\boldsymbol{k}_0)\cdot\boldsymbol{r}-(\omega'-\omega_0)t]}\,dt d\boldsymbol{r}$$

$$= \iint_{\boldsymbol{r}}\int_{t}\left(\iint_{\boldsymbol{k}_1}\int_{\omega_1} h(\boldsymbol{k}_1,\omega_1)\,\mathrm{e}^{i(\boldsymbol{k}_1\cdot\boldsymbol{r}-\omega_1 t)}\,d\omega_1 d\boldsymbol{k}_1\right)\left(\iint_{\boldsymbol{k}_2}\int_{\omega_2} h(\boldsymbol{k}_2,\omega_2)\,\mathrm{e}^{i(\boldsymbol{k}_2\cdot\boldsymbol{r}-\omega_2 t)}\,d\omega_2 d\boldsymbol{k}_2\right)\mathrm{e}^{-i[(\boldsymbol{k}'-\boldsymbol{k}_0)\cdot\boldsymbol{r}-(\omega'-\omega_0)t]}\,dt d\boldsymbol{r}$$

$$= (2\pi)^3\iint_{\boldsymbol{k}_1}\int_{\omega_1}\iint_{\boldsymbol{k}_2}\int_{\omega_2} h(\boldsymbol{k}_1,\omega_1)h(\boldsymbol{k}_2,\omega_2)\delta(\boldsymbol{k}_1+\boldsymbol{k}_2-\boldsymbol{k}'+\boldsymbol{k}_0)\delta(\omega_1+\omega_2-\omega'+\omega_0)\,d\omega_2 d\boldsymbol{k}_2 d\omega_1 d\boldsymbol{k}_1$$

$$= (2\pi)^3\iint_{\boldsymbol{k}_1}\int_{\omega_1} h(\boldsymbol{k}'-\boldsymbol{k}_0-\boldsymbol{k}_1,\omega'-\omega_0-\omega_1)h(\boldsymbol{k}_1,\omega_1)\,d\omega_1 d\boldsymbol{k}_1$$

$$= (2\pi)^3\iint_{\boldsymbol{k}}\int_{\omega} h(\boldsymbol{k}'-\boldsymbol{k},\omega'-\omega)h(\boldsymbol{k}-\boldsymbol{k}_0,\omega-\omega_0)\,d\omega d\boldsymbol{k} \quad (\text{by } \boldsymbol{k}=\boldsymbol{k}_0+\boldsymbol{k}_1,\ \omega=\omega_0+\omega_1)$$

$$= (2\pi)^3 h*h(\boldsymbol{k}'-\boldsymbol{k}_0,\omega'-\omega_0) \tag{3.45}$$

where $h*h$ denotes a convolution integral defined in the wave number / frequency domain.

$$h*h(\boldsymbol{k},\omega)\equiv\iint_{\boldsymbol{k}_1}\int_{\omega_1} h(\boldsymbol{k}-\boldsymbol{k}_1,\omega-\omega_1)h(\boldsymbol{k}_1,\omega_1)\,d\omega_1 d\boldsymbol{k}_1 \tag{3.46}$$

Eq. (3.41) can be written as (using Eqs. (3.45), (3.19), and (3.26))

$$\rho_1\Bigg[-\frac{1}{2}\omega_0\left(1+R(\boldsymbol{k}_0)\right)(\rho_1 q_0^{(1)})^{-1/2}\left(q_0^{(1)}\right)^2 h*h(\boldsymbol{k}'-\boldsymbol{k}_0,\omega'-\omega_0)$$

$$-i\int_{\omega}\iint_{\boldsymbol{k}}\omega(\rho_1 q_k^{(1)})^{-1/2}q_k^{(1)}h(\boldsymbol{k}'-\boldsymbol{k},\omega'-\omega)S_1^{11}(\boldsymbol{k},\boldsymbol{k}_0,\omega,\omega_0)\,d\boldsymbol{k}d\omega+\omega'(\rho_1 q_{k'}^{(1)})^{-1/2}S_2^{11}(\boldsymbol{k}',\boldsymbol{k}_0,\omega',\omega_0)\Bigg]$$

$$=\rho_2\Bigg[-\frac{1}{2}\omega_0 D(\boldsymbol{k}_0)(\rho_2 q_0^{(2)})^{-1/2}\left(q_0^{(2)}\right)^2 h*h(\boldsymbol{k}'-\boldsymbol{k}_0,\omega'-\omega_0)$$

$$+i\int_{\omega}\iint_{\boldsymbol{k}}\omega(\rho_2 q_k^{(2)})^{-1/2}q_k^{(2)}h(\boldsymbol{k}'-\boldsymbol{k},\omega'-\omega)S_1^{21}(\boldsymbol{k},\boldsymbol{k}_0,\omega,\omega_0)\,d\boldsymbol{k}d\omega+\omega'(\rho_2 q_{k'}^{(2)})^{-1/2}S_2^{21}(\boldsymbol{k}',\boldsymbol{k}_0,\omega',\omega_0)\Bigg] \tag{3.47}$$

Similarly, Eq. (3.43) can be written as (using (3.45) and (3.26))

$$-\frac{1}{2}\left(1-R(\boldsymbol{k}_0)\right)(\rho_1 q_0^{(1)})^{-1/2}q_0^{(1)}\left[\left(q_0^{(1)}\right)^2-(\boldsymbol{k}'-\boldsymbol{k}_0)\cdot\boldsymbol{k}_0\right]h*h(\boldsymbol{k}'-\boldsymbol{k}_0,\omega'-\omega_0)$$

$$+i\int_{\omega}\iint_{\boldsymbol{k}}(\rho_1 q_k^{(1)})^{-1/2}q_k^{(1)}\left\{q_k^{(1)}-\frac{(\boldsymbol{k}'-\boldsymbol{k})\cdot\boldsymbol{k}}{q_k^{(1)}}\right\}S_1^{11}(\boldsymbol{k},\boldsymbol{k}_0,\omega,\omega_0)h(\boldsymbol{k}'-\boldsymbol{k},\omega'-\omega)\,d\boldsymbol{k}d\omega$$

$$-(\rho_1 q_{k'}^{(1)})^{-1/2}q_{k'}^{(1)}S_2^{11}(\boldsymbol{k}',\boldsymbol{k}_0,\omega',\omega_0)$$

$$= -\frac{1}{2} D(\boldsymbol{k_0})(\rho_2 q_0^{(2)})^{-1/2} q_0^{(2)} \left[\left(q_0^{(2)} \right)^2 - (\boldsymbol{k}' - \boldsymbol{k_0}) \cdot \boldsymbol{k_0} \right] h * h(\boldsymbol{k}' - \boldsymbol{k_0}, \omega' - \omega_0)$$
$$+ i \int_{\omega} \iint_{\boldsymbol{k}} (\rho_2 q_k^{(2)})^{-1/2} q_k^{(2)} \left\{ q_k^{(2)} - \frac{(\boldsymbol{k}' - \boldsymbol{k}) \cdot \boldsymbol{k}}{q_k^{(2)}} \right\} S_1^{21}(\boldsymbol{k}, \boldsymbol{k_0}, \omega, \omega_0) h(\boldsymbol{k}' - \boldsymbol{k}, \omega' - \omega) d\boldsymbol{k} d\omega$$
$$+ (\rho_2 q_{k'}^{(2)})^{-1/2} q_{k'}^{(2)} S_2^{21}(\boldsymbol{k}', \boldsymbol{k_0}, \omega', \omega_0) \tag{3.48}$$

Eqs. (3.47) and (3.48) can be rearranged in the following forms using Eqs. (3.28) and (3.29).

$$(\rho_1 / q_{k'}^{(1)})^{1/2} S_2^{11}(\boldsymbol{k}', \boldsymbol{k_0}, \omega', \omega_0) - (\rho_2 / q_{k'}^{(2)})^{1/2} S_2^{21}(\boldsymbol{k}', \boldsymbol{k_0}, \omega', \omega_0)$$
$$= \int_{\omega} \iint_{\boldsymbol{k}} A_2(\boldsymbol{k}, \boldsymbol{k_0}, \omega, \omega_0, \omega') h(\boldsymbol{k}' - \boldsymbol{k}, \omega' - \omega) h(\boldsymbol{k} - \boldsymbol{k_0}, \omega - \omega_0) d\boldsymbol{k} d\omega \tag{3.49}$$

$$(q_{k'}^{(1)} / \rho_1)^{1/2} S_2^{11}(\boldsymbol{k}', \boldsymbol{k_0}, \omega', \omega_0) + (q_{k'}^{(2)} / \rho_2)^{1/2} S_2^{21}(\boldsymbol{k}', \boldsymbol{k_0}, \omega', \omega_0)$$
$$= \int_{\omega} \iint_{\boldsymbol{k}} B_2(\boldsymbol{k}, \boldsymbol{k_0}, \boldsymbol{k}', \omega, \omega_0) h(\boldsymbol{k}' - \boldsymbol{k}, \omega' - \omega) h(\boldsymbol{k} - \boldsymbol{k_0}, \omega - \omega_0) d\boldsymbol{k} d\omega \tag{3.50}$$

where

$$A_2(\boldsymbol{k}, \boldsymbol{k_0}, \omega, \omega_0, \omega')$$
$$= \frac{\omega_0}{2\omega'} \left[\left(1 + R(\boldsymbol{k_0}) \right) (\rho_1 q_0^{(1)})^{1/2} q_0^{(1)} - D(\boldsymbol{k_0}) (\rho_2 q_0^{(2)})^{1/2} q_0^{(2)} \right] \tag{3.51}$$
$$+ i \frac{\omega}{\omega'} \left[(\rho_1 q_k^{(1)})^{1/2} A(\boldsymbol{k}, \boldsymbol{k_0}, \omega, \omega_0) + (\rho_2 q_k^{(2)})^{1/2} B(\boldsymbol{k}, \boldsymbol{k_0}, \omega, \omega_0) \right]$$

$$B_2(\boldsymbol{k}, \boldsymbol{k_0}, \boldsymbol{k}', \omega, \omega_0)$$
$$= -\frac{1}{2} \left(1 - R(\boldsymbol{k_0}) \right) (q_0^{(1)} / \rho_1)^{1/2} \left[\left(q_0^{(1)} \right)^2 - (\boldsymbol{k}' - \boldsymbol{k_0}) \cdot \boldsymbol{k_0} \right]$$
$$+ \frac{1}{2} D(\boldsymbol{k_0}) (q_0^{(2)} / \rho_2)^{1/2} \left[\left(q_0^{(2)} \right)^2 - (\boldsymbol{k}' - \boldsymbol{k_0}) \cdot \boldsymbol{k_0} \right] \tag{3.52}$$
$$+ i (\rho_1 q_k^{(1)})^{-1/2} \left\{ \left(q_k^{(1)} \right)^2 - (\boldsymbol{k}' - \boldsymbol{k}) \cdot \boldsymbol{k} \right\} A(\boldsymbol{k}, \boldsymbol{k_0}, \omega, \omega_0)$$
$$- i (\rho_2 q_k^{(2)})^{-1/2} \left\{ \left(q_k^{(2)} \right)^2 - (\boldsymbol{k}' - \boldsymbol{k}) \cdot \boldsymbol{k} \right\} B(\boldsymbol{k}, \boldsymbol{k_0}, \omega, \omega_0)$$

The second equality in Eq. (3.51) is obtained by replacing $R(\boldsymbol{k_0})$ and $D(\boldsymbol{k_0})$ with those in Eqs. (3.20) and (3.21).

$$\left(1+R(\boldsymbol{k_0})\right)(\rho_1 q_0^{(1)})^{1/2} q_0^{(1)} - D(\boldsymbol{k_0})(\rho_2 q_0^{(2)})^{1/2} q_0^{(2)}$$
$$= \frac{2(\rho_1 q_0^{(1)})^{1/2}\rho_2}{\rho_2 q_0^{(1)} + \rho_1 q_0^{(2)}}\left[\left(q_0^{(1)}\right)^2 - \left(q_0^{(2)}\right)^2\right] = \frac{2(\rho_1 q_0^{(1)})^{1/2}\rho_2}{\rho_2 q_0^{(1)} + \rho_1 q_0^{(2)}}\left[\left(\frac{\omega_0}{c_1}\right)^2 - \left(\frac{\omega_0}{c_2}\right)^2\right] \tag{3.53}$$

The second equality in Eq. (3.52) is obtained by using $R(\boldsymbol{k_0})$ and $D(\boldsymbol{k_0})$ in Eqs. (3.20) and (3.21) together with $q_k^{(m)} = [(\omega/c_m)^2 - k^2]^{1/2}$, $q_0^{(m)} = [(\omega_0/c_m)^2 - k_0^2]^{1/2}$ (m =1,2) in Eqs. (2.18) and (2.20). Solving for S_2^{11} and S_2^{21} in Eqs. (3.49) and (3.50) and changing $\boldsymbol{k}' \to \boldsymbol{k}$ and $\omega' \to \omega$ yields:

$$\begin{Bmatrix} S_2^{11}(\boldsymbol{k},\boldsymbol{k_0},\omega,\omega_0) \\ S_2^{21}(\boldsymbol{k},\boldsymbol{k_0},\omega,\omega_0) \end{Bmatrix} = \frac{\left(\rho_1\rho_2 q_k^{(1)} q_k^{(2)}\right)^{1/2}}{\rho_1 q_k^{(2)} + \rho_2 q_k^{(1)}} \begin{bmatrix} (q_k^{(2)}/\rho_2)^{1/2} & (\rho_2/q_k^{(2)})^{1/2} \\ -(q_k^{(1)}/\rho_1)^{1/2} & (\rho_1/q_k^{(1)})^{1/2} \end{bmatrix}$$

$$\times \begin{Bmatrix} \int_{\omega'}\iint_{\boldsymbol{k}'} A_2(\boldsymbol{k}',\boldsymbol{k_0},\omega',\omega_0,\omega)h(\boldsymbol{k}-\boldsymbol{k}',\omega-\omega')h(\boldsymbol{k}'-\boldsymbol{k_0},\omega'-\omega_0)d\boldsymbol{k}'d\omega' \\ \int_{\omega'}\iint_{\boldsymbol{k}'} B_2(\boldsymbol{k}',\boldsymbol{k_0},\boldsymbol{k},\omega',\omega_0)h(\boldsymbol{k}-\boldsymbol{k}',\omega-\omega')h(\boldsymbol{k}'-\boldsymbol{k_0},\omega'-\omega_0)d\boldsymbol{k}'d\omega' \end{Bmatrix} \tag{3.54}$$

$$= \frac{\left(\rho_1\rho_2 q_k^{(1)} q_k^{(2)}\right)^{1/2}}{\rho_1 q_k^{(2)} + \rho_2 q_k^{(1)}} \begin{Bmatrix} \int_{\omega'}\iint_{\boldsymbol{k}'} F(\boldsymbol{k}',\boldsymbol{k_0},\boldsymbol{k},\omega',\omega_0,\omega)h(\boldsymbol{k}-\boldsymbol{k}',\omega-\omega')h(\boldsymbol{k}'-\boldsymbol{k_0},\omega'-\omega_0)d\boldsymbol{k}'d\omega' \\ \int_{\omega'}\iint_{\boldsymbol{k}'} G(\boldsymbol{k}',\boldsymbol{k_0},\boldsymbol{k},\omega',\omega_0,\omega)h(\boldsymbol{k}-\boldsymbol{k}',\omega-\omega')h(\boldsymbol{k}'-\boldsymbol{k_0},\omega'-\omega_0)d\boldsymbol{k}'d\omega' \end{Bmatrix}$$

where

$$F(\boldsymbol{k}',\boldsymbol{k_0},\boldsymbol{k},\omega',\omega_0,\omega) = (q_k^{(2)}/\rho_2)^{1/2} A_2(\boldsymbol{k}',\boldsymbol{k_0},\omega',\omega_0,\omega) + (\rho_2/q_k^{(2)})^{1/2} B_2(\boldsymbol{k}',\boldsymbol{k_0},\boldsymbol{k},\omega',\omega_0) \tag{3.55}$$

$$G(\boldsymbol{k}',\boldsymbol{k_0},\boldsymbol{k},\omega',\omega_0,\omega) = -(q_k^{(1)}/\rho_1)^{1/2} A_2(\boldsymbol{k}',\boldsymbol{k_0},\omega',\omega_0,\omega) + (\rho_1/q_k^{(1)})^{1/2} B_2(\boldsymbol{k}',\boldsymbol{k_0},\boldsymbol{k},\omega',\omega_0) \tag{3.56}$$

Substituting R, D, A, and B from Eqs. (3.20), (3.21), (3.30), and (3.31), respectively, into A_2 and B_2 in Eqs. (3.51) and (3.52) and changing arguments of A_2 and B_2 yields:

$$A_2(\boldsymbol{k}',\boldsymbol{k}_0,\omega',\omega_0,\omega)=\frac{\omega_0}{\omega}\frac{(\rho_1 q_0^{(1)})^{1/2}\rho_2}{\rho_2 q_0^{(1)}+\rho_1 q_0^{(2)}}\left[\left(\frac{\omega_0}{c_1}\right)^2-\left(\frac{\omega_0}{c_2}\right)^2\right]$$
$$+\frac{2\left(\rho_1 q_0^{(1)}\right)^{1/2}\left(\frac{\omega'}{\omega}\right)\left[\frac{\omega_0}{\omega'}\left(\rho_2-\rho_1\right)^2 q_0^{(2)}q_{k'}^{(1)}q_{k'}^{(2)}-\rho_2\left(q_{k'}^{(1)}+q_{k'}^{(2)}\right)\alpha(\boldsymbol{k}',\boldsymbol{k}_0,\omega_0)\right]}{\left(\rho_2 q_0^{(1)}+\rho_1 q_0^{(2)}\right)\left(\rho_2 q_{k'}^{(1)}+\rho_1 q_{k'}^{(2)}\right)} \tag{3.57}$$

$$B_2(\boldsymbol{k}',\boldsymbol{k}_0,\boldsymbol{k},\omega',\omega_0)=-\frac{(\rho_1 q_0^{(1)})^{1/2}q_0^{(2)}}{\rho_2 q_0^{(1)}+\rho_1 q_0^{(2)}}\left[\left(\frac{\omega_0}{c_1}\right)^2-\left(\frac{\omega_0}{c_2}\right)^2\right]-\frac{2\left(\frac{q_0^{(1)}}{\rho_1}\right)^{1/2}\alpha(\boldsymbol{k}',\boldsymbol{k}_0,\omega_0)\alpha(\boldsymbol{k}',\boldsymbol{k},\omega')}{\left(\rho_2 q_0^{(1)}+\rho_1 q_0^{(2)}\right)\left(\rho_2 q_{k'}^{(1)}+\rho_1 q_{k'}^{(2)}\right)}$$
$$-\frac{2\left(\rho_2-\rho_1\right)q_0^{(2)}\left(\rho_1 q_0^{(1)}\right)^{1/2}\left(\frac{\omega_0}{\omega'}\right)\left[q_{k'}^{(1)}\left\{\left(\frac{\omega'}{c_2}\right)^2-\boldsymbol{k}'\cdot\boldsymbol{k}\right\}+q_{k'}^{(2)}\left\{\left(\frac{\omega'}{c_1}\right)^2-\boldsymbol{k}'\cdot\boldsymbol{k}\right\}\right]}{\left(\rho_2 q_0^{(1)}+\rho_1 q_0^{(2)}\right)\left(\rho_2 q_{k'}^{(1)}+\rho_1 q_{k'}^{(2)}\right)} \tag{3.58}$$

Substituting Eqs. (3.57) and (3.58) into Eqs. (3.55) and (3.56) yields the final form of F and G.

$$F(\boldsymbol{k}',\boldsymbol{k}_0,\boldsymbol{k},\omega',\omega_0,\omega)$$
$$=\frac{(\rho_1\rho_2 q_0^{(1)}q_k^{(2)})^{1/2}}{\rho_2 q_0^{(1)}+\rho_1 q_0^{(2)}}\left(\frac{\omega_0}{\omega}-\frac{q_0^{(2)}}{q_k^{(2)}}\right)\left[\left(\frac{\omega_0}{c_1}\right)^2-\left(\frac{\omega_0}{c_2}\right)^2\right]+\frac{2\left(q_0^{(1)}\right)^{1/2}}{\left(\rho_2 q_0^{(1)}+\rho_1 q_0^{(2)}\right)\left(\rho_2 q_{k'}^{(1)}+\rho_1 q_{k'}^{(2)}\right)}\times$$
$$\left[\left(\frac{\omega'}{\omega}\right)\left(\frac{\rho_1 q_k^{(2)}}{\rho_2}\right)^{1/2}\left\{\frac{\omega_0}{\omega'}\left(\rho_2-\rho_1\right)^2 q_0^{(2)}q_{k'}^{(1)}q_{k'}^{(2)}-\rho_2\left(q_{k'}^{(1)}+q_{k'}^{(2)}\right)\alpha(\boldsymbol{k}',\boldsymbol{k}_0,\omega_0)\right\}\right.$$
$$-\left(\rho_2-\rho_1\right)q_0^{(2)}\left(\frac{\omega_0}{\omega'}\right)\left(\frac{\rho_1\rho_2}{q_k^{(2)}}\right)^{1/2}\left(q_{k'}^{(1)}\left\{\left(\frac{\omega'}{c_2}\right)^2-\boldsymbol{k}'\cdot\boldsymbol{k}\right\}+q_{k'}^{(2)}\left\{\left(\frac{\omega'}{c_1}\right)^2-\boldsymbol{k}'\cdot\boldsymbol{k}\right\}\right) \tag{3.59}$$
$$\left.-\left(\frac{\rho_2}{\rho_1 q_k^{(2)}}\right)^{1/2}\alpha(\boldsymbol{k}',\boldsymbol{k}_0,\omega_0)\alpha(\boldsymbol{k}',\boldsymbol{k},\omega')\right]$$

$$G(\boldsymbol{k}',\boldsymbol{k}_0,\boldsymbol{k},\omega',\omega_0,\omega)$$
$$=-\frac{\rho_2\left(q_0^{(1)}q_k^{(1)}\right)^{1/2}}{\rho_2 q_0^{(1)}+\rho_1 q_0^{(2)}}\left(\frac{\omega_0}{\omega}+\frac{\rho_1 q_0^{(2)}}{\rho_2 q_k^{(1)}}\right)\left[\left(\frac{\omega_0}{c_1}\right)^2-\left(\frac{\omega_0}{c_2}\right)^2\right]-\frac{2\left(q_0^{(1)}q_k^{(1)}\right)^{1/2}}{\left(\rho_2 q_0^{(1)}+\rho_1 q_0^{(2)}\right)\left(\rho_2 q_{k'}^{(1)}+\rho_1 q_{k'}^{(2)}\right)}\times$$

$$\left[\left(\frac{\omega'}{\omega}\right)\left\{\frac{\omega_0}{\omega'}\left(\rho_2-\rho_1\right)^2 q_0^{(2)} q_{k'}^{(1)} q_{k'}^{(2)} - \rho_2\left(q_{k'}^{(1)}+q_{k'}^{(2)}\right)\alpha(\boldsymbol{k}',\boldsymbol{k_0},\omega_0)\right\}\right.$$
$$+\rho_1\left(\rho_2-\rho_1\right)\frac{q_0^{(2)}}{q_k^{(1)}}\left(\frac{\omega_0}{\omega'}\right)\left(q_{k'}^{(1)}\left\{\left(\frac{\omega'}{c_2}\right)^2-\boldsymbol{k}'\cdot\boldsymbol{k}\right\}+q_{k'}^{(2)}\left\{\left(\frac{\omega'}{c_1}\right)^2-\boldsymbol{k}'\cdot\boldsymbol{k}\right\}\right) \tag{3.60}$$
$$\left.+\frac{1}{q_k^{(1)}}\alpha(\boldsymbol{k}',\boldsymbol{k_0},\omega_0)\alpha(\boldsymbol{k}',\boldsymbol{k},\omega')\right]$$

where α is defined in Eq. (3.32).

In the case where the incident waves originate from medium (2), S_2^{22} and S_2^{12} (the reflected and the transmitted scattering amplitude, respectively) can be obtained by exchanging $1 \leftrightarrow 2$ with an opposite sign of *h* as follows.

$$\begin{Bmatrix} S_2^{22}(\boldsymbol{k},\boldsymbol{k_0},\omega,\omega_0) \\ S_2^{12}(\boldsymbol{k},\boldsymbol{k_0},\omega,\omega_0) \end{Bmatrix} = \begin{Bmatrix} S_2^{11}(\boldsymbol{k},\boldsymbol{k_0},\omega,\omega_0) \\ S_2^{21}(\boldsymbol{k},\boldsymbol{k_0},\omega,\omega_0) \end{Bmatrix}_{\substack{1\leftrightarrow 2 \\ h\to(-)h}} \tag{3.61}$$

$$= \frac{\left(\rho_1\rho_2 q_k^{(1)} q_k^{(2)}\right)^{1/2}}{\rho_1 q_k^{(2)} + \rho_2 q_k^{(1)}} \begin{Bmatrix} \int_{\omega'}\iint_{\boldsymbol{k}'} F(\boldsymbol{k}',\boldsymbol{k_0},\boldsymbol{k},\omega',\omega_0,\omega)\big|_{1\leftrightarrow 2}\, h(\boldsymbol{k}-\boldsymbol{k}',\omega-\omega')h(\boldsymbol{k}'-\boldsymbol{k_0},\omega'-\omega_0)d\boldsymbol{k}'d\omega' \\ \int_{\omega'}\iint_{\boldsymbol{k}'} G(\boldsymbol{k}',\boldsymbol{k_0},\boldsymbol{k},\omega',\omega_0,\omega)\big|_{1\leftrightarrow 2}\, h(\boldsymbol{k}-\boldsymbol{k}',\omega-\omega')h(\boldsymbol{k}'-\boldsymbol{k_0},\omega'-\omega_0)d\boldsymbol{k}'d\omega' \end{Bmatrix}$$

where

$$F(\boldsymbol{k}',\boldsymbol{k_0},\boldsymbol{k},\omega',\omega_0,\omega)\big|_{1\leftrightarrow 2}$$
$$= -\frac{(\rho_1\rho_2 q_0^{(2)} q_k^{(1)})^{1/2}}{\rho_2 q_0^{(1)} + \rho_1 q_0^{(2)}}\left(\frac{\omega_0}{\omega}-\frac{q_0^{(1)}}{q_k^{(1)}}\right)\left[\left(\frac{\omega_0}{c_1}\right)^2-\left(\frac{\omega_0}{c_2}\right)^2\right]+\frac{2\left(q_0^{(2)}\right)^{1/2}}{\left(\rho_2 q_0^{(1)}+\rho_1 q_0^{(2)}\right)\left(\rho_2 q_{k'}^{(1)}+\rho_1 q_{k'}^{(2)}\right)}\times$$
$$\left[\left(\frac{\omega'}{\omega}\right)\left(\frac{\rho_2 q_k^{(1)}}{\rho_1}\right)^{1/2}\left\{\frac{\omega_0}{\omega'}\left(\rho_2-\rho_1\right)^2 q_0^{(1)} q_{k'}^{(1)} q_{k'}^{(2)} + \rho_1\left(q_{k'}^{(1)}+q_{k'}^{(2)}\right)\alpha(\boldsymbol{k}',\boldsymbol{k_0},\omega_0)\right\}\right.$$
$$+\left(\rho_2-\rho_1\right)q_0^{(1)}\left(\frac{\omega_0}{\omega'}\right)\left(\frac{\rho_1\rho_2}{q_k^{(1)}}\right)^{1/2}\left(q_{k'}^{(1)}\left\{\left(\frac{\omega'}{c_2}\right)^2-\boldsymbol{k}'\cdot\boldsymbol{k}\right\}+q_{k'}^{(2)}\left\{\left(\frac{\omega'}{c_1}\right)^2-\boldsymbol{k}'\cdot\boldsymbol{k}\right\}\right) \tag{3.62}$$
$$\left.-\left(\frac{\rho_1}{\rho_2 q_k^{(1)}}\right)^{1/2}\alpha(\boldsymbol{k}',\boldsymbol{k_0},\omega_0)\alpha(\boldsymbol{k}',\boldsymbol{k},\omega')\right]$$

$$
\begin{aligned}
&G(\boldsymbol{k}',\boldsymbol{k}_0,\boldsymbol{k},\omega',\omega_0,\omega)\big|_{1\leftrightarrow 2} \\
&= \frac{\rho_1\left(q_0^{(2)}q_k^{(2)}\right)^{1/2}}{\rho_2 q_0^{(1)}+\rho_1 q_0^{(2)}}\left(\frac{\omega_0}{\omega}+\frac{\rho_2 q_0^{(1)}}{\rho_1 q_k^{(2)}}\right)\left[\left(\frac{\omega_0}{c_1}\right)^2-\left(\frac{\omega_0}{c_2}\right)^2\right]-\frac{2\left(q_0^{(2)}q_k^{(2)}\right)^{1/2}}{\left(\rho_2 q_0^{(1)}+\rho_1 q_0^{(2)}\right)\left(\rho_2 q_{k'}^{(1)}+\rho_1 q_{k'}^{(2)}\right)}\times \\
&\left[\left(\frac{\omega'}{\omega}\right)\left\{\frac{\omega_0}{\omega'}\left(\rho_2-\rho_1\right)^2 q_0^{(1)}q_{k'}^{(1)}q_{k'}^{(2)}+\rho_1\left(q_{k'}^{(1)}+q_{k'}^{(2)}\right)\alpha(\boldsymbol{k}',\boldsymbol{k}_0,\omega_0)\right\}\right. \\
&-\rho_2\left(\rho_2-\rho_1\right)\frac{q_0^{(1)}}{q_k^{(2)}}\left(\frac{\omega_0}{\omega'}\right)\left(q_{k'}^{(1)}\left\{\left(\frac{\omega'}{c_2}\right)^2-\boldsymbol{k}'\cdot\boldsymbol{k}\right\}+q_{k'}^{(2)}\left\{\left(\frac{\omega'}{c_1}\right)^2-\boldsymbol{k}'\cdot\boldsymbol{k}\right\}\right) \\
&\left.+\frac{1}{q_k^{(2)}}\alpha(\boldsymbol{k}',\boldsymbol{k}_0,\omega_0)\alpha(\boldsymbol{k}',\boldsymbol{k},\omega')\right]
\end{aligned}
\tag{3.63}
$$

3.2 Reciprocity theorem

Scattering amplitudes for reflected/transmitted waves are known to observe the reciprocity theorem with respect to wave number vector $\boldsymbol{k}$ for a fixed frequency ω_0, which has the following form. [50]

$$
S^{N_1N_2}(\boldsymbol{k},\boldsymbol{k}_0;\omega_0)=S^{N_2N_1}(-\boldsymbol{k}_0,-\boldsymbol{k};\omega_0) \qquad \{N_1,N_2\}=\{1,2\} \tag{3.64}
$$

which is illustrated in Figure 5.

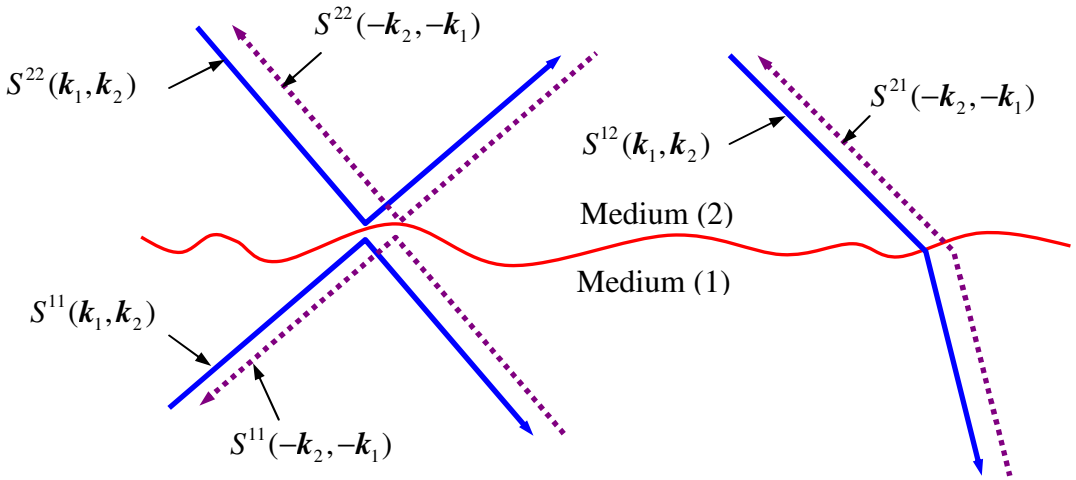

Figure 5 The schematics of reciprocity theorem

Reciprocity for zeroth-order scattering amplitude is confirmed trivially by Eqs. (3.20), (3.21), (3.35) and (3.36). Reciprocity for first-order scattering amplitude follows from Eqs. (3.28), (3.29) and (3.38).

For $N_1 = N_2 = 1$,

$$\begin{aligned} &S_1^{11}(-\boldsymbol{k}_0, -\boldsymbol{k}, \omega, \omega_0) = A(-\boldsymbol{k}_0, -\boldsymbol{k}, \omega, \omega_0) h(\boldsymbol{k} - \boldsymbol{k}_0, \omega - \omega_0) \\ &= A(\boldsymbol{k}, \boldsymbol{k}_0, \omega, \omega_0) h(\boldsymbol{k} - \boldsymbol{k}_0, \omega - \omega_0) = S_1^{11}(\boldsymbol{k}, \boldsymbol{k}_0, \omega, \omega_0) \end{aligned} \tag{3.65}$$

For $N_1 = 2$, $N_2 = 1$,

$$\begin{aligned} &S_1^{12}(-\boldsymbol{k}_0, -\boldsymbol{k}, \omega, \omega_0) = B(-\boldsymbol{k}_0, -\boldsymbol{k}, \omega, \omega_0)\big|_{1 \leftrightarrow 2} (-h)(\boldsymbol{k} - \boldsymbol{k}_0, \omega - \omega_0) \\ &= B(\boldsymbol{k}, \boldsymbol{k}_0, \omega, \omega_0) h(\boldsymbol{k} - \boldsymbol{k}_0, \omega - \omega_0) = S_1^{21}(\boldsymbol{k}, \boldsymbol{k}_0, \omega, \omega_0) \end{aligned} \tag{3.66}$$

where $B(-\boldsymbol{k}_0, -\boldsymbol{k}, \omega, \omega_0)\big|_{1 \leftrightarrow 2} = -B(\boldsymbol{k}, \boldsymbol{k}_0, \omega, \omega_0)$ is used. (3.67)

Reciprocity for 2nd order of SA has the following forms from Eq. (3.64).

$$S_2^{11}(\boldsymbol{k}, \boldsymbol{k}_0; \omega_0) = S_2^{11}(-\boldsymbol{k}_0, -\boldsymbol{k}; \omega_0) \tag{3.68}$$

$$S_2^{22}(\boldsymbol{k}, \boldsymbol{k}_0; \omega_0) = S_2^{22}(-\boldsymbol{k}_0, -\boldsymbol{k}; \omega_0) \tag{3.69}$$

$$S_2^{21}(\boldsymbol{k}, \boldsymbol{k}_0; \omega_0) = S_2^{12}(-\boldsymbol{k}_0, -\boldsymbol{k}; \omega_0) \tag{3.70}$$

To verify Eq. (3.68) first, recall from Eq. (3.54) that

$$\begin{aligned} &S_2^{11}(\boldsymbol{k}, \boldsymbol{k}_0, \omega, \omega_0) \\ &= \frac{\left(\rho_1 \rho_2 q_k^{(1)} q_k^{(2)}\right)^{1/2}}{\rho_1 q_k^{(2)} + \rho_2 q_k^{(1)}} \int_{\omega'} \iint_{\boldsymbol{k}'} F(\boldsymbol{k}', \boldsymbol{k}_0, \boldsymbol{k}, \omega', \omega_0, \omega) h(\boldsymbol{k} - \boldsymbol{k}', \omega - \omega') h(\boldsymbol{k}' - \boldsymbol{k}_0, \omega' - \omega_0) d\boldsymbol{k}' d\omega' \end{aligned} \tag{3.71}$$

It follows from exchanging $\boldsymbol{k}_0 \leftrightarrow -\boldsymbol{k}$ that

$$\begin{aligned} &S_2^{11}(-\boldsymbol{k}_0, -\boldsymbol{k}, \omega, \omega_0) \\ &= \frac{\left(\rho_1 \rho_2 q_0^{(1)} q_0^{(2)}\right)^{1/2}}{\rho_1 q_0^{(2)} + \rho_2 q_0^{(1)}} \int_{\omega'} \iint_{\boldsymbol{k}'} F(\boldsymbol{k}', -\boldsymbol{k}, -\boldsymbol{k}_0, \omega', \omega_0, \omega) h(-\boldsymbol{k}_0 - \boldsymbol{k}', \omega - \omega') h(\boldsymbol{k}' + \boldsymbol{k}, \omega' - \omega_0) d\boldsymbol{k}' d\omega' \end{aligned}$$

($\boldsymbol{k}'' = -\boldsymbol{k}'$ yields)

$$= \frac{-\left(\rho_1\rho_2 q_0^{(1)} q_0^{(2)}\right)^{1/2}}{\rho_1 q_0^{(2)} + \rho_2 q_0^{(1)}} \int_{\omega'} \iint_{\substack{\boldsymbol{k}''= \\ (\infty,-\infty)}} F(-\boldsymbol{k}'', -\boldsymbol{k}, -\boldsymbol{k_0}, \omega', \omega_0, \omega) h(-\boldsymbol{k_0} + \boldsymbol{k}'', \omega - \omega') h(-\boldsymbol{k}'' + \boldsymbol{k}, \omega' - \omega_0) d\boldsymbol{k}'' d\omega'$$

($\boldsymbol{k}'' \to \boldsymbol{k}'$ yields)

$$= \frac{\left(\rho_1\rho_2 q_0^{(1)} q_0^{(2)}\right)^{1/2}}{\rho_1 q_0^{(2)} + \rho_2 q_0^{(1)}} \int_{\omega'} \iint_{\substack{\boldsymbol{k}'= \\ (-\infty,\infty)}} F(-\boldsymbol{k}', -\boldsymbol{k}, -\boldsymbol{k_0}, \omega', \omega_0, \omega) h(\boldsymbol{k}' - \boldsymbol{k_0}, \omega - \omega') h(\boldsymbol{k} - \boldsymbol{k}', \omega' - \omega_0) d\boldsymbol{k}' d\omega' \tag{3.72}$$

h^2 term in Eq. (3.72) is the same as that in Eq.(3.71) with respect to wave number vector for a fixed frequency, which means that the reciprocity in Eq. (3.68) requires:

$$\frac{\left(\rho_1\rho_2 q_k^{(1)} q_k^{(2)}\right)^{1/2}}{\left(\rho_1 q_k^{(2)} + \rho_2 q_k^{(1)}\right)} F(\boldsymbol{k}', \boldsymbol{k_0}, \boldsymbol{k}; \omega_0) - \frac{\left(\rho_1\rho_2 q_0^{(1)} q_0^{(2)}\right)^{1/2}}{\left(\rho_1 q_0^{(2)} + \rho_2 q_0^{(1)}\right)} F(-\boldsymbol{k}', -\boldsymbol{k}, -\boldsymbol{k_0}; \omega_0) \overset{(?)}{=} 0 \tag{3.73}$$

It follows from Eq. (3.59) with invariant frequencies ($\omega = \omega' = \omega_0$) that

$$\left[\frac{\left(\rho_1\rho_2 q_k^{(1)} q_k^{(2)}\right)^{1/2}}{\left(\rho_1 q_k^{(2)} + \rho_2 q_k^{(1)}\right)} F(\boldsymbol{k}', \boldsymbol{k_0}, \boldsymbol{k}; \omega_0) - \frac{\left(\rho_1\rho_2 q_0^{(1)} q_0^{(2)}\right)^{1/2}}{\left(\rho_1 q_0^{(2)} + \rho_2 q_0^{(1)}\right)} F(-\boldsymbol{k}', -\boldsymbol{k}, -\boldsymbol{k_0}; \omega_0)\right] \Bigg/ \frac{\left(\rho_1\rho_2 q_0^{(1)} q_k^{(1)}\right)^{1/2}}{\left(\rho_1 q_k^{(2)} + \rho_2 q_k^{(1)}\right)\left(\rho_2 q_0^{(1)} + \rho_1 q_0^{(2)}\right)} \tag{3.74}$$

$$= \left(\rho_1\rho_2\right)^{1/2} q_k^{(2)} \left(1 - \frac{q_0^{(2)}}{q_k^{(2)}}\right)\left[\left(\frac{\omega_0}{c_1}\right)^2 - \left(\frac{\omega_0}{c_2}\right)^2\right] + \frac{2\left(q_k^{(2)}\right)^{1/2}}{\left(\rho_2 q_{k'}^{(1)} + \rho_1 q_{k'}^{(2)}\right)} \times$$

$$\left[\left(\frac{\rho_1}{\rho_2} q_k^{(2)}\right)^{1/2} \left\{\cancel{\left(\rho_2 - \rho_1\right)^2 q_0^{(2)}} q_{k'}^{(1)} q_{k'}^{(2)} - \rho_2\left(q_{k'}^{(1)} + q_{k'}^{(2)}\right)\alpha(\boldsymbol{k}', \boldsymbol{k_0}, \omega_0)\right\}\right.$$

$$-\left(\rho_2 - \rho_1\right) q_0^{(2)} \left(\frac{\rho_1\rho_2}{q_k^{(2)}}\right)^{1/2} \left(q_{k'}^{(1)} \left\{\left(\frac{\omega_0}{c_2}\right)^2 - \boldsymbol{k}' \cdot \boldsymbol{k}\right\} + q_{k'}^{(2)} \left\{\left(\frac{\omega_0}{c_1}\right)^2 - \boldsymbol{k}' \cdot \boldsymbol{k}\right\}\right)$$

$$\left. -\left(\frac{\rho_2}{\rho_1 q_k^{(2)}}\right)^{1/2} \alpha(\boldsymbol{k}', \cancel{\boldsymbol{k_0}, \omega_0)\alpha(\boldsymbol{k}', \boldsymbol{k}}, \omega_0)\right]$$

$$-\left(\rho_1\rho_2\right)^{1/2} q_0^{(2)} \left(1 - \frac{q_k^{(2)}}{q_0^{(2)}}\right)\left[\left(\frac{\omega_0}{c_1}\right)^2 - \left(\frac{\omega_0}{c_2}\right)^2\right] - \frac{2\left(q_0^{(2)}\right)^{1/2}}{\left(\rho_2 q_{k'}^{(1)} + \rho_1 q_{k'}^{(2)}\right)} \times$$

$$
\left[\left(\frac{\rho_1}{\rho_2}q_0^{(2)}\right)^{1/2}\left\{\cancel{(\rho_2-\rho_1)^2 q_k^{(2)}}\,q_{k'}^{(1)}q_{k'}^{(2)}-\rho_2\left(q_{k'}^{(1)}+q_{k'}^{(2)}\right)\alpha(-\boldsymbol{k}',-\boldsymbol{k},\omega_0)\right\}\right.
$$

$$
-(\rho_2-\rho_1)q_k^{(2)}\left(\frac{\rho_1\rho_2}{q_0^{(2)}}\right)^{1/2}\left(q_{k'}^{(1)}\left\{\left(\frac{\omega_0}{c_2}\right)^2-\boldsymbol{k}'\cdot\boldsymbol{k}_0\right\}+q_{k'}^{(2)}\left\{\left(\frac{\omega_0}{c_1}\right)^2-\boldsymbol{k}'\cdot\boldsymbol{k}_0\right\}\right)
$$

$$
\left.-\left(\frac{\rho_2}{\rho_1 q_0^{(2)}}\right)^{1/2}\alpha(-\boldsymbol{k}',\cancel{-\boldsymbol{k},\omega_0)\alpha(-\boldsymbol{k}',}-\boldsymbol{k}_0,\omega_0)\right]
$$

$$
=2(\rho_1\rho_2)^{1/2}\left(q_k^{(2)}-q_0^{(2)}\right)\left[\left(\frac{\omega_0}{c_1}\right)^2-\left(\frac{\omega_0}{c_2}\right)^2\right]+\frac{2(\rho_1\rho_2)^{1/2}}{\left(\rho_2 q_{k'}^{(1)}+\rho_1 q_{k'}^{(2)}\right)}\times
$$

$$
\left[-q_k^{(2)}\left\{\left(q_{k'}^{(1)}+q_{k'}^{(2)}\right)\alpha(\boldsymbol{k}',\boldsymbol{k}_0,\omega_0)-(\rho_2-\rho_1)\left(q_{k'}^{(1)}\left\{\left(\frac{\omega_0}{c_2}\right)^2-\boldsymbol{k}'\cdot\boldsymbol{k}_0\right\}+q_{k'}^{(2)}\left\{\left(\frac{\omega_0}{c_1}\right)^2-\boldsymbol{k}'\cdot\boldsymbol{k}_0\right\}\right)\right\}\right.
$$

$$
\left.+q_0^{(2)}\left\{\left(q_{k'}^{(1)}+q_{k'}^{(2)}\right)\alpha(-\boldsymbol{k}',-\boldsymbol{k},\omega_0)-(\rho_2-\rho_1)\left(q_{k'}^{(1)}\left\{\left(\frac{\omega_0}{c_2}\right)^2-\boldsymbol{k}'\cdot\boldsymbol{k}\right\}+q_{k'}^{(2)}\left\{\left(\frac{\omega_0}{c_1}\right)^2-\boldsymbol{k}'\cdot\boldsymbol{k}\right\}\right)\right\}\right]
$$

$$
=2(\rho_1\rho_2)^{1/2}\left(q_k^{(2)}-q_0^{(2)}\right)\left[\left(\frac{\omega_0}{c_1}\right)^2-\left(\frac{\omega_0}{c_2}\right)^2\right]+\frac{2(\rho_1\rho_2)^{1/2}}{\left(\rho_2 q_{k'}^{(1)}+\rho_1 q_{k'}^{(2)}\right)}\times
$$

$$
\left[\left(q_0^{(2)}-q_k^{(2)}\right)\left(\left(q_{k'}^{(1)}+q_{k'}^{(2)}\right)\left\{\rho_2\left(\frac{\omega_0}{c_1}\right)^2-\rho_1\left(\frac{\omega_0}{c_2}\right)^2\right\}-(\rho_2-\rho_1)\left\{q_{k'}^{(2)}\left(\frac{\omega_0}{c_1}\right)^2+q_{k'}^{(1)}\left(\frac{\omega_0}{c_2}\right)^2\right\}\right)
$$

$$
+q_k^{(2)}\left\{(\rho_2-\rho_1)\left(q_{k'}^{(1)}+q_{k'}^{(2)}\right)\cancel{\boldsymbol{k}'\cdot\boldsymbol{k}_0}-(\rho_2-\rho_1)\left(q_{k'}^{(1)}+q_{k'}^{(2)}\right)\cancel{\boldsymbol{k}'\cdot\boldsymbol{k}_0}\right\}
$$

$$
\left.-q_0^{(2)}\left\{(\rho_2-\rho_1)\left(q_{k'}^{(1)}+q_{k'}^{(2)}\right)\cancel{\boldsymbol{k}'\cdot\boldsymbol{k}}-(\rho_2-\rho_1)\left(q_{k'}^{(1)}+q_{k'}^{(2)}\right)\cancel{\boldsymbol{k}'\cdot\boldsymbol{k}}\right\}\right]
$$

$$
=0
$$

where α in Eq. (3.32) is used. The above equation verifies Eq. (3.73), which confirms the reciprocity, $S_2^{11}(\boldsymbol{k},\boldsymbol{k}_0;\omega_0)=S_2^{11}(-\boldsymbol{k}_0,-\boldsymbol{k};\omega_0)$, in Eq. (3.68). The reciprocity of S_2^{22} for $N_1=N_2=2$ in Eq. (3.69) follows immediately from Eq. (3.68).

$$
S_2^{22}(\boldsymbol{k},\boldsymbol{k}_0;\omega_0)=S_2^{11}(\boldsymbol{k},\boldsymbol{k}_0;\omega_0)\Big|_{\substack{1\leftrightarrow 2\\ h\rightarrow(-)h}}=S_2^{11}(-\boldsymbol{k}_0,-\boldsymbol{k};\omega_0)\Big|_{\substack{1\leftrightarrow 2\\ h\rightarrow(-)h}}=S_2^{22}(-\boldsymbol{k}_0,-\boldsymbol{k};\omega_0) \qquad (3.75)
$$

To show the reciprocity in Eq. (3.70) for $N_1=2$ and $N_2=1$, one can use Eq. (3.61) and change integral variables in the same way as in Eq. (3.72) to have the form.

$$S_2^{12}(-\boldsymbol{k_0},-\boldsymbol{k},\omega,\omega_0) \tag{3.76}$$

$$=\frac{\left(\rho_1\rho_2 q_0^{(1)}q_0^{(2)}\right)^{1/2}}{\rho_1 q_0^{(2)}+\rho_2 q_0^{(1)}}\int_{\omega'}\iint_{\boldsymbol{k}'} G(-\boldsymbol{k}',-\boldsymbol{k},-\boldsymbol{k_0},\omega',\omega_0,\omega)\big|_{1\leftrightarrow 2}\, h(\boldsymbol{k}'-\boldsymbol{k_0},\omega-\omega')h(\boldsymbol{k}-\boldsymbol{k}',\omega'-\omega_0)d\boldsymbol{k}'d\omega'$$

Then the reciprocity in Eq. (3.70) can be confirmed by showing the following equality.

$$\frac{\left(\rho_1\rho_2 q_k^{(1)}q_k^{(2)}\right)^{1/2}}{\rho_1 q_k^{(2)}+\rho_2 q_k^{(1)}}G(\boldsymbol{k}',\boldsymbol{k_0},\boldsymbol{k};\omega_0)-\frac{\left(\rho_1\rho_2 q_0^{(1)}q_0^{(2)}\right)^{1/2}}{\left(\rho_1 q_0^{(2)}+\rho_2 q_0^{(1)}\right)}G(-\boldsymbol{k}',-\boldsymbol{k},-\boldsymbol{k_0};\omega_0)\big|_{1\leftrightarrow 2}\overset{(?)}{=}0 \tag{3.77}$$

It follows from Eqs. (3.60) and (3.63) with constant frequencies($\omega=\omega'=\omega_0$) that

$$\left[\frac{\left(\rho_1\rho_2 q_k^{(1)}q_k^{(2)}\right)^{1/2}}{\left(\rho_1 q_k^{(2)}+\rho_2 q_k^{(1)}\right)}G(\boldsymbol{k}',\boldsymbol{k_0},\boldsymbol{k};\omega_0)-\frac{\left(\rho_1\rho_2 q_0^{(1)}q_0^{(2)}\right)^{1/2}}{\left(\rho_1 q_0^{(2)}+\rho_2 q_0^{(1)}\right)}G(-\boldsymbol{k}',-\boldsymbol{k},-\boldsymbol{k_0};\omega_0)\big|_{1\leftrightarrow 2}\right] \tag{3.78}$$
$$\Big/\ \frac{\left(\rho_1\rho_2 q_0^{(1)}q_k^{(2)}\right)^{1/2}}{\left(\rho_1 q_0^{(2)}+\rho_2 q_0^{(1)}\right)\left(\rho_1 q_k^{(2)}+\rho_2 q_k^{(1)}\right)}$$

$$=-\rho_2 q_k^{(1)}\left(1+\frac{\rho_1 q_0^{(2)}}{\rho_2 q_k^{(1)}}\right)\left[\left(\frac{\omega_0}{c_1}\right)^2-\left(\frac{\omega_0}{c_2}\right)^2\right]-\frac{2q_k^{(1)}}{\left(\rho_2 q_{k'}^{(1)}+\rho_1 q_{k'}^{(2)}\right)}\times$$

$$\Big[\cancel{\left(\rho_2-\rho_1\right)^2 q_0^{(2)}}\, q_{k'}^{(1)}q_{k'}^{(2)}-\rho_2\left(q_{k'}^{(1)}+q_{k'}^{(2)}\right)\alpha(\boldsymbol{k}',\boldsymbol{k_0},\omega_0)$$

$$+\rho_1\left(\rho_2-\rho_1\right)\frac{q_0^{(2)}}{q_k^{(1)}}\left(q_{k'}^{(1)}\left\{\left(\frac{\omega_0}{c_2}\right)^2-\boldsymbol{k}'\cdot\boldsymbol{k}\right\}+q_{k'}^{(2)}\left\{\left(\frac{\omega_0}{c_1}\right)^2-\boldsymbol{k}'\cdot\boldsymbol{k}\right\}\right)+\frac{1}{q_k^{(1)}}\alpha(\boldsymbol{k}',\cancel{\boldsymbol{k_0},\omega_0)\alpha(\boldsymbol{k}'},\boldsymbol{k},\omega_0)\Big]$$

$$-\rho_1 q_0^{(2)}\left(1+\frac{\rho_2 q_k^{(1)}}{\rho_1 q_0^{(2)}}\right)\left[\left(\frac{\omega_0}{c_1}\right)^2-\left(\frac{\omega_0}{c_2}\right)^2\right]+\frac{2q_0^{(2)}}{\left(\rho_2 q_{k'}^{(1)}+\rho_1 q_{k'}^{(2)}\right)}\times$$

$$\Big[\cancel{\left(\rho_2-\rho_1\right)^2 q_k^{(1)}}\, q_{k'}^{(1)}q_{k'}^{(2)}+\rho_1\left(q_{k'}^{(1)}+q_{k'}^{(2)}\right)\alpha(-\boldsymbol{k}',-\boldsymbol{k},\omega_0)-\rho_2\left(\rho_2-\rho_1\right)\frac{q_k^{(1)}}{q_0^{(2)}}\times$$

$$\left(q_{k'}^{(1)}\left\{\left(\frac{\omega_0}{c_2}\right)^2-\boldsymbol{k}'\cdot\boldsymbol{k_0}\right\}+q_{k'}^{(2)}\left\{\left(\frac{\omega_0}{c_1}\right)^2-\boldsymbol{k}'\cdot\boldsymbol{k_0}\right\}\right)+\frac{1}{q_0^{(2)}}\alpha(-\boldsymbol{k}',\cancel{-\boldsymbol{k},\omega_0)\alpha(-\boldsymbol{k}'},-\boldsymbol{k_0},\omega_0)\Big]$$

$$= -2\left(\rho_1 q_0^{(2)} + \rho_2 q_k^{(1)}\right)\left[\left(\frac{\omega_0}{c_1}\right)^2 - \left(\frac{\omega_0}{c_2}\right)^2\right] + \frac{2}{\left(\rho_2 q_{k'}^{(1)} + \rho_1 q_{k'}^{(2)}\right)} \times$$

$$\left[\rho_2 q_k^{(1)}\left\{\left(q_{k'}^{(1)} + q_{k'}^{(2)}\right)\alpha(\boldsymbol{k}', \boldsymbol{k_0}, \omega_0) - \left(\rho_2 - \rho_1\right)\left(q_{k'}^{(1)}\left\{\left(\frac{\omega_0}{c_2}\right)^2 - \boldsymbol{k}' \cdot \boldsymbol{k_0}\right\} + q_{k'}^{(2)}\left\{\left(\frac{\omega_0}{c_1}\right)^2 - \boldsymbol{k}' \cdot \boldsymbol{k_0}\right\}\right)\right\}\right.$$

$$\left. + \rho_1 q_0^{(2)}\left\{\left(q_{k'}^{(1)} + q_{k'}^{(2)}\right)\alpha(-\boldsymbol{k}', -\boldsymbol{k}, \omega_0) - \left(\rho_2 - \rho_1\right)\left(q_{k'}^{(1)}\left\{\left(\frac{\omega_0}{c_2}\right)^2 - \boldsymbol{k}' \cdot \boldsymbol{k}\right\} + q_{k'}^{(2)}\left\{\left(\frac{\omega_0}{c_1}\right)^2 - \boldsymbol{k}' \cdot \boldsymbol{k}\right\}\right)\right\}\right]$$

$$= -2\left(\rho_1 q_0^{(2)} + \rho_2 q_k^{(1)}\right)\left[\left(\frac{\omega_0}{c_1}\right)^2 - \left(\frac{\omega_0}{c_2}\right)^2\right] + \frac{2}{\left(\rho_2 q_{k'}^{(1)} + \rho_1 q_{k'}^{(2)}\right)} \times$$

$$\left[\left(\rho_1 q_0^{(2)} + \rho_2 q_k^{(1)}\right)\left(\left(q_{k'}^{(1)} + q_{k'}^{(2)}\right)\left\{\rho_2\left(\frac{\omega_0}{c_1}\right)^2 - \rho_1\left(\frac{\omega_0}{c_2}\right)^2\right\} - \left(\rho_2 - \rho_1\right)\left\{q_{k'}^{(2)}\left(\frac{\omega_0}{c_1}\right)^2 + q_{k'}^{(1)}\left(\frac{\omega_0}{c_2}\right)^2\right\}\right)\right.$$

$$-\rho_2 q_k^{(1)}\left\{\left(\rho_2 - \rho_1\right)\left(q_{k'}^{(1)} + q_{k'}^{(2)}\right)\cancel{\boldsymbol{k}' \cdot \boldsymbol{k_0}} - \left(\rho_2 - \rho_1\right)\left(q_{k'}^{(1)} + q_{k'}^{(2)}\right)\cancel{\boldsymbol{k}' \cdot \boldsymbol{k_0}}\right\}$$

$$\left. -\rho_1 q_0^{(2)}\left\{\left(\rho_2 - \rho_1\right)\left(q_{k'}^{(1)} + q_{k'}^{(2)}\right)\cancel{\boldsymbol{k}' \cdot \boldsymbol{k}} - \left(\rho_2 - \rho_1\right)\left(q_{k'}^{(1)} + q_{k'}^{(2)}\right)\cancel{\boldsymbol{k}' \cdot \boldsymbol{k}}\right\}\right]$$

$$= 0$$

where α in Eq. (3.32) is used. The above equation verifies Eq. (3.77), which confirms the reciprocity, $S_2^{21}(\boldsymbol{k}, \boldsymbol{k_0}; \omega_0) = S_2^{12}(-\boldsymbol{k_0}, -\boldsymbol{k}; \omega_0)$, in Eq. (3.70).

3.3 Evaluation of scattering amplitudes with jump conditions

Matching conditions used in the previous section are not valid across unsteady flame front because unsteady gas expansion across unsteady flame front causes jump conditions in acoustic pressure and velocity. These jump conditions have been derived by many researchers using conservation relations and reported to be associated with mean flame speed Mach number for unburned gas, M_S ($= \overline{S}_L^{(1)} / c_1$), and perturbations in mass burning rate and pressure. [18,20,26] The jump condition in acoustic pressure across the flame front can be derived by linearizing normal momentum conservation.

$$p^{(1)} - p^{(2)} = \rho_2 S_L^{(2)2} - \rho_1 S_L^{(1)2} = m^2 \left(\frac{1}{\rho_2} - \frac{1}{\rho_1} \right) \; ; \; m = \rho_1 S_L^{(1)} = \rho_2 S_L^{(2)} \tag{3.79}$$

which leads to the form by expanding variables

$$\begin{aligned}
&\left(p_0^{(1)} + \varepsilon p_1^{(1)} + O(\varepsilon^2) \right) - \left(p_0^{(2)} + \varepsilon p_1^{(2)} + O(\varepsilon^2) \right) \\
&= \left(m_0 + \varepsilon m_1 + O(\varepsilon^2) \right)^2 \left(\frac{1}{\rho_{2,0} + \varepsilon \rho_{2,1} + O(\varepsilon^2)} - \frac{1}{\rho_{1,0} + \varepsilon \rho_{1,1} + O(\varepsilon^2)} \right) \\
&= \left(m_0 + \varepsilon m_1 + O(\varepsilon^2) \right)^2 \left[\rho_{2,0}^{-1} (1 - \varepsilon \rho_{2,1} \rho_{2,0}^{-1} + O(\varepsilon^2)) - \rho_{1,0}^{-1} (1 - \varepsilon \rho_{1,1} \rho_{1,0}^{-1} + O(\varepsilon^2)) \right] \\
&= \left(m_0^2 + 2\varepsilon m_0 m_1 + O(\varepsilon^2) \right) \left[(\rho_{2,0}^{-1} - \rho_{1,0}^{-1}) + \varepsilon (\rho_{1,1} \rho_{1,0}^{-2} - \rho_{2,1} \rho_{2,0}^{-2}) + O(\varepsilon^2) \right]
\end{aligned} \tag{3.80}$$

where superscripts (1) and (2) denote media (1) and (2) and subscripts 0 and 1 denote mean value and perturbation value of first order, respectively, for all variables except for ρ and c. (Note that j and n in $\rho_{n,j}$ and c_n denote values of j^{th} order in medium (n).) It follows by taking $O(\varepsilon)$ in Eq. (3.80) and using $\rho_{n,0} = \gamma p_0^{(n)} / c_n^2$, $\rho_{n,1} = p_1^{(n)} / c_n^2$ (n $=\{1,2\}$) with $p_0^{(1)} = p_0^{(2)} = p_0$ and $M_S = m_0 / (\rho_{1,0} c_1) = m_0 c_1 / (\gamma p_0)$ that

$$\begin{aligned}
&p_1^{(1)} - p_1^{(2)} = m_0^2 (\rho_{1,1} \rho_{1,0}^{-2} - \rho_{2,1} \rho_{2,0}^{-2}) + 2 m_0 m_1 (\rho_{2,0}^{-1} - \rho_{1,0}^{-1}) \\
&= m_0^2 [p_1^{(1)} c_1^{-2} (\gamma p_0)^{-2} c_1^4 - p_1^{(2)} c_2^{-2} (\gamma p_0)^{-2} c_2^4] + 2 m_0 m_1 (\gamma p_0)^{-1} (c_2^2 - c_1^2) \\
&= M_S^2 (p_1^{(1)} - \Lambda p_1^{(2)}) + 2\gamma p_0 M_S^2 (\Lambda - 1) \frac{m_1}{m_0}
\end{aligned}$$

which is rearranged to yield

$$\begin{aligned}
2\gamma M_S^2 (\Lambda - 1) \frac{m_1}{m_0} &= \frac{p_1^{(1)}}{p_0} (1 - M_S^2) - \frac{p_1^{(2)}}{p_0} (1 - \Lambda M_S^2) \\
&\approx \frac{p_1^{(1)} - p_1^{(2)}}{p_0} \qquad (\because O(M_S^2) << O(1))
\end{aligned} \tag{3.81}$$

which means that the difference in a linearized acoustic pressure across a flame front is $O(M_S^2)$ smaller than linearized mass burning rate perturbation, m_1 / m_0, and, therefore, the pressure jump condition can simply reduce to the continuity condition, $p_1^{(1)} = p_1^{(2)}$, up

to first order approximation as in Eq. (3.1). The velocity jump condition at the flame front can be obtained from linearized energy equation. For instance, the energy equation was linearized by Lieuwen. (Eq. (10) in reference [26])

$$\frac{v_{1,n}^{(2)}}{c_1}-\frac{v_{1,n}^{(1)}}{c_1}=M_S\left(\frac{(\gamma+\Lambda-1)}{\gamma}\frac{p_1^{(1)}}{p_0}-\Lambda\frac{p_1^{(2)}}{p_0}+(\Lambda-1)\frac{S_{L,1}^{(1)}}{S_{L,0}^{(1)}}\right)+O(M_S^2) \tag{3.82}$$

where $v_{1,n}$ denotes acoustic velocity component that is normal to wrinkled flame surface. The left hand side results from difference in flame speed across a flame, $(S_{L,1}^{(2)}-S_{L,1}^{(1)})/c_1$. Note that Lieuwen[26] used vertical component of velocity, $v_{1,z}$, in the left hand side, which is replaced by $v_{1,n}$ in Eq. (3.82). Such replacement depends upon whether a flow field and flame kinematics are coupled or not, as demonstrated below. By definition,

$$\text{Flame front speed} = (\vec{\boldsymbol{v}}\cdot\vec{\boldsymbol{n}}-S_L)^{(1)}=(\vec{\boldsymbol{v}}\cdot\vec{\boldsymbol{n}}-S_L)^{(2)} \tag{3.83}$$

where the velocity terms are expanded by incident acoustic pressure amplitude, $\varepsilon\equiv|P_1|/(\rho_1 c_1^2)$, see Eq. (6.6).

$$\vec{\boldsymbol{v}}=\vec{\boldsymbol{v}}_0+\varepsilon\vec{\boldsymbol{v}}_1+O(\varepsilon^2),\qquad S_L=S_{L,0}+\varepsilon S_{L,1}+O(\varepsilon^2) \tag{3.84}$$

where terms of $O(\varepsilon)$ and higher can further be expanded in terms of flame front height h as flow field is scattered by a wrinkling flame, see Eq. (6.7).

$$\vec{\boldsymbol{v}}_1=\vec{\boldsymbol{v}}_{10}+h\vec{\boldsymbol{v}}_{11}+h^2\vec{\boldsymbol{v}}_{12}+O(h^3),\quad S_{L,1}=S_{L,10}+hS_{L,11}+h^2S_{L,12}+O(h^3) \tag{3.85}$$

Flame's unit normal can also be expanded in terms of h using Eq. (3.4).

$$\begin{aligned}\vec{\boldsymbol{n}}&=\left(1+|\nabla h|^2\right)^{-1/2}(\vec{\boldsymbol{e}}_z-\nabla h)=\left(1-\frac{1}{2}|\nabla h|^2+O(h^4)\right)(\vec{\boldsymbol{e}}_z-\nabla h)\\&=\vec{\boldsymbol{e}}_z-\nabla h-\frac{1}{2}|\nabla h|^2\vec{\boldsymbol{e}}_z+O(h^3)\end{aligned} \tag{3.86}$$

Eqs. (3.84) - (3.86) are substituted into Eq. (3.83) to yield

$$
\begin{aligned}
&\{[\vec{v}_0 + \varepsilon(\vec{v}_{10} + h\vec{v}_{11} + h^2\vec{v}_{12} + O(h^3))]^{(2)} \\
&-[\vec{v}_0 + \varepsilon(\vec{v}_{10} + h\vec{v}_{11} + h^2\vec{v}_{12} + O(h^3))]^{(1)} + O(\varepsilon^2)\} \cdot (\vec{e}_z - \nabla h - \left|\nabla h\right|^2 \vec{e}_z / 2 + O(h^3)) \\
&= [S_{L,0} + \varepsilon(S_{L,10} + hS_{L,11} + h^2 S_{L,12} + O(h^3))]^{(2)} \\
&-[S_{L,0} + \varepsilon(S_{L,10} + hS_{L,11} + h^2 S_{L,12} + O(h^3))]^{(1)} + O(\varepsilon^2)
\end{aligned}
\tag{3.87}
$$

In the case where flow field and flame kinematics are coupled and relative magnitude of ε and h is such that $O(\varepsilon) = O(h)$, then collecting terms of $O(\varepsilon)$ (or $O(h)$) in Eq. (3.87) yields the form

$$
\varepsilon(\vec{v}_{10}^{(2)} - \vec{v}_{10}^{(1)}) \cdot \vec{e}_z - (\vec{v}_0^{(2)} - \vec{v}_0^{(1)}) \cdot \nabla h = \varepsilon(S_{L,10}^{(2)} - S_{L,10}^{(1)}) \tag{3.88}
$$

where the second term on the left hand side vanishes identically by using continuity of tangential momentum

$$
(\vec{v}^{(2)} - \vec{v}^{(1)}) \times \vec{\nabla} G = 0 \text{ with } \vec{\nabla} G = \vec{e}_z - \nabla h
$$

terms of $O(1)$ of which has the form

$$
(\vec{v}_0^{(2)} - \vec{v}_0^{(1)}) \times \vec{e}_z = 0
$$

which implies that $(\vec{v}_0^{(2)} - \vec{v}_0^{(1)}) // \vec{e}_z$ or $(\vec{v}_0^{(2)} - \vec{v}_0^{(1)}) \perp \nabla h$ that leads to the form

$$
\nabla h \cdot (\vec{v}_0^{(2)} - \vec{v}_0^{(1)}) = 0 \tag{3.89}
$$

which leads Eq. (3.88) to the form which is equivalent to the result of Lieuwen[26].

$$
(\vec{v}_{10}^{(2)} - \vec{v}_{10}^{(1)}) \cdot \vec{e}_z = S_{L,10}^{(2)} - S_{L,10}^{(1)} \tag{3.90}
$$

On the other hand, if a flame surface is prescribed and uncoupled with flow field as is assumed in this analysis, then h is not affected by ε even when ε is brought to zero, i.e.; turbulent flame wrinkling still exists even without an acoustic flow excitation. This leads to the following form simply by substituting Eq. (3.84) to Eq. (3.83) and collecting terms of $O(\varepsilon)$.

$$(\vec{v}_1^{(2)} - \vec{v}_1^{(1)}) \cdot \vec{n} = S_{L,1}^{(2)} - S_{L,1}^{(1)} \tag{3.91}$$

which justifies the usage of velocity component normal to flame surface, $v_{1,n}$, instead of using vertical component of velocity in Eq. (3.82). Eq. (3.91) implies that acoustic velocity jump arises from difference in flame speed fluctuation. Perturbation in mass burning rate, $m = \rho_1 S_L^{(1)}$, can be obtained by expanding $m = m_0 + \varepsilon m_1 + O(\varepsilon^2)$, $\rho_1 = \rho_{1,0} + \varepsilon\rho_{1,1} + O(\varepsilon^2)$, $S_L^{(1)} = S_{L,0}^{(1)} + \varepsilon S_{L,1}^{(1)} + O(\varepsilon^2)$ and taking terms of $O(\varepsilon)$, which yields

$$\frac{m_1}{m_0} = \frac{\rho_{1,1}}{\rho_{1,0}} + \frac{S_{L,1}^{(1)}}{S_{L,0}^{(1)}} \qquad \text{or} \qquad \frac{S_{L,1}^{(1)}}{S_{L,0}^{(1)}} = \frac{m_1}{m_0} - \frac{p_1^{(1)}}{\gamma p_0} \tag{3.92}$$

where $p_1^{(1)} / \rho_{1,1} = c_1^2 = \gamma p_0 / \rho_{1,0}$ is used. Then Eq. (3.82) can be rewritten in terms of normalized mass burning rate perturbation, m_1 / m_0, in Eq. (3.92) and $p_1^{(1)} = p_1^{(2)} = p_1$ on the first order of M_S from Eq. (3.81).

$$\frac{v_{1,n}^{(2)}}{c_1} - \frac{v_{1,n}^{(1)}}{c_1} = (\Lambda - 1) M_S \left(\frac{m_1}{m_0} - \frac{p_1}{p_0} \right) + O(M_S^2) \tag{3.93}$$

Taking inverse Fourier transform of the above equation yields

$$\frac{v_{1,n}^{(2)}(t)}{c_1} - \frac{v_{1,n}^{(1)}(t)}{c_1} = (\Lambda - 1) M_S \left(\frac{m_1(t)}{m_0} - \frac{p_1(t)}{p_0} \right) + O(M_S^2) \tag{3.94}$$

$m_1(t)/m_0$ can be calculated by linearizing the expression for the burning rate, $M(\tau)$ ($\equiv m(t)/M_r$), reported by Peters and Ludford [52](Eq. (22) in their publication).

$$b \frac{d \ln M(\tau)}{d\tau} - M^2(\tau) \left\{ \ln M^2(\tau) + \alpha \left(1 - P\ (\tau)^{(\gamma-1)/\gamma} \right) \right\} = -2 \frac{\gamma - 1}{\gamma} \frac{d \ln P\ (\tau)}{d\tau} \tag{3.95}$$

where $b = 1 - Le^{-1}$, $P(\tau) = p(t)/p_r$, $\tau = (\theta t_r)^{-1} t$, Le = Lewis number, θ = dimensionless activation energy, p_r = reference pressure, $t_r = \rho_r \lambda_r / c_{pr} M_r^2$ = reference time of flame's diffusion, M_r = reference mass flux per unit area. (Note that the above $\tau = (\theta t_r)^{-1} t$ is different from $\tau = t_r / t_c$ that will be introduced in Eq. (4.73).)

Expand M and P in Eq. (3.95) in the power series of θ^{-1} yields:

$$M = 1 + \theta^{-1} M_1 + O(\theta^{-2}), \qquad P = 1 + \theta^{-1} P_1 + O(\theta^{-2}), \tag{3.96}$$

$$\ln M = \ln\left(1 + \theta^{-1} M_1 + O(\theta^{-2})\right) = \theta^{-1} M_1 + O(\theta^{-2}) \text{ using } \ln(1+x) = x - x^2/2 + x^3/3 + O(x^4),$$

$$M^2 = 1 + 2\theta^{-1} M_1 + O(\theta^{-2}), \qquad P^{(\gamma-1)/\gamma} = 1 + \theta^{-1} \frac{(\gamma-1)}{\gamma} P_1 + O(\theta^{-2})$$

Substituting Eq. (3.96) into Eq. (3.95) and collecting $O(\theta^{-1})$ yields a linearized form of mass burning rate.

$$b \frac{dM_1(\tau)}{d\tau} - 2M_1(\tau) + \alpha \frac{\gamma-1}{\gamma} P_1(\tau) = -2 \frac{\gamma-1}{\gamma} \frac{dP_1(\tau)}{d\tau} \tag{3.97}$$

The case of $Le = 1$ will be examined where b vanishes. Then $m_1(t)/m_0$ $(= M_1(\tau)$ with $M_r = m_0)$ has the form in terms of linearized acoustic pressure, $p_1(t)$ $(= p_0 P_1(\tau)$ with $p_r = p_0)$, from Eq. (3.97).

$$\frac{m_1(t)}{m_0} = \frac{\gamma-1}{\gamma p_0} \left(\frac{\alpha}{2} p_1(t) + \theta t_r \frac{\partial p_1(t)}{\partial t} \right) \tag{3.98}$$

which is then substituted into Eq. (3.94) to yield the acoustic velocity jump across a flame front of the order of $O(M_S)$ where $p_1^{(1)}(t) = p_1^{(2)}(t) = p_1(t)$ is valid.

$$\frac{v_{1,n}^{(2)}(t)}{c_1}-\frac{v_{1,n}^{(1)}(t)}{c_1}=(\Lambda-1)M_S\left(\frac{m_1(t)}{m_0}-\frac{p_1(t)}{p_0}\right)+O(M_S^2)$$

$$v_{1,n}^{(2)}(t)-v_{1,n}^{(1)}(t)=\frac{(\Lambda-1)\bar{S}_L^{(1)}}{p_0}\left[\left(\frac{\alpha}{2}\frac{(\gamma-1)}{\gamma}-1\right)p_1^{(2)}(t)+\theta t_r\frac{(\gamma-1)}{\gamma}\frac{\partial p_1^{(2)}(t)}{\partial t}\right] \tag{3.99}$$

where the ratio of magnitude of pressure term, p_1, to that of time derivative of pressure term, $\partial p_1/\partial t$, in the right hand side can be evaluated using $\alpha=2$, $\gamma=1.4$, $\theta=10$ [52], $t_r=D_T/\bar{S}_L^2\approx d/\bar{S}_L\approx 0.001/0.4=0.0025\,(s)$. (Note that $t_r:=\rho_r\lambda_r/c_{pr}M_r^2=D_T/\bar{S}_L^2$ using $D_T=\lambda_r/(\rho_r c_{pr})$ and $M_r=\rho_r\bar{S}_L$.)

$$\left|\frac{\alpha}{2}\frac{(\gamma-1)}{\gamma}-1\right|\Big/\left|i\omega\theta t_r\frac{(\gamma-1)}{\gamma}\right|\approx\frac{16}{f} \tag{3.100}$$

which ensures the dominance of $\partial p_1/\partial t$ term for $f\geq 100$ Hz. Eq. (3.99) can be expressed as velocity potential by means of Eqs. (2.2) and (2.3).

$$\left(\frac{\partial\psi_c^{(2)}(\vec{\boldsymbol{R}},t)}{\partial n}-\frac{\partial\psi_c^{(1)}(\vec{\boldsymbol{R}},t)}{\partial n}+\beta_X\frac{\partial\psi_c^{(2)}(\vec{\boldsymbol{R}},t)}{\partial t}+\beta_Y\frac{\partial^2\psi_c^{(2)}(\vec{\boldsymbol{R}},t)}{\partial t^2}\right)_{z=h(\boldsymbol{r},t)}=0 \tag{3.101}$$

where $\beta_X=\dfrac{(\Lambda-1)\rho_2\bar{S}_L^{(1)}}{p_0}\left(\dfrac{\alpha}{2}\dfrac{(\gamma-1)}{\gamma}-1\right)$, $\beta_Y=\dfrac{(\Lambda-1)(\gamma-1)}{\gamma}\dfrac{\rho_2 t_r\theta\bar{S}_L^{(1)}}{p_0}$

which are rewritten in another form using $\rho_2/p_0=\gamma/c_2^2$, $c_2/c_1=\Lambda^{1/2}$, and mean flame speed Mach number $M_S\,(=\bar{S}_L^{(1)}/c_1)$.

$$c_2\beta_X=\frac{(\Lambda-1)}{\Lambda^{1/2}}\left(\frac{\alpha}{2}(\gamma-1)-\gamma\right)M_S\ , \qquad c_2\beta_Y=\frac{(\Lambda-1)(\gamma-1)t_r\theta}{\Lambda^{1/2}}M_S \tag{3.102}$$

Eq. (3.5) leads the above equation to the form

$$\left(1+\left|\nabla h\right|^2\right)^{-1/2}\left(\frac{\partial}{\partial z}-\nabla h\cdot\nabla\right)\psi_c^{(1)}(\vec{\boldsymbol{R}},t)\Big|_{z=h(\boldsymbol{r},t)}$$
$$=\left[\left(1+\left|\nabla h\right|^2\right)^{-1/2}\left(\frac{\partial}{\partial z}-\nabla h\cdot\nabla\right)-\beta_X\frac{\partial}{\partial t}-\beta_Y\frac{\partial^2}{\partial t^2}\right]\psi_c^{(2)}(\vec{\boldsymbol{R}},t)\Big|_{z=h(\boldsymbol{r},t)} \tag{3.103}$$

which, using Eqs. (2.18) and (2.20), can be written as

$$\left(1+\left|\nabla h\right|^2\right)^{-1/2}\left(\rho_1 q_0^{(1)}\right)^{-1/2}\left(q_0^{(1)}-\nabla h(\boldsymbol{r},t)\cdot\boldsymbol{k_0}\right)\mathrm{e}^{i(\boldsymbol{k_0}\cdot\boldsymbol{r}+q_0^{(1)}h(\boldsymbol{r},t)-\omega_0 t)} \tag{3.104}$$

$$-\left(1+\left|\nabla h\right|^2\right)^{-1/2}\int_{\omega}\iint_{\boldsymbol{k}}S^{11}(\boldsymbol{k},\boldsymbol{k_0},\omega,\omega_0)\left(\rho_1 q_k^{(1)}\right)^{-1/2}\left(q_k^{(1)}+\nabla h(\boldsymbol{r},t)\cdot\boldsymbol{k}\right)\mathrm{e}^{i(\boldsymbol{k}\cdot\boldsymbol{r}-q_k^{(1)}h(\boldsymbol{r},t)-\omega t)}\,d\boldsymbol{k}d\omega$$
$$=\int_{\omega}\iint_{\boldsymbol{k}}S^{21}(\boldsymbol{k},\boldsymbol{k_0},\omega,\omega_0)\left(\rho_2 q_k^{(2)}\right)^{-1/2}\left[\left(1+\left|\nabla h\right|^2\right)^{-1/2}\left(q_k^{(2)}-\nabla h(\boldsymbol{r},t)\cdot\boldsymbol{k}\right)+\beta_X\omega-i\beta_Y\omega^2\right]d\boldsymbol{k}d\omega$$
$$\mathrm{e}^{i(\boldsymbol{k}\cdot\boldsymbol{r}+q_k^{(2)}h(\boldsymbol{r},t)-\omega t)}$$

It follows, by expanding in power series of h for $\left(1+\left|\nabla h\right|^2\right)^{-1/2}$, $\exp(iqh(\boldsymbol{r},t))$, and the scattering amplitudes as in Eq. (3.8), that

$$\left(1-\frac{1}{2}\left|\nabla h\right|^2+O(h^4)\right)\left(\rho_1 q_0^{(1)}\right)^{-1/2}\left(q_0^{(1)}-\nabla h(\boldsymbol{r},t)\cdot\boldsymbol{k_0}\right)\left\{1+iq_0^{(1)}h(\boldsymbol{r},t)-\frac{1}{2}(q_0^{(1)}h(\boldsymbol{r},t))^2+O(h^3)\right\}\mathrm{e}^{i(\boldsymbol{k_0}\cdot\boldsymbol{r}-\omega_0 t)}$$

$$-\int_{\omega}\iint_{\boldsymbol{k}}\left(1-\frac{1}{2}\left|\nabla h\right|^2+O(h^4)\right)\left(S_0^{11}+S_1^{11}+S_2^{11}+O(h^3)\right)\left(\rho_1 q_k^{(1)}\right)^{-1/2}\left(q_k^{(1)}+\nabla h(\boldsymbol{r},t)\cdot\boldsymbol{k}\right)$$
$$\times\left\{1-iq_k^{(1)}h(\boldsymbol{r},t)-\frac{1}{2}(q_k^{(1)}h(\boldsymbol{r},t))^2+O(h^3)\right\}\mathrm{e}^{i(\boldsymbol{k}\cdot\boldsymbol{r}-\omega t)}\,d\boldsymbol{k}d\omega$$
$$=\int_{\omega}\iint_{\boldsymbol{k}}\left(S_0^{21}+S_1^{21}+S_2^{21}+O(h^3)\right)\left(\rho_2 q_k^{(2)}\right)^{-1/2}\left[\left(1-\frac{1}{2}\left|\nabla h\right|^2+O(h^4)\right)\left(q_k^{(2)}-\nabla h(\boldsymbol{r},t)\cdot\boldsymbol{k}\right)+\beta(\omega)\right]$$
$$\times\left\{1+iq_k^{(2)}h(\boldsymbol{r},t)-\frac{1}{2}(q_k^{(2)}h(\boldsymbol{r},t))^2+O(h^3)\right\}\mathrm{e}^{i(\boldsymbol{k}\cdot\boldsymbol{r}-\omega t)}\,d\boldsymbol{k}d\omega \tag{3.105}$$

Collecting the terms of $O(h^0)$ in Eq. (3.105) leads to the solution of zeroth order of scattering amplitude.

$$(q_0^{(1)}/\rho_1)^{1/2}\,\mathrm{e}^{i(\boldsymbol{k_0}\cdot\boldsymbol{r}-\omega_0 t)} - \int_{\omega}\iint_{\boldsymbol{k}} S_0^{11}(\boldsymbol{k},\boldsymbol{k_0},\omega,\omega_0)(q_k^{(1)}/\rho_1)^{1/2}\,\mathrm{e}^{i(\boldsymbol{k}\cdot\boldsymbol{r}-\omega t)}\,d\boldsymbol{k}d\omega$$
$$= \int_{\omega}\iint_{\boldsymbol{k}} S_0^{21}(\boldsymbol{k},\boldsymbol{k_0},\omega,\omega_0)\left(\frac{q_k^{(2)}}{\rho_2}\right)^{1/2}\left(1+\frac{(\beta_X\omega - i\beta_Y\omega^2)}{q_k^{(2)}}\right)\mathrm{e}^{i(\boldsymbol{k}\cdot\boldsymbol{r}-\omega t)}\,d\boldsymbol{k}d\omega \qquad (3.106)$$

Algebraic form of scattering amplitude is obtained by multiplying $\exp[-i(\boldsymbol{k}'\cdot\boldsymbol{r}-\omega' t)]/(2\pi)^3$ in Eq. (3.106) and integrating with respect to $\boldsymbol{r}$ and t as in Eq.(3.16).

$$(q_0^{(1)}/\rho_1)^{1/2}\,\delta(\boldsymbol{k_0}-\boldsymbol{k}')\delta(\omega_0-\omega') - S_0^{11}(\boldsymbol{k}',\boldsymbol{k_0},\omega',\omega_0)(q_{k'}^{(1)}/\rho_1)^{1/2}$$
$$= S_0^{21}(\boldsymbol{k}',\boldsymbol{k_0},\omega',\omega_0)\left(\rho_2 q_{k'}^{(2)}\right)^{-1/2}\left(q_{k'}^{(2)}+\beta_X\omega'-i\beta_Y\omega'^2\right) \qquad (3.107)$$

The above expression for velocity jump condition and Eq. (3.17) for pressure continuity yield the explicit solution for the zeroth order scattering amplitudes.

$$S_0^{11}(\boldsymbol{k},\boldsymbol{k_0},\omega,\omega_0) = R_J(\boldsymbol{k},\omega)\delta(\boldsymbol{k}-\boldsymbol{k_0})\delta(\omega-\omega_0) \qquad (3.108)$$

where $\quad R_J(\boldsymbol{k},\omega) = \dfrac{\rho_2 q_k^{(1)} - \rho_1\left(q_k^{(2)}+\beta(\omega)\right)}{\rho_2 q_k^{(1)} + \rho_1\left(q_k^{(2)}+\beta(\omega)\right)}$; $\quad \beta(\omega) = \beta_X\omega - i\beta_Y\omega^2$

$$S_0^{21}(\boldsymbol{k},\boldsymbol{k_0},\omega,\omega_0) = D_J(\boldsymbol{k},\omega)\delta(\boldsymbol{k}-\boldsymbol{k_0})\delta(\omega-\omega_0) \qquad (3.109)$$

where $\quad D_J(\boldsymbol{k},\omega) = \dfrac{2\left(\rho_1\rho_2 q_k^{(1)} q_k^{(2)}\right)^{1/2}}{\rho_2 q_k^{(1)} + \rho_1\left(q_k^{(2)}+\beta(\omega)\right)}$

Reflection / transmission coefficients in above equations represent specular reflection / transmission from flat mean flame surface and reduce to R and D in Eqs. (3.20) and (3.21), respectively, by setting $\beta = 0$ which corresponds to the continuity condition of acoustic velocity. Note that this reflection / transmission coefficient is actually not a function of frequency when $\beta(\omega) \approx \beta_X\omega$ for low frequency regime, $\omega << |\beta_X/\beta_Y|$; e.g.,

$$R_J(\boldsymbol{k},\omega)=\frac{\rho_2 q_k^{(1)}-\rho_1\left(q_k^{(2)}+\beta_X\omega\right)}{\rho_2 q_k^{(1)}+\rho_1\left(q_k^{(2)}+\beta_X\omega\right)}=\frac{\rho_2 c_2\cos\phi^{(1)}-\rho_1 c_1\left(\cos\phi^{(2)}+c_2\beta_X\right)}{\rho_2 c_2\cos\phi^{(1)}-\rho_1 c_1\left(\cos\phi^{(2)}+c_2\beta_X\right)}\neq fun(\omega) \quad (3.110)$$

For higher frequency, however, dependence of these coefficients upon frequency becomes significant as $\beta_Y\omega^2$ term becomes more dominant than $\beta_X\omega$. Collecting the terms of $O(h^1)$ in Eq. (3.105) leads to the solution of first order of scattering amplitude.

$$\begin{aligned}&\left(\rho_1 q_0^{(1)}\right)^{-1/2}\left[i\left(q_0^{(1)}\right)^2 h(\boldsymbol{r},t)-\nabla h(\boldsymbol{r},t)\cdot\boldsymbol{k_0}\right]\mathrm{e}^{i(\boldsymbol{k_0}\cdot\boldsymbol{r}-\omega_0 t)}\\&-\int_{\omega}\iint_{\boldsymbol{k}}\left(\rho_1 q_k^{(1)}\right)^{-1/2}\left[q_k^{(1)}S_1^{11}+S_0^{11}\left(\nabla h(\boldsymbol{r},t)\cdot\boldsymbol{k}-i\left(q_k^{(1)}\right)^2 h(\boldsymbol{r},t)\right)\right]\mathrm{e}^{i(\boldsymbol{k}\cdot\boldsymbol{r}-\omega t)}\,d\boldsymbol{k}d\omega \quad (3.111)\\&=\int_{\omega}\iint_{\boldsymbol{k}}\left[S_1^{21}\left(q_k^{(2)}+\beta_X\omega-i\beta_Y\omega^2\right)+S_0^{21}\left\{iq_k^{(2)}h(\boldsymbol{r},t)\left(q_k^{(2)}+\beta_X\omega-i\beta_Y\omega^2\right)-\nabla h(\boldsymbol{r},t)\cdot\boldsymbol{k}\right\}\right]\\&\qquad\times\left(\rho_2 q_k^{(2)}\right)^{-1/2}\mathrm{e}^{i(\boldsymbol{k}\cdot\boldsymbol{r}-\omega t)}\,d\boldsymbol{k}d\omega\end{aligned}$$

An algebraic form of the scattering amplitude is obtained by multiplying $\exp[-i(\boldsymbol{k}'\cdot\boldsymbol{r}-\omega' t)]/(2\pi)^3$ in Eq. (3.111) and integrating with respect to $\boldsymbol{r}$ and t, using S_0^{11}, S_0^{21} from Eqs. (3.108) and (3.109).

$$\begin{aligned}&i\left(1+R_J(\boldsymbol{k_0},\omega_0)\right)(\rho_1 q_0^{(1)})^{-1/2}\left[\left(q_0^{(1)}\right)^2-(\boldsymbol{k}'-\boldsymbol{k_0})\cdot\boldsymbol{k_0}\right]h(\boldsymbol{k}'-\boldsymbol{k_0},\omega'-\omega_0)\\&-(\rho_1 q_{k'}^{(1)})^{-1/2}q_{k'}^{(1)}S_1^{11}(\boldsymbol{k}',\boldsymbol{k_0},\omega',\omega_0)=\\&iD_J(\boldsymbol{k_0},\omega_0)(\rho_2 q_0^{(2)})^{-1/2}\left[q_0^{(2)}\left(q_0^{(2)}+\beta(\omega_0)\right)-(\boldsymbol{k}'-\boldsymbol{k_0})\cdot\boldsymbol{k_0}\right]h(\boldsymbol{k}'-\boldsymbol{k_0},\omega'-\omega_0)\\&+(\rho_2 q_{k'}^{(2)})^{-1/2}\left(q_{k'}^{(2)}+\beta(\omega')\right)S_1^{21}(\boldsymbol{k}',\boldsymbol{k_0},\omega',\omega_0) \quad (3.112)\end{aligned}$$

Pressure continuity has a similar form to Eq. (3.24) by replacing $R(\boldsymbol{k_0},\omega_0)$ and $D(\boldsymbol{k_0},\omega_0)$ with $R_J(\boldsymbol{k_0},\omega_0)$ and $D_J(\boldsymbol{k_0},\omega_0)$, respectively.

$$\rho_1\left[i\omega_0\left(1-R_J(\boldsymbol{k_0},\omega_0)\right)\left(\frac{q_0^{(1)}}{\rho_1}\right)^{1/2} h(\boldsymbol{k'}-\boldsymbol{k_0},\omega'-\omega_0)+\omega'(\rho_1 q_{k'}^{(1)})^{-1/2} S_1^{11}(\boldsymbol{k'},\boldsymbol{k_0},\omega',\omega_0)\right]$$

$$=\rho_2\left[i\omega_0 D_J(\boldsymbol{k_0},\omega_0)\left(\frac{q_0^{(2)}}{\rho_2}\right)^{1/2} h(\boldsymbol{k'}-\boldsymbol{k_0},\omega'-\omega_0)+\omega'(\rho_2 q_{k'}^{(2)})^{-1/2} S_1^{21}(\boldsymbol{k'},\boldsymbol{k_0},\omega',\omega_0)\right] \quad (3.113)$$

Solving for S_1^{11} and S_1^{21} in Eqs. (3.112) and (3.113) yields

$$S_1^{11}(\boldsymbol{k},\boldsymbol{k_0},\omega,\omega_0)=A_J(\boldsymbol{k},\boldsymbol{k_0},\omega,\omega_0)h(\boldsymbol{k}-\boldsymbol{k_0},\omega-\omega_0) \quad (3.114)$$

$$S_1^{21}(\boldsymbol{k},\boldsymbol{k_0},\omega,\omega_0)=B_J(\boldsymbol{k},\boldsymbol{k_0},\omega,\omega_0)h(\boldsymbol{k}-\boldsymbol{k_0},\omega-\omega_0) \quad (3.115)$$

where

$$A_J(\boldsymbol{k},\boldsymbol{k_0},\omega,\omega_0)=\frac{(q_k^{(1)}/\rho_1)^{1/2}\rho_2}{\left[\rho_2 q_k^{(1)}+\rho_1\left(q_k^{(2)}+\beta(\omega)\right)\right]}\times$$

$$\left[i\rho_1\left(1+R_J(\boldsymbol{k_0},\omega_0)\right)(\rho_1 q_0^{(1)})^{-1/2}\left\{\left(\frac{\omega_0}{c_1}\right)^2-\boldsymbol{k}\cdot\boldsymbol{k_0}\right\}\right.$$

$$-i\rho_1 D_J(\boldsymbol{k_0},\omega_0)(\rho_2 q_0^{(2)})^{-1/2}\left\{\left(\frac{\omega_0}{c_2}\right)^2-\boldsymbol{k}\cdot\boldsymbol{k_0}+q_0^{(2)}\beta(\omega_0)\right\}$$

$$\left.+iq_k^{(1)}\frac{\omega_0}{\omega}\left\{\left(1-R_J(\boldsymbol{k_0},\omega_0)\right)\left(\rho_1 q_0^{(1)}\right)^{1/2}-D_J(\boldsymbol{k_0},\omega_0)\left(\rho_2 q_0^{(2)}\right)^{1/2}\right\}\right]$$

$$+\frac{i\omega_0}{\omega}\left(\frac{q_k^{(1)}}{\rho_1}\right)^{1/2}\left[D_J(\boldsymbol{k_0},\omega_0)\left(\rho_2 q_0^{(2)}\right)^{1/2}-\left(1-R_J(\boldsymbol{k_0},\omega_0)\right)\left(\rho_1 q_0^{(1)}\right)^{1/2}\right]$$

$$B_J(\boldsymbol{k},\boldsymbol{k_0},\omega,\omega_0)=\frac{i(\rho_2 q_k^{(2)})^{1/2}}{\left[\rho_2 q_k^{(1)}+\rho_1\left(q_k^{(2)}+\beta(\omega)\right)\right]}\times$$

$$\left[\rho_1\left(1+R_J(\boldsymbol{k_0},\omega_0)\right)(\rho_1 q_0^{(1)})^{-1/2}\left\{\left(\frac{\omega_0}{c_1}\right)^2-\boldsymbol{k}\cdot\boldsymbol{k_0}\right\}\right.$$

$$-\rho_1 D_J(\boldsymbol{k_0},\omega_0)(\rho_2 q_0^{(2)})^{-1/2}\left\{\left(\frac{\omega_0}{c_2}\right)^2-\boldsymbol{k}\cdot\boldsymbol{k_0}+q_0^{(2)}\beta(\omega_0)\right\}$$

$$\left.+q_k^{(1)}\frac{\omega_0}{\omega}\left\{\left(1-R_J(\boldsymbol{k_0},\omega_0)\right)\left(\rho_1 q_0^{(1)}\right)^{1/2}-D_J(\boldsymbol{k_0},\omega_0)\left(\rho_2 q_0^{(2)}\right)^{1/2}\right\}\right]$$

The forms of $R_J(\boldsymbol{k_0},\omega_0)$ and $D_J(\boldsymbol{k_0},\omega_0)$ in Eqs. (3.108) and (3.109) are used to yield the final forms of A_J and B_J.

$$A_J(\boldsymbol{k},\boldsymbol{k_0},\omega,\omega_0)=\frac{2i(q_0^{(1)}q_k^{(1)})^{1/2}}{\left[\rho_2 q_0^{(1)}+\rho_1\left(q_0^{(2)}+\beta(\omega_0)\right)\right]\left[\rho_2 q_k^{(1)}+\rho_1\left(q_k^{(2)}+\beta(\omega)\right)\right]}\times$$
$$\left[\frac{\omega_0}{\omega}\rho_1\left(q_k^{(2)}+\beta(\omega)\right)\left\{(\rho_2-\rho_1)q_0^{(2)}-\rho_1\beta(\omega_0)\right\}+\rho_2\alpha_J(\boldsymbol{k},\boldsymbol{k_0},\omega_0)\right] \tag{3.116}$$

$$B_J(\boldsymbol{k},\boldsymbol{k_0},\omega,\omega_0)=\frac{2i(\rho_1\rho_2 q_0^{(1)}q_k^{(2)})^{1/2}}{\left[\rho_2 q_0^{(1)}+\rho_1\left(q_0^{(2)}+\beta(\omega_0)\right)\right]\left[\rho_2 q_k^{(1)}+\rho_1\left(q_k^{(2)}+\beta(\omega)\right)\right]}\times$$
$$\left[-\frac{\omega_0}{\omega}q_k^{(1)}\left\{(\rho_2-\rho_1)q_0^{(2)}-\rho_1\beta(\omega_0)\right\}+\alpha_J(\boldsymbol{k},\boldsymbol{k_0},\omega_0)\right] \tag{3.117}$$

$$\alpha_J(\boldsymbol{k},\boldsymbol{k_0},\omega_0)=\rho_2\left\{\left(\frac{\omega_0}{c_1}\right)^2-\boldsymbol{k}\cdot\boldsymbol{k_0}\right\}-\rho_1\left\{\left(\frac{\omega_0}{c_2}\right)^2-\boldsymbol{k}\cdot\boldsymbol{k_0}+q_0^{(2)}\beta(\omega_0)\right\} \tag{3.118}$$

Note that A_J and B_J reduce to A and B in Eqs. (3.30) and (3.31), respectively, by setting $\beta=0$. Second order approximation of scattering amplitude, $S_2^{N_1N_2}$, can be obtained by collecting the terms of $O(h^2)$ in Eq. (3.105).

$$\begin{aligned}
&(q_0^{(1)}/\rho_1)^{1/2}\left[-\frac{1}{2}\left(q_0^{(1)}h(\boldsymbol{r},t)\right)^2-\frac{i}{2}\nabla h^2(\boldsymbol{r},t)\cdot\boldsymbol{k_0}-\frac{1}{2}|\nabla h|^2\right]\mathrm{e}^{i(\boldsymbol{k_0}\cdot\boldsymbol{r}-\omega_0 t)}\\
&-\int_{\omega}\iint_{\boldsymbol{k}}(q_k^{(1)}/\rho_1)^{1/2}\left[S_0^{11}\left\{-\frac{1}{2}\left(q_k^{(1)}h(\boldsymbol{r},t)\right)^2-\frac{i}{2}\nabla h^2(\boldsymbol{r},t)\cdot\boldsymbol{k}-\frac{1}{2}|\nabla h|^2\right\}\right.\\
&\qquad\left.+S_1^{11}\left\{-iq_k^{(1)}h(\boldsymbol{r},t)+\frac{\nabla h(\boldsymbol{r},t)\cdot\boldsymbol{k}}{q_k^{(1)}}\right\}+S_2^{11}\right]\mathrm{e}^{i(\boldsymbol{k}\cdot\boldsymbol{r}-\omega t)}\,d\boldsymbol{k}d\omega\\
&=\int_{\omega}\iint_{\boldsymbol{k}}(q_k^{(2)}/\rho_2)^{1/2}\left[S_0^{21}\left\{-\frac{1}{2}\left(1+\frac{\beta(\omega)}{q_k^{(2)}}\right)\left(q_k^{(2)}h(\boldsymbol{r},t)\right)^2-\frac{i}{2}\nabla h^2(\boldsymbol{r},t)\cdot\boldsymbol{k}-\frac{1}{2}|\nabla h|^2\right\}\right.\\
&\qquad\left.+S_1^{21}\left\{i\left(q_k^{(2)}+\beta(\omega)\right)h(\boldsymbol{r},t)-\frac{\nabla h(\boldsymbol{r},t)\cdot\boldsymbol{k}}{q_k^{(2)}}\right\}+\left(1+\frac{\beta(\omega)}{q_k^{(2)}}\right)S_2^{21}\right]\mathrm{e}^{i(\boldsymbol{k}\cdot\boldsymbol{r}-\omega t)}\,d\boldsymbol{k}d\omega
\end{aligned} \tag{3.119}$$

Substituting into the above equation the solutions of S_0^{11}, S_0^{21}, S_1^{11}, and S_1^{21} from Eqs. (3.108), (3.109), (3.114), (3.115), respectively, leads to

$$
\begin{aligned}
&-\frac{(q_0^{(1)}/\rho_1)^{1/2}}{2}\left(1-R_J(\boldsymbol{k}_0,\omega_0)\right)\left[\left(q_0^{(1)}h(\boldsymbol{r},t)\right)^2+i\nabla h^2(\boldsymbol{r},t)\cdot\boldsymbol{k}_0+\left|\nabla h\right|^2\right]\mathrm{e}^{i(\boldsymbol{k}_0\cdot\boldsymbol{r}-\omega_0 t)}\\
&-\int_{\omega}\iint_{\boldsymbol{k}}(q_k^{(1)}/\rho_1)^{1/2}\left[A_J(\boldsymbol{k},\boldsymbol{k}_0,\omega,\omega_0)h(\boldsymbol{k}-\boldsymbol{k}_0,\omega-\omega_0)\left\{-iq_k^{(1)}h(\boldsymbol{r},t)+\frac{\nabla h(\boldsymbol{r},t)\cdot\boldsymbol{k}}{q_k^{(1)}}\right\}\right.\\
&\qquad\left.+S_2^{11}(\boldsymbol{k},\boldsymbol{k}_0,\omega,\omega_0)\right]\mathrm{e}^{i(\boldsymbol{k}\cdot\boldsymbol{r}-\omega t)}\,d\boldsymbol{k}d\omega \qquad (3.120)\\
&=-\frac{(q_0^{(2)}/\rho_2)^{1/2}}{2}D_J(\boldsymbol{k}_0,\omega_0)\left[\left(1+\frac{\beta(\omega_0)}{q_0^{(2)}}\right)\left(q_0^{(2)}h(\boldsymbol{r},t)\right)^2+i\nabla h^2(\boldsymbol{r},t)\cdot\boldsymbol{k}_0+\left|\nabla h\right|^2\right]\mathrm{e}^{i(\boldsymbol{k}_0\cdot\boldsymbol{r}-\omega_0 t)}\\
&+\int_{\omega}\iint_{\boldsymbol{k}}(q_k^{(2)}/\rho_2)^{1/2}\left[B_J(\boldsymbol{k},\boldsymbol{k}_0,\omega,\omega_0)h(\boldsymbol{k}-\boldsymbol{k}_0,\omega-\omega_0)\left\{i\left(q_k^{(2)}+\beta(\omega)\right)h(\boldsymbol{r},t)-\frac{\nabla h(\boldsymbol{r},t)\cdot\boldsymbol{k}}{q_k^{(2)}}\right\}\right.\\
&\qquad\left.+\left(1+\frac{\beta(\omega)}{q_k^{(2)}}\right)S_2^{21}(\boldsymbol{k},\boldsymbol{k}_0,\omega,\omega_0)\right]\mathrm{e}^{i(\boldsymbol{k}\cdot\boldsymbol{r}-\omega t)}\,d\boldsymbol{k}d\omega
\end{aligned}
$$

The next step is to multiply Eq. (3.120) by $\exp[-i(\boldsymbol{k}'\cdot\boldsymbol{r}-\omega' t)]/(2\pi)^3$ and integrate with respect to $\boldsymbol{r}$ and t. Then $\nabla h^2(\boldsymbol{r},t)$ can be replaced by $i(\boldsymbol{k}'-\boldsymbol{k}_0)h^2(\boldsymbol{r},t)$ using $\boldsymbol{a}=\mathrm{e}^{-i(\boldsymbol{k}'-\boldsymbol{k}_0)\cdot\boldsymbol{r}}\boldsymbol{k}_0$ from Eq. (3.27) and, similarly, $\nabla h(\boldsymbol{r},t)$ in $\nabla h(\boldsymbol{r},t)\cdot\boldsymbol{k}$ can be replaced by $i(\boldsymbol{k}'-\boldsymbol{k})h(\boldsymbol{r},t)$ using $\boldsymbol{a}=\mathrm{e}^{-i(\boldsymbol{k}'-\boldsymbol{k})\cdot\boldsymbol{r}}\boldsymbol{k}$. Expressing the terms including $\left|\nabla h\right|^2$ in terms of h^2 requires a different approach, using the following procedure:

$$
\begin{aligned}
&\frac{1}{(2\pi)^3}\iint_{\boldsymbol{r}}\int_{t}\left|\nabla h(\boldsymbol{r},t)\right|^2\mathrm{e}^{-i[(\boldsymbol{k}'-\boldsymbol{k}_0)\cdot\boldsymbol{r}-(\omega'-\omega_0)t]}\,dtd\boldsymbol{r}\\
&=\frac{1}{(2\pi)^3}\iint_{\boldsymbol{r}}\int_{t}\left(\iint_{\boldsymbol{k}_1}\int_{\omega_1}ih(\boldsymbol{k}_1,\omega_1)\boldsymbol{k}_1\,\mathrm{e}^{i(\boldsymbol{k}_1\cdot\boldsymbol{r}-\omega_1 t)}\,d\omega_1 d\boldsymbol{k}_1\right)\cdot\left(\iint_{\boldsymbol{k}_2}\int_{\omega_2}ih(\boldsymbol{k}_2,\omega_2)\boldsymbol{k}_2\,\mathrm{e}^{i(\boldsymbol{k}_2\cdot\boldsymbol{r}-\omega_2 t)}\,d\omega_2 d\boldsymbol{k}_2\right)\\
&\qquad\times\mathrm{e}^{-i[(\boldsymbol{k}'-\boldsymbol{k}_0)\cdot\boldsymbol{r}-(\omega'-\omega_0)t]}\,dtd\boldsymbol{r}\\
&=-\iint_{\boldsymbol{k}_1}\int_{\omega_1}\iint_{\boldsymbol{k}_2}\int_{\omega_2}\boldsymbol{k}_1\cdot\boldsymbol{k}_2h(\boldsymbol{k}_1,\omega_1)h(\boldsymbol{k}_2,\omega_2)\delta(\boldsymbol{k}_1+\boldsymbol{k}_2-\boldsymbol{k}'+\boldsymbol{k}_0)\delta(\omega_1+\omega_2-\omega'+\omega_0)d\omega_2 d\boldsymbol{k}_2 d\omega_1 d\boldsymbol{k}_1\\
&=-\iint_{\boldsymbol{k}_1}\int_{\omega_1}\boldsymbol{k}_1\cdot(\boldsymbol{k}'-\boldsymbol{k}_0-\boldsymbol{k}_1)h(\boldsymbol{k}'-\boldsymbol{k}_0-\boldsymbol{k}_1,\omega'-\omega_0-\omega_1)h(\boldsymbol{k}_1,\omega_1)d\omega_1 d\boldsymbol{k}_1
\end{aligned}
$$

($\boldsymbol{k} = \boldsymbol{k}_0 + \boldsymbol{k}_1$, $\omega = \omega_0 + \omega_1$ yields)

$$= -\iint_{\boldsymbol{k}} \int_{\omega} (\boldsymbol{k}' - \boldsymbol{k}) \cdot (\boldsymbol{k} - \boldsymbol{k}_0) h(\boldsymbol{k}' - \boldsymbol{k}, \omega' - \omega) h(\boldsymbol{k} - \boldsymbol{k}_0, \omega - \omega_0) d\omega d\boldsymbol{k} \tag{3.121}$$

The first equality was obtained writing the gradient of h in Eq. (3.44) as $\nabla h(\boldsymbol{r}, t) = \iint_{\boldsymbol{k}} \int_{\omega} i\boldsymbol{k} h(\boldsymbol{k}, \omega) \mathrm{e}^{i(\boldsymbol{k}\cdot\boldsymbol{r} - \omega t)} \, d\omega d\boldsymbol{k}$. Then it follows from Eqs. (3.45) and (3.121) that Eq. (3.120) can be written as:

$$\begin{aligned}
&(q_{k'}^{(1)} / \rho_1)^{1/2} S_2^{11}(\boldsymbol{k}', \boldsymbol{k}_0, \omega', \omega_0) + (q_{k'}^{(2)} / \rho_2)^{1/2} \left(1 + \frac{\beta(\omega')}{q_{k'}^{(2)}}\right) S_2^{21}(\boldsymbol{k}', \boldsymbol{k}_0, \omega', \omega_0) \\
&= \int_{\omega} \iint_{\boldsymbol{k}} B_2^J(\boldsymbol{k}, \boldsymbol{k}_0, \boldsymbol{k}', \omega, \omega_0) h(\boldsymbol{k}' - \boldsymbol{k}, \omega' - \omega) h(\boldsymbol{k} - \boldsymbol{k}_0, \omega - \omega_0) d\boldsymbol{k} d\omega
\end{aligned} \tag{3.122}$$

where

$$\begin{aligned}
&B_2^J(\boldsymbol{k}, \boldsymbol{k}_0, \boldsymbol{k}', \omega, \omega_0) = \\
&-\frac{(q_0^{(1)} / \rho_1)^{1/2}}{2} \left(1 - R_J(\boldsymbol{k}_0, \omega_0)\right) \left[\left(q_0^{(1)}\right)^2 - (\boldsymbol{k}' - \boldsymbol{k}_0) \cdot \boldsymbol{k}_0 - (\boldsymbol{k}' - \boldsymbol{k}) \cdot (\boldsymbol{k} - \boldsymbol{k}_0) \right] \\
&+\frac{(q_0^{(2)} / \rho_2)^{1/2}}{2} D_J(\boldsymbol{k}_0, \omega_0) \left[\left(1 + \frac{\beta(\omega_0)}{q_0^{(2)}}\right) \left(q_0^{(2)}\right)^2 - (\boldsymbol{k}' - \boldsymbol{k}_0) \cdot \boldsymbol{k}_0 - (\boldsymbol{k}' - \boldsymbol{k}) \cdot (\boldsymbol{k} - \boldsymbol{k}_0) \right] \\
&+i(\rho_1 q_k^{(1)})^{-1/2} \left[\left(q_k^{(1)}\right)^2 - (\boldsymbol{k}' - \boldsymbol{k}) \cdot \boldsymbol{k} \right] A_J(\boldsymbol{k}, \boldsymbol{k}_0, \omega, \omega_0) \\
&-i(\rho_2 q_k^{(2)})^{-1/2} \left[q_k^{(2)} \left(q_k^{(2)} + \beta(\omega)\right) - (\boldsymbol{k}' - \boldsymbol{k}) \cdot \boldsymbol{k} \right] B_J(\boldsymbol{k}, \boldsymbol{k}_0, \omega, \omega_0)
\end{aligned}$$

$$\begin{aligned}
&= \frac{\left(\rho_1 q_0^{(1)}\right)^{1/2} \left[\left(q_0^{(2)} + \beta(\omega_0)\right) \left\{ \left(\frac{\omega_0}{c_2}\right)^2 - \left(\frac{\omega_0}{c_1}\right)^2 \right\} + \beta(\omega_0) \{ \boldsymbol{k} \cdot (\boldsymbol{k}' - \boldsymbol{k}) + \boldsymbol{k}_0 \cdot (\boldsymbol{k} - \boldsymbol{k}_0) \} \right]}{\rho_2 q_0^{(1)} + \rho_1 \left(q_0^{(2)} + \beta(\omega_0)\right)} \\
&+i(\rho_1 q_k^{(1)})^{-1/2} \left[\left(\frac{\omega}{c_1}\right)^2 - \boldsymbol{k}' \cdot \boldsymbol{k} \right] A_J(\boldsymbol{k}, \boldsymbol{k}_0, \omega, \omega_0) \\
&-i(\rho_2 q_k^{(2)})^{-1/2} \left[\left(\frac{\omega}{c_2}\right)^2 - \boldsymbol{k}' \cdot \boldsymbol{k} + \beta(\omega) q_k^{(2)} \right] B_J(\boldsymbol{k}, \boldsymbol{k}_0, \omega, \omega_0)
\end{aligned} \tag{3.123}$$

where the solutions of $R_J(\boldsymbol{k}, \omega)$ and $D_J(\boldsymbol{k}, \omega)$ in Eqs. (3.108) and (3.109) were used.

Note that, by setting $\beta = 0$ (no jump condition), the terms including $(\boldsymbol{k}' - \boldsymbol{k}) \cdot (\boldsymbol{k} - \boldsymbol{k_0})$ in the first equality in Eq. (3.123), which result from $|\nabla h|^2$, vanish and B_2^J reduces to B_2 obtained from continuity condition in Eq. (3.52). Pressure continuity condition from Eq. (3.49) also yields an algebraic equation of S_2^{11} and S_2^{21} by replacing A_2 with A_2^J.

$$
\begin{aligned}
&(\rho_1 / q_{k'}^{(1)})^{1/2} S_2^{11}(\boldsymbol{k}', \boldsymbol{k_0}, \omega', \omega_0) - (\rho_2 / q_{k'}^{(2)})^{1/2} S_2^{21}(\boldsymbol{k}', \boldsymbol{k_0}, \omega', \omega_0) \\
&= \int_{\omega} \iint_{\boldsymbol{k}} A_2^J(\boldsymbol{k}, \boldsymbol{k_0}, \omega, \omega_0, \omega') h(\boldsymbol{k}' - \boldsymbol{k}, \omega' - \omega) h(\boldsymbol{k} - \boldsymbol{k_0}, \omega - \omega_0) d\boldsymbol{k} d\omega
\end{aligned} \tag{3.124}
$$

where

$$
\begin{aligned}
&A_2^J(\boldsymbol{k}, \boldsymbol{k_0}, \omega, \omega_0, \omega') \\
&= \frac{\omega_0}{2\omega'} \left[\left(1 + R_J(\boldsymbol{k_0}, \omega_0)\right) (\rho_1 q_0^{(1)})^{1/2} q_0^{(1)} - D_J(\boldsymbol{k_0}, \omega_0) (\rho_2 q_0^{(2)})^{1/2} q_0^{(2)} \right] \\
&+ i \frac{\omega}{\omega'} \left[(\rho_1 q_k^{(1)})^{1/2} A_J(\boldsymbol{k}, \boldsymbol{k_0}, \omega, \omega_0) + (\rho_2 q_k^{(2)})^{1/2} B_J(\boldsymbol{k}, \boldsymbol{k_0}, \omega, \omega_0) \right] \\
&= \frac{\omega_0}{\omega'} \frac{(\rho_1 q_0^{(1)})^{1/2} \rho_2}{\rho_2 q_0^{(1)} + \rho_1 \left(q_0^{(2)} + \beta(\omega_0) \right)} \left[\left(\frac{\omega_0}{c_1} \right)^2 - \left(\frac{\omega_0}{c_2} \right)^2 \right] \\
&+ i \frac{\omega}{\omega'} \left[(\rho_1 q_k^{(1)})^{1/2} A_J(\boldsymbol{k}, \boldsymbol{k_0}, \omega, \omega_0) + (\rho_2 q_k^{(2)})^{1/2} B_J(\boldsymbol{k}, \boldsymbol{k_0}, \omega, \omega_0) \right]
\end{aligned} \tag{3.125}
$$

Note that A_2^J above reduces to A_2 obtained from continuity condition in Eq. (3.51). Solving for S_2^{11} and S_2^{21} in Eqs. (3.122) and (3.124) and changing $\boldsymbol{k}' \to \boldsymbol{k}$ and $\omega' \to \omega$ yields:

$$
\begin{aligned}
\begin{Bmatrix} S_2^{11}(\boldsymbol{k}, \boldsymbol{k_0}, \omega, \omega_0) \\ S_2^{21}(\boldsymbol{k}, \boldsymbol{k_0}, \omega, \omega_0) \end{Bmatrix} &= \frac{\left(\rho_1 \rho_2 q_k^{(1)} q_k^{(2)} \right)^{1/2}}{\rho_2 q_k^{(1)} + \rho_1 \left(q_k^{(2)} + \beta(\omega) \right)} \begin{bmatrix} \left(1 + \dfrac{\beta(\omega)}{q_k^{(2)}} \right) (q_k^{(2)} / \rho_2)^{1/2} & (\rho_2 / q_k^{(2)})^{1/2} \\ -(q_k^{(1)} / \rho_1)^{1/2} & (\rho_1 / q_k^{(1)})^{1/2} \end{bmatrix} \\
&\times \begin{Bmatrix} \displaystyle\int_{\omega'} \iint_{\boldsymbol{k}'} A_2^J(\boldsymbol{k}', \boldsymbol{k_0}, \omega', \omega_0, \omega) h(\boldsymbol{k} - \boldsymbol{k}', \omega - \omega') h(\boldsymbol{k}' - \boldsymbol{k_0}, \omega' - \omega_0) d\boldsymbol{k}' d\omega' \\ \displaystyle\int_{\omega'} \iint_{\boldsymbol{k}'} B_2^J(\boldsymbol{k}', \boldsymbol{k_0}, \boldsymbol{k}, \omega', \omega_0) h(\boldsymbol{k} - \boldsymbol{k}', \omega - \omega') h(\boldsymbol{k}' - \boldsymbol{k_0}, \omega' - \omega_0) d\boldsymbol{k}' d\omega' \end{Bmatrix}
\end{aligned} \tag{3.126}
$$

$$= \frac{\left(\rho_1\rho_2 q_k^{(1)} q_k^{(2)}\right)^{1/2}}{\rho_2 q_k^{(1)} + \rho_1\left(q_k^{(2)} + \beta(\omega)\right)} \begin{Bmatrix} \int_{\omega'}\iint_{\boldsymbol{k}'} F_J(\boldsymbol{k}', \boldsymbol{k}_0, \boldsymbol{k}, \omega', \omega_0, \omega) h(\boldsymbol{k}-\boldsymbol{k}', \omega-\omega') h(\boldsymbol{k}'-\boldsymbol{k}_0, \omega'-\omega_0) d\boldsymbol{k}' d\omega' \\ \int_{\omega'}\iint_{\boldsymbol{k}'} G_J(\boldsymbol{k}', \boldsymbol{k}_0, \boldsymbol{k}, \omega', \omega_0, \omega) h(\boldsymbol{k}-\boldsymbol{k}', \omega-\omega') h(\boldsymbol{k}'-\boldsymbol{k}_0, \omega'-\omega_0) d\boldsymbol{k}' d\omega' \end{Bmatrix}$$

where

$$F_J(\boldsymbol{k}', \boldsymbol{k}_0, \boldsymbol{k}, \omega', \omega_0, \omega) = \left(1 + \frac{\beta(\omega)}{q_k^{(2)}}\right)(q_k^{(2)}/\rho_2)^{1/2} A_2^J(\boldsymbol{k}', \boldsymbol{k}_0, \omega', \omega_0, \omega) + (\rho_2/q_k^{(2)})^{1/2} B_2^J(\boldsymbol{k}', \boldsymbol{k}_0, \boldsymbol{k}, \omega', \omega_0) \tag{3.127}$$

$$G_J(\boldsymbol{k}', \boldsymbol{k}_0, \boldsymbol{k}, \omega', \omega_0, \omega) = -(q_k^{(1)}/\rho_1)^{1/2} A_2^J(\boldsymbol{k}', \boldsymbol{k}_0, \omega', \omega_0, \omega) + (\rho_1/q_k^{(1)})^{1/2} B_2^J(\boldsymbol{k}', \boldsymbol{k}_0, \boldsymbol{k}, \omega', \omega_0) \tag{3.128}$$

A_2^J and B_2^J in Eqs. (3.125) and (3.123), whose arguments are exchanged by $\boldsymbol{k}' \leftrightarrow \boldsymbol{k}$ and $\omega' \leftrightarrow \omega$, are substituted into Eqs. (3.127) and (3.128) to yield F_J and G_J in terms of first order scattering amplitudes A_J and B_J.

$$\begin{aligned} F_J(\boldsymbol{k}', \boldsymbol{k}_0, \boldsymbol{k}, \omega', \omega_0, \omega) &= \frac{(\rho_1\rho_2 q_0^{(1)}/q_k^{(2)})^{1/2}}{\rho_2 q_0^{(1)} + \rho_1\left(q_0^{(2)} + \beta(\omega_0)\right)} \times \\ &\left\{\left[\left(\frac{\omega_0}{c_1}\right)^2 - \left(\frac{\omega_0}{c_2}\right)^2\right]\left[\frac{\omega_0}{\omega}\left(q_k^{(2)} + \beta(\omega)\right) - \left(q_0^{(2)} + \beta(\omega_0)\right)\right] + \beta(\omega_0)\left[\boldsymbol{k}' \cdot (\boldsymbol{k}-\boldsymbol{k}') + \boldsymbol{k}_0 \cdot (\boldsymbol{k}'-\boldsymbol{k}_0)\right]\right\} \\ &+ \frac{i}{\left(q_k^{(2)}\right)^{1/2}}\left\{\frac{\omega'}{\omega}\left(\frac{\rho_1 q_{k'}^{(1)}}{\rho_2}\right)^{1/2}\left(q_k^{(2)} + \beta(\omega)\right) + \left(\frac{\rho_2}{\rho_1 q_{k'}^{(1)}}\right)^{1/2}\left[\left(\frac{\omega'}{c_1}\right)^2 - \boldsymbol{k}' \cdot \boldsymbol{k}\right]\right\} A_J(\boldsymbol{k}', \boldsymbol{k}_0, \omega', \omega_0) \\ &+ \frac{i}{\left(q_k^{(2)}\right)^{1/2}}\left\{\frac{\omega'}{\omega}\left(q_{k'}^{(2)}\right)^{1/2}\left(q_k^{(2)} + \beta(\omega)\right) - \left(q_{k'}^{(2)}\right)^{-1/2}\left[\left(\frac{\omega'}{c_2}\right)^2 - \boldsymbol{k}' \cdot \boldsymbol{k} + \beta(\omega') q_{k'}^{(2)}\right]\right\} B_J(\boldsymbol{k}', \boldsymbol{k}_0, \omega', \omega_0) \end{aligned} \tag{3.129}$$

$$\begin{aligned} G_J(\boldsymbol{k}', \boldsymbol{k}_0, \boldsymbol{k}, \omega', \omega_0, \omega) &= \frac{-(q_0^{(1)}/q_k^{(1)})^{1/2}}{\rho_2 q_0^{(1)} + \rho_1\left(q_0^{(2)} + \beta(\omega_0)\right)} \times \\ &\left\{\left[\left(\frac{\omega_0}{c_1}\right)^2 - \left(\frac{\omega_0}{c_2}\right)^2\right]\left[\frac{\omega_0}{\omega}\rho_2 q_k^{(1)} + \rho_1\left(q_0^{(2)} + \beta(\omega_0)\right)\right] - \rho_1\beta(\omega_0)\left[\boldsymbol{k}' \cdot (\boldsymbol{k}-\boldsymbol{k}') + \boldsymbol{k}_0 \cdot (\boldsymbol{k}'-\boldsymbol{k}_0)\right]\right\} \end{aligned}$$

$$+i\left\{-\frac{\omega'}{\omega}\left(q_k^{(1)}q_{k'}^{(1)}\right)^{1/2}+\left(q_k^{(1)}q_{k'}^{(1)}\right)^{-1/2}\left[\left(\frac{\omega'}{c_1}\right)^2-\boldsymbol{k}'\cdot\boldsymbol{k}\right]\right\}A_J(\boldsymbol{k}',\boldsymbol{k_0},\omega',\omega_0)$$

$$-i\left\{\frac{\omega'}{\omega}\left(\frac{\rho_2}{\rho_1}q_k^{(1)}q_{k'}^{(2)}\right)^{1/2}+\left(\frac{\rho_2}{\rho_1}q_k^{(1)}q_{k'}^{(2)}\right)^{-1/2}\left[\left(\frac{\omega'}{c_2}\right)^2-\boldsymbol{k}'\cdot\boldsymbol{k}+\beta(\omega')q_{k'}^{(2)}\right]\right\}B_J(\boldsymbol{k}',\boldsymbol{k_0},\omega',\omega_0) \tag{3.130}$$

The scattering amplitude up to 2nd order of flame front height can now be written as, by combining Eqs. (3.108), (3.109), (3.114), (3.115), and (3.126).

$$\begin{aligned}
&S^{11}(\boldsymbol{k},\boldsymbol{k_0},\omega,\omega_0)\\
&=\sum_{n=0}^{2}S_n^{11}(\boldsymbol{k},\boldsymbol{k_0},\omega,\omega_0)+O(h^3)\\
&=R_J(\boldsymbol{k},\omega)\delta(\boldsymbol{k}-\boldsymbol{k_0})\delta(\omega-\omega_0)+A_J(\boldsymbol{k},\boldsymbol{k_0},\omega,\omega_0)h(\boldsymbol{k}-\boldsymbol{k_0},\omega-\omega_0)\\
&+\frac{1}{2}D_J(\boldsymbol{k},\omega)\int_{\omega'}\iint_{\boldsymbol{k}'}F_J(\boldsymbol{k}',\boldsymbol{k_0},\boldsymbol{k},\omega',\omega_0,\omega)h(\boldsymbol{k}-\boldsymbol{k}',\omega-\omega')h(\boldsymbol{k}'-\boldsymbol{k_0},\omega'-\omega_0)d\boldsymbol{k}'d\omega'
\end{aligned} \tag{3.131}$$

$$\begin{aligned}
&S^{21}(\boldsymbol{k},\boldsymbol{k_0},\omega,\omega_0)\\
&=\sum_{n=0}^{2}S_n^{21}(\boldsymbol{k},\boldsymbol{k_0},\omega,\omega_0)+O(h^3)\\
&=D_J(\boldsymbol{k},\omega)\delta(\boldsymbol{k}-\boldsymbol{k_0})\delta(\omega-\omega_0)+B_J(\boldsymbol{k},\boldsymbol{k_0},\omega,\omega_0)h(\boldsymbol{k}-\boldsymbol{k_0},\omega-\omega_0)\\
&+\frac{1}{2}D_J(\boldsymbol{k},\omega)\int_{\omega'}\iint_{\boldsymbol{k}'}G_J(\boldsymbol{k}',\boldsymbol{k_0},\boldsymbol{k},\omega',\omega_0,\omega)h(\boldsymbol{k}-\boldsymbol{k}',\omega-\omega')h(\boldsymbol{k}'-\boldsymbol{k_0},\omega'-\omega_0)d\boldsymbol{k}'d\omega'
\end{aligned} \tag{3.132}$$

The velocity potential in medium (1) and (2) from Eqs. (2.18) and (2.20) can be similarly expressed as:

$$\begin{aligned}
&\frac{\psi_c^{(1)}(\vec{\boldsymbol{R}},t)}{A_1}=(\rho_1q_0^{(1)})^{-1/2}\,\mathrm{e}^{i(\boldsymbol{k_0}\cdot\boldsymbol{r}+q_0^{(1)}z-\omega_0t)}+(\rho_1q_0^{(1)})^{-1/2}R_J(\boldsymbol{k_0},\omega_0)\,\mathrm{e}^{i(\boldsymbol{k_0}\cdot\boldsymbol{r}-q_0^{(1)}z-\omega_0t)}\\
&+\int_{\omega}\iint_{\boldsymbol{k}}(\rho_1q_k^{(1)})^{-1/2}A_J(\boldsymbol{k},\boldsymbol{k_0},\omega,\omega_0)h(\boldsymbol{k}-\boldsymbol{k_0},\omega-\omega_0)\,\mathrm{e}^{i(\boldsymbol{k}\cdot\boldsymbol{r}-q_k^{(1)}z-\omega t)}\,d\boldsymbol{k}d\omega\\
&+\frac{1}{2}\int_{\omega}\iint_{\boldsymbol{k}}(\rho_1q_k^{(1)})^{-1/2}D_J(\boldsymbol{k},\omega)\,\mathrm{e}^{i(\boldsymbol{k}\cdot\boldsymbol{r}-q_k^{(1)}z-\omega t)}\times\\
&\qquad\left[\int_{\omega'}\iint_{\boldsymbol{k}'}F_J(\boldsymbol{k}',\boldsymbol{k_0},\boldsymbol{k},\omega',\omega_0,\omega)h(\boldsymbol{k}-\boldsymbol{k}',\omega-\omega')h(\boldsymbol{k}'-\boldsymbol{k_0},\omega'-\omega_0)d\boldsymbol{k}'d\omega'\right]d\boldsymbol{k}d\omega
\end{aligned} \tag{3.133}$$

$$\frac{\psi_c^{(2)}(\vec{\boldsymbol{R}},t)}{A_1} = (\rho_2 q_0^{(2)})^{-1/2} D_J(\boldsymbol{k_0},\omega_0)\, \mathrm{e}^{i(\boldsymbol{k_0}\cdot\boldsymbol{r}+q_0^{(2)}z-\omega_0 t)}$$
$$+\int_{\omega}\iint_{\boldsymbol{k}} (\rho_2 q_k^{(2)})^{-1/2} B_J(\boldsymbol{k},\boldsymbol{k_0},\omega,\omega_0) h(\boldsymbol{k}-\boldsymbol{k_0},\omega-\omega_0)\, \mathrm{e}^{i(\boldsymbol{k}\cdot\boldsymbol{r}+q_k^{(2)}z-\omega t)}\, d\boldsymbol{k}d\omega$$
$$+\frac{1}{2}\int_{\omega}\iint_{\boldsymbol{k}} (\rho_2 q_k^{(2)})^{-1/2} D_J(\boldsymbol{k},\omega)\, \mathrm{e}^{i(\boldsymbol{k}\cdot\boldsymbol{r}+q_k^{(2)}z-\omega t)} \times \tag{3.134}$$
$$\left[\int_{\omega'}\iint_{\boldsymbol{k}'} G_J(\boldsymbol{k}',\boldsymbol{k_0},\boldsymbol{k},\omega',\omega_0,\omega) h(\boldsymbol{k}-\boldsymbol{k}',\omega-\omega') h(\boldsymbol{k}'-\boldsymbol{k_0},\omega'-\omega_0) d\boldsymbol{k}'d\omega'\right] d\boldsymbol{k}d\omega$$

where the forms of R_J, D_J, A_J, B_J, F_J, and G_J are found in Eqs. (3.108), (3.109), (3.116), (3.117), (3.129), and (3.130). Dimensionless form of acoustic pressure and velocity fields then follows from substituting the above forms of velocity potential into Eq. (2.3).

In medium (1),

$$\tilde{p}^{(1)}(\vec{\boldsymbol{R}},t) \equiv \frac{p^{(1)}}{|P_1|} = -\frac{\rho_1}{|P_1|}\mathrm{Re}\left[\frac{\partial \psi_c^{(1)}(\vec{\boldsymbol{R}},t)}{\partial t}\right] = \tilde{p}_I^{(1)}(\vec{\boldsymbol{R}},t) + \tilde{p}_R^{(1)}(\vec{\boldsymbol{R}},t) \tag{3.135}$$

where

$$\tilde{p}_I^{(1)}(\vec{\boldsymbol{R}},t) = \mathrm{Re}\left[i\,\mathrm{e}^{i(\boldsymbol{k_0}\cdot\boldsymbol{r}+q_0^{(1)}z-\omega_0 t)}\right]$$
$$\tilde{p}_R^{(1)}(\vec{\boldsymbol{R}},t) = \mathrm{Re}\left[i\int_{\omega}\iint_{\boldsymbol{k}} \frac{\omega}{\omega_0}\left(\frac{q_0^{(1)}}{q_k^{(1)}}\right)^{1/2} S^{11}(\boldsymbol{k},\boldsymbol{k_0},\omega,\omega_0)\, \mathrm{e}^{i(\boldsymbol{k}\cdot\boldsymbol{r}-q_k^{(1)}z-\omega t)}\, d\boldsymbol{k}d\omega\right]$$
$$= \mathrm{Re}\Big\{iR_J(\boldsymbol{k_0},\omega_0)\, \mathrm{e}^{i(\boldsymbol{k_0}\cdot\boldsymbol{r}-q_0^{(1)}z-\omega_0 t)}$$
$$+i\int_{\omega}\iint_{\boldsymbol{k}} \frac{\omega}{\omega_0}(q_0^{(1)}/q_k^{(1)})^{1/2} A_J(\boldsymbol{k},\boldsymbol{k_0},\omega,\omega_0) h(\boldsymbol{k}-\boldsymbol{k_0},\omega-\omega_0)\, \mathrm{e}^{i(\boldsymbol{k}\cdot\boldsymbol{r}-q_k^{(1)}z-\omega t)}\, d\boldsymbol{k}d\omega$$
$$+\frac{i}{2}\int_{\omega}\iint_{\boldsymbol{k}} \frac{\omega}{\omega_0}(q_0^{(1)}/q_k^{(1)})^{1/2} D_J(\boldsymbol{k},\omega)\, \mathrm{e}^{i(\boldsymbol{k}\cdot\boldsymbol{r}-q_k^{(1)}z-\omega t)} \times$$
$$\left[\int_{\omega'}\iint_{\boldsymbol{k}'} F_J(\boldsymbol{k}',\boldsymbol{k_0},\boldsymbol{k},\omega',\omega_0,\omega) h(\boldsymbol{k}-\boldsymbol{k}',\omega-\omega') h(\boldsymbol{k}'-\boldsymbol{k_0},\omega'-\omega_0) d\boldsymbol{k}'d\omega'\right] d\boldsymbol{k}d\omega\Big\}$$

$$\tilde{\vec{\boldsymbol{v}}}^{(1)}(\vec{\boldsymbol{R}},t) \equiv \frac{\vec{\boldsymbol{v}}^{(1)}}{c_1} = \frac{1}{c_1}\mathrm{Re}\left[\vec{\nabla}\psi_c^{(1)}(\vec{\boldsymbol{R}},t)\right] = \tilde{\vec{\boldsymbol{v}}}_I^{(1)}(\vec{\boldsymbol{R}},t) + \tilde{\vec{\boldsymbol{v}}}_R^{(1)}(\vec{\boldsymbol{R}},t) \tag{3.136}$$

where $\tilde{\vec{v}}_I^{(1)}(\vec{R},t) = \dfrac{\varepsilon c_1}{\omega_0}\,\mathrm{Re}\left[i\vec{K}_{0+}^{(1)}\, \mathrm{e}^{i(\boldsymbol{k}_0\cdot\boldsymbol{r}+q_0^{(1)}z-\omega_0 t)} \right]$

$$\tilde{\vec{v}}_R^{(1)}(\vec{R},t) = \frac{\varepsilon c_1}{\omega_0}\,\mathrm{Re}\left[i\int_{\omega}\iint_{\boldsymbol{k}} (q_0^{(1)}/q_k^{(1)})^{1/2} S^{11}(\boldsymbol{k},\boldsymbol{k}_0,\omega,\omega_0)\vec{K}_-^{(1)}\, \mathrm{e}^{i(\boldsymbol{k}\cdot\boldsymbol{r}-q_k^{(1)}z-\omega t)}\, d\boldsymbol{k}d\omega \right]$$

$$= \frac{\varepsilon c_1}{\omega_0}\,\mathrm{Re}\Big\{ iR_J(\boldsymbol{k}_0,\omega_0)\vec{K}_{0-}^{(1)}\, \mathrm{e}^{i(\boldsymbol{k}_0\cdot\boldsymbol{r}-q_0^{(1)}z-\omega_0 t)}$$

$$+ i\int_{\omega}\iint_{\boldsymbol{k}} (q_0^{(1)}/q_k^{(1)})^{1/2} A_J(\boldsymbol{k},\boldsymbol{k}_0,\omega,\omega_0) h(\boldsymbol{k}-\boldsymbol{k}_0,\omega-\omega_0)\vec{K}_-^{(1)}\, \mathrm{e}^{i(\boldsymbol{k}\cdot\boldsymbol{r}-q_k^{(1)}z-\omega t)}\, d\boldsymbol{k}d\omega$$

$$+ \frac{i}{2}\int_{\omega}\iint_{\boldsymbol{k}} (q_0^{(1)}/q_k^{(1)})^{1/2} D_J(\boldsymbol{k},\omega)\vec{K}_-^{(1)}\, \mathrm{e}^{i(\boldsymbol{k}\cdot\boldsymbol{r}-q_k^{(1)}z-\omega t)} \times$$

$$\left[\int_{\omega'}\iint_{\boldsymbol{k}'} F_J(\boldsymbol{k}',\boldsymbol{k}_0,\boldsymbol{k},\omega',\omega_0,\omega) h(\boldsymbol{k}-\boldsymbol{k}',\omega-\omega') h(\boldsymbol{k}'-\boldsymbol{k}_0,\omega'-\omega_0)\, d\boldsymbol{k}'d\omega' \right] d\boldsymbol{k}d\omega \Big\}$$

In medium (2),

$$\tilde{p}^{(2)}(\vec{R},t) \equiv \frac{p^{(2)}}{|P_1|} = -\frac{\rho_2}{|P_1|}\,\mathrm{Re}\left[\frac{\partial \psi_c^{(2)}(\vec{R},t)}{\partial t} \right]$$

$$= \mathrm{Re}\left[i\int_{\omega}\iint_{\boldsymbol{k}} \frac{\omega}{\omega_0}\left(\frac{\rho_2 q_0^{(1)}}{\rho_1 q_k^{(2)}} \right)^{1/2} S^{21}(\boldsymbol{k},\boldsymbol{k}_0,\omega,\omega_0)\, \mathrm{e}^{i(\boldsymbol{k}\cdot\boldsymbol{r}+q_k^{(2)}z-\omega t)}\, d\boldsymbol{k}d\omega \right] \tag{3.137}$$

$$= \mathrm{Re}\Big\{ i\left(\frac{\rho_2 q_0^{(1)}}{\rho_1 q_0^{(2)}} \right)^{1/2} D_J(\boldsymbol{k}_0,\omega_0)\, \mathrm{e}^{i(\boldsymbol{k}_0\cdot\boldsymbol{r}+q_0^{(2)}z-\omega_0 t)}$$

$$+ i\int_{\omega}\iint_{\boldsymbol{k}} \frac{\omega}{\omega_0}\left(\frac{\rho_2 q_0^{(1)}}{\rho_1 q_k^{(2)}} \right)^{1/2} B_J(\boldsymbol{k},\boldsymbol{k}_0,\omega,\omega_0) h(\boldsymbol{k}-\boldsymbol{k}_0,\omega-\omega_0)\, \mathrm{e}^{i(\boldsymbol{k}\cdot\boldsymbol{r}+q_k^{(2)}z-\omega t)}\, d\boldsymbol{k}d\omega$$

$$+ \frac{i}{2}\int_{\omega}\iint_{\boldsymbol{k}} \frac{\omega}{\omega_0}\left(\frac{\rho_2 q_0^{(1)}}{\rho_1 q_k^{(2)}} \right)^{1/2} D_J(\boldsymbol{k},\omega) \times$$

$$\left[\int_{\omega'}\iint_{\boldsymbol{k}'} G_J(\boldsymbol{k}',\boldsymbol{k}_0,\boldsymbol{k},\omega',\omega_0,\omega) h(\boldsymbol{k}-\boldsymbol{k}',\omega-\omega') h(\boldsymbol{k}'-\boldsymbol{k}_0,\omega'-\omega_0)\, d\boldsymbol{k}'d\omega' \right] d\boldsymbol{k}d\omega \Big\}$$

$$\tilde{\vec{v}}_T^{(2)}(\vec{R},t) \equiv \frac{\vec{v}^{(2)}}{c_1} = \frac{1}{c_1}\,\mathrm{Re}\left[\vec{\nabla}\psi_c^{(2)}(\vec{R},t) \right]$$

$$= \frac{\varepsilon c_1}{\omega_0}\,\mathrm{Re}\left[i\int_{\omega}\iint_{\boldsymbol{k}} \left(\frac{\rho_1 q_0^{(1)}}{\rho_2 q_k^{(2)}} \right)^{1/2} S^{21}(\boldsymbol{k},\boldsymbol{k}_0,\omega,\omega_0)\vec{K}_+^{(2)}\, \mathrm{e}^{i(\boldsymbol{k}\cdot\boldsymbol{r}+q_k^{(2)}z-\omega t)}\, d\boldsymbol{k}d\omega \right] \tag{3.138}$$

$$= \frac{\varepsilon c_1}{\omega_0}\left(\frac{\rho_1 q_0^{(1)}}{\rho_2 q_0^{(2)}}\right)^{1/2} \mathrm{Re}\Big\{ iD_J(\boldsymbol{k_0},\omega_0)\vec{\boldsymbol{K}}_{\boldsymbol{0}+}^{(2)}\, \mathrm{e}^{i(\boldsymbol{k_0}\cdot\boldsymbol{r}+q_0^{(2)}z-\omega_0 t)}$$

$$+ i\int_{\omega}\iint_{\boldsymbol{k}} (q_0^{(2)}/q_k^{(2)})^{1/2} B_J(\boldsymbol{k},\boldsymbol{k_0},\omega,\omega_0) h(\boldsymbol{k}-\boldsymbol{k_0},\omega-\omega_0)\vec{\boldsymbol{K}}_{+}^{(2)}\, \mathrm{e}^{i(\boldsymbol{k}\cdot\boldsymbol{r}+q_k^{(2)}z-\omega t)}\, d\boldsymbol{k}d\omega$$

$$+ \frac{i}{2}\int_{\omega}\iint_{\boldsymbol{k}} (q_0^{(2)}/q_k^{(2)})^{1/2} D_J(\boldsymbol{k},\omega)\vec{\boldsymbol{K}}_{+}^{(2)}\, \mathrm{e}^{i(\boldsymbol{k}\cdot\boldsymbol{r}+q_k^{(2)}z-\omega t)} \times$$

$$\left[\int_{\omega'}\iint_{\boldsymbol{k}'} G_J(\boldsymbol{k}',\boldsymbol{k_0},\boldsymbol{k},\omega',\omega_0,\omega) h(\boldsymbol{k}-\boldsymbol{k}',\omega-\omega') h(\boldsymbol{k}'-\boldsymbol{k_0},\omega'-\omega_0) d\boldsymbol{k}'d\omega'\right] d\boldsymbol{k}d\omega\Big\}$$

where $\vec{\boldsymbol{K}}_{\boldsymbol{0}\pm}^{(m)} = \boldsymbol{k_0} \pm q_0^{(m)}\vec{\boldsymbol{e}}_z$, $\vec{\boldsymbol{K}}_{\pm}^{(m)} = \boldsymbol{k} \pm q_k^{(m)}\vec{\boldsymbol{e}}_z$ $(m = \{1,2\})$, $\varepsilon \equiv \left|P_1\right| / (\rho_1 c_1^2)$

3.4 Bragg scattering and Doppler shifted frequency effects

The characteristics, e.g., directivity and frequency, of scattered acoustic fields due to a moving rough surface can be demonstrated in the context of Bragg scattering and Doppler frequency shift. A two-dimensional problem will be illustrated where an incident plane wave of $\boldsymbol{k_0} = (k_0, 0)$ and frequency ω_0 from medium (1) impinges upon a sinusoidal surface propagating in x-direction whose roughness is expressed as:

$$h(\boldsymbol{r},t) = h(x,t) = a\cos(k_S x - \Omega t) \tag{3.139}$$

where $k_S = 2\pi / L$ is surface wave number and L is a period of surface irregularities. The spectral form of roughness is

$$h(\boldsymbol{k},\omega) = \frac{a}{2}[\delta(k_x - k_S)\delta(\omega-\Omega) + \delta(k_x + k_S)\delta(\omega+\Omega)]\delta(k_y) \tag{3.140}$$

$$h(\boldsymbol{k}-\boldsymbol{k_0},\omega-\omega_0) = \frac{a}{2}[\delta(k_x - k_0 - k_S)\delta(\omega-\omega_0-\Omega) + \delta(k_x - k_0 + k_S)\delta(\omega-\omega_0+\Omega)]\delta(k_y)$$

$$h(\boldsymbol{k}-\boldsymbol{k}',\omega-\omega') = \frac{a}{2}[\delta(k_x - k_x' - k_S)\delta(\omega-\omega'-\Omega) + \delta(k_x - k_x' + k_S)\delta(\omega-\omega'+\Omega)]\delta(k_y - k_y')$$

where (k_x, k_y) and (k_x', k_y') are x- and y-component of the wave number $\boldsymbol{k}$ and $\boldsymbol{k}'$, respectively. The next step is to calculate the reflection and transmission coefficients for

both media, i.e., R_J , D_J , A_J , B_J , F_J , and G_J from Eqs. (3.108), (3.109), (3.116), (3.117), (3.129), and (3.130) to evaluate reflected and transmitted scattered pressure fields. The jump condition ($\beta \neq 0$) is still utilized to describe unsteady gas expansion across a wrinkling surface. Then the total pressure field in medium (1) has the form from Eq. (3.135).

$$\begin{aligned}
&\tilde{p}^{(1)}(x,z,t) = \cos\left(k_0 x + q_0^{(1)} z - \omega_0 t + \pi/2\right) \\
&+R_0 \cos\left(k_0 x - q_0^{(1)} z - \omega_0 t + \pi/2\right) \\
&+A_+ \cos\left((k_0 + k_S)x - q_{0+S}^{(1)} z - (\omega_0 + \Omega)t\right) + A_- \cos\left((k_0 - k_S)x - q_{0-S}^{(1)} z - (\omega_0 - \Omega)t\right) \\
&+F_+ \cos\left((k_0 + 2k_S)x - q_{0+2S}^{(1)} z - (\omega_0 + 2\Omega)t + \pi/2\right) + F_0 \cos\left(k_0 x - q_0^{(1)} z - \omega_0 t + \pi/2\right) \\
&+F_- \cos\left((k_0 - 2k_S)x - q_{0-2S}^{(1)} z - (\omega_0 - 2\Omega)t + \pi/2\right)
\end{aligned} \tag{3.141}$$

$$\begin{aligned}
&\tilde{p}^{(2)}(x,z,t) = D_0 \cos\left(k_0 x + q_0^{(2)} z - \omega_0 t + \pi/2\right) \\
&+B_+ \cos\left((k_0 + k_S)x + q_{0+S}^{(2)} z - (\omega_0 + \Omega)t\right) + B_- \cos\left((k_0 - k_S)x + q_{0-S}^{(2)} z - (\omega_0 - \Omega)t\right) \\
&+G_+ \cos\left((k_0 + 2k_S)x + q_{0+2S}^{(2)} z - (\omega_0 + 2\Omega)t + \pi/2\right) + G_0 \cos\left(k_0 x + q_0^{(2)} z - \omega_0 t + \pi/2\right) \\
&+G_- \cos\left((k_0 - 2k_S)x + q_{0-2S}^{(2)} z - (\omega_0 - 2\Omega)t + \pi/2\right)
\end{aligned} \tag{3.142}$$

where q's are assumed to be real values and

$$q_0^{(m)} = \left[\left(\omega_0 / c_m\right)^2 - \left(k_0\right)^2\right]^{1/2} = (\omega_0 / c_m)\cos\phi_0^{(m)} \quad ; \; m = \{1,2\} \tag{3.143}$$

$$q_{0\pm S}^{(m)} = \left[\left((\omega_0 \pm \Omega)/c_m\right)^2 - \left(k_0 \pm k_S\right)^2\right]^{1/2} = \frac{(\omega_0 \pm \Omega)}{c_m}\cos\phi_{\pm 1}^{(m)}, \qquad q_{0\pm 2S}^{(m)} = \frac{(\omega_0 \pm 2\Omega)}{c_m}\cos\phi_{\pm 2}^{(m)}$$

$$R_0 = \frac{\rho_2 q_0^{(1)} - \rho_1\left(q_0^{(2)} + \beta(\omega_0)\right)}{\rho_2 q_0^{(1)} + \rho_1\left(q_0^{(2)} + \beta(\omega_0)\right)} = \frac{\cos\phi_0^{(1)} - \Lambda^{1/2}\cos\phi_0^{(2)} + (\Lambda - 1)M_S(1 + 4i\omega_0 t_r)}{\cos\phi_0^{(1)} + \Lambda^{1/2}\cos\phi_0^{(2)} - (\Lambda - 1)M_S(1 + 4i\omega_0 t_r)} \tag{3.144}$$

$$D_0 = \frac{2\left(\rho_1\rho_2 q_0^{(1)} q_0^{(2)}\right)^{1/2}}{\rho_2 q_0^{(1)} + \rho_1\left(q_0^{(2)} + \beta(\omega_0)\right)} = \frac{2\Lambda^{1/4}\left(\cos\phi_0^{(1)}\cos\phi_0^{(2)}\right)^{1/2}}{\cos\phi_0^{(1)} + \Lambda^{1/2}\cos\phi_0^{(2)} - (\Lambda - 1)M_S(1 + 4i\omega_0 t_r)} \tag{3.145}$$

$$A_{\pm} = i\frac{a}{2}\frac{(\omega_0 \pm \Omega)}{\omega_0}\left(\frac{q_0^{(1)}}{q_{0\pm S}^{(1)}}\right)^{1/2} A_J((k_0 \pm k_S, 0), (k_0, 0), \omega_0 \pm \Omega, \omega_0)$$
$$= -(a\omega_0 / c_1)(\Lambda - 1)\cos\phi_0^{(1)}\left[\cos\phi_0^{(1)} + \Lambda^{1/2}\cos\phi_0^{(2)} - (\Lambda - 1)M_S(1 + 4i\omega_0 t_r)\right]^{-1} \times$$
$$\left[\cos\phi_{\pm 1}^{(1)} + \Lambda^{1/2}\cos\phi_{\pm 1}^{(2)} - (\Lambda - 1)M_S\left(1 + 4i\omega_0 t_r(1 \pm \Omega/\omega_0)\right)\right]^{-1} \times \tag{3.146}$$
$$\left\{-\left[\Lambda^{-1/2}\cos\phi_0^{(2)} - M_S(1 + 4i\omega_0 t_r)\right]\left[\Lambda^{1/2}\cos\phi_{\pm 1}^{(2)} - (\Lambda - 1)M_S\left(1 + 4i\omega_0 t_r(1 \pm \Omega/\omega_0)\right)\right]\right.$$
$$\left. + (1 \pm \Omega/\omega_0)\sin\phi_0^{(1)}\sin\phi_{\pm 1}^{(1)} + \Lambda^{-1/2}M_S(1 + 4i\omega_0 t_r)\cos\phi_0^{(2)}\right\}$$

$$B_{\pm} = i\frac{a}{2}\frac{(\omega_0 \pm \Omega)}{\omega_0}\left(\frac{q_0^{(2)}}{q_{0\pm S}^{(2)}}\right)^{1/2} B_J((k_0 \pm k_S, 0), (k_0, 0), \omega_0 \pm \Omega, \omega_0)$$
$$= -\frac{a\omega_0}{c_1}(\Lambda - 1)\Lambda^{1/4}\left(\cos\phi_0^{(1)}\cos\phi_0^{(2)}\right)^{1/2}\left[\cos\phi_0^{(1)} + \Lambda^{1/2}\cos\phi_0^{(2)} - (\Lambda - 1)M_S(1 + 4i\omega_0 t_r)\right]^{-1}$$
$$\times\left[\cos\phi_{\pm 1}^{(1)} + \Lambda^{1/2}\cos\phi_{\pm 1}^{(2)} - (\Lambda - 1)M_S\left(1 + 4i\omega_0 t_r(1 \pm \Omega/\omega_0)\right)\right]^{-1}$$
$$\times\left\{\left[\Lambda^{-1/2}\cos\phi_0^{(2)} - M_S(1 + 4i\omega_0 t_r)\right]\cos\phi_{\pm 1}^{(1)}\right. \tag{3.147}$$
$$\left. + (1 \pm \Omega/\omega_0)\sin\phi_0^{(1)}\sin\phi_{\pm 1}^{(1)} + \Lambda^{-1/2}M_S(1 + 4i\omega_0 t_r)\cos\phi_0^{(2)}\right\}$$

where $\Lambda \equiv T_2 / T_1$ is temperature ratio between medium (1) and (2) and $\rho_2 / \rho_1 = \Lambda^{-1}$ and $c_2 / c_1 = \sqrt{\Lambda}$ are used assuming that specific heat and gas constant are invariant. ϕ is a polar angle of incident and scattering waves measured from +z-axis. Eqs. (3.141) and (3.142) implies that scattered waves propagate not only in specular direction, ϕ_0, but also in off-specular directions, $\phi_{\pm 1}$ and $\phi_{\pm 2}$ (up to 2nd order), which have the form, see also Figure 6.

For a reflection field,

$$\phi_{\pm n}^{(1)} = \sin^{-1}\left(\frac{k_0 \pm nk_S}{(\omega_0 \pm n\Omega)/c_1}\right) \quad (n = \{0, 1, 2\}) \tag{3.148}$$

For a transmission field,

$$\phi_{\pm n}^{(2)} = \sin^{-1}\left(\frac{k_0 \pm nk_S}{(\omega_0 \pm n\Omega)/c_2}\right) \quad (n = \{0, 1, 2\}) \tag{3.149}$$

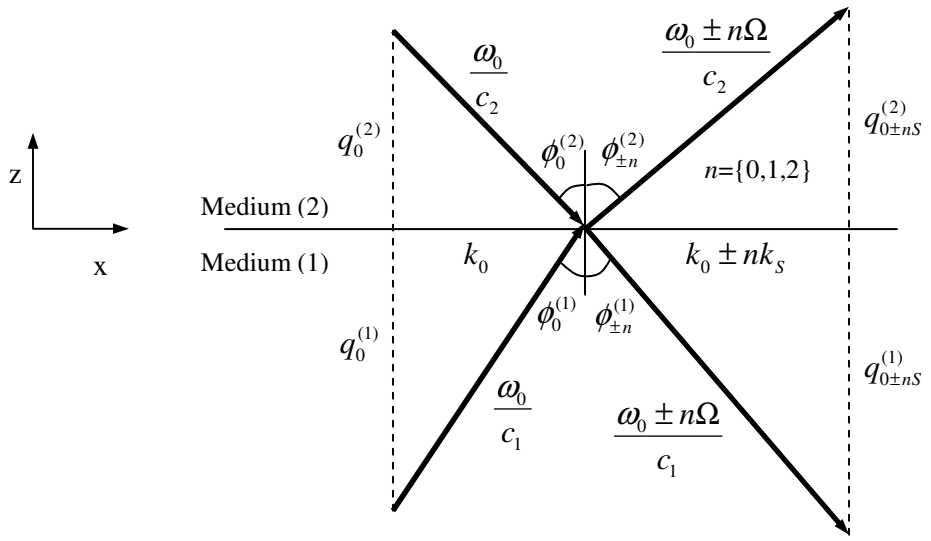

Figure 6 Notation of propagation angles of incident and scattering fields

These scattered waves propagate in discrete directions, depending upon the period, $L = 2\pi / k_S$, and frequency, Ω, of surface roughness. Note in Eqs. (3.148)and (3.149) that scattering occurs only in a specular direction if $\Omega / k_S = \omega_0 / k_0$, i.e., $\phi_{\pm 1} = \phi_{\pm 2} = \phi_0$ if the surface's propagation speed, Ω / k_S, is coincident with the phase speed, ω_0 / k_0, of incident waves along mean surface. It is known in general that such discrete scattering directions are $k = k_0 \pm np$ (n = 0, 1, …), which results from taking into account higher order terms of h in evaluating scattering amplitudes.[50] The frequency is also shifted from the incident frequency by the frequency of the moving surface. This is called "Doppler frequency shift". Figure 7 illustrates Bragg scattering and Doppler frequency shift by wave scattering from moving rough surface.

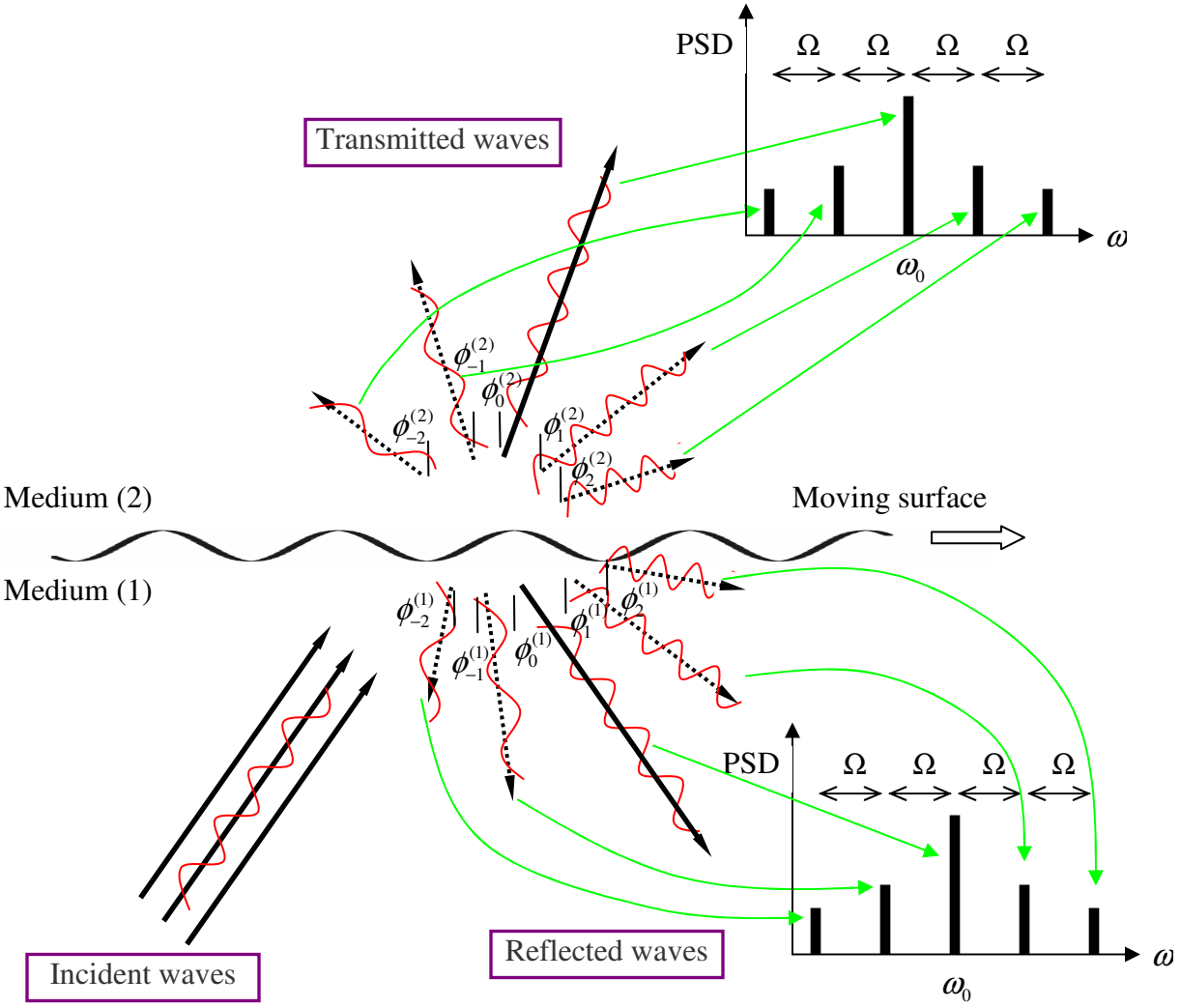

Figure 7 Wave scattering from a sinusoidally moving surface

For instance, Wunenburger *et al*. [53] demonstrated that scattering waves by a harmonically vibrating flat scatterer have a frequency spectrum with peaks at $\omega = \omega_0 \pm n\Omega$ (n = 0, 1, …), which is due to phase modulation when the measurement time interval is much larger than time interval of scatterer oscillation, see Figure 8. They called this "quasi-static Doppler effect". Since our example above deals with scattering

fields by a sinusoidal surface in a sinusoidal motion (in a vertical direction), it exhibits both "Bragg scattering" and "Doppler shift", and the resultant scattering amplitude is expected to have the form:

$$S(\boldsymbol{k},\boldsymbol{k}_0,\omega,\omega_0)=\sum_{n=-\infty}^{\infty}A_n\delta(\boldsymbol{k}-\boldsymbol{k}_0+np)\delta(\omega-\omega_0+n\Omega) \tag{3.150}$$

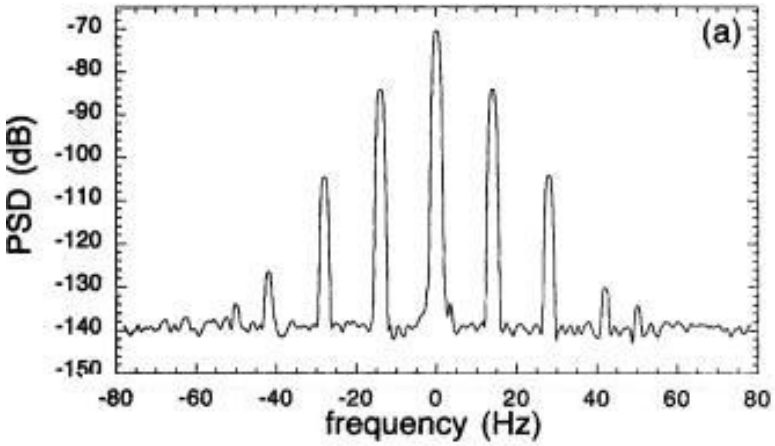

Figure 8 Dependence of power spectra of the wave scattered by the vibrating plate upon frequency (courtesy of Wunenburger *et al*)

"Quasi-static Doppler effect" can be compared to "static Doppler effect" which is observed when the measurement time interval is much shorter than time interval of scatterer oscillation. Static Doppler effect is characterized by the frequency shift Δf of scattered field which is $2Mf$ for $M \ll 1$ ($M = V/c$: V is scatterer velocity, see also Figure 9) and, therefore, the frequency spectrum of scattered field conforms to probability density function (PDF) of the scatterer velocity. Figure 9 illustrates how much frequency shift occurs when a sound source and a receiver are moving or stationary. (a) is the case of a moving source with a stationary receiver. A wavelength is reduced to λ' by the distance l_1 that the source travels during time period T. This enables one to calculate the shifted frequency, f' by

$$f' = \frac{c}{\lambda'} = \frac{c}{\lambda - l_1} = \frac{c}{(c-v)T} = \frac{1}{1-M} f \tag{3.151}$$

(b) is the case of a stationary source with a moving receiver where time period recognized by the receiver is shortened to T' because the receiver sweeps one wavelength faster than a case when a receiver is stationary.

$$l_1 + l_2 = cT' + vT' = \lambda = cT \quad \Rightarrow f' = \frac{1}{T'} = \frac{(c+v)}{cT} = (1+M) f \tag{3.152}$$

(c) is the case of stationary source and receiver with a moving scatterer. It constists of two parts. Part (1) corresponds to a situation of "source → scatterer". Note that a scatterer acts as a moving receiver and, therefore, (b) applies to get scatterer frequency, f_{sc}, as

$$f_{sc} = (1 - \vec{M} \cdot \vec{n}_S) f \tag{3.153}$$

Part (2) corresponds to a situation of "scatterer → receiver" where a scatterer acts as a moving source and, therefore, (a) applies to get receiver frequency, f_R, as

$$f_R = \frac{1}{1 - \vec{M} \cdot \vec{n}_R} f_{sc} = \frac{1 - \vec{M} \cdot \vec{n}_S}{1 - \vec{M} \cdot \vec{n}_R} f \tag{3.154}$$

If the angle by which a signal is projected and received is normal to scatterer surface, then Eq. (3.154) is simplified to $f_R = \frac{1+M}{1-M} f$ and the frequency shift is of the form for M <<1.

$$\Delta f_R = f_R - f = \frac{2M}{1-M} f \approx 2Mf \tag{3.155}$$

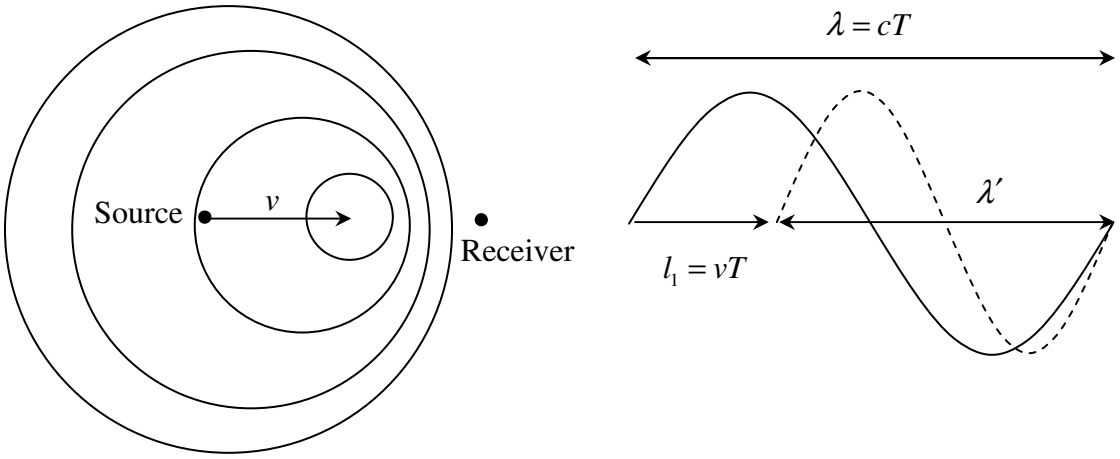

(a) A moving source with a stationary receiver

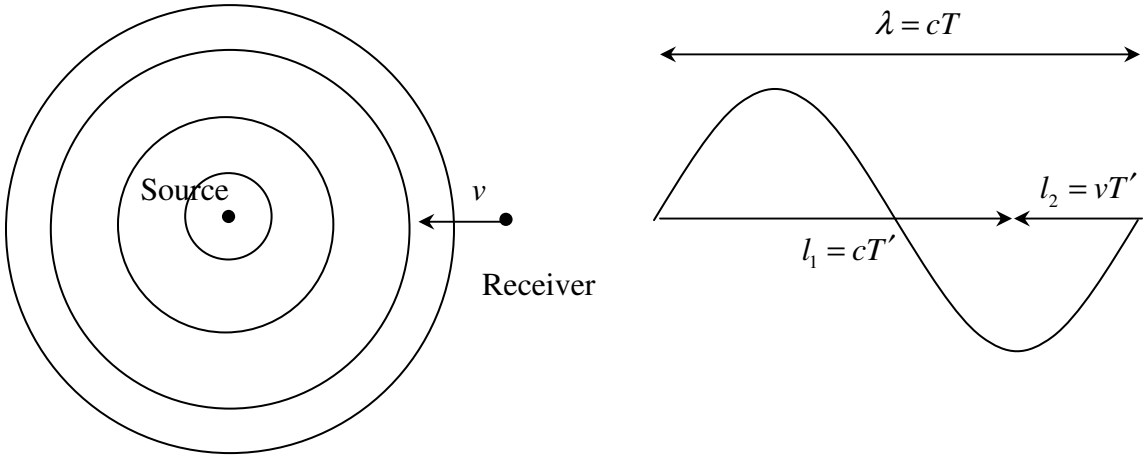

(b) A stationary source with a moving receiver

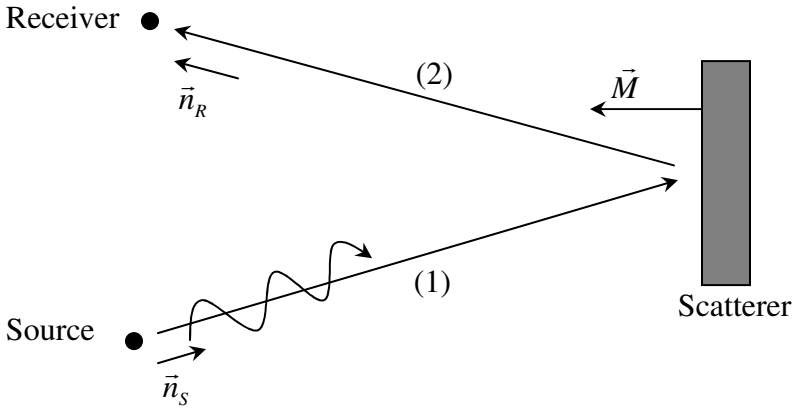

(c) Stationary source and receiver with a moving scatterer

Figure 9 Illustration of static Doppler shift effect

CHAPTER 4 STOCHASTIC ANALYSIS OF SCATTERED FIELDS

This section deals with evaluation of acoustic energy flux before and after scattering to see how the acoustic energy is balanced or amplified / damped through the scattering process when the incident waves are scattered by randomly moving turbulent flames. Statistical analysis will be incorporated to describe the random motion of turbulent flame and resultant scattered acoustic fields. Statistics of spatial homogeneity and temporal stationarity will be assumed in the following analysis.

4.1 Formulation of averaged acoustic energy flux

Recalling time-averaged intensity first, the mean acoustic energy flux is defined as being averaged over some time, T, which is either an acoustic time period or interminably long time interval ([54], p. 25)

$$\boldsymbol{I}_{av\_time} = \frac{1}{T}\int_{-T/2}^{T/2} p(t)\vec{\boldsymbol{v}}(t)dt = \frac{1}{2}\mathrm{Re}(P\vec{\boldsymbol{V}}^{*}) \tag{4.1}$$

which is valid for a single frequency wave, i.e., $p(t) = \mathrm{Re}(Pe^{-i\omega t})$ and $\vec{\boldsymbol{v}}(t) = \mathrm{Re}(\vec{\boldsymbol{V}}e^{-i\omega t})$. The wave fields of interest in this paper, however, are those of multi-frequencies which are produced by scattering from randomly moving turbulent flames due to Doppler frequency shift. Note that the scattered waves are of multi-frequencies even if an incident wave is of single frequency. The following analysis introduces an approach of evaluating a time-averaged intensity of varying frequency wave fields in the broader sense that it also applies to the case of a single-frequency wave as in Eq. (4.1) and of discrete multi-frequency waves as will be shown in Eq. (4.6).

It follows from $p(t) = \mathrm{Re}\left[\int_{\omega} P(\omega) e^{-i\omega t} d\omega\right]$ and $\vec{v}(t) = \mathrm{Re}\left[\int_{\omega} \vec{V}(\omega) e^{-i\omega t} d\omega\right]$ that

$$
\begin{aligned}
p(t)\vec{v}(t) &= \frac{1}{4}\int_{\omega} P(\omega) e^{-i\omega t} d\omega \left[\int_{\omega} \left(\vec{V}(\omega) e^{-i\omega t} + \vec{V}^{*}(\omega) e^{i\omega t}\right) d\omega\right] + C.C. \\
&= \frac{1}{4}\int_{\omega}\int_{\omega'} P(\omega)\left(\vec{V}(\omega') e^{-i(\omega+\omega')t} + \vec{V}^{*}(\omega') e^{-i(\omega-\omega')t}\right) d\omega' d\omega + C.C.
\end{aligned}
\tag{4.2}
$$

Time-averaged intensity is then of the form

$$
\begin{aligned}
\boldsymbol{I}_{av\_time} &= \lim_{T\to\infty} \frac{1}{T} \int_{-T/2}^{T/2} p(t)\vec{v}(t) dt \\
&= \frac{1}{4}\int_{\omega}\int_{\omega'} P(\omega)\left[\vec{V}(\omega')\left(\lim_{T\to\infty}\frac{1}{T}\int_{-T/2}^{T/2} e^{-i(\omega+\omega')t} dt\right) + \vec{V}^{*}(\omega')\left(\lim_{T\to\infty}\frac{1}{T}\int_{-T/2}^{T/2} e^{-i(\omega-\omega')t} dt\right)\right] d\omega' d\omega + C.C. \\
&= \frac{1}{4}\int_{\omega} P(\omega)\left(\int_{\omega'\to-\omega} \vec{V}(\omega') d\omega' + \int_{\omega'\to\omega} \vec{V}^{*}(\omega') d\omega'\right) d\omega + C.C. \\
&= \frac{1}{2}\mathrm{Re}\left\{\int_{\omega} P(\omega)\left(\int_{\omega'\to\omega} \left[\vec{V}(-\omega') + \vec{V}^{*}(\omega')\right] d\omega'\right) d\omega\right\}
\end{aligned}
\tag{4.3}
$$

where use is made of

$$
\lim_{T\to\infty}\frac{1}{T}\int_{-T/2}^{T/2} e^{-2i\omega t} dt = \begin{cases} \lim_{T\to\infty}\dfrac{\sin(\omega T)}{\omega T} = 0 & (\omega \neq 0) \\ 1 & (\omega = 0) \end{cases}
\tag{4.4}
$$

Note that (4.3) reduces to $\mathrm{Re}(P\vec{V}^{*})/2$ for a single-frequency wave, i.e., $P(\omega) = P\delta(\omega-\omega_0)$ and $\vec{V}(\omega) = \vec{V}\delta(\omega-\omega_0)$ since, for nonzero ω_0,

$$
\begin{aligned}
\boldsymbol{I}_{av\_time} &= \frac{1}{2}\mathrm{Re}\left\{\int_{\omega} P\delta(\omega-\omega_0)\left(\vec{V}\delta_{\omega(-\omega_0)} + \vec{V}^{*}\delta_{\omega\omega_0}\right) d\omega\right\} \\
&= \frac{1}{2}\mathrm{Re}\left\{P\left(\vec{V}\delta_{\omega_0(-\omega_0)} + \vec{V}^{*}\delta_{\omega_0\omega_0}\right)\right\} = \frac{1}{2}\mathrm{Re}(P\vec{V}^{*})
\end{aligned}
\tag{4.5}
$$

where $\delta_{\omega\omega_0}$ is Kronecker's delta function and

$$\int_{\omega'\to\omega} \delta(\omega'-\omega_0)d\omega' = \delta_{\omega\omega_0} = \begin{cases} 1 & (\omega=\omega_0) \\ 0 & (\omega\neq\omega_0) \end{cases}$$

are used. For waves of discrete multi-frequencies, i.e., $P(\omega)=\sum_m P_m\delta(\omega-\omega_m)$ and $\vec{\boldsymbol{V}}(\omega)=\sum_n \vec{\boldsymbol{V}}_n\delta(\omega-\omega_n)$ for $\omega_m\neq\omega_n>0 \quad (m\neq n)$, it is found that

$$\begin{aligned} \boldsymbol{I}_{av\_time} &= \frac{1}{2}\sum_m\sum_n \mathrm{Re}\left\{\int_\omega P_m\delta(\omega-\omega_m)\left(\vec{\boldsymbol{V}}_n\delta_{\omega(-\omega_n)}+\vec{\boldsymbol{V}}_n^{\,*}\delta_{\omega\omega_n}\right)d\omega\right\} \\ &= \frac{1}{2}\sum_m\sum_n \mathrm{Re}\left\{P_m\left(\vec{\boldsymbol{V}}_n\delta_{\omega_m(-\omega_n)}+\vec{\boldsymbol{V}}_n^{\,*}\delta_{\omega_m\omega_n}\right)\right\} = \frac{1}{2}\sum_n \mathrm{Re}(P_n\vec{\boldsymbol{V}}_n^{\,*}) = \sum_n \boldsymbol{I}_{n,av} \end{aligned} \tag{4.6}$$

which coincides with the expression from Pierce ([54], p. 56). Parseval theorem can be obtained in a similar manner to (4.3):

$$\begin{aligned} &\int_{-\infty}^{\infty} p(t)\vec{\boldsymbol{v}}(t)dt \\ &= \frac{1}{4}\int_\omega\int_{\omega'} P(\omega)\left[\vec{\boldsymbol{V}}(\omega')\left(\int_{-\infty}^{\infty} e^{-i(\omega+\omega')t}dt\right)+\vec{\boldsymbol{V}}^{\,*}(\omega')\left(\int_{-\infty}^{\infty} e^{-i(\omega-\omega')t}dt\right)\right]d\omega' d\omega + C.C. \\ &= \frac{\pi}{2}\int_\omega\int_{\omega'} P(\omega)\left[\vec{\boldsymbol{V}}(\omega')\delta(\omega+\omega')+\vec{\boldsymbol{V}}^{\,*}(\omega')\delta(\omega-\omega')\right]d\omega' d\omega + C.C. \\ &= \frac{\pi}{2}\int_{-\infty}^{\infty} P(\omega)\left[\vec{\boldsymbol{V}}(-\omega)+\vec{\boldsymbol{V}}^{\,*}(\omega)\right]d\omega + C.C. = \pi\int_{-\infty}^{\infty}\mathrm{Re}\left\{P(\omega)\left[\vec{\boldsymbol{V}}(-\omega)+\vec{\boldsymbol{V}}^{\,*}(\omega)\right]\right\}d\omega \end{aligned} \tag{4.7}$$

Similarly, space-averaged intensity can be utilized in order to obtain a time and space-averaged intensity for multi-frequency and multi-directional waves of the form

$$p(\vec{\boldsymbol{R}},t) = \mathrm{Re}\left[\int_\omega\iiint_{\boldsymbol{k}} P(\boldsymbol{k},\omega,z)e^{i(\boldsymbol{k}\cdot\boldsymbol{r}-\omega t)}d\boldsymbol{k}d\omega\right] \tag{4.8}$$

$$\vec{\boldsymbol{v}}(\vec{\boldsymbol{R}},t) = \mathrm{Re}\left[\int_\omega\iiint_{\boldsymbol{k}} \vec{\boldsymbol{V}}(\boldsymbol{k},\omega,z)e^{i(\boldsymbol{k}\cdot\boldsymbol{r}-\omega t)}d\boldsymbol{k}d\omega\right]$$

which yields

$$
\begin{aligned}
&p(\vec{\boldsymbol{R}},t)\vec{\boldsymbol{v}}(\vec{\boldsymbol{R}},t) \\
&= \frac{1}{4}\int_{\omega}\iiint_{\boldsymbol{k}}\int_{\omega'}\iiint_{\boldsymbol{k}'} P(\boldsymbol{k},\omega,z)\begin{pmatrix}\vec{\boldsymbol{V}}(\boldsymbol{k}',\omega',z)e^{i[(\boldsymbol{k}+\boldsymbol{k}')\cdot\boldsymbol{r}-(\omega+\omega')t]} \\ +\vec{\boldsymbol{V}}^{*}(\boldsymbol{k}',\omega',z)e^{i[(\boldsymbol{k}-\boldsymbol{k}')\cdot\boldsymbol{r}-(\omega-\omega')t]}\end{pmatrix} d\boldsymbol{k}'d\omega' d\boldsymbol{k}d\omega + C.C.
\end{aligned} \tag{4.9}
$$

A time and space-averaged intensity can then be evaluated by adding spatial integration to Eq. (4.3).

$$
\begin{aligned}
&\vec{\boldsymbol{I}}_{av} = \lim_{A,T\to\infty}\frac{1}{AT}\int_{|x|,|y|\le\sqrt{A}/2}\int_{-T/2}^{T/2} p(\vec{\boldsymbol{R}},t)\vec{\boldsymbol{v}}(\vec{\boldsymbol{R}},t)dtd\boldsymbol{r} \\
&= \frac{1}{2}\mathrm{Re}\left\{\int_{\omega}\iiint_{\boldsymbol{k}} P(\boldsymbol{k},\omega,z)\left[\int_{\omega'\to\omega}\iiint_{\boldsymbol{k}'\to\boldsymbol{k}}\left(\vec{\boldsymbol{V}}(-\boldsymbol{k}',-\omega',z)+\vec{\boldsymbol{V}}^{*}(\boldsymbol{k}',\omega',z)\right)d\boldsymbol{k}'d\omega'\right]d\boldsymbol{k}d\omega\right\}
\end{aligned} \tag{4.10}
$$

Note that space average is taken over horizontal coordinates $\boldsymbol{r}$ on a mean flame surface. Ensemble average for the above equation can be taken to describe the statistical characteristics of acoustic fields.

$$
\left\langle\vec{\boldsymbol{I}}_{av}\right\rangle = \frac{1}{2}\mathrm{Re}\left\{\int_{\omega}\iiint_{\boldsymbol{k}}\left[\int_{\omega'\to\omega}\iiint_{\boldsymbol{k}'\to\boldsymbol{k}}\begin{pmatrix}\left\langle P(\boldsymbol{k},\omega,z)\vec{\boldsymbol{V}}(-\boldsymbol{k}',-\omega',z)\right\rangle \\ +\left\langle P(\boldsymbol{k},\omega,z)\vec{\boldsymbol{V}}^{*}(\boldsymbol{k}',\omega',z)\right\rangle\end{pmatrix}d\boldsymbol{k}'d\omega'\right]d\boldsymbol{k}d\omega\right\} \tag{4.11}
$$

4.2 Evaluation of acoustic energy flux of scattered fields

To account for the statistical characteristics of scattered acoustic fields, analysis of the scattering amplitude should be examined first. Taking ensemble average of scattering amplitude in Eq. (3.131).

$$
\begin{aligned}
&\left\langle S^{11}(\boldsymbol{k},\boldsymbol{k_0},\omega,\omega_0)\right\rangle \\
&= R_J(\boldsymbol{k},\omega)\delta(\boldsymbol{k}-\boldsymbol{k_0})\delta(\omega-\omega_0) + A_J(\boldsymbol{k},\boldsymbol{k_0},\omega,\omega_0)\left\langle h(\boldsymbol{k}-\boldsymbol{k_0},\omega-\omega_0)\right\rangle \\
&+\frac{1}{2}D_J(\boldsymbol{k},\omega)\int_{\omega'}\iint_{\boldsymbol{k}'} F_J(\boldsymbol{k}',\boldsymbol{k_0},\boldsymbol{k},\omega',\omega_0,\omega)\left\langle h(\boldsymbol{k}-\boldsymbol{k}',\omega-\omega')h(\boldsymbol{k}'-\boldsymbol{k_0},\omega'-\omega_0)\right\rangle d\boldsymbol{k}'d\omega'
\end{aligned} \tag{4.12}
$$

where ensemble average of h vanishes using Eq. (3.26).

$$\left\langle h(\boldsymbol{k}-\boldsymbol{k_0},\omega-\omega_0)\right\rangle = \frac{1}{(2\pi)^3}\iint_{\boldsymbol{r}}\int_{t}\left\langle h(\boldsymbol{r},t)\right\rangle e^{-i[(\boldsymbol{k}-\boldsymbol{k_0})\cdot\boldsymbol{r}-(\omega-\omega_0)t]}dtd\boldsymbol{r} = 0 \tag{4.13}$$

Ensemble average of h^2 term is correlation function of $h(\boldsymbol{k},\omega)$ in wave number and frequency domain which is related to the power spectral density as follows. ([50], p. 80)

$$\left\langle h(\boldsymbol{k}_1,\omega_1)h(\boldsymbol{k}_2,\omega_2)\right\rangle = W(\boldsymbol{k}_1,\omega_1)\delta(\boldsymbol{k}_1+\boldsymbol{k}_2)\delta(\omega_1+\omega_2) \tag{4.14}$$

$W(\boldsymbol{k}_1,\omega_1)$ is the power spectral density of flame front height, which is defined as Fourier transform of correlation function of flame front height ([55], pp. 490)

$$W(\boldsymbol{k}_1,\omega_1) = \frac{1}{(2\pi)^3}\iint_{\boldsymbol{\xi}}\int_{\eta}\breve{W}(\boldsymbol{\xi},\eta)e^{-i(\boldsymbol{k}_1\cdot\boldsymbol{\xi}-\omega_1\eta)}d\eta d\boldsymbol{\xi} \tag{4.15}$$

Eq. (4.14) can be verified by expressing the correlation function $\breve{W}(\boldsymbol{\xi},\eta)$ in terms of power spectral density using inverse Fourier transform.

$$\breve{W}(\boldsymbol{\xi},\eta) = \iint_{\boldsymbol{k}_1}\int_{\omega_1} W(\boldsymbol{k}_1,\omega_1)e^{i(\boldsymbol{k}_1\cdot\boldsymbol{\xi}-\omega_1\eta)}d\omega_1 d\boldsymbol{k}_1 \tag{4.16}$$

where $\boldsymbol{\xi} = \boldsymbol{r}_1 - \boldsymbol{r}_2$ and $\eta = t_1 - t_2$ are difference in space and time, respectively, between two points. Note that the correlation function is only a function of $\boldsymbol{\xi}$ and η in case of spatially homogeneous and temporally stationary statistics. The correlation function $\breve{W}(\boldsymbol{\xi},\eta)$ can also be expressed as the following by its definition.

$$\begin{aligned}
\breve{W}(\boldsymbol{\xi},\eta) &= \left\langle h(\boldsymbol{r}_1,t_1)h(\boldsymbol{r}_2,t_2)\right\rangle \\
&= \left\langle \iint_{\boldsymbol{k}_1}\int_{\omega_1} h(\boldsymbol{k}_1,\omega_1)e^{i(\boldsymbol{k}_1\cdot\boldsymbol{r}_1-\omega_1 t_1)}d\omega_1 d\boldsymbol{k}_1 \times \iint_{\boldsymbol{k}_2}\int_{\omega_2} h(\boldsymbol{k}_2,\omega_2)e^{i(\boldsymbol{k}_2\cdot\boldsymbol{r}_2-\omega_2 t_2)}d\omega_2 d\boldsymbol{k}_2 \right\rangle \\
&= \iint_{\boldsymbol{k}_1}\int_{\omega_1}\iint_{\boldsymbol{k}_2}\int_{\omega_2}\left\langle h(\boldsymbol{k}_1,\omega_1)h(\boldsymbol{k}_2,\omega_2)\right\rangle e^{i(\boldsymbol{k}_1\cdot\boldsymbol{r}_1+\boldsymbol{k}_2\cdot\boldsymbol{r}_2-\omega_1 t_1-\omega_2 t_2)}d\omega_2 d\boldsymbol{k}_2 d\omega_1 d\boldsymbol{k}_1 \\
&= \iint_{\boldsymbol{k}_1}\int_{\omega_1}\iint_{\boldsymbol{k}_2}\int_{\omega_2}\left\langle h(\boldsymbol{k}_1,\omega_1)h(\boldsymbol{k}_2,\omega_2)\right\rangle e^{i[\boldsymbol{k}_1\cdot\boldsymbol{\xi}+(\boldsymbol{k}_1+\boldsymbol{k}_2)\cdot\boldsymbol{r}_2-\omega_1\eta-(\omega_1+\omega_2)t_2]}d\omega_2 d\boldsymbol{k}_2 d\omega_1 d\boldsymbol{k}_1
\end{aligned} \tag{4.17}$$

where $(\boldsymbol{k}_1+\boldsymbol{k}_2)\cdot\boldsymbol{r}_2-(\omega_1+\omega_2)t_2$ in the exponential term in the last equation should vanish in order for $\breve{W}(\xi,\eta)$ to be a function of ξ and η only. This leads to the fact that $\langle h(\boldsymbol{k}_1,\omega_1)h(\boldsymbol{k}_2,\omega_2)\rangle$ is required to vanish unless $\boldsymbol{k}_1+\boldsymbol{k}_2=0$ and $\omega_1+\omega_2=0$, which yields Eq. (4.14). From Eq. (4.14)

$$\langle h(\boldsymbol{k}-\boldsymbol{k}',\omega-\omega')h(\boldsymbol{k}'-\boldsymbol{k_0},\omega'-\omega_0)\rangle = W(\boldsymbol{k}-\boldsymbol{k}',\omega-\omega')\delta(\boldsymbol{k}-\boldsymbol{k_0})\delta(\omega-\omega_0) \tag{4.18}$$

Substituting Eqs. (4.13) and (4.18) into Eq. (4.12) yields the form

$$\langle S^{11}(\boldsymbol{k},\boldsymbol{k_0},\omega,\omega_0)\rangle = \langle V_J(\boldsymbol{k},\omega)\rangle\delta(\boldsymbol{k}-\boldsymbol{k_0})\delta(\omega-\omega_0) \tag{4.19}$$

where

$$\langle V_J(\boldsymbol{k},\omega)\rangle \equiv R_J(\boldsymbol{k},\omega)+\frac{1}{2}D_J(\boldsymbol{k},\omega)\int_{\omega'}\iint_{\boldsymbol{k}'}F_J(\boldsymbol{k}',\boldsymbol{k_0},\boldsymbol{k},\omega',\omega_0,\omega)W(\boldsymbol{k}-\boldsymbol{k}',\omega-\omega')d\boldsymbol{k}'d\omega'$$

which implies that mean (ensemble-averaged) scattering amplitude consists only of the waves that propagate in a specular direction and that 1st order term has no contribution to mean scattering amplitude while zeroth and 2nd order terms do have a contribution. $\langle V_J(\boldsymbol{k},\omega)\rangle$ in the above equation is referred to as the mean reflection coefficient. In case of pressure release condition ($\rho_2/\rho_1\to 0$) at a flame surface without velocity jump, $\beta=$ 0, the mean reflection coefficient reduces to the form

$$\langle V(\boldsymbol{k},\omega)\rangle \equiv \langle V_J(\boldsymbol{k},\omega)_{\beta=0}\rangle = -1+2(q_0^{(1)}q_k^{(1)})^{1/2}\int_{\omega'}\iint_{\boldsymbol{k}'}\frac{\omega_0}{\omega}q_{k'}^{(1)}W(\boldsymbol{k}-\boldsymbol{k}',\omega-\omega')d\boldsymbol{k}'d\omega' \tag{4.20}$$

where Eqs. (3.108), (3.109), (3.116), (3.117), and (3.129) are used to yield as $\rho_2/\rho_1\to 0$

$$R_J(\boldsymbol{k},\omega)_{\beta=0}=-1,\quad D_J(\boldsymbol{k},\omega)_{\beta=0}=0,\quad A_J(\boldsymbol{k}',\boldsymbol{k_0},\omega',\omega_0)_{\beta=0}=-2i\frac{\omega_0}{\omega'}(q_0^{(1)}q_{k'}^{(1)})^{1/2}, \tag{4.21}$$

$$B_J(\boldsymbol{k}',\boldsymbol{k_0},\omega',\omega_0)_{\beta=0}=0\,,\qquad D_J(\boldsymbol{k},\omega)F_J(\boldsymbol{k}',\boldsymbol{k_0},\boldsymbol{k},\omega',\omega_0,\omega)\big|_{\beta=0}=4\frac{\omega_0}{\omega}(q_0^{(1)}q_k^{(1)})^{1/2}q_{k'}^{(1)}$$

Eq. (4.20) reduces further to the form using $W(\boldsymbol{k},\omega)\equiv W(\boldsymbol{k})\delta(\omega)$.

$$\left\langle V(\boldsymbol{k_0},\omega_0)\right\rangle=-1+2q_0^{(1)}\iint_{\boldsymbol{k}'}q_{k'}^{(1)}W(\boldsymbol{k_0}-\boldsymbol{k}')d\boldsymbol{k}' \tag{4.22}$$

which is equivalent to the expression from Voronovich ([50], p.80). (Note that $\left\langle V(\boldsymbol{k},\omega)\right\rangle\delta(\boldsymbol{k}-\boldsymbol{k_0})\delta(\omega-\omega_0)=\left\langle V(\boldsymbol{k_0},\omega_0)\right\rangle\delta(\boldsymbol{k}-\boldsymbol{k_0})\delta(\omega-\omega_0)$.)

The above analysis enables one to evaluate ensemble average of acoustic fields. Note that the energy flux of incident wave field must be evaluated first as a reference value, using Eqs. (3.135), (3.136), (4.8), and (4.10).

$$P(\boldsymbol{k},\omega,z)=i\,\mathrm{e}^{iq_k^{(1)}z}\,\delta(\boldsymbol{k}-\boldsymbol{k_0})\delta(\omega-\omega_0)$$

$$\vec{\boldsymbol{V}}(\boldsymbol{k},\omega,z)=i\frac{\varepsilon c_1}{\omega_0}\vec{\boldsymbol{K}}_+^{(1)}\,\mathrm{e}^{iq_k^{(1)}z}\,\delta(\boldsymbol{k}-\boldsymbol{k_0})\delta(\omega-\omega_0)$$

$$\vec{\boldsymbol{I}}_{av,I}=-\frac{1}{2}\frac{\varepsilon c_1}{\omega_0}\mathrm{Re}\left\{\int_{\omega}\iint_{\boldsymbol{k}}\mathrm{e}^{iq_k^{(1)}z}\,\delta(\boldsymbol{k}-\boldsymbol{k_0})\delta(\omega-\omega_0)\begin{bmatrix}\left(-\vec{\boldsymbol{K}}_-^{(1)}\right)\mathrm{e}^{iq_k^{(1)}z}\,\delta_{\boldsymbol{k}(-\boldsymbol{k_0})}\delta_{\omega(-\omega_0)}\\ -\left(\vec{\boldsymbol{K}}_+^{(1)}\,\mathrm{e}^{iq_k^{(1)}z}\right)^*\delta_{\boldsymbol{k}\boldsymbol{k_0}}\delta_{\omega\omega_0}\end{bmatrix}d\boldsymbol{k}\,d\omega\right\}$$

$$=\frac{1}{2}\frac{\varepsilon c_1}{\omega_0}\mathrm{Re}\left[\mathrm{e}^{iq_0^{(1)}z}\left(\vec{\boldsymbol{K}}_{0+}^{(1)}\,\mathrm{e}^{iq_0^{(1)}z}\right)^*\right]=\frac{1}{2}\frac{\varepsilon c_1}{\omega_0}\vec{\boldsymbol{K}}_{0+}^{(1)}$$

where $q_0^{(1)}$ is a real value for an incident plane wave. The acoustic energy flux incident upon unit area of mean flame surface (z = 0) with its normal vector $\vec{\boldsymbol{n}}$ equal to $\vec{\boldsymbol{e}}_z$ is of the form

$$\vec{\boldsymbol{I}}_{av,I}\cdot\vec{\boldsymbol{n}}=\frac{\varepsilon c_1 q_0^{(1)}}{2\omega_0} \tag{4.23}$$

The reflected /transmitted scattered fields have stochastic properties whose ensemble averaged energy flux can be calculated using Eq. (4.11). Comparing Eq. (4.8) with reflected acoustic pressure / velocity fields in Eqs. (3.135) and (3.136) yields:

$$P(\boldsymbol{k},\omega,z) = i\frac{\omega}{\omega_0}\left(\frac{q_0^{(1)}}{q_k^{(1)}}\right)^{1/2} S^{11}(\boldsymbol{k},\boldsymbol{k_0},\omega,\omega_0)\,\mathrm{e}^{-iq_k^{(1)}z} \tag{4.24}$$

$$\vec{\boldsymbol{V}}(\boldsymbol{k},\omega,z) = i\frac{\varepsilon c_1}{\omega_0}(q_0^{(1)}/q_k^{(1)})^{1/2} S^{11}(\boldsymbol{k},\boldsymbol{k_0},\omega,\omega_0)\vec{\boldsymbol{K}}_-^{(1)}\,\mathrm{e}^{-iq_k^{(1)}z}$$

The first and the second terms of ensemble averaged quantities in the integral on the R.H.S. of Eq. (4.11) are then expressed in terms of the second moments of scattering amplitude.

$$\begin{aligned}&\left\langle P(\boldsymbol{k},\omega,z)\vec{\boldsymbol{V}}(-\boldsymbol{k}',-\omega',z)\right\rangle \\ &= \frac{\varepsilon c_1\omega}{\omega_0^2}\frac{q_0^{(1)}}{(q_k^{(1)}q_{k'}^{(1)})^{1/2}}\left\langle S^{11}(\boldsymbol{k},\boldsymbol{k_0},\omega,\omega_0)S^{11}(-\boldsymbol{k}',\boldsymbol{k_0},-\omega',\omega_0)\right\rangle \vec{\boldsymbol{K}}_+'^{(1)}\,\mathrm{e}^{-i(q_k^{(1)}+q_{k'}^{(1)})z}\end{aligned} \tag{4.25}$$

$$\begin{aligned}&\left\langle P(\boldsymbol{k},\omega,z)\vec{\boldsymbol{V}}^*(\boldsymbol{k}',\omega',z)\right\rangle \\ &= \frac{\varepsilon c_1\omega}{\omega_0^2}\left(\frac{q_0^{(1)}}{q_k^{(1)}}\right)^{1/2}\left(\frac{q_0^{(1)}}{q_{k'}^{(1)}}\right)^{1/2*}\left\langle S^{11}(\boldsymbol{k},\boldsymbol{k_0},\omega,\omega_0)S^{11*}(\boldsymbol{k}',\boldsymbol{k_0},\omega',\omega_0)\right\rangle \vec{\boldsymbol{K}}_-'^{(1)*}\,\mathrm{e}^{-i[q_k^{(1)}-(q_{k'}^{(1)})^*]z}\end{aligned} \tag{4.26}$$

; $\vec{\boldsymbol{K}}_\pm'^{(m)} = \boldsymbol{k}' \pm q_{k'}^{(m)}\vec{\boldsymbol{e}}_z$

The scattering amplitude is decomposed of mean and fluctuating terms.

$$S^{11}(\boldsymbol{k},\boldsymbol{k_0},\omega,\omega_0) = \left\langle S^{11}(\boldsymbol{k},\boldsymbol{k_0},\omega,\omega_0)\right\rangle + \Delta S^{11}_{(\boldsymbol{k},\boldsymbol{k_0},\omega,\omega_0)} \tag{4.27}$$

which can be rewritten using Eqs. (3.131) and (4.19):

$$\begin{aligned}&\Delta S^{11}_{(\boldsymbol{k},\boldsymbol{k_0},\omega,\omega_0)} = S^{11}(\boldsymbol{k},\boldsymbol{k_0},\omega,\omega_0) - \left\langle S^{11}(\boldsymbol{k},\boldsymbol{k_0},\omega,\omega_0)\right\rangle \\ &= A_J(\boldsymbol{k},\boldsymbol{k_0},\omega,\omega_0)h(\boldsymbol{k}-\boldsymbol{k_0},\omega-\omega_0) + O(h^2)\end{aligned} \tag{4.28}$$

Eqs. (4.19), (4.27), and (4.28) then leads the second moments of scattering amplitude in Eqs. (4.25) and (4.26) to the forms

$$
\begin{aligned}
&\left\langle S^{11}(\boldsymbol{k},\boldsymbol{k_0},\omega,\omega_0)S^{11}(-\boldsymbol{k}',\boldsymbol{k_0},-\omega',\omega_0)\right\rangle \\
&=\left\langle\left[\left\langle S^{11}_{(\boldsymbol{k},\boldsymbol{k_0},\omega,\omega_0)}\right\rangle+\Delta S^{11}_{(\boldsymbol{k},\boldsymbol{k_0},\omega,\omega_0)}\right]\left[\left\langle S^{11}_{(-\boldsymbol{k}',\boldsymbol{k_0},-\omega',\omega_0)}\right\rangle+\Delta S^{11}_{(-\boldsymbol{k}',\boldsymbol{k_0},-\omega',\omega_0)}\right]\right\rangle \\
&=\left\langle S^{11}_{(\boldsymbol{k},\boldsymbol{k_0},\omega,\omega_0)}\right\rangle\left\langle S^{11}_{(-\boldsymbol{k}',\boldsymbol{k_0},-\omega',\omega_0)}\right\rangle+\left\langle\Delta S^{11}_{(\boldsymbol{k},\boldsymbol{k_0},\omega,\omega_0)}\Delta S^{11}_{(-\boldsymbol{k}',\boldsymbol{k_0},-\omega',\omega_0)}\right\rangle \\
&=\left\langle V_J(\boldsymbol{k},\omega)\right\rangle\left\langle V_J(-\boldsymbol{k}',-\omega')\right\rangle\delta(\boldsymbol{k}-\boldsymbol{k_0})\delta(\omega-\omega_0)\delta(\boldsymbol{k}'+\boldsymbol{k_0})\delta(\omega'+\omega_0) \\
&+A_J(\boldsymbol{k},\boldsymbol{k_0},\omega,\omega_0)A_J(-\boldsymbol{k}',\boldsymbol{k_0},-\omega',\omega_0)\left\langle h(\boldsymbol{k}-\boldsymbol{k_0},\omega-\omega_0)h(-\boldsymbol{k}'-\boldsymbol{k_0},-\omega'-\omega_0)\right\rangle+O(h^3) \\
&=\left\langle V_J(\boldsymbol{k},\omega)\right\rangle\left\langle V_J(-\boldsymbol{k}',-\omega')\right\rangle\delta(\boldsymbol{k}-\boldsymbol{k_0})\delta(\omega-\omega_0)\delta(\boldsymbol{k}'+\boldsymbol{k_0})\delta(\omega'+\omega_0) \\
&+A_J(\boldsymbol{k},\boldsymbol{k_0},\omega,\omega_0)A_J(-\boldsymbol{k}',\boldsymbol{k_0},-\omega',\omega_0)W(\boldsymbol{k}-\boldsymbol{k_0},\omega-\omega_0)\delta(\boldsymbol{k}-\boldsymbol{k}'-2\boldsymbol{k_0})\delta(\omega-\omega'-2\omega_0)+O(h^3)
\end{aligned}
\tag{4.29}
$$

$$
\begin{aligned}
&\left\langle S^{11}(\boldsymbol{k},\boldsymbol{k_0},\omega,\omega_0)S^{11*}(\boldsymbol{k}',\boldsymbol{k_0},\omega',\omega_0)\right\rangle \\
&=\left\langle S^{11}_{(\boldsymbol{k},\boldsymbol{k_0},\omega,\omega_0)}\right\rangle\left\langle S^{11*}_{(\boldsymbol{k}',\boldsymbol{k_0},\omega',\omega_0)}\right\rangle+\left\langle\Delta S^{11}_{(\boldsymbol{k},\boldsymbol{k_0},\omega,\omega_0)}\Delta S^{11*}_{(\boldsymbol{k}',\boldsymbol{k_0},\omega',\omega_0)}\right\rangle \\
&=\left\langle V_J(\boldsymbol{k},\omega)\right\rangle\left\langle V_J{}^*(\boldsymbol{k}',\omega')\right\rangle\delta(\boldsymbol{k}-\boldsymbol{k_0})\delta(\omega-\omega_0)\delta(\boldsymbol{k}'-\boldsymbol{k_0})\delta(\omega'-\omega_0) \\
&+A_J(\boldsymbol{k},\boldsymbol{k_0},\omega,\omega_0)A_J^*(\boldsymbol{k}',\boldsymbol{k_0},\omega',\omega_0)\left\langle h(\boldsymbol{k}-\boldsymbol{k_0},\omega-\omega_0)h^*(\boldsymbol{k}'-\boldsymbol{k_0},\omega'-\omega_0)\right\rangle+O(h^3) \\
&=\left\langle V_J(\boldsymbol{k},\omega)\right\rangle\left\langle V_J{}^*(\boldsymbol{k}',\omega')\right\rangle\delta(\boldsymbol{k}-\boldsymbol{k_0})\delta(\omega-\omega_0)\delta(\boldsymbol{k}'-\boldsymbol{k_0})\delta(\omega'-\omega_0) \\
&+A_J(\boldsymbol{k},\boldsymbol{k_0},\omega,\omega_0)A_J^*(\boldsymbol{k}',\boldsymbol{k_0},\omega',\omega_0)W(\boldsymbol{k}-\boldsymbol{k_0},\omega-\omega_0)\delta(\boldsymbol{k}-\boldsymbol{k}')\delta(\omega-\omega')+O(h^3)
\end{aligned}
\tag{4.30}
$$

where Eq. (4.14) is used together with

$$
h^*(\boldsymbol{k},\omega)=\iint_{\boldsymbol{r}}\int_t h(\boldsymbol{r},t)e^{i(\boldsymbol{k}\cdot\boldsymbol{r}-\omega t)}dtd\boldsymbol{r}/(2\pi)^3=h(-\boldsymbol{k},-\omega) \tag{4.31}
$$

Substituting Eqs. (4.25) and (4.29) into Eq. (4.11) yields the form for the first term on the R.H.S. of (4.11).

The first term =

$$
\begin{aligned}
&\frac{\varepsilon c_1\omega}{\omega_0^2}\frac{q_0^{(1)}}{(q_k^{(1)}q_{k'}^{(1)})^{1/2}}\vec{\boldsymbol{K}}_+'^{(1)}\,\mathrm{e}^{-i(q_k^{(1)}+q_{k'}^{(1)})z}\times \\
&\frac{\mathrm{Re}}{2}\int_\omega\iint_{\boldsymbol{k}}\int_{\omega'\to\omega}\iint_{\boldsymbol{k}'\to\boldsymbol{k}}\left[\begin{array}{l}\left\langle V_J(\boldsymbol{k},\omega)\right\rangle\left\langle V_J(-\boldsymbol{k}',-\omega')\right\rangle\delta(\boldsymbol{k}-\boldsymbol{k_0})\delta(\omega-\omega_0)\delta(\boldsymbol{k}'+\boldsymbol{k_0})\delta(\omega'+\omega_0) \\ +A_J(\boldsymbol{k},\boldsymbol{k_0},\omega,\omega_0)A_J(-\boldsymbol{k}',\boldsymbol{k_0},-\omega',\omega_0)W(\boldsymbol{k}-\boldsymbol{k_0},\omega-\omega_0)\times \\ \delta(\boldsymbol{k}-\boldsymbol{k}'-2\boldsymbol{k_0})\delta(\omega-\omega'-2\omega_0)\end{array}\right]d\boldsymbol{k}'d\omega'd\boldsymbol{k}d\omega \\
&+O(h^3)
\end{aligned}
$$

$$= \frac{\varepsilon c_1}{2\omega_0} \mathrm{Re} \int_{\omega} \iint_{\boldsymbol{k}} \frac{\omega}{\omega_0} \frac{q_0^{(1)}}{q_k^{(1)}} \vec{\boldsymbol{K}}_+^{(1)} \mathrm{e}^{-2iq_k^{(1)} z} \begin{bmatrix} \langle V_J(\boldsymbol{k},\omega)\rangle \langle V_J(\boldsymbol{k_0},\omega_0)\rangle \delta(\boldsymbol{k}-\boldsymbol{k_0})\delta(\omega-\omega_0)\delta_{\boldsymbol{k}(-\boldsymbol{k_0})}\delta_{\omega(-\omega_0)} \\ +A_J(\boldsymbol{k},\boldsymbol{k_0},\omega,\omega_0)A_J(-\boldsymbol{k},\boldsymbol{k_0},-\omega,\omega_0)\times \\ W(\boldsymbol{k}-\boldsymbol{k_0},\omega-\omega_0)\delta_{\boldsymbol{k}(\boldsymbol{k}-2\boldsymbol{k_0})}\delta_{\omega(\omega-2\omega_0)} \end{bmatrix} d\boldsymbol{k}d\omega$$

$$+O(h^3)$$

$$= \frac{\varepsilon c_1}{2\omega_0} \mathrm{Re} \left\{ \begin{array}{l} \vec{\boldsymbol{K}}_{0+}^{(1)} \mathrm{e}^{-2iq_0^{(1)} z} \langle V(\boldsymbol{k_0},\omega_0)\rangle^2 \delta_{\boldsymbol{k_0}(-\boldsymbol{k_0})}\delta_{\omega_0(-\omega_0)} \\ \int_{\omega} \iint_{\boldsymbol{k}} \frac{\omega}{\omega_0} \frac{q_0^{(1)}}{q_k^{(1)}} \vec{\boldsymbol{K}}_+^{(1)} \mathrm{e}^{-2iq_k^{(1)} z} \begin{bmatrix} A_J(\boldsymbol{k},\boldsymbol{k_0},\omega,\omega_0)A_J(-\boldsymbol{k},\boldsymbol{k_0},-\omega,\omega_0)\times \\ W(\boldsymbol{k}-\boldsymbol{k_0},\omega-\omega_0)\delta_{\boldsymbol{k}(\boldsymbol{k}-2\boldsymbol{k_0})}\delta_{\omega(\omega-2\omega_0)} \end{bmatrix} d\boldsymbol{k}d\omega \end{array} \right\} + O(h^3)$$

$$= 0 + O(h^3) \qquad (4.32)$$

where the use is made that $\delta_{\omega_0(-\omega_0)} = 0$ and $\delta_{\omega(\omega-2\omega_0)} = 0$ if $\omega_0 \neq 0$. Similarly, the second term on the R.H.S. of (4.11) is of the form using (4.26) and (4.30).

The second term =

$$\frac{\varepsilon c_1 \omega}{\omega_0^2} \left(\frac{q_0^{(1)}}{q_k^{(1)}} \right)^{1/2} \left(\frac{q_0^{(1)}}{q_{k'}^{(1)}} \right)^{1/2*} \vec{\boldsymbol{K}}_-'^{(1)*} \mathrm{e}^{-i[q_k^{(1)} - (q_{k'}^{(1)})^*]z} \times$$

$$\frac{\mathrm{Re}}{2} \int_{\omega} \iint_{\boldsymbol{k}} \int_{\omega' \to \omega} \iint_{\boldsymbol{k}' \to \boldsymbol{k}} \begin{bmatrix} \langle V_J(\boldsymbol{k},\omega)\rangle \langle V_J^*(\boldsymbol{k}',\omega')\rangle \delta(\boldsymbol{k}-\boldsymbol{k_0})\delta(\omega-\omega_0)\delta(\boldsymbol{k}'-\boldsymbol{k_0})\delta(\omega'-\omega_0) \\ +A_J(\boldsymbol{k},\boldsymbol{k_0},\omega,\omega_0)A_J^*(\boldsymbol{k}',\boldsymbol{k_0},\omega',\omega_0)\times \\ W(\boldsymbol{k}-\boldsymbol{k_0},\omega-\omega_0)\delta(\boldsymbol{k}-\boldsymbol{k}')\delta(\omega-\omega') \end{bmatrix} d\boldsymbol{k}'d\omega' d\boldsymbol{k}d\omega$$

$$+O(h^3)$$

$$= \frac{\varepsilon c_1}{2\omega_0} \mathrm{Re} \left\{ \begin{array}{l} \int_{\omega} \iint_{\boldsymbol{k}} \frac{\omega}{\omega_0} \left(\frac{q_0^{(1)}}{q_k^{(1)}} \right)^{1/2} \vec{\boldsymbol{K}}_{0-}^{(1)*} \mathrm{e}^{-i[q_k^{(1)} - (q_0^{(1)})^*]z} \times \qquad d\boldsymbol{k}d\omega \\ \langle V_J(\boldsymbol{k},\omega)\rangle \langle V_J^*(\boldsymbol{k_0},\omega_0)\rangle \delta(\boldsymbol{k}-\boldsymbol{k_0})\delta(\omega-\omega_0)\delta_{\boldsymbol{k}\boldsymbol{k_0}}\delta_{\omega\omega_0} \\ +\int_{\omega} \iint_{\boldsymbol{k}} \frac{\omega}{\omega_0} \left| \left(\frac{q_0^{(1)}}{q_k^{(1)}} \right)^{1/2} A_J(\boldsymbol{k},\boldsymbol{k_0},\omega,\omega_0) \right|^2 W(\boldsymbol{k}-\boldsymbol{k_0},\omega-\omega_0) \vec{\boldsymbol{K}}_-^{(1)*} \mathrm{e}^{-i[q_k^{(1)} - (q_k^{(1)})^*]z} d\boldsymbol{k}d\omega \end{array} \right\}$$

$$+O(h^3)$$

$$= \frac{\varepsilon c_1}{2\omega_0} \mathrm{Re} \left\{ \begin{array}{l} \vec{\boldsymbol{K}}_{0-}^{(1)*} \left| \langle V_J(\boldsymbol{k_0},\omega_0)\rangle \right|^2 \mathrm{e}^{-i[q_0^{(1)} - (q_0^{(1)})^*]z} \\ +\int_{\omega} \iint_{\boldsymbol{k}} \frac{\omega}{\omega_0} \left| \left(\frac{q_0^{(1)}}{q_k^{(1)}} \right)^{1/2} A_J(\boldsymbol{k},\boldsymbol{k_0},\omega,\omega_0) \right|^2 W(\boldsymbol{k}-\boldsymbol{k_0},\omega-\omega_0) \vec{\boldsymbol{K}}_-^{(1)*} \mathrm{e}^{-i[q_k^{(1)} - (q_k^{(1)})^*]z} d\boldsymbol{k}d\omega \end{array} \right\} + O(h^3)$$

$$= \frac{\varepsilon c_1}{2\omega_0}\left[\begin{array}{l} \mathrm{Re}\left(\vec{\boldsymbol{K}}_{0-}^{(1)}\right)\left|\left\langle V_J(\boldsymbol{k_0},\omega_0)\right\rangle\right|^2 \mathrm{e}^{2\,\mathrm{Im}(q_0^{(1)})z} \\ +\int_{\omega}\iint_{\boldsymbol{k}} \frac{\omega}{\omega_0}\left|\frac{q_0^{(1)}}{q_k^{(1)}}\right|\left|A_J(\boldsymbol{k},\boldsymbol{k_0},\omega,\omega_0)\right|^2 W(\boldsymbol{k}-\boldsymbol{k_0},\omega-\omega_0)\,\mathrm{Re}\left(\vec{\boldsymbol{K}}_{-}^{(1)}\right)\mathrm{e}^{2\,\mathrm{Im}(q_k^{(1)})z}\,d\boldsymbol{k}d\omega \end{array}\right] + O(h^3)$$

; $\vec{\boldsymbol{K}}_{0-}^{(1)} = \boldsymbol{k_0} - q_0^{(1)}\vec{\boldsymbol{e}}_z$, $\vec{\boldsymbol{K}}_{-}^{(1)} = \boldsymbol{k} - q_k^{(1)}\vec{\boldsymbol{e}}_z$ (4.33)

Note that, for complex number $z = ae^{i\theta}$, $\left|z^{1/2}\right|^2 = \left|\sqrt{a}\,e^{i\theta/2}\right|^2 = \left|\sqrt{a}\right|^2 = a = |z|$. Substituting Eqs. (4.32) and (4.33) into Eq. (4.11) yields the acoustic energy flux reflected from unit area of mean flame surface (z = 0) whose normal vector $\vec{\boldsymbol{n}}$ is equal to $\vec{\boldsymbol{e}}_z$.

$$\left\langle \vec{\boldsymbol{I}}_{av} \right\rangle_R \cdot \vec{\boldsymbol{n}} =$$

$$-\frac{\varepsilon c_1 q_0^{(1)}}{2\omega_0}\left[\left|\left\langle V_J(\boldsymbol{k_0},\omega_0)\right\rangle\right|^2 + \int_{\omega}\iint_{\boldsymbol{k}} \frac{\omega}{\omega_0}\left|q_k^{(1)}\right|^{-1}\left|A_J(\boldsymbol{k},\boldsymbol{k_0},\omega,\omega_0)\right|^2 W(\boldsymbol{k}-\boldsymbol{k_0},\omega-\omega_0)\,\mathrm{Re}(q_k^{(1)})\,d\boldsymbol{k}d\omega\right]$$

$$+O(h^3)$$

$$= -\frac{\varepsilon c_1 q_0^{(1)}}{2\omega_0}\left[\left|\left\langle V_J(\boldsymbol{k_0},\omega_0)\right\rangle\right|^2 + \int_{\omega}\iint_{|\boldsymbol{k}|<\frac{|\omega|}{c_1}} \frac{\omega}{\omega_0}\left|A_J(\boldsymbol{k},\boldsymbol{k_0},\omega,\omega_0)\right|^2 W(\boldsymbol{k}-\boldsymbol{k_0},\omega-\omega_0)\,d\boldsymbol{k}d\omega\right] + O(h^3)$$

(4.34)

where $q_0^{(1)}$ is a positive real value. Last equality results from the fact that $\mathrm{Re}\left(q_k^{(1)*}\right) = 0$ if $\omega/c_1 \le |\boldsymbol{k}|$ since $q_k^{(1)} = i\left|q_k^{(1)}\right|$ for $\omega/c_1 \le |\boldsymbol{k}|$. Note also that W is real because, by taking conjugate in Eq. (4.15),

$$W^*(\boldsymbol{k}_1,\omega_1) = \frac{1}{(2\pi)^3}\int_{-\infty}^{\infty}\int_{-\infty}^{\infty}\int_{-\infty}^{\infty}\breve{W}(\boldsymbol{\xi},\eta)e^{i(\boldsymbol{k}_1\cdot\boldsymbol{\xi}-\omega_1\eta)}d\eta d\boldsymbol{\xi}$$

$$= \frac{-1}{(2\pi)^3}\int_{\infty}^{-\infty}\int_{\infty}^{-\infty}\int_{\infty}^{-\infty}\breve{W}(-\boldsymbol{\xi}',-\eta')e^{-i(\boldsymbol{k}_1\cdot\boldsymbol{\xi}'-\omega_1\eta')}d\eta' d\boldsymbol{\xi}' \qquad (4.35)$$

$$= \frac{1}{(2\pi)^3}\int_{-\infty}^{\infty}\int_{-\infty}^{\infty}\int_{-\infty}^{\infty}\breve{W}(-\boldsymbol{\xi}',-\eta')e^{-i(\boldsymbol{k}_1\cdot\boldsymbol{\xi}'-\omega_1\eta')}d\eta' d\boldsymbol{\xi}' = W(\boldsymbol{k}_1,\omega_1)$$

where $\breve{W}(-\boldsymbol{\xi},-\eta)=\left\langle h(\boldsymbol{r}_2,t_2)h(\boldsymbol{r}_1,t_1)\right\rangle=\left\langle h(\boldsymbol{r}_1,t_1)h(\boldsymbol{r}_2,t_2)\right\rangle=\breve{W}(\boldsymbol{\xi},\eta)$ is used.

The first term in Eq. (4.34) represents coherent energy flux of the waves reflected from the mean flame surface reflection of scattering waves, which are in phase and simply add to give total amplitude. On the other hand, the second term is related to incoherent energy flux. This results from fluctuation in scattering waves which have random phase difference and can add destructively to give a smaller amplitude than the ones which are coherent.

Transmitted acoustic energy flux can be evaluated in a similar way to the preceding analysis of reflection energy flux. Comparing Eq. (4.8) with transmitted acoustic pressure / velocity fields in Eqs. (3.137) and (3.138) yields

$$P(\boldsymbol{k},\omega,z)=i\frac{\omega}{\omega_0}\left(\frac{\rho_2 q_0^{(1)}}{\rho_1 q_k^{(2)}}\right)^{1/2}S^{21}(\boldsymbol{k},\boldsymbol{k_0},\omega,\omega_0)\,\mathrm{e}^{iq_k^{(2)}z}$$

$$\vec{\boldsymbol{V}}(\boldsymbol{k},\omega,z)=i\frac{\varepsilon c_1}{\omega_0}\left(\frac{\rho_1 q_0^{(1)}}{\rho_2 q_k^{(2)}}\right)^{1/2}S^{21}(\boldsymbol{k},\boldsymbol{k_0},\omega,\omega_0)\vec{\boldsymbol{K}}_+^{(2)}\,\mathrm{e}^{iq_k^{(2)}z}$$

The first and the second terms on the R.H.S. of (4.11) are of the form

$$\left\langle P(\boldsymbol{k},\omega,z)\vec{\boldsymbol{V}}(-\boldsymbol{k}',-\omega',z)\right\rangle$$
$$=\frac{\varepsilon c_1\omega}{\omega_0^2}\frac{q_0^{(1)}}{(q_k^{(2)}q_{k'}^{(2)})^{1/2}}\left\langle S^{21}(\boldsymbol{k},\boldsymbol{k_0},\omega,\omega_0)S^{21}(-\boldsymbol{k}',\boldsymbol{k_0},-\omega',\omega_0)\right\rangle\vec{\boldsymbol{K}}_-'^{(2)}\,\mathrm{e}^{i(q_k^{(2)}+q_{k'}^{(2)})z} \tag{4.36}$$

$$\left\langle P(\boldsymbol{k},\omega,z)\vec{\boldsymbol{V}}^*(\boldsymbol{k}',\omega',z)\right\rangle$$
$$=\frac{\varepsilon c_1\omega}{\omega_0^2}\left(\frac{q_0^{(1)}}{q_k^{(2)}}\right)^{1/2}\left(\frac{q_0^{(1)}}{q_{k'}^{(2)}}\right)^{1/2*}\left\langle S^{21}(\boldsymbol{k},\boldsymbol{k_0},\omega,\omega_0)S^{21*}(\boldsymbol{k}',\boldsymbol{k_0},\omega',\omega_0)\right\rangle\vec{\boldsymbol{K}}_+'^{(2)*}\,\mathrm{e}^{i[q_k^{(2)}-(q_{k'}^{(2)})^*]z} \tag{4.37}$$

; $\vec{\boldsymbol{K}}_\pm'^{(m)}=\boldsymbol{k}'\pm q_{k'}^{(m)}\vec{\boldsymbol{e}}_z$

Taking ensemble average of Eq. (3.132) yields the form

$$\left\langle S^{21}(\boldsymbol{k},\boldsymbol{k_0},\omega,\omega_0)\right\rangle=\left\langle T_J(\boldsymbol{k},\omega)\right\rangle\delta(\boldsymbol{k}-\boldsymbol{k_0})\delta(\omega-\omega_0) \tag{4.38}$$

where $\left\langle T_J(\boldsymbol{k},\omega)\right\rangle = D_J(\boldsymbol{k},\omega)\left[1+\frac{1}{2}\int_{\omega'}\iint_{k'} G_J(\boldsymbol{k}',\boldsymbol{k_0},\boldsymbol{k},\omega',\omega_0,\omega)W(\boldsymbol{k}-\boldsymbol{k}',\omega-\omega')d\boldsymbol{k}'d\omega'\right]$

which leads to fluctuation in scattering amplitude in the form

$$\begin{aligned}\Delta S^{21}_{(\boldsymbol{k},\boldsymbol{k_0},\omega,\omega_0)} &= S^{21}(\boldsymbol{k},\boldsymbol{k_0},\omega,\omega_0)-\left\langle S^{21}(\boldsymbol{k},\boldsymbol{k_0},\omega,\omega_0)\right\rangle \\ &= B_J(\boldsymbol{k},\boldsymbol{k_0},\omega,\omega_0)h(\boldsymbol{k}-\boldsymbol{k_0},\omega-\omega_0)+O(h^2)\end{aligned} \tag{4.39}$$

which yields the second moment of scattering amplitude

$$\begin{aligned}&\left\langle S^{21}(\boldsymbol{k},\boldsymbol{k_0},\omega,\omega_0)S^{21}(-\boldsymbol{k}',\boldsymbol{k_0},-\omega',\omega_0)\right\rangle \\ &=\left\langle S^{21}_{(\boldsymbol{k},\boldsymbol{k_0},\omega,\omega_0)}\right\rangle\left\langle S^{21}_{(-\boldsymbol{k}',\boldsymbol{k_0},-\omega',\omega_0)}\right\rangle+\left\langle \Delta S^{21}_{(\boldsymbol{k},\boldsymbol{k_0},\omega,\omega_0)}\Delta S^{21}_{(-\boldsymbol{k}',\boldsymbol{k_0},-\omega',\omega_0)}\right\rangle\end{aligned} \tag{4.40}$$

$$\begin{aligned}&=\left\langle T_J(\boldsymbol{k},\omega)\right\rangle\left\langle T_J(-\boldsymbol{k}',-\omega')\right\rangle\delta(\boldsymbol{k}-\boldsymbol{k_0})\delta(\omega-\omega_0)\delta(\boldsymbol{k}'+\boldsymbol{k_0})\delta(\omega'+\omega_0) \\ &+B_J(\boldsymbol{k},\boldsymbol{k_0},\omega,\omega_0)B_J(-\boldsymbol{k}',\boldsymbol{k_0},-\omega',\omega_0)W(\boldsymbol{k}-\boldsymbol{k_0},\omega-\omega_0)\delta(\boldsymbol{k}-\boldsymbol{k}'-2\boldsymbol{k_0})\delta(\omega-\omega'-2\omega_0)+O(h^3)\end{aligned}$$

$$\begin{aligned}&\left\langle S^{21}(\boldsymbol{k},\boldsymbol{k_0},\omega,\omega_0)S^{21*}(\boldsymbol{k}',\boldsymbol{k_0},\omega',\omega_0)\right\rangle \\ &=\left\langle S^{21}_{(\boldsymbol{k},\boldsymbol{k_0},\omega,\omega_0)}\right\rangle\left\langle S^{21*}_{(\boldsymbol{k}',\boldsymbol{k_0},\omega',\omega_0)}\right\rangle+\left\langle \Delta S^{21}_{(\boldsymbol{k},\boldsymbol{k_0},\omega,\omega_0)}\Delta S^{21*}_{(\boldsymbol{k}',\boldsymbol{k_0},\omega',\omega_0)}\right\rangle \\ &=\left\langle T_J(\boldsymbol{k},\omega)\right\rangle\left\langle T_J^{\,*}(\boldsymbol{k}',\omega')\right\rangle\delta(\boldsymbol{k}-\boldsymbol{k_0})\delta(\omega-\omega_0)\delta(\boldsymbol{k}'-\boldsymbol{k_0})\delta(\omega'-\omega_0) \\ &+B_J(\boldsymbol{k},\boldsymbol{k_0},\omega,\omega_0)B_J^*(\boldsymbol{k}',\boldsymbol{k_0},\omega',\omega_0)W(\boldsymbol{k}-\boldsymbol{k_0},\omega-\omega_0)\delta(\boldsymbol{k}-\boldsymbol{k}')\delta(\omega-\omega')+O(h^3)\end{aligned} \tag{4.41}$$

It is found by substituting Eqs. (4.36) and (4.40) into Eq. (4.11) that the first term on the R.H.S. of Eq. (4.11) vanishes as does Eq. (4.32). The second term on the R.H.S. of Eq. (4.11) yields the form using Eqs. (4.37) and (4.41)

The second term =

$$\frac{\varepsilon c_1\omega}{\omega_0^2}\left(\frac{q_0^{(1)}}{q_k^{(2)}}\right)^{1/2}\left(\frac{q_0^{(1)}}{q_{k'}^{(2)}}\right)^{1/2*}\vec{\boldsymbol{K}}_+'^{(2)*}\,\mathrm{e}^{i[q_k^{(2)}-(q_{k'}^{(2)})^*]z}\times$$

$$\frac{1}{2}\mathrm{Re}\int_{\omega}\iint_{k}\int_{\omega'\to\omega}\iint_{k'\to k}\left[\begin{array}{l}\left\langle T_J(\boldsymbol{k},\omega)\right\rangle\left\langle T_J^{\,*}(\boldsymbol{k}',\omega')\right\rangle\delta(\boldsymbol{k}-\boldsymbol{k_0})\delta(\omega-\omega_0)\delta(\boldsymbol{k}'-\boldsymbol{k_0})\delta(\omega'-\omega_0) \\ +B_J(\boldsymbol{k},\boldsymbol{k_0},\omega,\omega_0)B_J^*(\boldsymbol{k}',\boldsymbol{k_0},\omega',\omega_0)\times \\ W(\boldsymbol{k}-\boldsymbol{k_0},\omega-\omega_0)\delta(\boldsymbol{k}-\boldsymbol{k}')\delta(\omega-\omega')\end{array}\right]d\boldsymbol{k}'d\omega'd\boldsymbol{k}d\omega$$

$$+O(h^3)$$

$$= \frac{\varepsilon c_1}{2\omega_0} \mathrm{Re} \left\{ \begin{array}{l} \vec{\boldsymbol{K}}_{0+}^{(2)*} \left| \left(\frac{q_0^{(1)}}{q_0^{(2)}} \right)^{1/2} \left\langle T_J(\boldsymbol{k}_0, \omega_0) \right\rangle \right|^2 \mathrm{e}^{i[q_0^{(2)} - (q_0^{(2)})^*]z} \\ + \int_{\omega} \iint_{\boldsymbol{k}} \frac{\omega}{\omega_0} \left| \left(\frac{q_0^{(1)}}{q_k^{(2)}} \right)^{1/2} B_J(\boldsymbol{k}, \boldsymbol{k}_0, \omega, \omega_0) \right|^2 W(\boldsymbol{k} - \boldsymbol{k}_0, \omega - \omega_0) \vec{\boldsymbol{K}}_{+}^{(2)*} \mathrm{e}^{i[q_k^{(2)} - (q_k^{(2)})^*]z} d\boldsymbol{k} d\omega \end{array} \right\} + O(h^3)$$

$$= \frac{\varepsilon c_1}{2\omega_0} \left[\begin{array}{l} \mathrm{Re}\left(\vec{\boldsymbol{K}}_{0+}^{(2)} \right) \left| \frac{q_0^{(1)}}{q_0^{(2)}} \right| \left| \left\langle T_J(\boldsymbol{k}_0, \omega_0) \right\rangle \right|^2 \mathrm{e}^{-2\,\mathrm{Im}(q_0^{(2)})z} \\ + \int_{\omega} \iint_{\boldsymbol{k}} \frac{\omega}{\omega_0} \left| \frac{q_0^{(1)}}{q_k^{(2)}} \right| \left| B_J(\boldsymbol{k}, \boldsymbol{k}_0, \omega, \omega_0) \right|^2 W(\boldsymbol{k} - \boldsymbol{k}_0, \omega - \omega_0) \mathrm{Re}\left(\vec{\boldsymbol{K}}_{+}^{(2)} \right) \mathrm{e}^{-2\,\mathrm{Im}(q_k^{(2)})z} d\boldsymbol{k} d\omega \end{array} \right] + O(h^3)$$

with $\vec{\boldsymbol{K}}_{0+}^{(2)} = \boldsymbol{k}_0 + q_0^{(2)} \vec{\boldsymbol{e}}_z$ (4.42)

where the first and the second term of the last equation corresponds to coherent and incoherent part of transmission energy, respectively. Note that $e^{-2\,\mathrm{Im}(q_0^{(2)})z} = 1$ for a real value of $q_0^{(2)}$ when an incident angle is below critical angle (See Figure 10), which implies that coherent transmission energy propagates without attenuation in the specular direction.

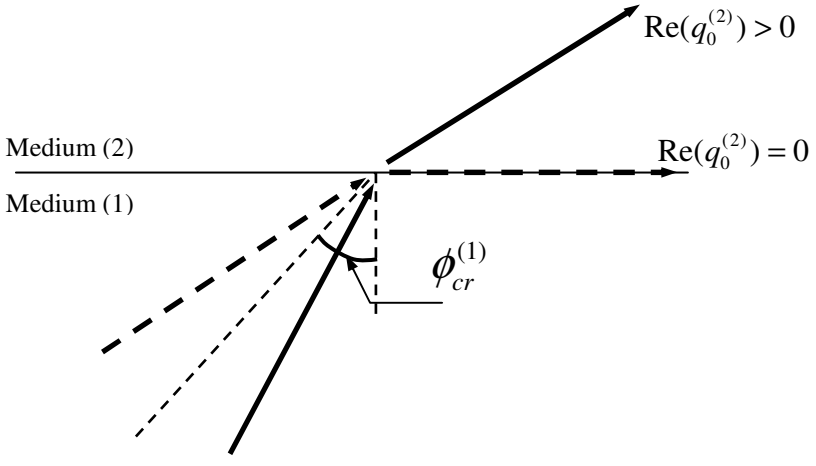

Figure 10 An incident wave angle below / above critical angle

On the other hand, when the incident angle is above the critical angle and $q_0^{(2)}$ has a pure imaginary value, coherent transmission energy can not penetrate into medium (2) and only propagates horizontally along the mean flame surface since $\mathrm{Re}\left(\vec{\boldsymbol{K}}_{0+}^{(2)}\right)=\mathrm{Re}\left(\boldsymbol{k_0}+q_0^{(2)}\vec{\boldsymbol{e}}_z\right)=\boldsymbol{k_0}$. Substituting Eq. (4.42) into Eq. (4.11) yields the acoustic energy flux transmitted from unit area of mean flame surface (z = 0) whose normal vector $\vec{\boldsymbol{n}}$ is equal to $\vec{\boldsymbol{e}}_z$.

$$\left\langle \vec{\boldsymbol{I}}_{av} \right\rangle_T \cdot \vec{\boldsymbol{n}} =$$

$$\frac{\varepsilon c_1 q_0^{(1)}}{2\omega_0}\left[\mathrm{Re}\left(\frac{q_0^{(2)}}{\left|q_0^{(2)}\right|}\right)\left|\left\langle T_J(\boldsymbol{k_0},\omega_0)\right\rangle\right|^2+\int_{\omega}\iint_{\boldsymbol{k}}\frac{\omega}{\omega_0}\left|B_J(\boldsymbol{k},\boldsymbol{k_0},\omega,\omega_0)\right|^2 W(\boldsymbol{k}-\boldsymbol{k_0},\omega-\omega_0)\frac{\mathrm{Re}(q_k^{(2)})}{\left|q_k^{(2)}\right|}d\boldsymbol{k}d\omega\right]$$

$$+O(h^3)$$

$$=\frac{\varepsilon c_1 q_0^{(1)}}{2\omega_0}\left[\mathrm{Re}\left(\frac{q_0^{(2)}}{\left|q_0^{(2)}\right|}\right)\left|\left\langle T_J(\boldsymbol{k_0},\omega_0)\right\rangle\right|^2+\int_{\omega}\iint_{|\boldsymbol{k}|<\frac{|\omega|}{c_2}}\frac{\omega}{\omega_0}\left|B_J(\boldsymbol{k},\boldsymbol{k_0},\omega,\omega_0)\right|^2 W(\boldsymbol{k}-\boldsymbol{k_0},\omega-\omega_0)d\boldsymbol{k}d\omega\right]+O(h^3) \tag{4.43}$$

where $q_0^{(1)}$ is a positive real value.

The reflected / transmitted energy flux normalized by incident energy flux can be obtained by dividing Eqs. (4.34) and (4.43) by Eq. (4.23), respectively, where terms of $O(h^3)$ and higher are neglected.

$$
\begin{aligned}
E_R &\equiv \left\langle \vec{\boldsymbol{I}}_{av} \right\rangle_R \cdot (-\vec{\boldsymbol{n}}) \Big/ \vec{\boldsymbol{I}}_{av,I} \cdot \vec{\boldsymbol{n}} \\
&= \left| \left\langle V_J(\boldsymbol{k_0}, \omega_0) \right\rangle \right|^2 + \int_{\omega} \iint_{|\boldsymbol{k}| < \frac{|\omega|}{c_1}} \frac{\omega}{\omega_0} \left| A_J(\boldsymbol{k}, \boldsymbol{k_0}, \omega, \omega_0) \right|^2 W(\boldsymbol{k} - \boldsymbol{k_0}, \omega - \omega_0) d\boldsymbol{k} d\omega \\
&= \left| R_J(\boldsymbol{k_0}, \omega_0) \right|^2 + \mathrm{Re}\left(R_J^*(\boldsymbol{k_0}, \omega_0) D_J(\boldsymbol{k_0}, \omega_0) \int_{\omega} \iint_{\boldsymbol{k}} F_J(\boldsymbol{k}, \boldsymbol{k_0}, \boldsymbol{k_0}, \omega, \omega_0, \omega_0) W(\boldsymbol{k_0} - \boldsymbol{k}, \omega_0 - \omega) d\boldsymbol{k} d\omega \right) \\
&+ \int_{\omega} \iint_{|\boldsymbol{k}| < \frac{|\omega|}{c_1}} \frac{\omega}{\omega_0} \left| A_J(\boldsymbol{k}, \boldsymbol{k_0}, \omega, \omega_0) \right|^2 W(\boldsymbol{k} - \boldsymbol{k_0}, \omega - \omega_0) d\boldsymbol{k} d\omega
\end{aligned}
\tag{4.44}
$$

$$
\begin{aligned}
E_T &\equiv \left\langle \vec{\boldsymbol{I}}_{av} \right\rangle_T \cdot \vec{\boldsymbol{n}} \Big/ \vec{\boldsymbol{I}}_{av,I} \cdot \vec{\boldsymbol{n}} \\
&= \mathrm{Re}\left(\frac{q_0^{(2)}}{\left| q_0^{(2)} \right|} \right) \left| \left\langle T_J(\boldsymbol{k_0}, \omega_0) \right\rangle \right|^2 + \int_{\omega} \iint_{|\boldsymbol{k}| < \frac{|\omega|}{c_2}} \frac{\omega}{\omega_0} \left| B_J(\boldsymbol{k}, \boldsymbol{k_0}, \omega, \omega_0) \right|^2 W(\boldsymbol{k} - \boldsymbol{k_0}, \omega - \omega_0) d\boldsymbol{k} d\omega \\
&= \mathrm{Re}\left(\frac{q_0^{(2)}}{\left| q_0^{(2)} \right|} \right) \left| D_J(\boldsymbol{k_0}, \omega_0) \right|^2 \left(1 + \int_{\omega} \iint_{\boldsymbol{k}} \mathrm{Re}\left[G_J(\boldsymbol{k}, \boldsymbol{k_0}, \boldsymbol{k_0}, \omega, \omega_0, \omega_0) \right] W(\boldsymbol{k_0} - \boldsymbol{k}, \omega_0 - \omega) d\boldsymbol{k} d\omega \right) \\
&+ \int_{\omega} \iint_{|\boldsymbol{k}| < \frac{|\omega|}{c_2}} \frac{\omega}{\omega_0} \left| B_J(\boldsymbol{k}, \boldsymbol{k_0}, \omega, \omega_0) \right|^2 W(\boldsymbol{k} - \boldsymbol{k_0}, \omega - \omega_0) d\boldsymbol{k} d\omega
\end{aligned}
\tag{4.45}
$$

where the mean reflection / transmission coefficients, V and T, were re-expressed using Eqs. (4.19) and (4.38). Combining Eqs. (4.44) and (4.45) yields total scattering energy flux.

$$
\begin{aligned}
E_{total} &= E_R + E_T \\
&= \left| R_J(\boldsymbol{k_0}, \omega_0) \right|^2 + \mathrm{Re}\left(\frac{q_0^{(2)}}{\left| q_0^{(2)} \right|} \right) \left| D_J(\boldsymbol{k_0}, \omega_0) \right|^2 + \int_{\omega} \iint_{\boldsymbol{k}} \mathrm{Re}\left[H_J(\boldsymbol{k}, \boldsymbol{k_0}, \boldsymbol{k_0}, \omega, \omega_0, \omega_0) \right] W(\boldsymbol{k_0} - \boldsymbol{k}, \omega_0 - \omega) d\boldsymbol{k} d\omega \\
&+ \int_{\omega} \iint_{\boldsymbol{k}} \frac{\omega}{\omega_0} \left[\mathrm{Re}\left(\frac{q_k^{(1)}}{\left| q_k^{(1)} \right|} \right) \left| A_J(\boldsymbol{k}, \boldsymbol{k_0}, \omega, \omega_0) \right|^2 + \mathrm{Re}\left(\frac{q_k^{(2)}}{\left| q_k^{(2)} \right|} \right) \left| B_J(\boldsymbol{k}, \boldsymbol{k_0}, \omega, \omega_0) \right|^2 \right] W(\boldsymbol{k} - \boldsymbol{k_0}, \omega - \omega_0) d\boldsymbol{k} d\omega \\
&+ O(h^3)
\end{aligned}
\tag{4.46}
$$

where

$$H_J(\boldsymbol{k},\boldsymbol{k_0},\boldsymbol{k_0},\omega,\omega_0,\omega_0) = R_J^*(\boldsymbol{k_0},\omega_0)D_J(\boldsymbol{k_0},\omega_0)F_J(\boldsymbol{k},\boldsymbol{k_0},\boldsymbol{k_0},\omega,\omega_0,\omega_0)$$
$$+\mathrm{Re}\left(\frac{q_0^{(2)}}{\left|q_0^{(2)}\right|}\right)\left|D_J(\boldsymbol{k_0},\omega_0)\right|^2 G_J(\boldsymbol{k},\boldsymbol{k_0},\boldsymbol{k_0},\omega,\omega_0,\omega_0)$$

and, Eqs. (3.108), (3.109), (3.116), (3.117), (3.129), and (3.130) yield

$$R_J(\boldsymbol{k}_0,\omega_0) = \frac{\rho_2 q_0^{(1)} - \rho_1\left(q_0^{(2)} + \beta(\omega_0)\right)}{\rho_2 q_0^{(1)} + \rho_1\left(q_0^{(2)} + \beta(\omega_0)\right)}\ ,\quad D_J(\boldsymbol{k}_0,\omega_0) = \frac{2\left(\rho_1\rho_2 q_0^{(1)} q_0^{(2)}\right)^{1/2}}{\rho_2 q_0^{(1)} + \rho_1\left(q_0^{(2)} + \beta(\omega_0)\right)} \qquad (4.47)$$

$$A_J(\boldsymbol{k},\boldsymbol{k_0},\omega,\omega_0) = \frac{iD_J(\boldsymbol{k}_0,\omega_0)D_J(\boldsymbol{k},\omega)}{2\rho_1\rho_2(q_0^{(2)}q_k^{(2)})^{1/2}}\left[\begin{array}{l}\dfrac{\omega_0}{\omega}\rho_1\left(q_k^{(2)} + \beta(\omega)\right)\left\{(\rho_2-\rho_1)q_0^{(2)} - \rho_1\beta(\omega_0)\right\} \\ +\rho_2\alpha_J(\boldsymbol{k},\boldsymbol{k_0},\omega_0)\end{array}\right]$$

$$B_J(\boldsymbol{k},\boldsymbol{k_0},\omega,\omega_0) = \frac{iD_J(\boldsymbol{k}_0,\omega_0)D_J(\boldsymbol{k},\omega)}{2(\rho_1\rho_2 q_k^{(1)} q_0^{(2)})^{1/2}}\left[-\frac{\omega_0}{\omega}q_k^{(1)}\left\{(\rho_2-\rho_1)q_0^{(2)} - \rho_1\beta(\omega_0)\right\} + \alpha_J(\boldsymbol{k},\boldsymbol{k_0},\omega_0)\right]$$

$$F_J(\boldsymbol{k},\boldsymbol{k_0},\boldsymbol{k_0},\omega,\omega_0,\omega_0) = \frac{-D_J(\boldsymbol{k}_0,\omega_0)\beta(\omega_0)\left|\boldsymbol{k}-\boldsymbol{k_0}\right|^2}{2q_0^{(2)}}$$
$$+\frac{i}{\left(q_0^{(2)}\right)^{1/2}}\left\{\frac{\omega}{\omega_0}\left(\frac{\rho_1 q_k^{(1)}}{\rho_2}\right)^{1/2}\left(q_0^{(2)} + \beta(\omega_0)\right) + \left(\frac{\rho_2}{\rho_1 q_k^{(1)}}\right)^{1/2}\left[\left(\frac{\omega}{c_1}\right)^2 - \boldsymbol{k}\cdot\boldsymbol{k_0}\right]\right\}A_J(\boldsymbol{k},\boldsymbol{k_0},\omega,\omega_0)$$
$$+\frac{i}{\left(q_0^{(2)}\right)^{1/2}}\left\{\frac{\omega}{\omega_0}\left(q_k^{(2)}\right)^{1/2}\left(q_0^{(2)} + \beta(\omega_0)\right) - \left(q_k^{(2)}\right)^{-1/2}\left[\left(\frac{\omega}{c_2}\right)^2 - \boldsymbol{k}\cdot\boldsymbol{k_0} + \beta(\omega)q_k^{(2)}\right]\right\}B_J(\boldsymbol{k},\boldsymbol{k_0},\omega,\omega_0)$$
$$G_J(\boldsymbol{k},\boldsymbol{k_0},\boldsymbol{k_0},\omega,\omega_0,\omega_0) = \left(\frac{\omega_0}{c_2}\right)^2 - \left(\frac{\omega_0}{c_1}\right)^2 - \frac{\rho_1\beta(\omega_0)\left|\boldsymbol{k}-\boldsymbol{k_0}\right|^2}{\rho_2 q_0^{(1)} + \rho_1\left(q_0^{(2)} + \beta(\omega_0)\right)}$$
$$+i\left\{-\frac{\omega}{\omega_0}\left(q_0^{(1)}q_k^{(1)}\right)^{1/2} + \left(q_0^{(1)}q_k^{(1)}\right)^{-1/2}\left[\left(\frac{\omega}{c_1}\right)^2 - \boldsymbol{k}\cdot\boldsymbol{k_0}\right]\right\}A_J(\boldsymbol{k},\boldsymbol{k_0},\omega,\omega_0)$$
$$-i\left\{\frac{\omega}{\omega_0}\left(\frac{\rho_2}{\rho_1}q_0^{(1)}q_k^{(2)}\right)^{1/2} + \left(\frac{\rho_2}{\rho_1}q_0^{(1)}q_k^{(2)}\right)^{-1/2}\left[\left(\frac{\omega}{c_2}\right)^2 - \boldsymbol{k}\cdot\boldsymbol{k_0} + \beta(\omega)q_k^{(2)}\right]\right\}B_J(\boldsymbol{k},\boldsymbol{k_0},\omega,\omega_0)$$

The first three terms, which include *R*, *D*, and *H*, on the right-hand side of Eq. (4.46) represent coherent energy flux of scattering acoustic fields. The last two terms, which include *A* and *B*, represent incoherent energy flux of reflection and transmission

scattering fields, respectively. The terms including R and D arise from zeroth order scattering amplitude which represent reflection and transmission, respectively, from the mean flame surface. The term including H is responsible for reduction of the coherent field, which describes coherent energy transfer to incoherent field due to the wrinkled flame surface, as will be shown in the accompanying analysis.

4.3 Acoustic energy balance

Since acoustic energy amplification / damping is caused either by the acoustic velocity jump due to unsteady heat release or by unsteady motion of flame, neglecting these effects must lead to acoustic energy balance. Acoustic energy balance states that total energy flux of scattering (reflection and transmission) fields is equal to original energy flux from incident wave fields. Alternatively, it can be stated that Eq. (4.46) yields unity in case that $\beta = 0$ to second order in h. To prove this, the following analysis will show that coherent energy reduction (H term) has the same magnitude as, but an opposite sign to, incoherent energy production (sum of A and B terms). Note that H, R, D, A, B, F, G below denote the values corresponding to no jump condition, i.e., $\beta = 0$. Constant frequency assumption will be invoked in the middle of analysis as needed. $q_0^{(2)}$ is assumed to be a real value since an imaginary value of $q_0^{(2)}$ allows some transmission energy terms to vanish, which should be proved more easily.

$$\begin{aligned} &H(\boldsymbol{k},\boldsymbol{k_0},\boldsymbol{k_0},\omega,\omega_0,\omega_0) \equiv H_J(\boldsymbol{k},\boldsymbol{k_0},\boldsymbol{k_0},\omega,\omega_0,\omega_0)_{\beta=0} \\ &= R^*(\boldsymbol{k_0},\omega_0)D(\boldsymbol{k_0},\omega_0)F(\boldsymbol{k},\boldsymbol{k_0},\boldsymbol{k_0},\omega,\omega_0,\omega_0) + \left|D(\boldsymbol{k_0},\omega_0)\right|^2 G(\boldsymbol{k},\boldsymbol{k_0},\boldsymbol{k_0},\omega,\omega_0,\omega_0) \end{aligned} \tag{4.48}$$

$$= R^*(\boldsymbol{k_0},\omega_0)D(\boldsymbol{k_0},\omega_0)\begin{bmatrix} \dfrac{i}{\left(q_0^{(2)}\right)^{1/2}}\left\{\dfrac{\omega}{\omega_0}\left(\dfrac{\rho_1 q_k^{(1)}}{\rho_2}\right)^{1/2} q_0^{(2)} + \left(\dfrac{\rho_2}{\rho_1 q_k^{(1)}}\right)^{1/2}\left[\left(\dfrac{\omega}{c_1}\right)^2 - \boldsymbol{k}\cdot\boldsymbol{k_0}\right]\right\} A(\boldsymbol{k},\boldsymbol{k_0},\omega,\omega_0) \\ + \dfrac{i}{\left(q_0^{(2)}\right)^{1/2}}\left\{\dfrac{\omega}{\omega_0}\left(q_k^{(2)}\right)^{1/2} q_0^{(2)} - \left(q_k^{(2)}\right)^{-1/2}\left[\left(\dfrac{\omega}{c_2}\right)^2 - \boldsymbol{k}\cdot\boldsymbol{k_0}\right]\right\} B(\boldsymbol{k},\boldsymbol{k_0},\omega,\omega_0) \end{bmatrix}$$

$$+\left|D(\boldsymbol{k_0},\omega_0)\right|^2\begin{bmatrix} \left[\left(\dfrac{\omega_0}{c_2}\right)^2 - \left(\dfrac{\omega_0}{c_1}\right)^2\right] \\ +i\left\{-\dfrac{\omega}{\omega_0}\left(q_0^{(1)}q_k^{(1)}\right)^{1/2} + \left(q_0^{(1)}q_k^{(1)}\right)^{-1/2}\left[\left(\dfrac{\omega}{c_1}\right)^2 - \boldsymbol{k}\cdot\boldsymbol{k_0}\right]\right\} A(\boldsymbol{k},\boldsymbol{k_0},\omega,\omega_0) \\ -i\left\{\dfrac{\omega}{\omega_0}\left(\dfrac{\rho_2}{\rho_1} q_0^{(1)} q_k^{(2)}\right)^{1/2} + \left(\dfrac{\rho_2}{\rho_1} q_0^{(1)} q_k^{(2)}\right)^{-1/2}\left[\left(\dfrac{\omega}{c_2}\right)^2 - \boldsymbol{k}\cdot\boldsymbol{k_0}\right]\right\} B(\boldsymbol{k},\boldsymbol{k_0},\omega,\omega_0) \end{bmatrix}$$

$$= \left|D(\boldsymbol{k_0},\omega_0)\right|^2\left[\left(\frac{\omega_0}{c_2}\right)^2 - \left(\frac{\omega_0}{c_1}\right)^2\right] + iD(\boldsymbol{k_0},\omega_0)A(\boldsymbol{k},\boldsymbol{k_0},\omega,\omega_0)\times$$

$$\begin{Bmatrix} \dfrac{\omega}{\omega_0}\left(\dfrac{\rho_1 q_k^{(1)} q_0^{(2)}}{\rho_2}\right)^{1/2}\left[R^*(\boldsymbol{k_0},\omega_0) - \left(\dfrac{\rho_2 q_0^{(1)}}{\rho_1 q_0^{(2)}}\right)^{1/2} D^*(\boldsymbol{k_0},\omega_0)\right] \\ +\left(\dfrac{\rho_2}{\rho_1 q_k^{(1)} q_0^{(2)}}\right)^{1/2}\left[\left(\dfrac{\omega}{c_1}\right)^2 - \boldsymbol{k}\cdot\boldsymbol{k_0}\right]\left[R^*(\boldsymbol{k_0},\omega_0) + \left(\dfrac{\rho_1 q_0^{(2)}}{\rho_2 q_0^{(1)}}\right)^{1/2} D^*(\boldsymbol{k_0},\omega_0)\right] \end{Bmatrix}$$

$$+iD(\boldsymbol{k_0},\omega_0)B(\boldsymbol{k},\boldsymbol{k_0},\omega,\omega_0)\times$$

$$\begin{Bmatrix} \dfrac{\omega}{\omega_0}\left(q_0^{(2)}q_k^{(2)}\right)^{1/2}\left[R^*(\boldsymbol{k_0},\omega_0) - \left(\dfrac{\rho_2 q_0^{(1)}}{\rho_1 q_0^{(2)}}\right)^{1/2} D^*(\boldsymbol{k_0},\omega_0)\right] \\ -\left(q_0^{(2)}q_k^{(2)}\right)^{-1/2}\left[\left(\dfrac{\omega}{c_2}\right)^2 - \boldsymbol{k}\cdot\boldsymbol{k_0}\right]\left[R^*(\boldsymbol{k_0},\omega_0) + \left(\dfrac{\rho_1 q_0^{(2)}}{\rho_2 q_0^{(1)}}\right)^{1/2} D^*(\boldsymbol{k_0},\omega_0)\right] \end{Bmatrix}$$

(Note that $q_0^{(1)}$ and $q_0^{(2)}$ are real values, which leads to)

$$= \left|D(\boldsymbol{k}_0,\omega_0)\right|^2 \left[\left(\frac{\omega_0}{c_2}\right)^2 - \left(\frac{\omega_0}{c_1}\right)^2\right]$$

$$+iD(\boldsymbol{k}_0,\omega_0)A(\boldsymbol{k},\boldsymbol{k}_0,\omega,\omega_0)\left\{-\frac{\omega}{\omega_0}\left(\frac{\rho_1 q_k^{(1)} q_0^{(2)}}{\rho_2}\right)^{1/2} + \left(\frac{\rho_2}{\rho_1 q_k^{(1)} q_0^{(2)}}\right)^{1/2}\left[\left(\frac{\omega}{c_1}\right)^2 - \boldsymbol{k}\cdot\boldsymbol{k}_0\right]\right\} \quad (4.49)$$

$$-iD(\boldsymbol{k}_0,\omega_0)B(\boldsymbol{k},\boldsymbol{k}_0,\omega,\omega_0)\left\{\frac{\omega}{\omega_0}\left(q_0^{(2)} q_k^{(2)}\right)^{1/2} + \left(q_0^{(2)} q_k^{(2)}\right)^{-1/2}\left[\left(\frac{\omega}{c_2}\right)^2 - \boldsymbol{k}\cdot\boldsymbol{k}_0\right]\right\}$$

where A and B are of the form setting $\beta = 0$ in Eq. (4.47)

$$A(\boldsymbol{k},\boldsymbol{k}_0,\omega,\omega_0) = \frac{iD(\boldsymbol{k}_0,\omega_0)D(\boldsymbol{k},\omega)}{2}\left[\frac{\omega_0}{\omega}(1-\rho_1/\rho_2)(q_0^{(2)}q_k^{(2)})^{1/2} + \rho_1^{-1}(q_0^{(2)}q_k^{(2)})^{-1/2}\alpha(\boldsymbol{k},\boldsymbol{k}_0,\omega_0)\right]$$

$$B(\boldsymbol{k},\boldsymbol{k}_0,\omega,\omega_0) = \frac{iD(\boldsymbol{k}_0,\omega_0)D(\boldsymbol{k},\omega)}{2}\left(\frac{\rho_2}{\rho_1}\right)^{1/2}\left[-\frac{\omega_0}{\omega}\left(1-\frac{\rho_1}{\rho_2}\right)\left(q_k^{(1)}q_0^{(2)}\right)^{1/2} + \frac{\alpha(\boldsymbol{k},\boldsymbol{k}_0,\omega_0)}{\rho_2\left(q_k^{(1)}q_0^{(2)}\right)^{1/2}}\right]$$

(4.50)

which leads Eq. (4.49) to:

$$= \left|D(\boldsymbol{k}_0,\omega_0)\right|^2 \left[\left(\frac{\omega_0}{c_2}\right)^2 - \left(\frac{\omega_0}{c_1}\right)^2\right]$$

$$+\frac{D^2(\boldsymbol{k}_0,\omega_0)D(\boldsymbol{k},\omega)}{2}\left[\frac{\omega_0}{\omega}(1-\rho_1/\rho_2)(q_0^{(2)}q_k^{(2)})^{1/2} + \rho_1^{-1}(q_0^{(2)}q_k^{(2)})^{-1/2}\alpha(\boldsymbol{k},\boldsymbol{k}_0,\omega_0)\right]\times$$

$$\left\{\frac{\omega}{\omega_0}\left(\frac{\rho_1 q_k^{(1)} q_0^{(2)}}{\rho_2}\right)^{1/2} - \left(\frac{\rho_1 q_k^{(1)} q_0^{(2)}}{\rho_2}\right)^{-1/2}\left[\left(\frac{\omega}{c_1}\right)^2 - \boldsymbol{k}\cdot\boldsymbol{k}_0\right]\right\}$$

$$+\frac{D^2(\boldsymbol{k}_0,\omega_0)D(\boldsymbol{k},\omega)}{2}\left(\frac{\rho_2}{\rho_1}\right)^{1/2}\left[-\frac{\omega_0}{\omega}(1-\rho_1/\rho_2)\left(q_k^{(1)}q_0^{(2)}\right)^{1/2} + \rho_2^{-1}\left(q_k^{(1)}q_0^{(2)}\right)^{-1/2}\alpha(\boldsymbol{k},\boldsymbol{k}_0,\omega_0)\right]\times$$

$$\left\{\frac{\omega}{\omega_0}\left(q_0^{(2)}q_k^{(2)}\right)^{1/2} + \left(q_0^{(2)}q_k^{(2)}\right)^{-1/2}\left[\left(\frac{\omega}{c_2}\right)^2 - \boldsymbol{k}\cdot\boldsymbol{k}_0\right]\right\}$$

$$= \left|D(\boldsymbol{k}_0,\omega_0)\right|^2\left[\left(\frac{\omega_0}{c_2}\right)^2-\left(\frac{\omega_0}{c_1}\right)^2\right]+\frac{D^2(\boldsymbol{k}_0,\omega_0)D(\boldsymbol{k},\omega)}{2}\frac{\omega_0}{\omega}(1-\rho_1/\rho_2)(q_0^{(2)})^{1/2}\times$$

$$\left[\begin{array}{l}(q_k^{(2)})^{1/2}\left\{\dfrac{\omega}{\omega_0}\left(\dfrac{\rho_1 q_k^{(1)}q_0^{(2)}}{\rho_2}\right)^{1/2}-\left(\dfrac{\rho_1 q_k^{(1)}q_0^{(2)}}{\rho_2}\right)^{-1/2}\left[\left(\dfrac{\omega}{c_1}\right)^2-\boldsymbol{k}\cdot\boldsymbol{k}_0\right]\right\}\\ -\left(\dfrac{\rho_2 q_k^{(1)}}{\rho_1}\right)^{1/2}\left\{\dfrac{\omega}{\omega_0}\left(q_0^{(2)}q_k^{(2)}\right)^{1/2}+\left(q_0^{(2)}q_k^{(2)}\right)^{-1/2}\left[\left(\dfrac{\omega}{c_2}\right)^2-\boldsymbol{k}\cdot\boldsymbol{k}_0\right]\right\}\end{array}\right]$$

$$+\frac{D^2(\boldsymbol{k}_0,\omega_0)D(\boldsymbol{k},\omega)}{2}\rho_2^{-1}\left(q_0^{(2)}\right)^{-1/2}\alpha(\boldsymbol{k},\boldsymbol{k}_0,\omega_0)\times$$

$$\left[\begin{array}{l}\left(\dfrac{\rho_2}{\rho_1 q_k^{(1)}}\right)^{1/2}\left\{\dfrac{\omega}{\omega_0}\left(q_0^{(2)}q_k^{(2)}\right)^{1/2}+\left(q_0^{(2)}q_k^{(2)}\right)^{-1/2}\left[\left(\dfrac{\omega}{c_2}\right)^2-\boldsymbol{k}\cdot\boldsymbol{k}_0\right]\right\}\\ \dfrac{\rho_2}{\rho_1}(q_k^{(2)})^{-1/2}\left\{\dfrac{\omega}{\omega_0}\left(\dfrac{\rho_1 q_k^{(1)}q_0^{(2)}}{\rho_2}\right)^{1/2}-\left(\dfrac{\rho_1 q_k^{(1)}q_0^{(2)}}{\rho_2}\right)^{-1/2}\left[\left(\dfrac{\omega}{c_1}\right)^2-\boldsymbol{k}\cdot\boldsymbol{k}_0\right]\right\}\end{array}\right]$$

$$= \left|D(\boldsymbol{k}_0,\omega_0)\right|^2\left[\left(\frac{\omega_0}{c_2}\right)^2-\left(\frac{\omega_0}{c_1}\right)^2\right]+\frac{D^2(\boldsymbol{k}_0,\omega_0)D(\boldsymbol{k},\omega)}{2}\frac{\omega_0}{\omega}\left(\frac{\rho_2}{\rho_1}\right)^{1/2}\left(1-\frac{\rho_1}{\rho_2}\right)\times$$

$$\left[-\frac{\omega}{\omega_0}\left(q_k^{(1)}q_k^{(2)}\right)^{1/2}q_0^{(2)}\left(1-\frac{\rho_1}{\rho_2}\right)-\left\{\left(\frac{q_k^{(2)}}{q_k^{(1)}}\right)^{1/2}\left[\left(\frac{\omega}{c_1}\right)^2-\boldsymbol{k}\cdot\boldsymbol{k}_0\right]+\left(\frac{q_k^{(1)}}{q_k^{(2)}}\right)^{1/2}\left[\left(\frac{\omega}{c_2}\right)^2-\boldsymbol{k}\cdot\boldsymbol{k}_0\right]\right\}\right]$$

$$+\frac{D^2(\boldsymbol{k}_0,\omega_0)D(\boldsymbol{k},\omega)}{2}\left(\frac{\rho_2}{\rho_1}\right)^{1/2}\rho_2^{-1}\alpha(\boldsymbol{k},\boldsymbol{k}_0,\omega_0)\times$$

$$\left[\frac{\omega}{\omega_0}\left[\left(\frac{q_k^{(2)}}{q_k^{(1)}}\right)^{1/2}+\left(\frac{q_k^{(1)}}{q_k^{(2)}}\right)^{1/2}\right]-\frac{1}{\left(q_k^{(1)}q_k^{(2)}\right)^{1/2}q_0^{(2)}}\left\{\frac{\rho_2}{\rho_1}\left[\left(\frac{\omega}{c_1}\right)^2-\boldsymbol{k}\cdot\boldsymbol{k}_0\right]-\left[\left(\frac{\omega}{c_2}\right)^2-\boldsymbol{k}\cdot\boldsymbol{k}_0\right]\right\}\right]$$

(4.51)

In case of constant frequency, $\omega=\omega_0$, which occurs when the flame surface moves so slowly that the Doppler frequency shift effect is negligible, Eq. (4.51) further reduces to the following form. Note that $q_k^{(m)}=\left((\omega_0/c_m)^2-k^2\right)^{1/2}$ (m = {1, 2}) for $\omega=\omega_0$.

$$H(\boldsymbol{k},\boldsymbol{k_0},\boldsymbol{k_0},\omega,\omega_0,\omega_0) =$$

$$\left|D(\boldsymbol{k_0},\omega_0)\right|^2\left[\left(\frac{\omega_0}{c_2}\right)^2-\left(\frac{\omega_0}{c_1}\right)^2\right]+\frac{D^2(\boldsymbol{k}_0,\omega_0)D(\boldsymbol{k},\omega_0)}{2}\left(\frac{\rho_2}{\rho_1}\right)^{1/2}\times$$

$$\left[\begin{array}{l}-\left(q_k^{(1)}q_k^{(2)}\right)^{1/2}q_0^{(2)}\left(1-\dfrac{\rho_1}{\rho_2}\right)^2-\left(1-\dfrac{\rho_1}{\rho_2}\right)\left\{\left(\dfrac{q_k^{(2)}}{q_k^{(1)}}\right)^{1/2}\left[\left(\dfrac{\omega_0}{c_1}\right)^2-\boldsymbol{k}\cdot\boldsymbol{k_0}\right]+\left(\dfrac{q_k^{(1)}}{q_k^{(2)}}\right)^{1/2}\left[\left(\dfrac{\omega_0}{c_2}\right)^2-\boldsymbol{k}\cdot\boldsymbol{k_0}\right]\right\}\\ \rho_2^{-1}\alpha(\boldsymbol{k},\boldsymbol{k_0},\omega_0)\left[\left(\dfrac{q_k^{(2)}}{q_k^{(1)}}\right)^{1/2}+\left(\dfrac{q_k^{(1)}}{q_k^{(2)}}\right)^{1/2}\right]-\dfrac{\alpha^2(\boldsymbol{k},\boldsymbol{k_0},\omega_0)}{\rho_1\rho_2\left(q_k^{(1)}q_k^{(2)}\right)^{1/2}q_0^{(2)}}\end{array}\right]$$

$$=\left|D(\boldsymbol{k_0},\omega_0)\right|^2\left[\left(\frac{\omega_0}{c_2}\right)^2-\left(\frac{\omega_0}{c_1}\right)^2\right]+\frac{D^2(\boldsymbol{k}_0,\omega_0)D(\boldsymbol{k},\omega_0)}{2}\left(\frac{\rho_2}{\rho_1}\right)^{1/2}\times$$

$$\left[\begin{array}{l}-\left(q_k^{(1)}q_k^{(2)}\right)^{1/2}q_0^{(2)}\left(1-\dfrac{\rho_1}{\rho_2}\right)^2-\left(1-\dfrac{\rho_1}{\rho_2}\right)\left\{\left(\dfrac{q_k^{(2)}}{q_k^{(1)}}\right)^{1/2}\left[\left(\dfrac{\omega_0}{c_1}\right)^2-\boldsymbol{k}\cdot\boldsymbol{k_0}\right]+\left(\dfrac{q_k^{(1)}}{q_k^{(2)}}\right)^{1/2}\left[\left(\dfrac{\omega_0}{c_2}\right)^2-\boldsymbol{k}\cdot\boldsymbol{k_0}\right]\right\}\\ \rho_2^{-1}\left\{\rho_2\left[\left(\dfrac{\omega_0}{c_1}\right)^2-\boldsymbol{k}\cdot\boldsymbol{k_0}\right]-\rho_1\left[\left(\dfrac{\omega_0}{c_2}\right)^2-\boldsymbol{k}\cdot\boldsymbol{k_0}\right]\right\}\left[\left(\dfrac{q_k^{(2)}}{q_k^{(1)}}\right)^{1/2}+\left(\dfrac{q_k^{(1)}}{q_k^{(2)}}\right)^{1/2}\right]-\dfrac{\alpha^2(\boldsymbol{k},\boldsymbol{k_0},\omega_0)}{\rho_1\rho_2\left(q_k^{(1)}q_k^{(2)}\right)^{1/2}q_0^{(2)}}\end{array}\right]$$

$$=\left|D(\boldsymbol{k_0},\omega_0)\right|^2\left[\left(\frac{\omega_0}{c_2}\right)^2-\left(\frac{\omega_0}{c_1}\right)^2\right]+\frac{D^2(\boldsymbol{k}_0,\omega_0)D(\boldsymbol{k},\omega_0)}{2}\left(\frac{\rho_2}{\rho_1}\right)^{1/2}\times$$

$$\left[-\left(q_k^{(1)}q_k^{(2)}\right)^{1/2}q_0^{(2)}\left(1-\frac{\rho_1}{\rho_2}\right)^2+\left[\left(\frac{q_k^{(1)}}{q_k^{(2)}}\right)^{1/2}+\frac{\rho_1}{\rho_2}\left(\frac{q_k^{(2)}}{q_k^{(1)}}\right)^{1/2}\right]\left[\left(\frac{\omega_0}{c_1}\right)^2-\left(\frac{\omega_0}{c_2}\right)^2\right]-\frac{\alpha^2(\boldsymbol{k},\boldsymbol{k_0},\omega_0)}{\rho_1\rho_2\left(q_k^{(1)}q_k^{(2)}\right)^{1/2}q_0^{(2)}}\right]$$

$$=-\frac{D^2(\boldsymbol{k}_0,\omega_0)D(\boldsymbol{k},\omega_0)}{2}\left(\frac{\rho_2}{\rho_1}\right)^{1/2}\left[\left(q_k^{(1)}q_k^{(2)}\right)^{1/2}q_0^{(2)}\left(1-\frac{\rho_1}{\rho_2}\right)^2+\frac{\alpha^2(\boldsymbol{k},\boldsymbol{k_0},\omega_0)}{\rho_1\rho_2\left(q_k^{(1)}q_k^{(2)}\right)^{1/2}q_0^{(2)}}\right] \quad (4.52)$$

where $\left(\dfrac{q_k^{(1)}}{q_k^{(2)}}\right)^{1/2}+\dfrac{\rho_1}{\rho_2}\left(\dfrac{q_k^{(2)}}{q_k^{(1)}}\right)^{1/2}=2\left(\dfrac{\rho_1}{\rho_2}\right)^{1/2}D^{-1}(\boldsymbol{k},\omega_0)$ is used. Eq. (4.52) leads finally to the form

$$\mathrm{Re}\left[H(\boldsymbol{k},\boldsymbol{k_0},\boldsymbol{k_0},\omega_0,\omega_0,\omega_0)\right] = -\frac{D^2(\boldsymbol{k}_0,\omega_0)}{2}\left(\frac{\rho_2}{\rho_1}\right)^{1/2} \times$$

$$\left\{ q_0^{(2)}\left(1-\frac{\rho_1}{\rho_2}\right)^2 \mathrm{Re}\left[\left(q_k^{(1)}q_k^{(2)}\right)^{1/2} D(\boldsymbol{k},\omega_0)\right] + \frac{\alpha^2(\boldsymbol{k},\boldsymbol{k_0},\omega_0)}{\rho_1\rho_2 q_0^{(2)}} \mathrm{Re}\left[\left(q_k^{(1)}q_k^{(2)}\right)^{-1/2} D(\boldsymbol{k},\omega_0)\right]\right\}$$

$$= -D^2(\boldsymbol{k}_0,\omega_0)\left\{ q_0^{(2)}\left(1-\frac{\rho_1}{\rho_2}\right)^2 \mathrm{Re}\left[\frac{q_k^{(1)}q_k^{(2)}}{q_k^{(1)}+(\rho_1/\rho_2)q_k^{(2)}}\right] + \frac{\alpha^2(\boldsymbol{k},\boldsymbol{k_0},\omega_0)}{\rho_1 q_0^{(2)}} \mathrm{Re}\left[\frac{1}{\rho_2 q_k^{(1)}+\rho_1 q_k^{(2)}}\right]\right\}$$

(4.53)

which is a non-positive value since $\mathrm{Re}\left[q_k^{(1)}q_k^{(2)}/(\rho_2 q_k^{(1)}+\rho_1 q_k^{(2)})\right]$ and $\mathrm{Re}\left[1/(\rho_2 q_k^{(1)}+\rho_1 q_k^{(2)})\right]$ are non-negative for $q_k = a$ or ai ($a \geq 0$). This implies that coherent energy is damped, not amplified, by a wrinkled surface if neither velocity jump effect nor surface motion is considered. Now the incoherent energy flux is evaluated using velocity matching condition ($\beta = 0$) using Eqs. (4.46) and (4.50) to check the energy balance between coherent and incoherent fields.

$$\frac{\omega}{\omega_0}\left|A(\boldsymbol{k},\boldsymbol{k_0},\omega,\omega_0)\right|^2 \mathrm{Re}(q_k^{(1)})\Big/\left|q_k^{(1)}\right| + \frac{\omega}{\omega_0}\left|B(\boldsymbol{k},\boldsymbol{k_0},\omega,\omega_0)\right|^2 \mathrm{Re}(q_k^{(2)})\Big/\left|q_k^{(2)}\right|$$

$$= \frac{\omega}{4\omega_0}\frac{\mathrm{Re}(q_k^{(1)})}{\left|q_k^{(1)}\right|}\left| D(\boldsymbol{k}_0,\omega_0)D(\boldsymbol{k},\omega)\begin{bmatrix}\frac{\omega_0}{\omega}(1-\rho_1/\rho_2)(q_0^{(2)}q_k^{(2)})^{1/2} \\ +\rho_1^{-1}(q_0^{(2)}q_k^{(2)})^{-1/2}\alpha(\boldsymbol{k},\boldsymbol{k_0},\omega_0)\end{bmatrix}\right|^2$$

$$+\frac{\omega}{4\omega_0}\frac{\rho_2}{\rho_1}\frac{\mathrm{Re}(q_k^{(2)})}{\left|q_k^{(2)}\right|}\left| D(\boldsymbol{k}_0,\omega_0)D(\boldsymbol{k},\omega)\begin{bmatrix}-\frac{\omega_0}{\omega}(1-\rho_1/\rho_2)\left(q_k^{(1)}q_0^{(2)}\right)^{1/2} \\ +\rho_2^{-1}\left(q_k^{(1)}q_0^{(2)}\right)^{-1/2}\alpha(\boldsymbol{k},\boldsymbol{k_0},\omega_0)\end{bmatrix}\right|^2$$

$$= \frac{\omega}{4\omega_0}\frac{\mathrm{Re}(q_k^{(1)})}{\left|q_k^{(1)}\right|}\left|D(\boldsymbol{k}_0,\omega_0)D(\boldsymbol{k},\omega)\right|^2\left[\begin{array}{l}\left|\frac{\omega_0}{\omega}(1-\rho_1/\rho_2)(q_0^{(2)}q_k^{(2)})^{1/2}\right|^2+\left|\rho_1^{-1}(q_0^{(2)}q_k^{(2)})^{-1/2}\alpha(\boldsymbol{k},\boldsymbol{k_0},\omega_0)\right|^2\\ +\frac{2\omega_0}{\omega}\rho_1^{-1}(1-\rho_1/\rho_2)\alpha(\boldsymbol{k},\boldsymbol{k_0},\omega_0)\,\mathrm{Re}(q_k^{(2)})\Big/\left|q_k^{(2)}\right|\end{array}\right]$$

$$+\frac{\omega}{4\omega_0}\frac{\rho_2}{\rho_1}\frac{\mathrm{Re}(q_k^{(2)})}{\left|q_k^{(2)}\right|}\left|D(\boldsymbol{k}_0,\omega_0)D(\boldsymbol{k},\omega)\right|^2\left[\begin{array}{l}\left|\frac{\omega_0}{\omega}(1-\rho_1/\rho_2)\left(q_k^{(1)}q_0^{(2)}\right)^{1/2}\right|^2\\ +\left|\rho_2^{-1}\left(q_k^{(1)}q_0^{(2)}\right)^{-1/2}\alpha(\boldsymbol{k},\boldsymbol{k_0},\omega_0)\right|^2\\ -\frac{2\omega_0}{\omega}\rho_2^{-1}(1-\rho_1/\rho_2)\alpha(\boldsymbol{k},\boldsymbol{k_0},\omega_0)\,\mathrm{Re}(q_k^{(1)})\Big/\left|q_k^{(1)}\right|\end{array}\right]$$

where $\mathrm{Re}\left[(q_k^{(2)})^{1/2}(q_k^{(2)})^{-1/2*}\right]=\mathrm{Re}\left[q_k^{(2)}\left|(q_k^{(2)})^{-1/2}\right|^2\right]=\mathrm{Re}(q_k^{(2)})\Big/\left|q_k^{(2)}\right|$ is used.

$$=\frac{q_0^{(2)}\omega}{4\omega_0}\left|\frac{\omega_0}{\omega}\left(1-\frac{\rho_1}{\rho_2}\right)D(\boldsymbol{k}_0,\omega_0)D(\boldsymbol{k},\omega)\right|^2\left[\left|q_k^{(2)}/q_k^{(1)}\right|\mathrm{Re}(q_k^{(1)})+\frac{\rho_2}{\rho_1}\left|q_k^{(1)}/q_k^{(2)}\right|\mathrm{Re}(q_k^{(2)})\right]$$

$$+\frac{\omega}{4\omega_0}\left|q_k^{(1)}q_0^{(2)}q_k^{(2)}\right|^{-1}\left|D(\boldsymbol{k}_0,\omega_0)D(\boldsymbol{k},\omega)\right|^2\left(\rho_1^{-1}\alpha(\boldsymbol{k},\boldsymbol{k_0},\omega_0)\right)^2\rho_2^{-1}\,\mathrm{Re}\left(\rho_2q_k^{(1)}+\rho_1q_k^{(2)}\right)$$

Using $\left|D(\boldsymbol{k},\omega)\right|^2=4\rho_1\rho_2\left|q_k^{(1)}q_k^{(2)}\right|\Big/\left|\rho_2q_k^{(1)}+\rho_1q_k^{(2)}\right|^2$ leads to

$$=\frac{\omega_0}{\omega}\rho_1\rho_2\left(1-\frac{\rho_1}{\rho_2}\right)^2q_0^{(2)}D^2(\boldsymbol{k}_0,\omega_0)\left[\left|q_k^{(2)}\right|^2\mathrm{Re}(q_k^{(1)})+\frac{\rho_2}{\rho_1}\left|q_k^{(1)}\right|^2\mathrm{Re}(q_k^{(2)})\right]\left|\rho_2q_k^{(1)}+\rho_1q_k^{(2)}\right|^{-2}$$

$$+\frac{\omega}{\omega_0}\frac{1}{\rho_1q_0^{(2)}}D^2(\boldsymbol{k}_0,\omega_0)\alpha^2(\boldsymbol{k},\boldsymbol{k_0},\omega_0)\,\mathrm{Re}\left[\frac{1}{\left(\rho_2q_k^{(1)}+\rho_1q_k^{(2)}\right)^*}\right]$$

$$=D^2(\boldsymbol{k}_0,\omega_0)\left\{\frac{\omega_0}{\omega}\rho_2q_0^{(2)}\left(1-\frac{\rho_1}{\rho_2}\right)^2\mathrm{Re}\left[\frac{q_k^{(1)}q_k^{(2)}}{\rho_2q_k^{(1)}+\rho_1q_k^{(2)}}\right]+\frac{\omega}{\omega_0}\frac{\alpha^2(\boldsymbol{k},\boldsymbol{k_0},\omega_0)}{\rho_1q_0^{(2)}}\mathrm{Re}\left[\frac{1}{\rho_2q_k^{(1)}+\rho_1q_k^{(2)}}\right]\right\} \tag{4.54}$$

where use is made of

$$\left[\left|q_k^{(2)}\right|^2 \mathrm{Re}(q_k^{(1)}) + \frac{\rho_2}{\rho_1}\left|q_k^{(1)}\right|^2 \mathrm{Re}(q_k^{(2)})\right]\left|\rho_2 q_k^{(1)} + \rho_1 q_k^{(2)}\right|^{-2} = \rho_1^{-1}\,\mathrm{Re}\left[\frac{q_k^{(1)} q_k^{(2)}\left(\rho_2 q_k^{(1)*} + \rho_1 q_k^{(2)*}\right)}{\left|\rho_2 q_k^{(1)} + \rho_1 q_k^{(2)}\right|^2}\right]$$

$$= \rho_1^{-1}\,\mathrm{Re}\left[\frac{q_k^{(1)} q_k^{(2)}}{\rho_2 q_k^{(1)} + \rho_1 q_k^{(2)}}\right]$$

Note that, in case of constant frequency ($\omega = \omega_0$), Eq. (4.54) is equivalent to Eq. (4.53) except for the opposite sign, which implies that sum of Eqs. (4.53) and (4.54) vanishes and leads Eq. (4.46) to the form

$$E_R + E_T = \left|R(\boldsymbol{k_0}, \omega_0)\right|^2 + \left|D(\boldsymbol{k_0}, \omega_0)\right|^2 + O(h^3) = 1 + O(h^3) \tag{4.55}$$

This proves that energy is conserved if the flame's unsteady effects, i.e., unsteady heat release and unsteady motion, are not considered. Energy balance can also be expressed as sum of coherent and incoherent fluxes using V and T in Eqs. (4.44) and (4.45) and introducing the scattering cross section σ.

$$\left|\langle V(\boldsymbol{k_0}, \omega_0)\rangle\right|^2 + \mathrm{Re}\left(q_0^{(2)} / \left|q_0^{(2)}\right|\right)\left|\langle T(\boldsymbol{k_0}, \omega_0)\rangle\right|^2 + \iint\limits_{|\boldsymbol{k}|<\frac{\omega_0}{c_1}} \sigma_R(\boldsymbol{k}, \boldsymbol{k_0})d\boldsymbol{k} + \iint\limits_{|\boldsymbol{k}|<\frac{\omega_0}{c_2}} \sigma_T(\boldsymbol{k}, \boldsymbol{k_0})d\boldsymbol{k} \tag{4.56}$$

$$= 1 + O(h^3)$$

with $\sigma_R(\boldsymbol{k}, \boldsymbol{k_0}) \equiv \left|A(\boldsymbol{k}, \boldsymbol{k_0}, \omega_0, \omega_0)\right|^2 W(\boldsymbol{k} - \boldsymbol{k_0})$, $\sigma_T(\boldsymbol{k}, \boldsymbol{k_0}) \equiv \left|B(\boldsymbol{k}, \boldsymbol{k_0}, \omega_0, \omega_0)\right|^2 W(\boldsymbol{k} - \boldsymbol{k_0})$

where the first two terms, V and T, represent coherent energy flux of reflected and transmitted wave fields, respectively, and the last two terms, i.e., scattering cross sections σ_R and σ_T, represent incoherent (diffuse) energy flux for reflected and transmitted wave fields, respectively. In case of pressure release condition across a flame, Eq. (4.56) is reduced further to the following form by taking $\rho_2 / \rho_1 \to 0$ and using Eq. (4.21).

$$\left|\left\langle V(\boldsymbol{k}_0,\omega_0)\right\rangle\right|^2 + 4q_0^{(1)} \iint\limits_{|\boldsymbol{k}|<\frac{\omega_0}{c_1}} q_k^{(1)} W(\boldsymbol{k}-\boldsymbol{k}_0)d\boldsymbol{k} = 1 + O(h^3) \tag{4.57}$$

where $\left\langle T(\boldsymbol{k}_0,\omega_0)\right\rangle \to 0$ as $\rho_2/\rho_1 \to 0$ because $G(\boldsymbol{k}',\boldsymbol{k}_0,\boldsymbol{k}_0,\omega',\omega_0,\omega_0) < \infty$ and $D(\boldsymbol{k}_0,\omega_0) \to 0$ in Eqs. (4.38) and (4.47). Eq. (4.57) is equivalent to the expression in Voronovich. ([50], p. 81).

4.4 Budget of net energy fluxes

Note that energy balance in Eq. (4.56) does not hold if either velocity jump due to unsteady mass burning rate across flame surface or unsteady flame motion is considered. In another words, the acoustic energy amplification / damping can be attributed to two factors: the acoustic velocity jump due to unsteady heat release and unsteady motion of flame front. (As for unsteady motion effect, see also Ch. 14 in Crighton *et al.*[48] who describe how a source in unsteady motion changes the amplitude of sound field compared to the case of a stationary source.) Net energy flux can also be separated into coherent and incoherent fields for reflected and transmitted waves. Total acoustic energy in Eq. (4.46) can be rewritten in the form

$$\begin{aligned} E_{total} &= \left|\left\langle V_J(\boldsymbol{k}_0,\omega_0)\right\rangle\right|^2 + \mathrm{Re}\left(q_0^{(2)}/\left|q_0^{(2)}\right|\right)\left|\left\langle T_J(\boldsymbol{k}_0,\omega_0)\right\rangle\right|^2 \\ &+ \int_{\omega} \iint\limits_{|\boldsymbol{k}|<\frac{|\omega|}{c_1}} \sigma_{R,J}(\boldsymbol{k},\boldsymbol{k}_0,\omega,\omega_0)d\boldsymbol{k}d\omega + \int_{\omega} \iint\limits_{|\boldsymbol{k}|<\frac{|\omega|}{c_2}} \sigma_{T,J}(\boldsymbol{k},\boldsymbol{k}_0,\omega,\omega_0)d\boldsymbol{k}d\omega \end{aligned} \tag{4.58}$$

where the scattering cross sections are

$$\sigma_{R,J}(\boldsymbol{k},\boldsymbol{k}_0,\omega,\omega_0) := \frac{\omega}{\omega_0}\left|A_J(\boldsymbol{k},\boldsymbol{k}_0,\omega,\omega_0)\right|^2 W(\boldsymbol{k}-\boldsymbol{k}_0,\omega-\omega_0)$$

$$\sigma_{T,J}(\boldsymbol{k},\boldsymbol{k}_0,\omega,\omega_0) := \frac{\omega}{\omega_0}\left|B_J(\boldsymbol{k},\boldsymbol{k}_0,\omega,\omega_0)\right|^2 W(\boldsymbol{k}-\boldsymbol{k}_0,\omega-\omega_0)$$

Note that Eq. (4.56) is a special case of Eq. (4.58) with no jump (β = 0) and constant frequency ($\omega = \omega_0$; $W(\boldsymbol{k}-\boldsymbol{k_0}, \omega-\omega_0) = W(\boldsymbol{k}-\boldsymbol{k_0})\delta(\omega-\omega_0)$). Then total net energy flux as a result of scattering from a turbulent flame is evaluated by subtracting incident energy flux in Eq. (4.55) from total resultant energy flux in Eq. (4.58) to have the form

$$\Delta E = E_{total} - 1 = \Delta E_{R,co} + \Delta E_{T,co} + \Delta E_{R,inc} + \Delta E_{T,inc} \tag{4.59}$$

where

$$\Delta E_{R,co} = \left|\left\langle V_J(\boldsymbol{k_0}, \omega_0)\right\rangle\right|^2 - \left|R(\boldsymbol{k_0}, \omega_0)\right|^2$$

$$\Delta E_{T,co} = \mathrm{Re}\left(q_0^{(2)} / \left|q_0^{(2)}\right|\right)\left(\left|\left\langle T_J(\boldsymbol{k_0}, \omega_0)\right\rangle\right|^2 - \left|D(\boldsymbol{k_0}, \omega_0)\right|^2\right)$$

$$\Delta E_{R,inc} = \int_{\omega} \iint_{|\boldsymbol{k}|<\frac{|\omega|}{c_1}} \sigma_{R,J}(\boldsymbol{k}, \boldsymbol{k_0}, \omega, \omega_0) d\boldsymbol{k} d\omega$$

$$\Delta E_{T,inc} = \int_{\omega} \iint_{|\boldsymbol{k}|<\frac{|\omega|}{c_2}} \sigma_{T,J}(\boldsymbol{k}, \boldsymbol{k_0}, \omega, \omega_0) d\boldsymbol{k} d\omega$$

The first term, $\Delta E_{R,co}$, is net coherent energy flux of reflected waves. $\Delta E_{T,co}$ is net coherent energy flux of transmitted waves, which vanishes when the incident angle is beyond critical angle because no energy is transmitted($\mathrm{Re}(q_0^{(2)}) = 0$). $\Delta E_{R,inc}$ and $\Delta E_{T,inc}$ are net incoherent energy flux of reflected and transmitted waves, respectively, which results from surface wrinkling and unsteady heat release. Combining reflection and transmission energy yields net energy flux of coherent /incoherent fields.

$$\Delta E_{co} = \Delta E_{R,co} + \Delta E_{T,co} = \left|\left\langle V_J(\boldsymbol{k_0}, \omega_0)\right\rangle\right|^2 + \mathrm{Re}\left(q_0^{(2)} / \left|q_0^{(2)}\right|\right)\left|\left\langle T_J(\boldsymbol{k_0}, \omega_0)\right\rangle\right|^2 - 1 \tag{4.60}$$

$$\Delta E_{inc} = \Delta E_{R,inc} + \Delta E_{T,inc} = \int_{\omega} \iint_{|\boldsymbol{k}|<\frac{|\omega|}{c_1}} \sigma_{R,J}(\boldsymbol{k},\boldsymbol{k_0},\omega,\omega_0) d\boldsymbol{k} d\omega + \int_{\omega} \iint_{|\boldsymbol{k}|<\frac{|\omega|}{c_2}} \sigma_{T,J}(\boldsymbol{k},\boldsymbol{k_0},\omega,\omega_0) d\boldsymbol{k} d\omega$$

Net coherent energy flux, ΔE_{co}, is attributed to two factors: One is due to acoustic velocity jump due to unsteady heat release, $\Delta_J(E_{co})$. The other is due to flame's wrinkling, $\Delta_\omega(E_{co})$, which accounts for both temporal (unsteady motion) and spatial wrinkling of flame fronts. This is of the form

$$\Delta E_{co} = \Delta_J(E_{co}) + \Delta_\omega(E_{co}) \tag{4.61}$$

where

$$\Delta_J(E_{co}) = \left|\left\langle V_J(\boldsymbol{k_0},\omega_0)\right\rangle\right|^2 - \left|\left\langle V(\boldsymbol{k_0},\omega_0)\right\rangle\right|^2 + \mathrm{Re}\left(q_0^{(2)}/\left|q_0^{(2)}\right|\right)\left(\left|\left\langle T_J(\boldsymbol{k_0},\omega_0)\right\rangle\right|^2 - \left|\left\langle T(\boldsymbol{k_0},\omega_0)\right\rangle\right|^2\right)$$

$$\begin{aligned}\Delta_\omega(E_{co}) &= \left|\left\langle V(\boldsymbol{k_0},\omega_0)\right\rangle\right|^2 + \mathrm{Re}\left(q_0^{(2)}/\left|q_0^{(2)}\right|\right)\left|\left\langle T(\boldsymbol{k_0},\omega_0)\right\rangle\right|^2 - 1 \\ &= \int_{\omega}\iint_{\boldsymbol{k}} \mathrm{Re}\left[H(\boldsymbol{k},\boldsymbol{k_0},\boldsymbol{k_0},\omega,\omega_0,\omega_0)\right] W(\boldsymbol{k_0}-\boldsymbol{k},\omega_0-\omega) d\boldsymbol{k} d\omega\end{aligned}$$

where H is defined in Eq. (4.48). Note that $\Delta_\omega(E_{co}) < 0$ for constant frequency, $\omega = \omega_0$, as shown in Eq. (4.53), which implies that coherent energy only flows into the incoherent field due to spatial flame wrinkling. Net incoherent energy flux is also attributed to velocity jump and surface wrinkling effects.

$$\Delta E_{inc} = \Delta_J(E_{inc}) + \Delta_\omega(E_{inc}) \tag{4.62}$$

where

$$\begin{aligned}\Delta_J(E_{inc}) = &\int_{\omega} \iint_{|\boldsymbol{k}|<\frac{|\omega|}{c_1}} \left[\sigma_{R,J}(\boldsymbol{k},\boldsymbol{k_0},\omega,\omega_0) - \sigma_R(\boldsymbol{k},\boldsymbol{k_0},\omega,\omega_0)\right] d\boldsymbol{k} d\omega \\ &+ \int_{\omega} \iint_{|\boldsymbol{k}|<\frac{|\omega|}{c_2}} \left[\sigma_{T,J}(\boldsymbol{k},\boldsymbol{k_0},\omega,\omega_0) - \sigma_T(\boldsymbol{k},\boldsymbol{k_0},\omega,\omega_0)\right] d\boldsymbol{k} d\omega\end{aligned}$$

$$\Delta_\omega(E_{inc}) = \int_{\omega} \iint_{|\boldsymbol{k}|<\frac{|\omega|}{c_1}} \sigma_R(\boldsymbol{k},\boldsymbol{k_0},\omega,\omega_0)d\boldsymbol{k}d\omega + \int_{\omega} \iint_{|\boldsymbol{k}|<\frac{|\omega|}{c_2}} \sigma_T(\boldsymbol{k},\boldsymbol{k_0},\omega,\omega_0)d\boldsymbol{k}d\omega$$

Note that $\Delta_\omega(E_{inc}) > 0$ for constant frequency, $\omega = \omega_0$, as shown in Eq.(4.54), which implies that incoherent energy is only produced due to spatial flame wrinkling.

4.5 Calculation of net energy flux using Gaussian distribution

Evaluation of net energy flux requires integrations of the terms F_J, G_J, A_J, and B_J, over $\boldsymbol{k},\omega$-space as shown in Eqs. (4.44), (4.45), and (4.59). These integrations are described next.

4.5.1 Net coherent energy flux

F_J in Eq. (4.47) can be rewritten in terms of $\boldsymbol{k}$ and $\boldsymbol{k_0}$ by substituting A_J and B_J into F_J to yield the form:

$$F_J(\boldsymbol{k},\boldsymbol{k_0},\boldsymbol{k_0},\omega,\omega_0,\omega_0) =$$
$$\frac{D_J(\boldsymbol{k}_0,\omega_0)}{q_0^{(2)}}\left[-\frac{\beta(\omega_0)|\boldsymbol{k}-\boldsymbol{k_0}|^2}{2} + C_{10}(k,\omega) + C_{11}(k,\omega)\boldsymbol{k}\cdot\boldsymbol{k_0} + C_{12}(k,\omega)(\boldsymbol{k}\cdot\boldsymbol{k_0})^2\right] \tag{4.63}$$

where

$$C_{10}(k,\omega) = \frac{1}{(\rho_2/\rho_1)q_k^{(1)} + q_k^{(2)} + \beta(\omega)} \times$$
$$\left(\begin{array}{l} \left[(1-\rho_2/\rho_1)q_0^{(2)} + \beta(\omega_0)\right]\left(\begin{array}{l} q_k^{(1)}\left(q_0^{(2)}+\beta(\omega_0)\right)\left[(\rho_1/\rho_2-1)q_k^{(2)} + \rho_1/\rho_2\beta(\omega)\right] \\ +\frac{\omega_0}{\omega}\left\{\left(q_k^{(2)}+\beta(\omega)\right)\left(\frac{\omega}{c_1}\right)^2 + q_k^{(1)}\left[\left(\frac{\omega}{c_2}\right)^2 + \beta(\omega)q_k^{(2)}\right]\right\} \end{array}\right) + \\ \left[\left(\frac{\omega_0}{c_2}\right)^2 - \frac{\rho_2}{\rho_1}\left(\frac{\omega_0}{c_1}\right)^2 + q_0^{(2)}\beta(\omega_0)\right]\left[\frac{\omega}{\omega_0}\left(q_k^{(1)}+q_k^{(2)}\right)\left(q_0^{(2)}+\beta(\omega_0)\right) - q_k^{(2)}\beta(\omega) + \frac{\rho_2}{\rho_1}\left(\frac{\omega}{c_1}\right)^2 - \left(\frac{\omega}{c_2}\right)^2\right] \end{array}\right)$$

$$C_{11}(k,\omega)=\frac{1}{(\rho_2/\rho_1)q_k^{(1)}+q_k^{(2)}+\beta(\omega)}\times$$
$$\left(\begin{array}{l}\left(1-\dfrac{\rho_2}{\rho_1}\right)\left[\left(\dfrac{\omega_0}{c_2}\right)^2-\dfrac{\rho_2}{\rho_1}\left(\dfrac{\omega_0}{c_1}\right)^2+q_0^{(2)}\beta(\omega_0)\right]\\ +\left(1-\dfrac{\rho_2}{\rho_1}\right)\left[\left(\dfrac{\omega}{c_2}\right)^2-\dfrac{\rho_2}{\rho_1}\left(\dfrac{\omega}{c_1}\right)^2+q_k^{(2)}\beta(\omega)-\dfrac{\omega}{\omega_0}\left(q_k^{(1)}+q_k^{(2)}\right)\left(q_0^{(2)}+\beta(\omega_0)\right)\right]\\ -\dfrac{\omega_0}{\omega}\left[(1-\rho_2/\rho_1)q_0^{(2)}+\beta(\omega_0)\right]\left(q_k^{(1)}+q_k^{(2)}+\beta(\omega)\right)\end{array}\right)$$

$$C_{12}(k,\omega)=\frac{-(1-\rho_2/\rho_1)^2}{(\rho_2/\rho_1)q_k^{(1)}+q_k^{(2)}+\beta(\omega)}$$

Flame surface height statistics are assumed to exhibit Gaussian characteristics:

$$\breve{W}(\boldsymbol{\xi},\eta)\equiv\left\langle h(\boldsymbol{r}_1,t_1)h(\boldsymbol{r}_2,t_2)\right\rangle=\left\langle h^2(\boldsymbol{r},t)\right\rangle e^{-|\boldsymbol{r}_1-\boldsymbol{r}_2|^2/l_c^2-(t_1-t_2)^2/t_c^2}=\sigma^2 e^{-|\boldsymbol{\xi}|^2/l_c^2-\eta^2/t_c^2} \tag{4.64}$$

where l_c and t_c are correlation length and time of flame position, respectively. Then, the power spectrum of flame height is obtained from Eq. (4.15).

$$\begin{aligned}W(\boldsymbol{k},\omega)&=\frac{\sigma^2}{(2\pi)^3}\iint_{\boldsymbol{\xi}}\int_{\eta}e^{-|\boldsymbol{\xi}|^2/l_c^2-\eta^2/t_c^2}e^{-i(\boldsymbol{k}\cdot\boldsymbol{\xi}-\omega\eta)}d\eta d\boldsymbol{\xi}\\ &=\frac{\sigma^2}{(2\pi)^3}\int_{-\infty}^{+\infty}\int_{-\infty}^{+\infty}\int_{-\infty}^{+\infty}e^{-(\xi_1^2+\xi_2^2)/l_c^2-\eta^2/t_c^2-i(k_1\xi_1+k_2\xi_2-\omega\eta)}d\eta d\xi_1 d\xi_2\\ &=\frac{\sigma^2}{(2\pi)^3}\int_{-\infty}^{+\infty}e^{-\eta^2/t_c^2+i\omega\eta}d\eta\times\int_{-\infty}^{+\infty}e^{-\xi_1^2/l_c^2-ik_1\xi_1}d\xi_1\times\int_{-\infty}^{+\infty}e^{-\xi_2^2/l_c^2-ik_2\xi_2}d\xi_2\\ &=\frac{\sigma^2}{(2\pi)^3}\sqrt{\pi}t_c e^{-(\omega t_c)^2/4}\times\sqrt{\pi}l_c e^{-(k_1 l_c)^2/4}\times\sqrt{\pi}l_c e^{-(k_2 l_c)^2/4}\\ &=\frac{\sigma^2 t_c l_c^2}{8\pi^{3/2}}\exp\left\{-\left[(\omega t_c)^2+(|\boldsymbol{k}|l_c)^2\right]/4\right\}\end{aligned} \tag{4.65}$$

where use is made of

$$\int_{-\infty}^{+\infty} e^{-\eta^2/t_c^2+i\omega\eta}d\eta = e^{-(\omega t_c)^2/4}\int_{-\infty}^{+\infty} e^{-(\eta/t_c-i\omega t_c/2)^2}d\eta$$

$$= t_c e^{-(\omega t_c)^2/4}\int_{-\infty-i\omega t_c/2}^{+\infty-i\omega t_c/2} e^{-z^2}dz = t_c e^{-(\omega t_c)^2/4}\int_{-\infty}^{+\infty} e^{-z^2}dz \text{ (using residue theorem)} \quad (4.66)$$

$$= \pi^{1/2} t_c e^{-(\omega t_c)^2/4}$$

Eq. (4.65) implies that a Gaussian correlation function yields a Gaussian power spectrum. Note that if a surface is stationary, the correlation time goes to infinty ($t_c \to \infty$). The power spectrum of a stationary surface is then approximated by delta function, i.e., $\frac{t_c}{\sqrt{\pi}}\exp[-(\omega t_c)^2] \to \delta(\omega)$ as $t_c \to \infty$.[47, p. 580]

$$W(\boldsymbol{k},\omega) \equiv W(\boldsymbol{k})\delta(\omega) \text{ with } W(\boldsymbol{k}) = \frac{(\sigma l_c)^2}{4\pi}\exp\left[-(|\boldsymbol{k}|l_c)^2/4\right] \quad (4.67)$$

$F_J W$ in Eq. (4.44) is integrated over k_x, k_y, and ω, which is a triple integration. Utilizing a polar coordinate, however, reduces the order of integration.

$$\boldsymbol{k} = k_x\vec{\boldsymbol{e}}_{\boldsymbol{x}} + k_y\vec{\boldsymbol{e}}_{\boldsymbol{y}}, \qquad k_x = k\cos\theta, \quad k_y = k\sin\theta$$

$$\boldsymbol{k_0} = k_{x0}\vec{\boldsymbol{e}}_{\boldsymbol{x}} + k_{y0}\vec{\boldsymbol{e}}_{\boldsymbol{y}}, \qquad k_{x0} = k_0\cos\theta_0, \qquad k_{y0} = k_0\sin\theta_0$$

$$\boldsymbol{k}\cdot\boldsymbol{k_0} = kk_0\cos(\theta-\theta_0)$$

$$q_k^{(m)} = \left((\omega/c_m)^2 - k^2\right)^{1/2} \quad m = \{1, 2\}$$

$$W(\boldsymbol{k_0}-\boldsymbol{k}, \omega_0-\omega) = \frac{\sigma^2 t_c l_c^2}{8\pi^{3/2}}\exp\left\{-\left[\left((\omega_0-\omega)t_c\right)^2 + \left(|\boldsymbol{k_0}-\boldsymbol{k}|l_c\right)^2\right]/4\right\}$$
$$= \frac{\sigma^2 t_c l_c^2}{8\pi^{3/2}}\exp\left\{-\left[\left((\omega-\omega_0)t_c\right)^2 + \left(k^2+k_0^2-2kk_0\cos(\theta-\theta_0)\right)l_c^2\right]/4\right\} \quad (4.68)$$

The following integral formulas will also be used.

$$\int_0^{2\pi} \exp\left(\boldsymbol{k}\cdot\boldsymbol{k_0}l_c^2/2\right)d\theta$$
$$= \int_0^{2\pi} \exp\left[(kk_0l_c^2/2)\cos(\theta-\theta_0)\right]d\theta = \int_0^{2\pi} \exp\left[(kk_0l_c^2/2)\cos\theta\right]d\theta \tag{4.69}$$
$$= 2\pi J_0(-ikk_0l_c^2/2) = 2\pi I_0(-kk_0l_c^2/2) = 2\pi I_0(kk_0l_c^2/2)$$

where $J(\ )$ is a Bessel function and $I(\ )$ is a modified Bessel function. See p. 360 and 9.6.3 and 9.6.10 in p.375, in ref. [56].

$$\int_0^{2\pi} \boldsymbol{k}\cdot\boldsymbol{k_0}\exp\left(\boldsymbol{k}\cdot\boldsymbol{k_0}l_c^2/2\right)d\theta$$
$$= kk_0\int_0^{2\pi} \cos(\theta-\theta_0)\exp\left[(kk_0l_c^2/2)\cos(\theta-\theta_0)\right]d\theta \tag{4.70}$$
$$= kk_0\int_0^{2\pi} (\cos\theta)\exp\left[(kk_0l_c^2/2)\cos\theta\right]d\theta$$
$$= 2\pi ikk_0J_1(-ikk_0l_c^2/2) = -2\pi kk_0I_1(-kk_0l_c^2/2) = 2\pi kk_0I_1(kk_0l_c^2/2)$$

$$\int_0^{2\pi} (\boldsymbol{k}\cdot\boldsymbol{k_0})^2\exp\left(\boldsymbol{k}\cdot\boldsymbol{k_0}l_c^2/2\right)d\theta$$
$$= (kk_0)^2\int_0^{2\pi} \cos^2(\theta-\theta_0)\exp\left[(kk_0l_c^2/2)\cos(\theta-\theta_0)\right]d\theta \tag{4.71}$$
$$= \frac{(kk_0)^2}{2}\int_0^{2\pi} (1+\cos 2\theta)\exp\left[(kk_0l_c^2/2)\cos\theta\right]d\theta$$
$$= \pi(kk_0)^2\left[J_0(-ikk_0l_c^2/2) - J_2(-ikk_0l_c^2/2)\right] = \pi(kk_0)^2\left[I_0(kk_0l_c^2/2) + I_2(kk_0l_c^2/2)\right]$$

Integration of F_J can be done using Eqs. (4.63) and (4.68) - (4.71).

$$\iint_{\boldsymbol{k}} F_J(\boldsymbol{k},\boldsymbol{k_0},\boldsymbol{k_0},\omega,\omega_0,\omega_0)W(\boldsymbol{k_0}-\boldsymbol{k},\omega_0-\omega)d\boldsymbol{k}$$
$$= \frac{D_J(\boldsymbol{k}_0,\omega_0)}{q_0^{(2)}}\frac{\sigma^2t_cl_c^2}{8\pi^{3/2}}\exp\left[-\left((\omega_0-\omega)t_c\right)^2/4\right]\times$$
$$\left(-\frac{\beta(\omega_0)}{2}\int_{-\infty}^{\infty}\int_{-\infty}^{\infty}\left|\boldsymbol{k}-\boldsymbol{k_0}\right|^2\exp\left[-\left(\left|\boldsymbol{k_0}-\boldsymbol{k}\right|l_c\right)^2/4\right]d\boldsymbol{k}\right.$$
$$\left.+\int_{k=0}^{\infty}\int_{\theta=0}^{2\pi}\left(\sum_{j=0}^{2}C_{1j}(k,\omega)(\boldsymbol{k}\cdot\boldsymbol{k_0})^j\right)\exp\left[-\left(k^2+k_0^2-2\boldsymbol{k}\cdot\boldsymbol{k_0}\right)l_c^2/4\right]kd\theta dk\right)$$

$$= \frac{D_J(\boldsymbol{k}_0,\omega_0)}{q_0^{(2)}} \frac{\sigma^2 t_c l_c^2}{8\pi^{3/2}} \exp\left[-\left((\omega_0-\omega)t_c\right)^2/4\right] \times$$

$$\left(-\frac{\beta(\omega_0)}{2} \int_{-\infty}^{\infty}\int_{-\infty}^{\infty} |\boldsymbol{k}|^2 \exp\left[-\left(|\boldsymbol{k}|l_c\right)^2/4\right] d\boldsymbol{k} \right.$$

$$\left. + \int_{k=0}^{\infty} k \exp\left[-(k^2+k_0^2)l_c^2/4\right] \left(\sum_{j=0}^{2} C_{1j}(k,\omega) \int_{\theta=0}^{2\pi} (\boldsymbol{k}\cdot\boldsymbol{k}_0)^j \exp(\boldsymbol{k}\cdot\boldsymbol{k}_0 l_c^2/2) d\theta \right) dk \right)$$

$$= \frac{D_J(\boldsymbol{k}_0,\omega_0)}{q_0^{(2)}} \frac{\sigma^2 t_c l_c^2}{\pi^{1/2}} \exp\left(-(\omega_0-\omega)^2 t_c^2/4\right) \times$$

$$\left[-\frac{\beta(\omega_0)}{l_c^4} + \frac{\mathrm{e}^{-k_0^2 l_c^2/4}}{8} \int_{k=0}^{\infty} \left(\begin{array}{l} 2C_{10}(k,\omega) I_0(kk_0 l_c^2/2) + 2kk_0 C_{11}(k,\omega) I_1(kk_0 l_c^2/2) \\ +(kk_0)^2 C_{12}(k,\omega)\left[I_0(kk_0 l_c^2/2) + I_2(kk_0 l_c^2/2) \right] \end{array} \right) k\,\mathrm{e}^{-k^2 l_c^2/4}\, dk \right] \quad (4.72)$$

using $\int_{-\infty}^{\infty}\int_{-\infty}^{\infty} |\boldsymbol{k}|^2 \exp\left[-\left(|\boldsymbol{k}|l_c\right)^2/4\right] d\boldsymbol{k} = \int_{k=0}^{\infty}\int_{\theta=0}^{2\pi} k^2 \exp\left[-\left(kl_c\right)^2/4\right] kd\theta dk = 16\pi l_c^{-4}$.

Eq. (4.72) can be rearranged in terms of dimensionless parameters of rms height of flame front, $\tilde{\sigma} \coloneqq K_0\sigma$ ($K_0 = \omega_0/c_1$), correlation length of flame front, $\tilde{l}_c \coloneqq K_0 l_c$, incident wave frequency, $\tilde{\omega}_0 \coloneqq \omega_0 t_c$ (equivalently, $\tilde{f}_0 \coloneqq \omega_0 t_c/(2\pi) = f_0/f_c$), the ratio of flame's diffusion time to correlation time of flame front, $\tau \coloneqq t_r/t_c$, and polar angle of incidence, $\tilde{k}_0 \coloneqq k_0/K_0 = \sin\phi_0^{(1)}$ to yield

$$\iint_{\boldsymbol{k}} F_J(\boldsymbol{k},\boldsymbol{k}_0,\boldsymbol{k}_0,\omega,\omega_0,\omega_0) W(\boldsymbol{k}_0-\boldsymbol{k},\omega_0-\omega) d\boldsymbol{k}$$

$$= \frac{2\left((\rho_2/\rho_1)\tilde{q}_0^{(1)}/\tilde{q}_0^{(2)}\right)^{1/2}}{(\rho_2/\rho_1)\tilde{q}_0^{(1)} + \tilde{q}_0^{(2)} + \tilde{\beta}(\tilde{\omega}_0)} \frac{\tilde{\sigma}^2 t_c}{\pi^{1/2}} \mathrm{e}^{-(\tilde{\omega}_0-\tilde{\omega})^2/4} \times \quad (4.73)$$

$$\left[-\frac{\tilde{\beta}(\tilde{\omega}_0)}{\tilde{l}_c^{\,2}} + \frac{\tilde{l}_c^{\,2}}{8} \mathrm{e}^{-(\tilde{k}_0\tilde{l}_c)^2/4} \times \right.$$

$$\left. \int_{\tilde{k}=0}^{\infty} \left(\begin{array}{l} 2\tilde{C}_{10}(\tilde{k},\tilde{\omega}) I_0(\tilde{k}\tilde{k}_0\tilde{l}_c^{\,2}/2) + 2\tilde{k}\tilde{k}_0\tilde{C}_{11}(\tilde{k},\tilde{\omega}) I_1(\tilde{k}\tilde{k}_0\tilde{l}_c^{\,2}/2) \\ +(\tilde{k}\tilde{k}_0)^2 \tilde{C}_{12}(\tilde{k},\tilde{\omega})\left[I_0(\tilde{k}\tilde{k}_0\tilde{l}_c^{\,2}/2) + I_2(\tilde{k}\tilde{k}_0\tilde{l}_c^{\,2}/2) \right] \end{array} \right) \tilde{k}\,\mathrm{e}^{-(\tilde{k}\tilde{l}_c)^2/4}\, d\tilde{k} \right]$$

where

$$\tilde{C}_{1m}(\tilde{k},\tilde{\omega}) \coloneqq C_{1m}(\tilde{k}K_0,\tilde{\omega}/t_c)\big/(K_0)^3 \quad (\mathrm{m} = \{0, 1, 2\}),$$

$$\tilde{q}_{\tilde{k}}^{(1)} \coloneqq \frac{q_k^{(1)}}{K_0} = \left[\left(\frac{\tilde{\omega}}{\tilde{\omega}_0}\right)^2 - \tilde{k}^2\right]^{1/2}, \qquad \tilde{q}_{\tilde{k}}^{(2)} \coloneqq \frac{q_k^{(2)}}{K_0} = \left[\left(\frac{\tilde{\omega}}{\tilde{\omega}_0}\frac{c_1}{c_2}\right)^2 - \tilde{k}^2\right]^{1/2}$$

$$\tilde{q}_0^{(1)} \coloneqq \frac{q_0^{(1)}}{K_0} = \left(1-(\tilde{k}_0)^2\right)^{1/2}, \qquad \tilde{q}_0^{(2)} \coloneqq \frac{q_0^{(2)}}{K_0} = \left[\left(\frac{c_1}{c_2}\right)^2 - (\tilde{k}_0)^2\right]^{1/2}$$

$$\begin{aligned}\tilde{\beta}(\tilde{\omega}) &\coloneqq \frac{\beta(\omega)}{K_0} = \frac{\beta_X\omega - i\beta_Y\omega^2}{K_0} \\ &= \frac{c_1}{c_2}\frac{\tilde{\omega}}{\tilde{\omega}_0}\left[\frac{\alpha}{2}(\gamma-1) - \gamma - i(\gamma-1)\theta\tau\tilde{\omega}\right]\frac{(\Lambda-1)M_S}{\Lambda^{1/2}} \qquad \text{(from Eq. (3.102))}\end{aligned} \tag{4.74}$$

Note that the right hand side of Eq. (4.73) contains $\tilde{q}_0^{(2)}$ in the denominator, which implies that the integration in Eq. (4.73) diverges for a critical angle of incidence because $\tilde{q}_0^{(2)}\big|_{\phi_0^{(1)}=\phi_{cr}^{(1)}} = \left[(c_1/c_2)^2 - (\sin\phi_{cr}^{(1)})^2\right]^{1/2} = 0$ by Snell's law. This problem can be settled by multiplying Eq. (4.73) by $D_J(\boldsymbol{k}_0,\omega_0) = \dfrac{2\left(\Lambda^{-1}\tilde{q}_0^{(1)}\tilde{q}_0^{(2)}\right)^{1/2}}{\Lambda^{-1}\tilde{q}_0^{(1)} + \tilde{q}_0^{(2)} + \tilde{\beta}(\tilde{\omega}_0)}$ (using $\rho_2/\rho_1 = \Lambda^{-1}$). (Note that a term in Eq. (4.44) requires a product of D_J and F_J.)

$$\begin{aligned}&D_J(\boldsymbol{k}_0,\omega_0)\iint_{\boldsymbol{k}} F_J(\boldsymbol{k},\boldsymbol{k_0},\boldsymbol{k_0},\omega,\omega_0,\omega_0)W(\boldsymbol{k_0}-\boldsymbol{k},\omega_0-\omega)d\boldsymbol{k} \\ &= \frac{4\tilde{q}_0^{(1)}}{\Lambda\left[\Lambda^{-1}\tilde{q}_0^{(1)} + \tilde{q}_0^{(2)} + \tilde{\beta}(\tilde{\omega}_0)\right]^2}\frac{\tilde{\sigma}^2 t_c}{\pi^{1/2}}\mathrm{e}^{-(\tilde{\omega}_0-\tilde{\omega})^2/4}\times \\ &\left[-\frac{\tilde{\beta}(\tilde{\omega}_0)}{\tilde{l}_c^{\,2}} + \frac{\tilde{l}_c^{\,2}}{8}\mathrm{e}^{-(\tilde{k}_0\tilde{l}_c)^2/4}\times\right. \\ &\left.\int_{\tilde{k}=0}^{\infty}\left(\begin{array}{l}2\tilde{C}_{10}(\tilde{k},\tilde{\omega})I_0(\tilde{k}\tilde{k}_0\tilde{l}_c^{\,2}/2) + 2\tilde{k}\tilde{k}_0\tilde{C}_{11}(\tilde{k},\tilde{\omega})I_1(\tilde{k}\tilde{k}_0\tilde{l}_c^{\,2}/2) \\ +(\tilde{k}\tilde{k}_0)^2\tilde{C}_{12}(\tilde{k},\tilde{\omega})\left[I_0(\tilde{k}\tilde{k}_0\tilde{l}_c^{\,2}/2) + I_2(\tilde{k}\tilde{k}_0\tilde{l}_c^{\,2}/2)\right]\end{array}\right)\tilde{k}\,\mathrm{e}^{-(\tilde{k}\tilde{l}_c)^2/4}\,d\tilde{k}\right]\end{aligned}$$

which is further integrated over ω to yield (using $\rho_2/\rho_1 = \Lambda^{-1}$ and $c_2/c_1 = \Lambda^{1/2}$):

$$D_J(\boldsymbol{k}_0,\omega_0)\int_{\omega}\iint_{\boldsymbol{k}} F_J(\boldsymbol{k},\boldsymbol{k_0},\boldsymbol{k_0},\omega,\omega_0,\omega_0)W(\boldsymbol{k_0}-\boldsymbol{k},\omega_0-\omega)d\boldsymbol{k}d\omega$$

$$= \frac{2\tilde{q}_0^{(1)}\tilde{\sigma}^2}{\Lambda\left[\Lambda^{-1}\tilde{q}_0^{(1)}+\tilde{q}_0^{(2)}+\tilde{\beta}(\tilde{\omega}_0)\right]^2}\times \tag{4.75}$$

$$\left[-\frac{4\tilde{\beta}(\tilde{\omega}_0)}{\tilde{l}_c^{\,2}}+\frac{\tilde{l}_c^{\,2}\,\mathrm{e}^{-(\tilde{k}_0\tilde{l}_c)^2/4}}{4\pi^{1/2}}\times \int_{\omega=-\infty}^{\infty}\int_{k=0}^{\infty}\left(\begin{array}{l}2\tilde{C}_{10}(k,\omega)I_0(k\tilde{k}_0\tilde{l}_c^{\,2}/2)+2k\tilde{k}_0\tilde{C}_{11}(k,\omega)I_1(k\tilde{k}_0\tilde{l}_c^{\,2}/2)\\ +(k\tilde{k}_0)^2\tilde{C}_{12}(k,\omega)\left[I_0(k\tilde{k}_0\tilde{l}_c^{\,2}/2)+I_2(k\tilde{k}_0\tilde{l}_c^{\,2}/2)\right]\end{array}\right)k\,\mathrm{e}^{-[(k\tilde{l}_c)^2+(\tilde{\omega}_0-\omega)^2]/4}\,dkd\omega\right]$$

where

$$\tilde{C}_{10}(k,\omega)=\frac{1}{\Lambda^{-1}\tilde{q}_k^{(1)}+\tilde{q}_k^{(2)}+\tilde{\beta}(\omega)}\times$$

$$\left(\begin{array}{l}\left[\left(1-\Lambda^{-1}\right)\tilde{q}_0^{(2)}+\tilde{\beta}(\tilde{\omega}_0)\right]\left(\begin{array}{l}\tilde{q}_k^{(1)}\left(\tilde{q}_0^{(2)}+\tilde{\beta}(\tilde{\omega}_0)\right)\left[(\Lambda-1)\tilde{q}_k^{(2)}+\Lambda\tilde{\beta}(\omega)\right]\\ +\dfrac{\tilde{\omega}_0}{\omega}\left\{\left(\tilde{q}_k^{(2)}+\tilde{\beta}(\omega)\right)\left(\dfrac{\omega}{\tilde{\omega}_0}\right)^2+\tilde{q}_k^{(1)}\left[\Lambda^{-1}\left(\dfrac{\omega}{\tilde{\omega}_0}\right)^2+\tilde{\beta}(\omega)\tilde{q}_k^{(2)}\right]\right\}\end{array}\right)\\ -\tilde{q}_0^{(2)}\tilde{\beta}(\tilde{\omega}_0)\left[-\dfrac{\omega}{\tilde{\omega}_0}\left(\tilde{q}_k^{(1)}+\tilde{q}_k^{(2)}\right)\left(\tilde{q}_0^{(2)}+\tilde{\beta}(\tilde{\omega}_0)\right)+\tilde{q}_k^{(2)}\tilde{\beta}(\omega)\right]\end{array}\right)$$

$$\tilde{C}_{11}(k,\omega)=\frac{1}{\Lambda^{-1}\tilde{q}_k^{(1)}+\tilde{q}_k^{(2)}+\tilde{\beta}(\omega)}\times$$

$$\left(\begin{array}{l}\left(1-\Lambda^{-1}\right)\left[\tilde{q}_0^{(2)}\tilde{\beta}(\tilde{\omega}_0)+\tilde{q}_k^{(2)}\tilde{\beta}(\omega)-\dfrac{\omega}{\tilde{\omega}_0}\left(\tilde{q}_k^{(1)}+\tilde{q}_k^{(2)}\right)\left(\tilde{q}_0^{(2)}+\tilde{\beta}(\tilde{\omega}_0)\right)\right]\\ -\dfrac{\tilde{\omega}_0}{\omega}\left[\left(1-\Lambda^{-1}\right)\tilde{q}_0^{(2)}+\tilde{\beta}(\tilde{\omega}_0)\right]\left(\tilde{q}_k^{(1)}+\tilde{q}_k^{(2)}+\tilde{\beta}(\omega)\right)\end{array}\right)$$

$$\tilde{C}_{12}(k,\omega)=\frac{-(1-\Lambda^{-1})^2}{\Lambda^{-1}\tilde{q}_k^{(1)}+\tilde{q}_k^{(2)}+\tilde{\beta}(\omega)}$$

$$\tilde{q}_0^{(1)}=\left(1-\tilde{k}_0^{\,2}\right)^{1/2},\ \tilde{q}_0^{(2)}=(\Lambda^{-1}-\tilde{k}_0^{\,2})^{1/2},\ \tilde{q}_k^{(1)}=\left[\left(\frac{\omega}{\tilde{\omega}_0}\right)^2-k^2\right]^{1/2},\ \tilde{q}_k^{(2)}=\left[\Lambda^{-1}\left(\frac{\omega}{\tilde{\omega}_0}\right)^2-k^2\right]^{1/2}$$

$$\tilde{\beta}(\omega)=\frac{\omega}{\tilde{\omega}_0}\left[\frac{\alpha}{2}(\gamma-1)-\gamma-i(\gamma-1)\theta\tau\omega\right](1-\Lambda^{-1})M_S \tag{4.76}$$

Similarly G_J in Eq. (4.47) can be rewritten in terms of $\boldsymbol{k}$ and $\boldsymbol{k_0}$.

$$G_J(\boldsymbol{k},\boldsymbol{k_0},\boldsymbol{k_0},\omega,\omega_0,\omega_0) =$$

$$\left(\frac{\omega_0}{c_2}\right)^2 - \left(\frac{\omega_0}{c_1}\right)^2 + \frac{2\left[-\frac{\beta(\omega_0)}{2}\left|\boldsymbol{k}-\boldsymbol{k_0}\right|^2 + C_{30}(k,\omega) + C_{31}(k,\omega)\boldsymbol{k}\cdot\boldsymbol{k_0} + C_{32}(k,\omega)(\boldsymbol{k}\cdot\boldsymbol{k_0})^2\right]}{(\rho_2/\rho_1)q_0^{(1)} + q_0^{(2)} + \beta(\omega_0)} \quad (4.77)$$

where

$$C_{30}(k,\omega) = \frac{1}{(\rho_2/\rho_1)q_k^{(1)} + q_k^{(2)} + \beta(\omega)} \times$$

$$\left(\begin{array}{l} \left[\left(1-\frac{\rho_2}{\rho_1}\right)q_0^{(2)} + \beta(\omega_0)\right]\left\{ \begin{array}{l} q_0^{(1)}q_k^{(1)}\left[\left(\frac{\rho_2}{\rho_1}-1\right)q_k^{(2)} - \beta(\omega)\right] \\ +\frac{\omega_0}{\omega}\left\{\left(q_k^{(2)}+\beta(\omega)\right)\left(\frac{\omega}{c_1}\right)^2 + q_k^{(1)}\left[\left(\frac{\omega}{c_2}\right)^2 + \beta(\omega)q_k^{(2)}\right]\right\} \end{array}\right\} \\ +\left[\left(\frac{\omega_0}{c_2}\right)^2 - \frac{\rho_2}{\rho_1}\left(\frac{\omega_0}{c_1}\right)^2 + q_0^{(2)}\beta(\omega_0)\right]\left[-\frac{\omega}{\omega_0}\frac{\rho_2}{\rho_1}q_0^{(1)}\left(q_k^{(1)}+q_k^{(2)}\right) - \beta(\omega)q_k^{(2)} + \frac{\rho_2}{\rho_1}\left(\frac{\omega}{c_1}\right)^2 - \left(\frac{\omega}{c_2}\right)^2\right] \end{array}\right)$$

$$C_{31}(k,\omega) = \frac{1}{(\rho_2/\rho_1)q_k^{(1)} + q_k^{(2)} + \beta(\omega)} \times$$

$$\left(\begin{array}{l} \left(1-\frac{\rho_2}{\rho_1}\right)\left[\left(\frac{\omega_0}{c_2}\right)^2 - \frac{\rho_2}{\rho_1}\left(\frac{\omega_0}{c_1}\right)^2 + q_0^{(2)}\beta(\omega_0)\right] - \frac{\omega_0}{\omega}\left[\left(1-\frac{\rho_2}{\rho_1}\right)q_0^{(2)} + \beta(\omega_0)\right]\left(q_k^{(1)}+q_k^{(2)}+\beta(\omega)\right) \\ +\left(1-\frac{\rho_2}{\rho_1}\right)\left[\left(\frac{\omega}{c_2}\right)^2 - \frac{\rho_2}{\rho_1}\left(\frac{\omega}{c_1}\right)^2 + q_k^{(2)}\beta(\omega) + \frac{\omega}{\omega_0}\frac{\rho_2}{\rho_1}q_0^{(1)}\left(q_k^{(1)}+q_k^{(2)}\right)\right] \end{array}\right)$$

$$C_{32}(k,\omega) = -\frac{(1-\rho_2/\rho_1)^2}{(\rho_2/\rho_1)q_k^{(1)} + q_k^{(2)} + \beta(\omega)} = C_{12}(k,\omega)$$

Integrating Eq. (4.77) together with Eq. (4.68) yields

$$\iint_{\boldsymbol{k}} G_J(\boldsymbol{k},\boldsymbol{k_0},\boldsymbol{k_0},\omega,\omega_0,\omega_0)W(\boldsymbol{k_0}-\boldsymbol{k},\omega_0-\omega)d\boldsymbol{k} \quad (4.78)$$

$$= \frac{\sigma^2 t_c}{2\pi^{1/2}}\left[\left(\frac{\omega_0}{c_2}\right)^2 - \left(\frac{\omega_0}{c_1}\right)^2\right]\exp\left(-(\omega_0-\omega)^2 t_c^2/4\right) +$$

$$\frac{2}{(\rho_2/\rho_1)q_0^{(1)}+q_0^{(2)}+\beta(\omega_0)}\frac{\sigma^2 t_c l_c^2}{\pi^{1/2}}\exp\left(-(\omega_0-\omega)^2 t_c^2/4\right)\times$$
$$\left[-\frac{\beta(\omega_0)}{l_c^4}+\frac{\mathrm{e}^{-(k_0 l_c)^2/4}}{8}\int_{k=0}^{\infty}\left(\begin{array}{l}2C_{30}(k,\omega)I_0(kk_0 l_c^2/2)+2kk_0 C_{31}(k,\omega)I_1(kk_0 l_c^2/2)\\+(kk_0)^2 C_{32}(k,\omega)\left[I_0(kk_0 l_c^2/2)+I_2(kk_0 l_c^2/2)\right]\end{array}\right)k\,\mathrm{e}^{-(kl_c)^2/4}\,dk\right]$$

where use is made of

$$\iint_{\boldsymbol{k}} W(\boldsymbol{k_0}-\boldsymbol{k},\omega_0-\omega)d\boldsymbol{k}$$
$$=\frac{\sigma^2 t_c l_c^2}{8\pi^{3/2}}\exp\left(-(\omega_0-\omega)^2 t_c^2/4\right)\int_{-\infty}^{\infty}\int_{-\infty}^{\infty}\exp\left[-\left(|\boldsymbol{k_0}-\boldsymbol{k}|l_c\right)^2/4\right]d\boldsymbol{k}$$
$$=\frac{\sigma^2 t_c l_c^2}{8\pi^{3/2}}\exp\left(-(\omega_0-\omega)^2 t_c^2/4\right)\int_{k=0}^{\infty}\int_{\theta=0}^{2\pi}\exp\left[-\left(kl_c\right)^2/4\right]kd\theta dk$$
$$=\frac{\sigma^2 t_c}{2\pi^{1/2}}\exp\left(-(\omega_0-\omega)^2 t_c^2/4\right)$$

After integrating over ω, nondimensionalizing Eq. (4.78) yields:

$$\int_{\omega}\iint_{\boldsymbol{k}} G_J(\boldsymbol{k},\boldsymbol{k_0},\boldsymbol{k_0},\omega,\omega_0,\omega_0)W(\boldsymbol{k_0}-\boldsymbol{k},\omega_0-\omega)d\boldsymbol{k}d\omega$$
$$=\tilde{\sigma}^2(\Lambda^{-1}-1)+\frac{\tilde{\sigma}^2}{(\rho_2/\rho_1)\tilde{q}_0^{(1)}+\tilde{q}_0^{(2)}+\tilde{\beta}(\tilde{\omega}_0)}\times \tag{4.79}$$
$$\left[-\frac{4\tilde{\beta}(\tilde{\omega}_0)}{\tilde{l}_c^{\,2}}+\frac{\tilde{l}_c^{\,2}\,\mathrm{e}^{-(\tilde{k}_0\tilde{l}_c)^2/4}}{4\pi^{1/2}}\times\right.$$
$$\left.\int_{\omega=-\infty}^{\infty}\int_{k=0}^{\infty}\left(\begin{array}{l}2\tilde{C}_{30}(k,\omega)I_0(k\tilde{k}_0\tilde{l}_c^{\,2}/2)+2k\tilde{k}_0\tilde{C}_{31}(k,\omega)I_1(k\tilde{k}_0\tilde{l}_c^{\,2}/2)\\+(k\tilde{k}_0)^2\tilde{C}_{32}(k,\omega)\left[I_0(k\tilde{k}_0\tilde{l}_c^{\,2}/2)+I_2(k\tilde{k}_0\tilde{l}_c^{\,2}/2)\right]\end{array}\right)k\,\mathrm{e}^{-[(k\tilde{l}_c)^2+(\tilde{\omega}_0-\omega)^2]/4}\,dkd\omega\right]$$

where

$$\tilde{C}_{30}(k,\omega)=\left[\Lambda^{-1}\tilde{q}_k^{(1)}+\tilde{q}_k^{(2)}+\tilde{\beta}(\omega)\right]^{-1}\times$$
$$\left(\begin{array}{l}\left[\left(1-\Lambda^{-1}\right)\tilde{q}_0^{(2)}+\tilde{\beta}(\tilde{\omega}_0)\right]\left(\begin{array}{l}\tilde{q}_0^{(1)}\tilde{q}_k^{(1)}\left[\left(\Lambda^{-1}-1\right)\tilde{q}_k^{(2)}-\tilde{\beta}(\omega)\right]\\+\dfrac{\tilde{\omega}_0}{\omega}\left\{\left(\tilde{q}_k^{(2)}+\tilde{\beta}(\omega)\right)\left(\dfrac{\omega}{\tilde{\omega}_0}\right)^2+\tilde{q}_k^{(1)}\left[\Lambda^{-1}\left(\dfrac{\omega}{\tilde{\omega}_0}\right)^2+\tilde{\beta}(\omega)\tilde{q}_k^{(2)}\right]\right\}\end{array}\right)\\-\tilde{q}_0^{(2)}\tilde{\beta}(\tilde{\omega}_0)\left[\Lambda^{-1}\dfrac{\omega}{\tilde{\omega}_0}\tilde{q}_0^{(1)}\left(\tilde{q}_k^{(1)}+\tilde{q}_k^{(2)}\right)+\tilde{q}_k^{(2)}\tilde{\beta}(\omega)\right]\end{array}\right)$$

$$\tilde{C}_{31}(k,\omega)=\frac{1}{\Lambda^{-1}\tilde{q}_k^{(1)}+\tilde{q}_k^{(2)}+\tilde{\beta}(\omega)}\begin{pmatrix}\left(1-\Lambda^{-1}\right)\left[\Lambda^{-1}\dfrac{\omega}{\tilde{\omega}_0}\tilde{q}_0^{(1)}\left(\tilde{q}_k^{(1)}+\tilde{q}_k^{(2)}\right)+\tilde{q}_0^{(2)}\tilde{\beta}(\tilde{\omega}_0)+\tilde{q}_k^{(2)}\tilde{\beta}(\omega)\right]\\ -\dfrac{\tilde{\omega}_0}{\omega}\left[\left(1-\Lambda^{-1}\right)\tilde{q}_0^{(2)}+\tilde{\beta}(\tilde{\omega}_0)\right]\left(\tilde{q}_k^{(1)}+\tilde{q}_k^{(2)}+\tilde{\beta}(\omega)\right)\end{pmatrix}$$

$$\tilde{C}_{32}(k,\omega)=-\frac{(1-\Lambda^{-1})^2}{\Lambda^{-1}\tilde{q}_k^{(1)}+\tilde{q}_k^{(2)}+\tilde{\beta}(\omega)}=\tilde{C}_{12}(k,\omega)$$

q's and β are from Eq. (4.76).

4.5.2 Net incoherent energy flux

Incoherent energy flux of a reflected field can be obtained in a similar manner to the previous section. Eqs. (3.118) and (4.47) lead to

$$A_J(\boldsymbol{k},\boldsymbol{k_0},\omega,\omega_0)=\frac{2i(q_0^{(1)}q_k^{(1)})^{1/2}}{\left[(\rho_2/\rho_1)q_0^{(1)}+q_0^{(2)}+\beta(\omega_0)\right]\left[(\rho_2/\rho_1)q_k^{(1)}+q_k^{(2)}+\beta(\omega)\right]}\times$$

$$\left[\frac{\omega_0}{\omega}\left(q_k^{(2)}+\beta(\omega)\right)\left(\left(\frac{\rho_2}{\rho_1}-1\right)q_0^{(2)}-\beta(\omega_0)\right)+\frac{\rho_2}{\rho_1}\left(\frac{\rho_2}{\rho_1}\left(\frac{\omega_0}{c_1}\right)^2-\left(\frac{\omega_0}{c_2}\right)^2-q_0^{(2)}\beta(\omega_0)\right)+\frac{\rho_2}{\rho_1}\left(1-\frac{\rho_2}{\rho_1}\right)\boldsymbol{k}\cdot\boldsymbol{k_0}\right]$$

which leads to

$$\left|A_J(\boldsymbol{k},\boldsymbol{k_0},\omega,\omega_0)\right|^2_{|\boldsymbol{k}|<|\omega|/c_1}=\frac{4q_0^{(1)}\left[C_{20}(k,\omega)+C_{21}(k,\omega)\boldsymbol{k}\cdot\boldsymbol{k_0}+C_{22}(k,\omega)(\boldsymbol{k}\cdot\boldsymbol{k_0})^2\right]}{\left|(\rho_2/\rho_1)q_0^{(1)}+q_0^{(2)}+\beta(\omega_0)\right|^2}\qquad(4.80)$$

where

$$C_{20}(k,\omega)=\frac{q_k^{(1)}\left|C_{23}(k,\omega)\right|^2}{\left|(\rho_2/\rho_1)q_k^{(1)}+q_k^{(2)}+\beta(\omega)\right|^2},\ C_{21}(k,\omega)=\frac{2(\rho_2/\rho_1)(1-\rho_2/\rho_1)q_k^{(1)}\,\mathrm{Re}[C_{23}(k,\omega)]}{\left|(\rho_2/\rho_1)q_k^{(1)}+q_k^{(2)}+\beta(\omega)\right|^2},$$

$$C_{22}(k,\omega)=\frac{(\rho_2/\rho_1)^2(1-\rho_2/\rho_1)^2q_k^{(1)}}{\left|(\rho_2/\rho_1)q_k^{(1)}+q_k^{(2)}+\beta(\omega)\right|^2}$$

$$C_{23}(k,\omega)=\frac{\omega_0}{\omega}\left(q_k^{(2)}+\beta(\omega)\right)\left(\left(\frac{\rho_2}{\rho_1}-1\right)q_0^{(2)}-\beta(\omega_0)\right)+\frac{\rho_2}{\rho_1}\left(\frac{\rho_2}{\rho_1}\left(\frac{\omega_0}{c_1}\right)^2-\left(\frac{\omega_0}{c_2}\right)^2-q_0^{(2)}\beta(\omega_0)\right)$$

Note that $q_k^{(1)}$ is a real value if $|\boldsymbol{k}| < \omega / c_1$. Scattering cross section can be integrated over $\boldsymbol{k}$ using Eq. (4.80) to yield

$$\iint_{|\boldsymbol{k}|<\frac{|\omega|}{c_1}} \sigma_{R,J}(\boldsymbol{k},\boldsymbol{k_0},\omega,\omega_0)d\boldsymbol{k} = \iint_{|\boldsymbol{k}|<\frac{|\omega|}{c_1}} \frac{\omega}{\omega_0}\left|A_J(\boldsymbol{k},\boldsymbol{k_0},\omega,\omega_0)\right|^2 W(\boldsymbol{k}-\boldsymbol{k_0},\omega-\omega_0)d\boldsymbol{k}$$

$$= \frac{\sigma^2 t_c l_c^2 q_0^{(1)} \omega \exp\left[-\left((\omega_0-\omega)^2 t_c^2 + k_0^2 l_c^2\right)/4\right]}{2\pi^{3/2}\omega_0\left|(\rho_2/\rho_1)q_0^{(1)} + q_0^{(2)} + \beta(\omega_0)\right|^2}$$

$$\times \int_{k=0}^{|\omega|/c_1}\int_{\theta=0}^{2\pi}\left(\sum_{j=0}^{2} C_{2j}(k,\omega)(\boldsymbol{k}\cdot\boldsymbol{k_0})^j\right)\exp\left[-\left(k^2 - 2\boldsymbol{k}\cdot\boldsymbol{k_0}\right)l_c^2/4\right]kd\theta dk$$

$$= \frac{\sigma^2 t_c l_c^2 q_0^{(1)} \omega \exp\left[-\left((\omega_0-\omega)^2 t_c^2 + k_0^2 l_c^2\right)/4\right]}{2\pi^{3/2}\omega_0\left|(\rho_2/\rho_1)q_0^{(1)} + q_0^{(2)} + \beta(\omega_0)\right|^2}$$

$$\times \int_{k=0}^{|\omega|/c_1} k\exp(-k^2 l_c^2/4)\left(\sum_{j=0}^{2} C_{2j}(k,\omega)\int_{\theta=0}^{2\pi}(\boldsymbol{k}\cdot\boldsymbol{k_0})^j \exp(\boldsymbol{k}\cdot\boldsymbol{k_0}l_c^2/2)d\theta\right)dk$$

$$= \frac{\sigma^2 t_c l_c^2 q_0^{(1)} \omega \exp\left[-\left((\omega_0-\omega)^2 t_c^2 + k_0^2 l_c^2\right)/4\right]}{2\pi^{1/2}\omega_0\left|(\rho_2/\rho_1)q_0^{(1)} + q_0^{(2)} + \beta(\omega_0)\right|^2}$$

$$\times \int_{k=0}^{|\omega|/c_1}\left(\begin{array}{l} 2C_{20}(k,\omega)I_0(kk_0 l_c^2/2) + 2kk_0 C_{21}(k,\omega)I_1(kk_0 l_c^2/2) \\ +(kk_0)^2 C_{22}(k,\omega)\left[I_0(kk_0 l_c^2/2) + I_2(kk_0 l_c^2/2)\right]\end{array}\right)k\,\mathrm{e}^{-k^2 l_c^2/4}\,dk$$

which is further integrated over ω and nondimensionalized to yield:

$$\int_{\omega}\iint_{|\boldsymbol{k}|<\frac{|\omega|}{c_1}} \sigma_{R,J}(\boldsymbol{k},\boldsymbol{k_0},\omega,\omega_0)d\boldsymbol{k}d\omega = \frac{\tilde{\sigma}^2\tilde{l}_c^2\tilde{q}_0^{(1)}\exp\left(-(\tilde{k}_0\tilde{l}_c)^2/4\right)}{2\pi^{1/2}\tilde{\omega}_0\left|\Lambda^{-1}\tilde{q}_0^{(1)} + \tilde{q}_0^{(2)} + \tilde{\beta}(\tilde{\omega}_0)\right|^2}\times$$

$$\int_{\omega=-\infty}^{\infty}\int_{k=0}^{|\omega|/\tilde{\omega}_0}\left(\begin{array}{l} 2\tilde{C}_{20}(k,\omega)I_0(k\tilde{k}_0\tilde{l}_c^2/2) + 2k\tilde{k}_0\tilde{C}_{21}(k,\omega)I_1(k\tilde{k}_0\tilde{l}_c^2/2) \\ +(k\tilde{k}_0)^2\tilde{C}_{22}(k,\omega)\left[I_0(k\tilde{k}_0\tilde{l}_c^2/2) + I_2(k\tilde{k}_0\tilde{l}_c^2/2)\right]\end{array}\right)k\omega\,\mathrm{e}^{-[(k\tilde{l}_c)^2+(\tilde{\omega}_0-\omega)^2]/4}\,dkd\omega \quad (4.81)$$

For a stationary surface,

$$\iint_{|\boldsymbol{k}|<\frac{\omega_0}{c_1}} \sigma_{R,J}(\boldsymbol{k},\boldsymbol{k_0})d\boldsymbol{k} = \iint_{|\boldsymbol{k}|<\frac{\omega_0}{c_1}} \left|A_J(\boldsymbol{k},\boldsymbol{k_0},\omega_0,\omega_0)\right|^2 W(\boldsymbol{k}-\boldsymbol{k_0})d\boldsymbol{k}$$

$$= \frac{\tilde{\sigma}^2\tilde{l}_c^{\,2}\tilde{q}_0^{(1)}\exp\left(-(\tilde{k}_0\tilde{l}_c)^2/4\right)}{\left|\Lambda^{-1}\tilde{q}_0^{(1)}+\tilde{q}_0^{(2)}+\tilde{\beta}(\tilde{\omega}_0)\right|^2} \tag{4.82}$$

$$\times\int_0^1 \begin{pmatrix} 2\tilde{C}_{20}(k,\tilde{\omega}_0)I_0(k\tilde{k}_0\tilde{l}_c^{\,2}/2)+2k\tilde{k}_0\tilde{C}_{21}(k,\tilde{\omega}_0)I_1(k\tilde{k}_0\tilde{l}_c^{\,2}/2) \\ +(k\tilde{k}_0)^2\tilde{C}_{22}(k,\tilde{\omega}_0)\left[I_0(k\tilde{k}_0\tilde{l}_c^{\,2}/2)+I_2(k\tilde{k}_0\tilde{l}_c^{\,2}/2)\right] \end{pmatrix} k\,\mathrm{e}^{-(k\tilde{l}_c)^2/4}\,dk$$

where

$$\tilde{C}_{20}(k,\omega) = \frac{\tilde{q}_k^{(1)}\left|\tilde{C}_{23}(k,\omega)\right|^2}{\left|\Lambda^{-1}\tilde{q}_k^{(1)}+\tilde{q}_k^{(2)}+\tilde{\beta}(\omega)\right|^2},\ \tilde{C}_{21}(k,\omega) = \frac{2(\Lambda-1)\tilde{q}_k^{(1)}\,\mathrm{Re}[\tilde{C}_{23}(k,\omega)]}{\left|\tilde{q}_k^{(1)}+\Lambda[\tilde{q}_k^{(2)}+\tilde{\beta}(\omega)]\right|^2} \tag{4.83}$$

$$\tilde{C}_{22}(k,\omega) = \frac{(1-\Lambda^{-1})^2\tilde{q}_k^{(1)}}{\left|\tilde{q}_k^{(1)}+\Lambda[\tilde{q}_k^{(2)}+\tilde{\beta}(\omega)]\right|^2}$$

$$\tilde{C}_{23}(k,\omega) = \frac{\tilde{\omega}_0}{\omega}\left(\tilde{q}_k^{(2)}+\tilde{\beta}(\omega)\right)\left((\Lambda^{-1}-1)\tilde{q}_0^{(2)}-\tilde{\beta}(\tilde{\omega}_0)\right)-\Lambda^{-1}\tilde{q}_0^{(2)}\tilde{\beta}(\tilde{\omega}_0)$$

q's and β are from Eq. (4.76). Incoherent energy flux of the transmitted field can be obtained in a similar manner. Eqs. (3.118) and (4.47) yield

$$B_J(\boldsymbol{k},\boldsymbol{k_0},\omega,\omega_0) = \frac{2i\left((\rho_2/\rho_1)q_0^{(1)}q_k^{(2)}\right)^{1/2}}{\left[(\rho_2/\rho_1)q_0^{(1)}+q_0^{(2)}+\beta(\omega_0)\right]\left[(\rho_2/\rho_1)q_k^{(1)}+q_k^{(2)}+\beta(\omega)\right]}\times$$

$$\left[-\frac{\omega_0}{\omega}q_k^{(1)}\left(\left(\frac{\rho_2}{\rho_1}-1\right)q_0^{(2)}-\beta(\omega_0)\right)+\frac{\rho_2}{\rho_1}\left(\frac{\omega_0}{c_1}\right)^2-\left(\frac{\omega_0}{c_2}\right)^2-q_0^{(2)}\beta(\omega_0)+\left(1-\frac{\rho_2}{\rho_1}\right)\boldsymbol{k}\cdot\boldsymbol{k_0}\right]$$

which leads to the transmitted incoherent energy flux:

$$\int_\omega \iint_{|\boldsymbol{k}|<\frac{|\omega|}{c_2}} \sigma_{T,J}(\boldsymbol{k},\boldsymbol{k_0},\omega,\omega_0)d\boldsymbol{k}d\omega = \int_\omega \iint_{|\boldsymbol{k}|<\frac{|\omega|}{c_2}} \frac{\omega}{\omega_0}\left|B_J(\boldsymbol{k},\boldsymbol{k_0},\omega,\omega_0)\right|^2 W(\boldsymbol{k}-\boldsymbol{k_0},\omega-\omega_0)d\boldsymbol{k}d\omega \tag{4.84}$$

$$= \frac{\Lambda^{-1}\tilde{\sigma}^2\tilde{l}_c^{\,2}\tilde{q}_0^{(1)}\exp\left(-(\tilde{k}_0\tilde{l}_c)^2/4\right)}{2\pi^{1/2}\tilde{\omega}_0\left|\Lambda^{-1}\tilde{q}_0^{(1)}+\tilde{q}_0^{(2)}+\tilde{\beta}(\tilde{\omega}_0)\right|^2}\times$$

$$\int_{\omega=-\infty}^{\infty}\int_{k=0}^{\Lambda^{-1/2}\frac{|\omega|}{\tilde{\omega}_0}}\begin{pmatrix}2\tilde{C}_{40}(k,\omega)I_0(k\tilde{k}_0\tilde{l}_c^2/2)+2k\tilde{k}_0\tilde{C}_{41}(k,\omega)I_1(k\tilde{k}_0\tilde{l}_c^2/2)\\+(k\tilde{k}_0)^2\tilde{C}_{42}(k,\omega)\left[I_0(k\tilde{k}_0\tilde{l}_c^2/2)+I_2(k\tilde{k}_0\tilde{l}_c^2/2)\right]\end{pmatrix}k\omega\,\mathrm{e}^{-[(k\tilde{l}_c)^2+(\tilde{\omega}_0-\omega)^2]/4}\,dkd\omega$$

where $\tilde{C}_{40}(k,\omega)=\dfrac{\tilde{q}_k^{(2)}\left|\tilde{C}_{43}(k,\omega)\right|^2}{\left|\Lambda^{-1}\tilde{q}_k^{(1)}+\tilde{q}_k^{(2)}+\tilde{\beta}(\omega)\right|^2}$, $\quad\tilde{C}_{41}(k,\omega)=\dfrac{2(1-\Lambda^{-1})\tilde{q}_k^{(2)}\,\mathrm{Re}[\tilde{C}_{43}(k,\omega)]}{\left|\Lambda^{-1}\tilde{q}_k^{(1)}+\tilde{q}_k^{(2)}+\tilde{\beta}(\omega)\right|^2}$

$$\tilde{C}_{42}(k,\omega)=\frac{(1-\Lambda^{-1})^2\tilde{q}_k^{(2)}}{\left|\Lambda^{-1}\tilde{q}_k^{(1)}+\tilde{q}_k^{(2)}+\tilde{\beta}(\omega)\right|^2},\ \tilde{C}_{43}(k,\omega)=-\frac{\tilde{\omega}_0}{\omega}\tilde{q}_k^{(1)}\left((\Lambda^{-1}-1)\tilde{q}_0^{(2)}-\tilde{\beta}(\tilde{\omega}_0)\right)-\tilde{q}_0^{(2)}\tilde{\beta}(\tilde{\omega}_0)$$

q's and β are from Eq. (4.76). Note that $\tilde{q}_k^{(2)}$ is a positive real value for an integral range of k ($0<k<\Lambda^{-1/2}|\omega|/\tilde{\omega}_0$). For a stationary surface,

$$\begin{aligned}&\iint_{|\boldsymbol{k}|<\frac{\omega_0}{c_2}}\sigma_{T,J}(\boldsymbol{k},\boldsymbol{k_0})d\boldsymbol{k}=\iint_{|\boldsymbol{k}|<\frac{\omega_0}{c_2}}\left|B_J(\boldsymbol{k},\boldsymbol{k_0},\omega_0,\omega_0)\right|^2W(\boldsymbol{k}-\boldsymbol{k_0})d\boldsymbol{k}\\&=\frac{\Lambda^{-1}\tilde{\sigma}^2\tilde{l}_c^2\tilde{q}_0^{(1)}\exp\left(-(\tilde{k}_0\tilde{l}_c)^2/4\right)}{\left|\Lambda^{-1}\tilde{q}_0^{(1)}+\tilde{q}_0^{(2)}+\tilde{\beta}(\tilde{\omega}_0)\right|^2}\\&\times\int_0^{\Lambda^{-1/2}}\begin{pmatrix}2\tilde{C}_{40}(k,\tilde{\omega}_0)I_0(k\tilde{k}_0\tilde{l}_c^2/2)+2k\tilde{k}_0\tilde{C}_{41}(k,\tilde{\omega}_0)I_1(k\tilde{k}_0\tilde{l}_c^2/2)\\+(k\tilde{k}_0)^2\tilde{C}_{42}(k,\tilde{\omega}_0)\left[I_0(k\tilde{k}_0\tilde{l}_c^2/2)+I_2(k\tilde{k}_0\tilde{l}_c^2/2)\right]\end{pmatrix}k\,\mathrm{e}^{-(k\tilde{l}_c)^2/4}\,dk\end{aligned}\qquad(4.85)$$

CHAPTER 5 RESULTS OF CALCULATIONS OF NET ENERGY FLUXES

5.1 Estimation of Numerical Error and Ranges of Parameters

Integrals were numerically evaluated using Mathematica (version 5.2) to calculate energy fluxes. The accuracy of numerical integration was tested by evaluating a double integration over *k* and ω in Eq. (4.75) and the integration over *k* and ω was performed by 'NIntegrate' and 'CauchyPrincipleValue' in Mathematica. Figure 11 plots real and imaginary parts of numerical integration as a function of 'digits of precision' in Mathematica. This figure shows that digits of precision of greater than 4 yields an error of less than 10^{-4} for normalized value. The analysis that follows hereafter, therefore, uses 5 for digits of precision.

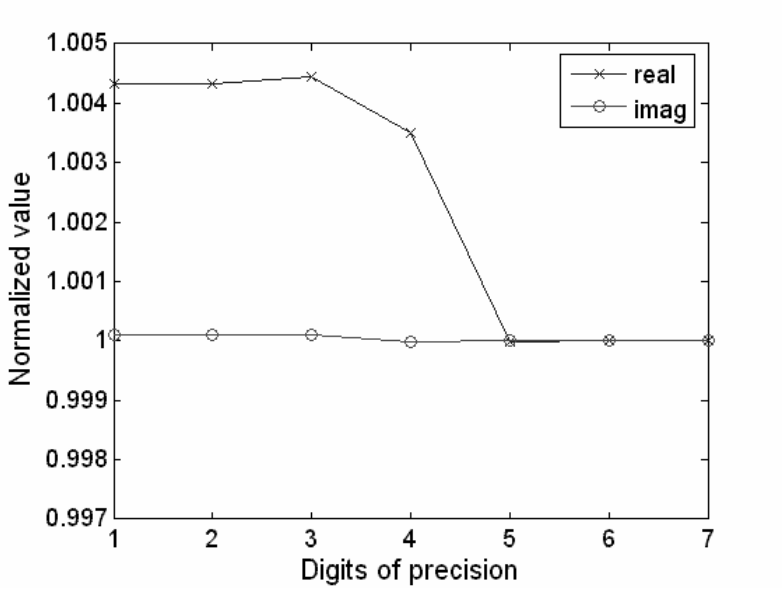

Figure 11 Precision test for numerical integrations using Mathematica ($\tilde{\sigma} = 0.1$, $\tilde{l}_c = 0.1$, $\tilde{f}_0 = 10$, $\phi_0^{(1)} = 30^\circ$, **τ= 0.025**)

Figure 12 shows the effect of integration range of ω upon the accuracy of numerical integration, where $\Delta\omega(=\tilde{\omega}_0-\omega) \geq 35$ yields the accuracy of $O(10^{-4})$. Note that the integration value depends mainly on $\exp[-(\Delta\omega)^2/4]$ for large $\Delta\omega$, which diminishes exponentially, as in Eq. (4.75). The analysis that follows hereafter approximates the integration over ω by applying a range of ω from $\tilde{\omega}_0-35$ to $\tilde{\omega}_0+35$ using $\Delta\omega$=35. Accordingly, the integral range over *k* is approximated by $0 \leq k \leq 35/\tilde{l}_c$ since $k\tilde{l}_c$ corresponds to $\Delta\omega$ as in $\exp\{-[(k\tilde{l}_c)^2+(\tilde{\omega}_0-\omega)^2]/4\}$.

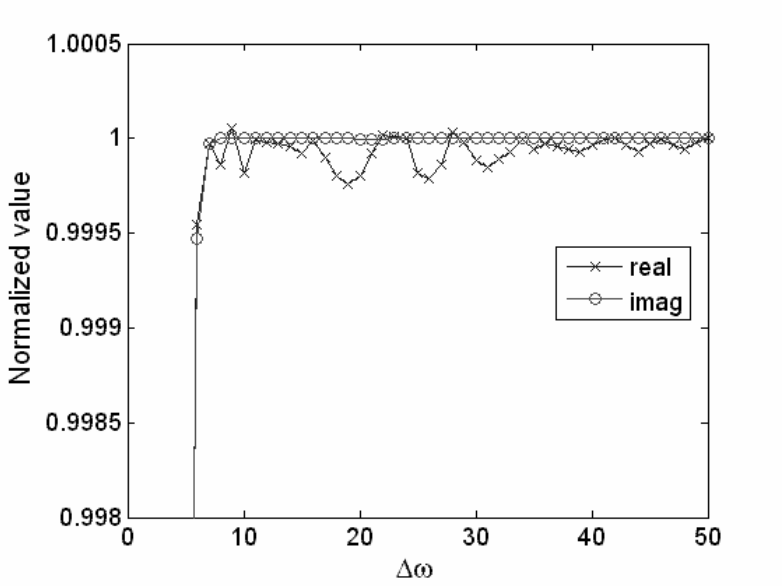

Figure 12 Dependence of accuracy of numerical integral upon integration range

Net energy fluxes will be simulated in the next section using dimensionless parameters whose ranges are based on Eqs. (3.13) and (3.14). Rms height, correlation length, and incidence angle have ranges such that

$$\tilde{\sigma} \leq 0.3, \qquad \tilde{l}_c \geq 1.5, \qquad 0° \leq \phi_0 \leq 40° \tag{5.1}$$

Note that $\tilde{l}_c \geq 1.5$ results from $\tilde{l}_c >> \sqrt{2}\,\tilde{\sigma}\tan\phi \approx 0.356$ for $\tilde{\sigma} = 0.3$, $\phi = 40$ °. $\tilde{f}_0 (= f_0 / f_c)$ and $\tau (= t_r / t_c)$ range from 0.1 to 10 to examine relative importance between f_0 and f_c and beween t_r and t_c, respectively. The variables related to β (jump factor; See Eq. (4.74)) have the values: $\alpha = 2$, $\gamma = 1.4$, $\theta = 10$, $\Lambda = 6$, $M_S = 0.001$.

5.2 Incidence angle dependence

Figure 13(a) shows a typical dependence of the reflected /transmitted energy flux upon incidence angle. The reflected energy flux is about 18 % of the total energy flux for normal incidence, and decreases slowly with increasing incidence angle (deviating more from a normal incidence) until it reaches the Brewster angle at about 22 °, where no reflection occurs. Reflected energy flux increases dramatically beyond the Brewster angle until it reaches the critical angle at about 24 °, beyond which all the energy is reflected. (The critical angle is: $\phi_{cr} = \sin^{-1}(c_1 / c_2) = \sin^{-1}(\Lambda^{-1/2}) = 24.1^{\circ}$ for $\Lambda = 6$.) This is typical wave reflection/ transmission behavior when incident waves originate from an unburned gas medium having a lower sound speed than that of hot burned gas medium. Figure 13(a) also shows the net energy flux due to the acoustic velocity jump condition. This effect is not significant enough to distinguish this result from the no jump condition, which is due to the fact that the velocity jump effect is proportional to $\tilde{f}_0 \tau$., whose value is quite small, $\tilde{f}_0 \tau = 0.01$. An enlarged view, shown in Figure 13(b), shows that the net energy flux due to the jump effect has a peak of about 2% at the critical angle. Such net energy flux at the critical angle goes to the reflection field, not to the transmission field because no energy is transmitted beyond the critical angle when a flame surface is flat.

Quantitative analysis of, for instance, the reflected energy flux in Figure 13(a) is as follows:

$$(E_{R,co})_{\sigma=0} = \left|\left\langle V_J(\boldsymbol{k_0}, \omega_0)\right\rangle\right|^2_{\sigma=0} = \left|R_J(\boldsymbol{k_0}, \omega_0)\right|^2 \tag{5.2}$$

where

$$R_J(\boldsymbol{k}_0, \omega_0) = \frac{\Lambda^{-1}\tilde{q}_0^{(1)} - \tilde{q}_0^{(2)} - \tilde{\beta}(\tilde{\omega}_0)}{\Lambda^{-1}\tilde{q}_0^{(1)} + \tilde{q}_0^{(2)} + \tilde{\beta}(\tilde{\omega}_0)}, \qquad \tilde{q}_0^{(1)} = \cos\phi_0^{(1)}, \qquad \tilde{q}_0^{(2)} = (\Lambda^{-1} - \sin^2\phi_0^{(1)})^{1/2},$$

$$\tilde{\beta}(\tilde{\omega}_0) = \left[\frac{\alpha}{2}(\gamma - 1) - \gamma - i(\gamma - 1)\theta\tau\tilde{\omega}_0\right](1 - \Lambda^{-1})M_S \qquad \text{(See Eq. (4.76))} \tag{5.3}$$

Setting $\beta = 0$ yields reflection /transmission energy flux with no jump effect.

$$(E_{R,co})_{\substack{\beta=0 \\ \sigma=0}} = \left|R(\boldsymbol{k_0}, \omega_0)\right|^2 = \begin{cases} \left(\dfrac{\Lambda^{-1}\cos\phi_0^{(1)} - (\Lambda^{-1} - \sin^2\phi_0^{(1)})^{1/2}}{\Lambda^{-1}\cos\phi_0^{(1)} + (\Lambda^{-1} - \sin^2\phi_0^{(1)})^{1/2}}\right)^2 & (\phi_0^{(1)} < \phi_{critical}) \\ 1 & (\phi_0^{(1)} \geq \phi_{critical}) \end{cases} \tag{5.4}$$

which has $(1-\sqrt{\Lambda})^2/(1+\sqrt{\Lambda})^2 = 0.177$ for case of normal angle of incidence with $\Lambda = 6$. The Brewster angle, ϕ_B, is defined as the angle where no reflection occurs with all the waves being transmitted. Thus, ϕ_B makes the numerator in Eq. (5.4) vanish.

$$\Lambda^{-1}\cos\phi_B - (\Lambda^{-1} - \sin^2\phi_B)^{1/2} = 0 \quad \Rightarrow \quad \Lambda^{-2}(1 - \sin^2\phi_B) = \Lambda^{-1} - \sin^2\phi_B$$

$$\phi_B = \arcsin\left(\frac{\Lambda^{-1/2}}{(1+\Lambda^{-1})^{1/2}}\right) = \arctan(\Lambda^{-1/2}) = 22.2^{\circ} \text{ for } \Lambda = 6 \tag{5.5}$$

which is equivalent to that in Modest ([57], p.58) with $n_2/n_1 = c_1/c_2 = \Lambda^{-1/2}$ (n is an index of refraction.).

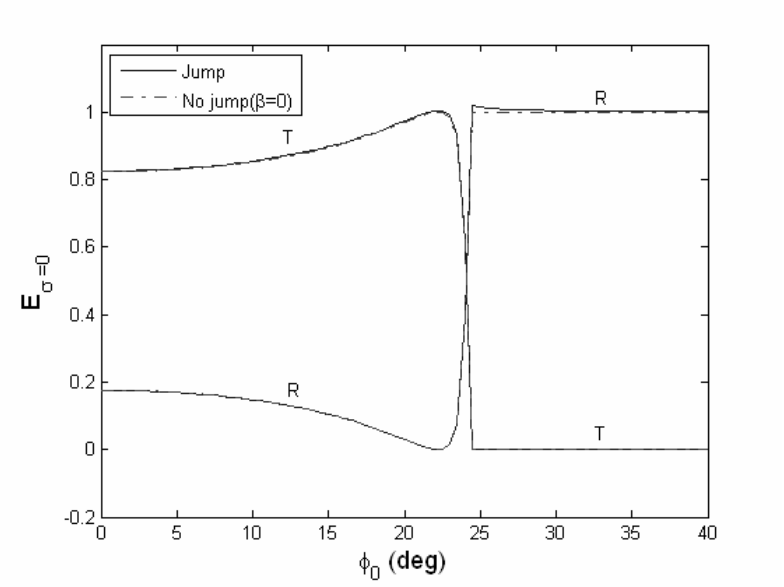

(a)

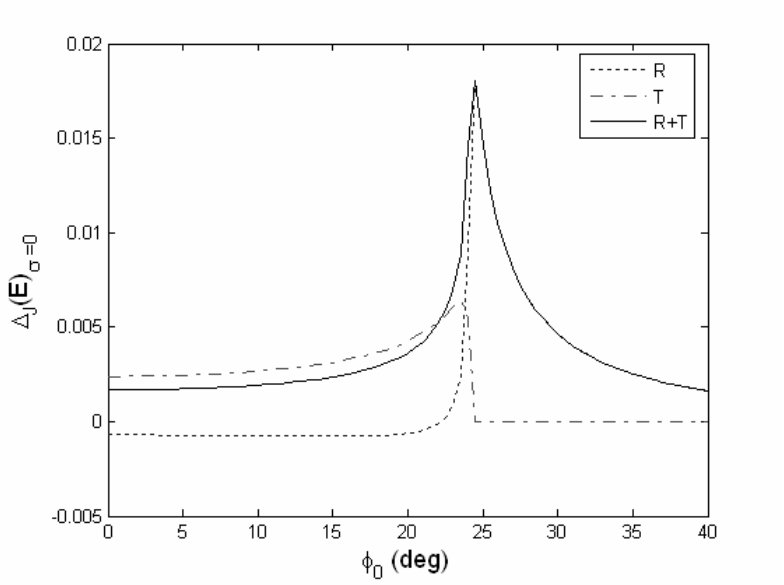

(b)

Figure 13 Dependence of acoustic energy flux upon incidence angle for a flat surface ($\sigma = 0$) (a) with and w/o jump effect, (b) Net energy flux due to jump effect ($\tilde{l}_c = 2$, $\tilde{f}_0 = \tau = 0.1$)

However, once the flame surface is wrinkled, incoherent energy is generated, which results from either, or both the jump effect and coherent energy damping. Such

wrinkling condition affects total energy flux, as shown in Figure 14(a), which exhibits noticeable net energy flux compared to jump condition in Figure 13. It is clearly shown in Figure 14(b) that, in case of small values of $\tilde{f}_0$ and τ, the total net energy flux depends primarily upon the surface wrinkling effect. ('J' and 'W' denote net energy flux due to jump and wrinkling effect, respectively.) This arises from that fact that a smaller $\tilde{f}_0$ implies a larger $f_c (\coloneqq 1/t_c)$, i.e., higher frequency of surface oscillation which leads to larger wrinkling effect. (Note that $\tilde{f}_0 = f_0 t_c = f_0 / f_c$; See also comments on Figure 19.) This figure shows that the total energy is damped (negative) except for near-critical incidence angle where energy flux is amplified (positive). Note that the wrinkling effect in Figure 14(b) is due to temporal wrinkling. Spatial wrinkling does not contribute to total net energy flux. It is worth recalling that surface wrinkling consists of two factors; temporal and spatial wrinkling. Temporal wrinkling is associated with unsteady motion of flame surface that amplifies /damps total energy flux as in Figure 14(b). On the other hand, spatial wrinkling is associated with energy transfer from coherent to incoherent flux due to spatial variation of a stationary wrinkled surface. Thus, spatial wrinkling does not alter total energy flux because it only redistributes energy flux between coherent and incoherent fields, as shown Figure 15, where coherent flux damping (negative value) is symmetric with incoherent flux production (positive value) leading to conservation of total energy flux (zero value).

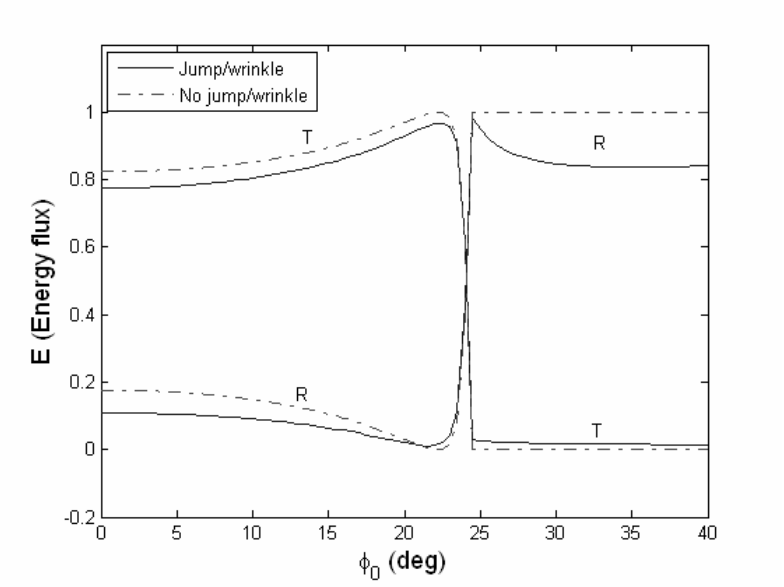

(a)

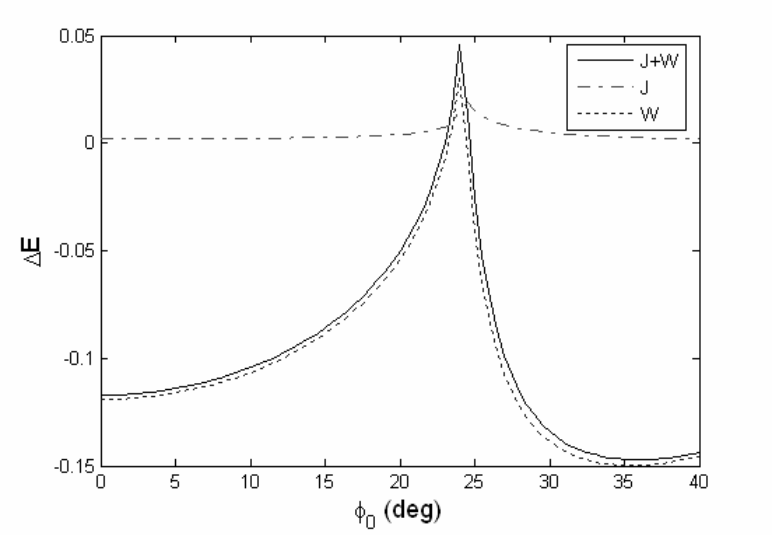

(b)

Figure 14 Dependence of acoustic energy flux upon incidence angle for a wrinkling surface (a) with and w/o jump and wrinkling effects, (b) net energy flux ($\tilde{\sigma}$ = 0.3, $\tilde{l}_c$ = 2, $\tilde{f}_0$ = τ = 0.1)

Note that a no jump condition is applied in Figure 15, to illustrate total energy conservation.

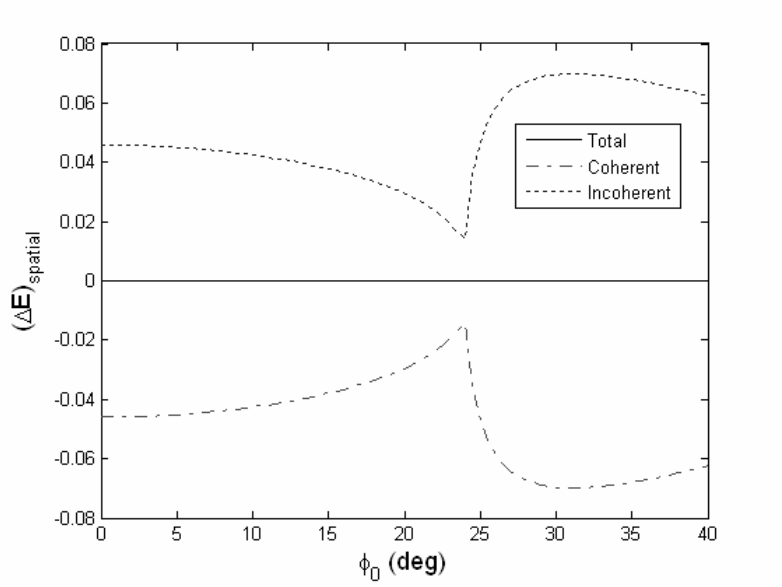

Figure 15 Dependence of coherent /incoherent energy fluxes upon incidence angle for a stationary wrinkling surface with no jump condition ($\tilde{\sigma}$ = 0.3, $\tilde{l}_c$ = 2, $\tilde{\beta} = 0$)

Figure 16 shows the total net energy flux and respective contribution of coherent and incoherent flux to the total flux for various τ. Figure 16(a) shows that the total net energy is amplified only near the critical angle and more damping occurs when the incidence angle deviates from the critical angle. It also shows that coherent energy is damped (negative) and incoherent energy is amplified (positive) for the entire range of incidence angle. Note that coherent and incoherent fluxes are no longer symmetric, see Figure 15 for comparison, since jump and temporal wrinkling effects are incorporated. The pattern of coherent flux is similar to that of total flux. Near the critical angle, coherent damping is minimized. As the incidence angle deviates from the critical angle, the coherent damping increases until reaching a maximum of about 23% at 34°. Incoherent flux production is almost invariant, at 2.5%, for subcritical angle, but displays a dramatic increase to 10% when crossing the critical angle and decreases slowly with further increasing incidence angle. The effect of $\tau (= t_r / t_c)$ in Figure 16(a) shows that, for

$\tilde{f}_0 = 0.1$, larger values of τ causes an increase of net coherent flux, leading to an increase of total net energy flux, for supercritical angles. However, τ does not affect net energy flux for subcritical angles. Figure 16(b) shows coherent flux for reflection and transmission fields. Note that coherent energy is not always damped, as reflected coherent energy is amplified near the critical angle. Transmitted coherent energy, however, is always damped for subcritical angles, with no net flux for supercritical angle. The effect of τ upon net coherent flux is only significant for the reflected part at supercritical angles. Figure 16(c) shows incoherent flux for reflection and transmission fields. Incoherent flux is higher for the reflected field than for the transmitted field, particularly for supercritical angles. Net incoherent fluxes increase abruptly near the critical angle. Note that some part of the incoherent flux is still transmitted even for supercritical angles in (c), as opposed to zero-coherent transmission flux for supercritical angles, as in (b). This is due to the fact that surface wrinkling, which produces incoherent energy, sometimes makes locally subcritical incidence angle even though the incidence angle from the mean surface is beyond the critical angle.

Figure 17 shows how the net energy flux varies with flame's rms height. For a flat surface with no roughness ($\tilde{\sigma} = 0$), total net energy flux is still generated by the jump effect due to unsteady heat release, as shown in (a). Such net energy flux is purely coherent as a flat surface produces no net incoherent flux, as in (c).

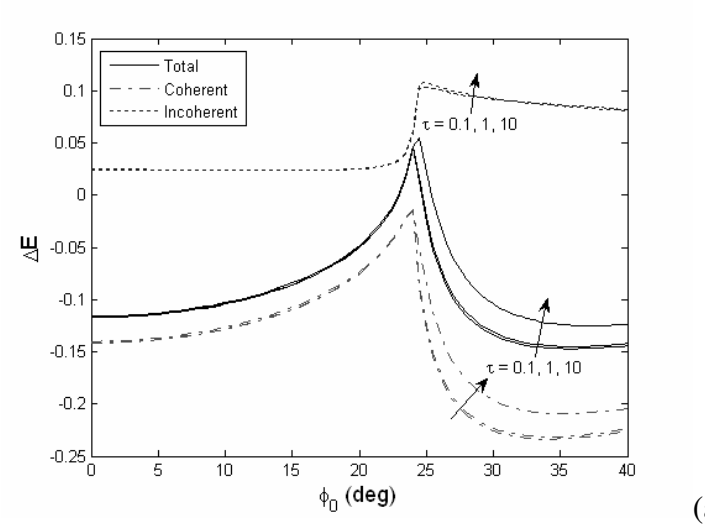

(a)

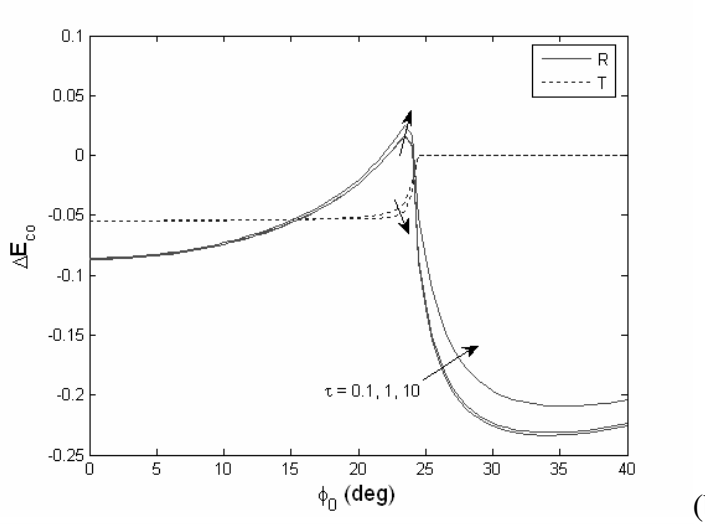

(b)

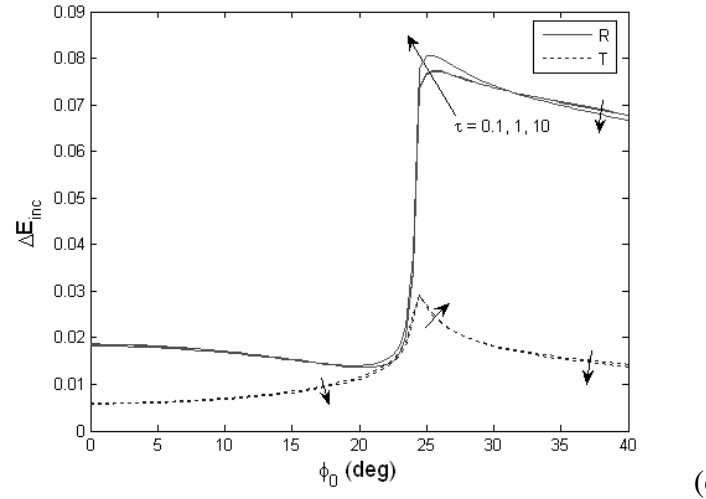

(c)

Figure 16 Dependence of net coherent /incoherent energy flux upon incidence angle for various τ($\tilde{f}_0$ = 0.1, $\tilde{\sigma}$ = 0.3, $\tilde{l}_c$ = 2)

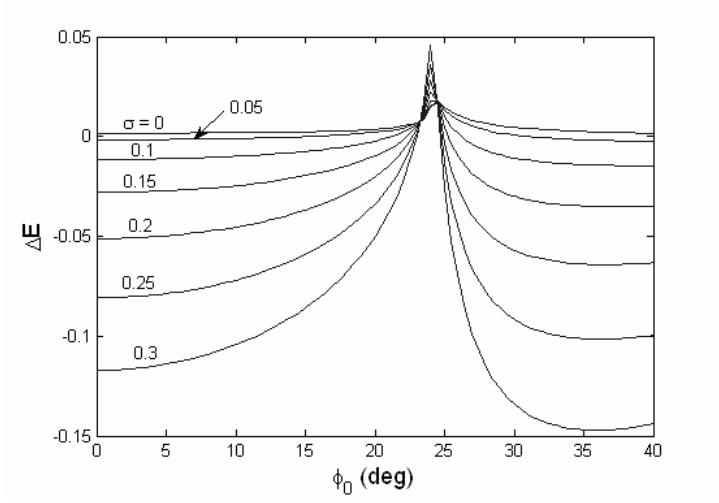

(a)

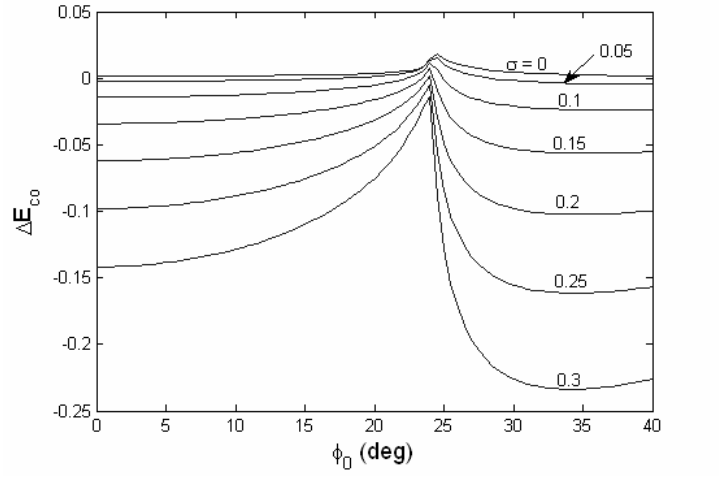

(b)

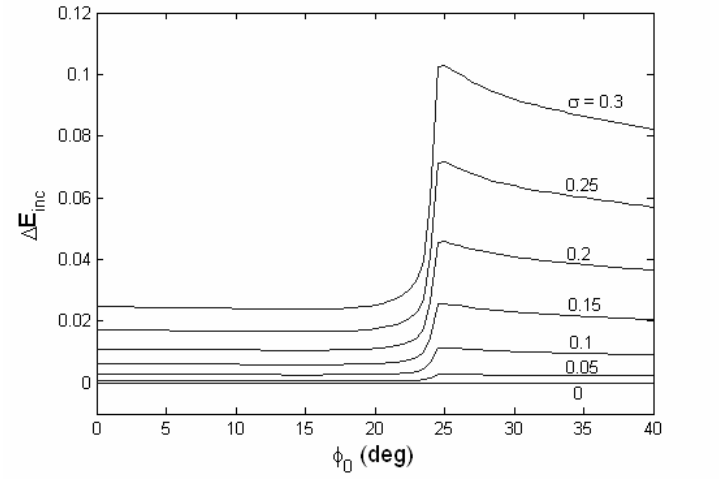

(c)

Figure 17 Dependence of net energy flux upon flame's rms height, $\tilde{\sigma} = K_0\sigma$, as a function of incidence angle ($\tilde{f}_0 = \tau = 0.1$, $\tilde{l}_c$ = 2)

Figure 17(b) shows that increasing rms height results in larger coherent flux damping. Damping is minimized near the critical angle. Figure 17(c) shows that increasing rms height results in more production of incoherent flux with a significant rate of production near the critical angle. Note that both coherent and incoherent fluxes vary with $\tilde{\sigma}^2$. The overall trend shows that larger portion of coherent flux is transferred to incoherent flux with increasing roughness of the flame surface. Note in (a) that the total net energy flux has a peak near the critical angle because coherent flux only has a slight damping while incoherent flux is amplified significantly near the critical angle.

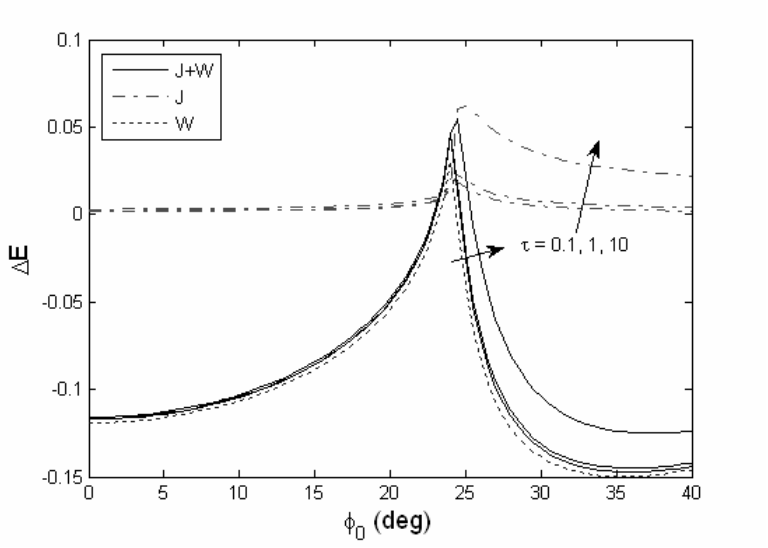

Figure 18 The effects of jump and wrinkling upon net energy flux as a function of incident angle for various τ. ($\tilde{f}_0$ = 0.1, $\tilde{\sigma}$ = 0.3, $\tilde{l}_c$ = 2)

Figure 18 shows the effects of jump (unsteady heat release) and wrinkling (unsteady motion) upon total net energy flux for various τ. For small values of τ (= 0.1, 1), total net energy flux is primarily due to wrinkling effects while the jump effect has a negligible contribution. For a large value of τ (=10), however, the jump effect becomes more significant. This is because a smaller τ (:= t_r / t_c ; the ratio of reference chemical time

to correlation time) can be regarded as smaller chemical time, which implies less interaction of flames with acoustic fields, leading to smaller unsteady heat release. Actually Eq. (5.3) states that β, which controls the jump effect, varies linearly with $\tau \tilde{f}_0 (= \tau \tilde{\omega}_0 / (2\pi))$ and, therefore, a smaller τ yields a smaller β. Note in Figure 18 that the jump effect causes energy amplification while wrinkling effect causes energy damping except for near-critical angle. Figure 19 shows how $\tilde{f}_0 (= f_0 t_c)$ affects the total energy flux and respective contribution of coherent and incoherent flux as a function of incidence angle. Figure 19(a) shows reflected /transmitted energy fluxes with and without unsteady (jump and wrinkling) effects for various $\tilde{f}_0$. For the smallest value of $\tilde{f}_0$ (= 0.1), reflected /transmitted energy fluxes are damped compared to the case without jump and wrinkling (solid line). Supercritical transmission is an exception, as it is amplified due to production of incoherent flux and zero-coherent flux as explained for Figure 16(c). For $\tilde{f}_0$=1, energy fluxes do not change significantly from no jump and wrinkling case. For the largest value of $\tilde{f}_0$ (= 10), reflected /transmitted energy fluxes deviate significantly from no jump and wrinkling case for subcritical angle only. The total net energy flux, however, is not significant, as shown in Figure 19(b), because reflected /transmitted energy fluxes cancel. Figure 19(b) shows that, for $\tilde{f}_0$ = 0.1, the total net energy flux is amplified only near the critical angle and its damping increases as the incidence angle deviates further from the critical angle. For $\tilde{f}_0$ = 1, both coherent flux damping and incoherent flux production become smaller and more symmetric, making the resultant total net energy flux negligibly small, except for near-critical angles. The case of a larger value of $\tilde{f}_0$ (= 10) is similar to the case of $\tilde{f}_0$ = 1, except that both

coherent and incoherent fluxes have little dependence upon incidence angle. Figure 19(c) shows, however, that the respective contribution from reflection and transmission for $\tilde{f}_0$= 1 has quite a different trend from the case of $\tilde{f}_0$= 10, whose reflected coherent flux is significantly amplified almost as much as the transmitted coherent flux is damped, for subcritical angles, These nearly cancel to yield only a small net energy flux, as shown in (b).

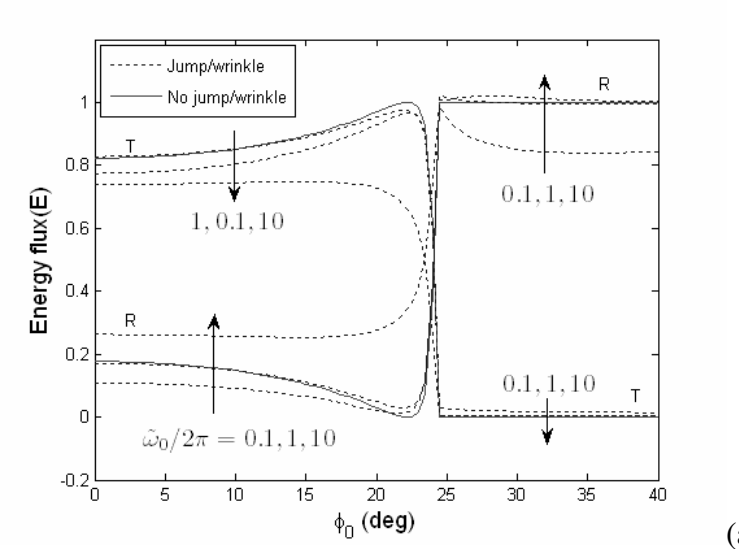

(a)

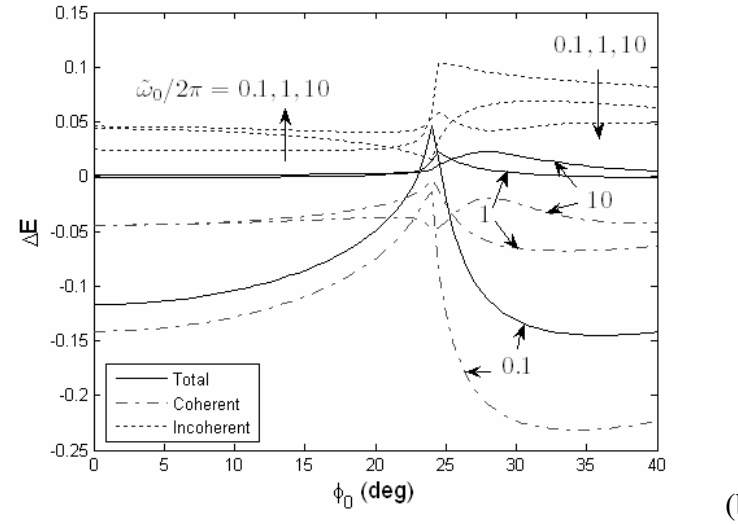

(b)

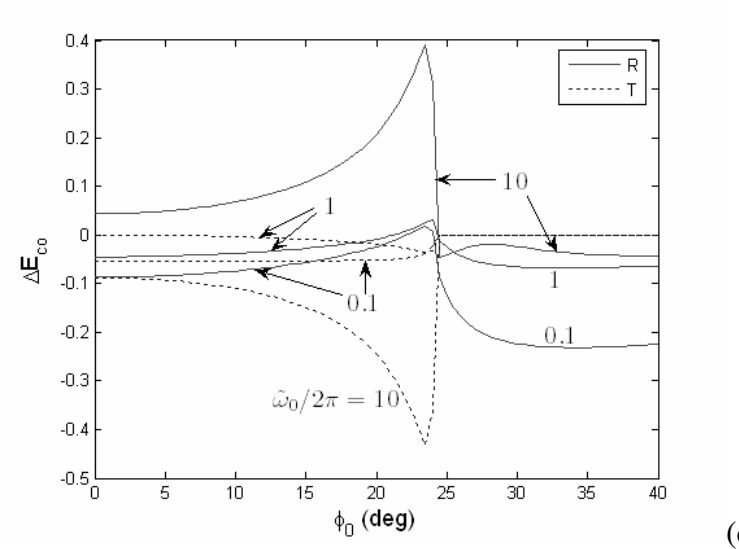

(c)

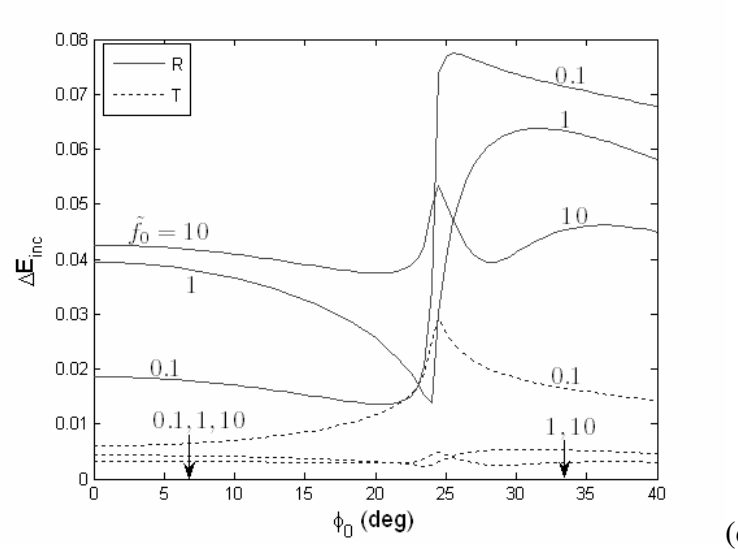

(d)

Figure 19 Dependence of net coherent /incoherent energy flux upon incidence angle for various $\tilde{f}_0$ (τ=1, $\tilde{\sigma}$ = 0.3, $\tilde{l}_c$ = 2)

Figure 19(d) shows incoherent flux for reflection and transmission fields. Incoherent flux increases more for the reflection field than for the transmission field, and more for a smaller value of $\tilde{f}_0$(= 0.1) than for larger values of $\tilde{f}_0$(= 1, 10), except for reflection field with subcritical angles. More production of incoherent flux at a smaller value of $\tilde{f}_0$ may be attributed to relatively larger values of the flame's characteristic

frequency, $f_c (\coloneqq 1/t_c)$, compared to the incident wave frequency, f_0 (note that $\tilde{f}_0 = f_0 t_c = f_0 / f_c$). This leads to larger flame surface oscillations, which enhance unsteady wrinkling and incoherent flux. Moreover, smaller values of $\tilde{f}_0$ yield a smaller value of $\tilde{\beta}(\tilde{\omega}_0)$ for a given τ, see Eq. (5.3), which results in smaller velocity jump. This dominance of the wrinkling effect to the jump effect at a smaller value of $\tilde{f}_0$ is more clearly illustrated in Figure 20(a), which shows that energy is significantly damped by the wrinkling effect for $\tilde{f}_0$= 0.1, while larger values $\tilde{f}_0$ have just slight effects on the net energy flux. Coherent and incoherent fluxes, as shown in Figure 20(b) and (c), respectively, are also attributed much more to the wrinkling than the jump effect, especially for smaller value of $\tilde{f}_0$. For a larger value of $\tilde{f}_0$(= 10), however, the jump effect becomes comparable to the wrinkling effect.

Figure 21 shows how the net energy flux varies with flame's rms height. This plot uses different values of $\tilde{f}_0$ and τ from Figure 17. What is to be noted in comparison with Figure 17 is that the rms height has little effect upon the total net energy flux, as shown in Figure 21(a). This is due to a large value of $\tilde{f}_0$(= 10) which makes the jump effect comparable to the wrinkling effect. Recall from the comment about Figure 20 that jump and wrinkling effects are comparable for larger $\tilde{f}_0$ values.

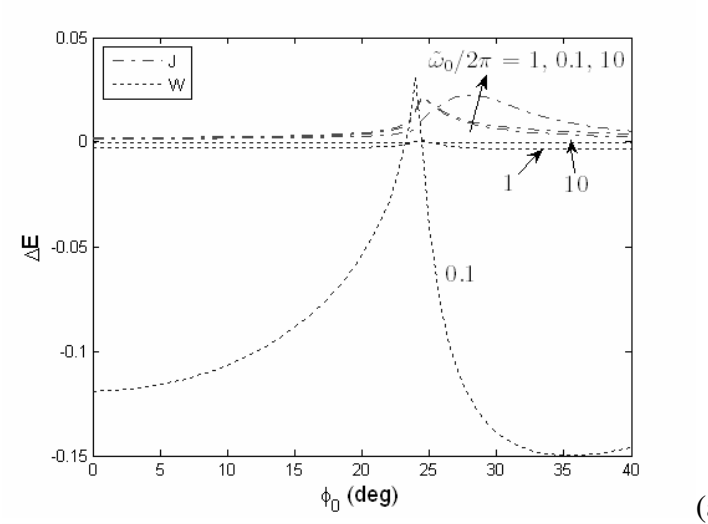

(a)

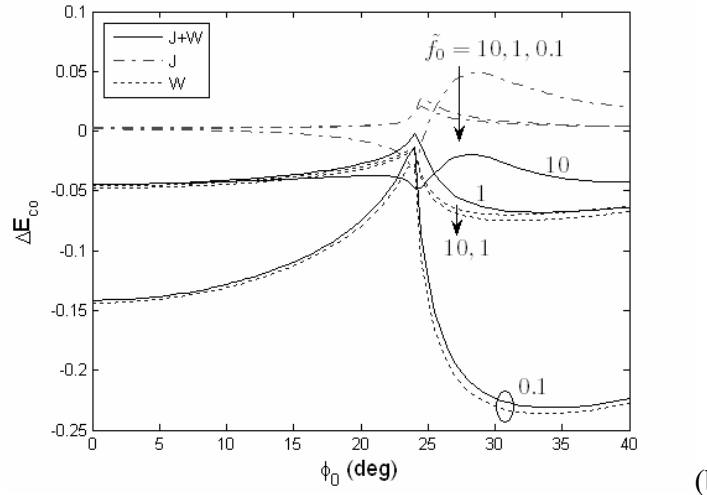

(b)

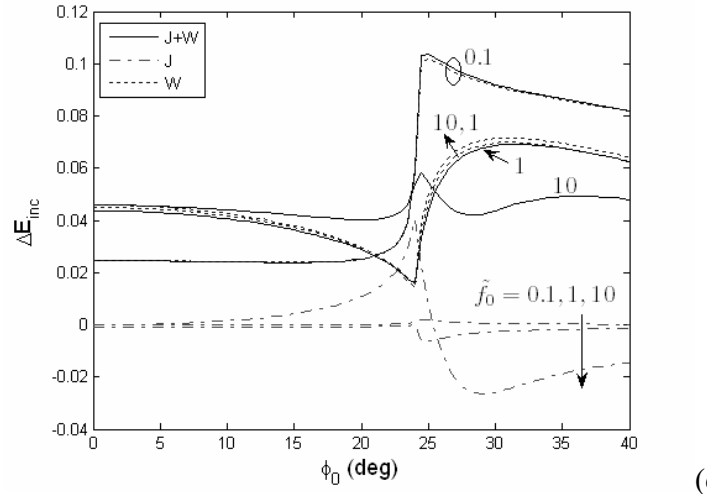

(c)

Figure 20 The effects of jump and wrinkling upon net energy flux as a function of incident angle for various $\tilde{f}_0$ (τ= 1, $\tilde{\sigma}$ = 0.3, $\tilde{l}_c$ = 2)

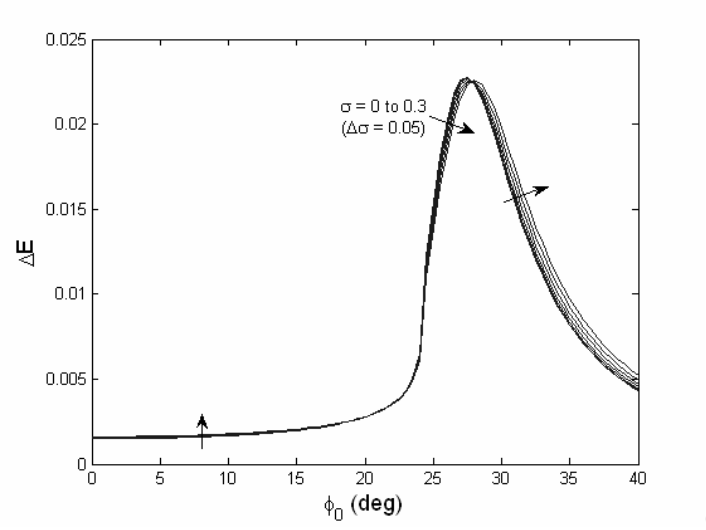

(a)

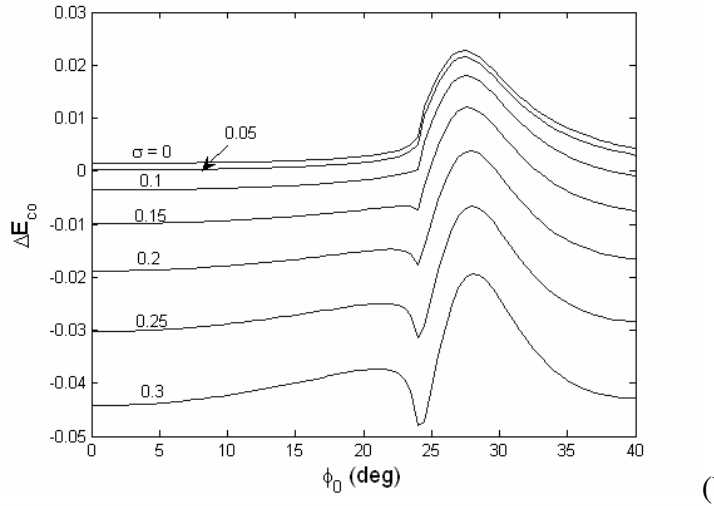

(b)

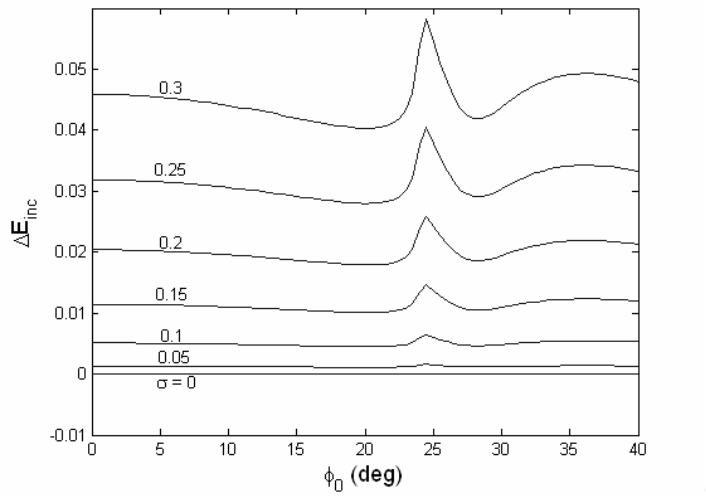

(c)

Figure 21 Dependence of net energy flux upon flame's rms height as a function of incidence angle ($\tilde{f}_0$=10, τ= 1, $\tilde{l}_c$= 2)

One should exercise caution in interpreting Figure 21(a), as the jump effect appears to be much more significant than the wrinkling effect, because of little variation of the total net energy with rms height. Figure 21(b) and (c), however, show that the effect of rms height upon coherent /incoherent fluxes is never less comparable than jump effect. Both coherent and incoherent fluxes depend largely upon rms height. Note that both fluxes vary with $\tilde{\sigma}^2$, as in Figure 17. However, the coherent flux is damped almost as much as the incoherent flux is amplified, which results in little variation in total net flux.

5.3 Dependence on two parameters

Figure 22 shows the variation of net energy flux with $\tilde{f}_0$ and τ for subcritical incidence angle. Total energy flux, as shown in (a), is damped by 10 % for $\tilde{f}_0 = 0.1$. Such damping results from coherent flux damping by 12 % and incoherent flux production by 2 %, as shown in (b) and (c). These net coherent /incoherent fluxes are due mostly to the wrinkling effect, not much to the jump effect, as shown in (d) and (e) for $\tilde{f}_0 = 0.1$. This follows from the same reasoning as made for Figure 20; i.e., a smaller value of $\tilde{f}_0$ not only yields higher oscillation of a flame surface ($f_c > f_0$) which enhances unsteady wrinkling effect, but it also yields a smaller value of β, leading to smaller jump effect. Note also in (a) that, for a smaller $\tilde{f}_0$ value, e.g., 0.1, the τ effect upon net energy flux is negligible because of a smaller $\tilde{f}_0\tau$ (τ only appears in β in form of $\tilde{f}_0\tau$.) For $\tilde{f}_0$ of O(1), the total net energy flux is very small, shown in (a), because coherent damping is almost as large as incoherent production, shown in (b) and (c). Incoherent energy production

increases slightly with $\tilde{f}_0$ for $\tilde{f}_0 \sim O(1)$, as shown in (c), and increases more rapidly and saturates for larger values of $\tilde{f}_0$ and τ. It may be noteworthy to compare this calculated incoherent energy with experimental data reported by Lieuwen et al.[65], as shown in Figure 23 and Figure 24. They performed measurements of acoustic wave scattering from a rim-stabilized turbulent premixed flame. Figure 23 shows the PSD of the sidebands of the scattered acoustic fields, where the sidebands broaden with driving (incident) frequency, f_{drive}. The generation of sidebands is attributable to Doppler frequency shift due to random oscillation of turbulent flame surface, which is characterized by broadband spectrum. Figure 24 shows the dependence of incoherent scattered power upon incident frequency. The incoherent scattered power was determined by calculating the area under the PSD in the relevant spectral region from Figure 23. The incoherent scattered power increases and saturates with driving frequency, which displays a similar pattern to the incoherent energy in Figure 22(c), even though this experimental data was measured at rather higher frequency range which is beyond the applicable regime of the present analysis. Note in (d) and (e) that jump effects on coherent and incoherent fluxes become significant for $\tilde{f}_0 > 1$, even though they almost cancel for $\tilde{f}_0 < 4$. For a larger value of $\tilde{f}_0 > 4$, however, the net coherent flux due to the jump effect, as in (d), starts to increase significantly, which results in amplification in total net energy flux for larger value of τ (> 4), as in (a). Local minimization of net coherent flux along a curve of $\tilde{f}_0 \tau \sim 40$, as in (b), is attributed mainly to the jump effect, as in (d).

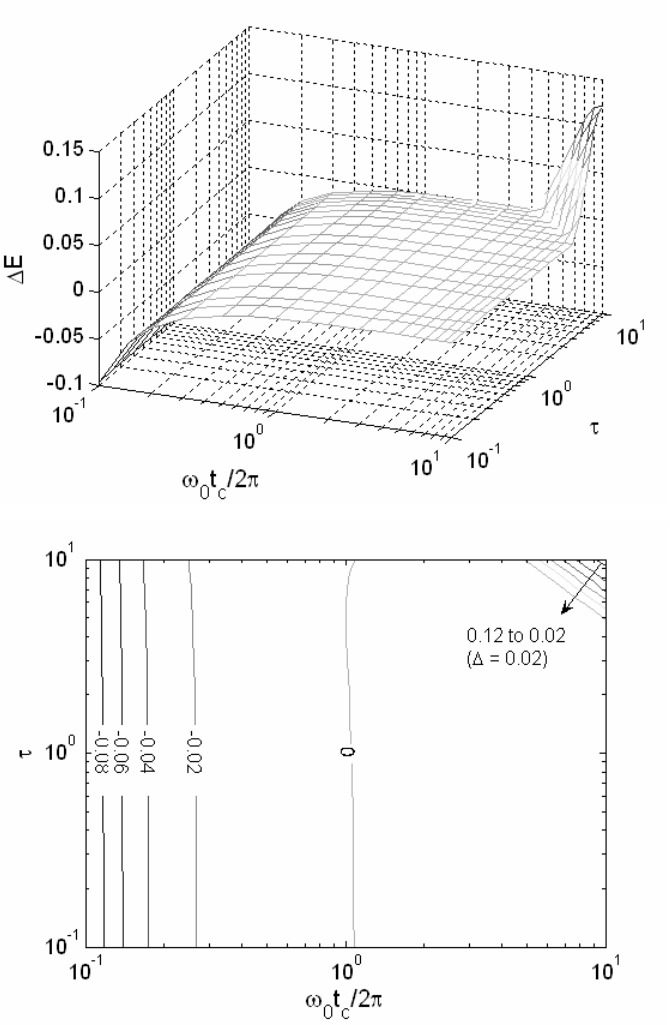

(a) Total net energy flux

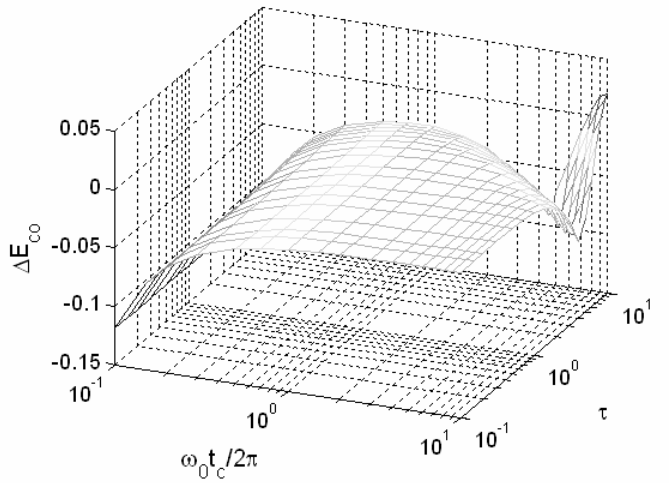

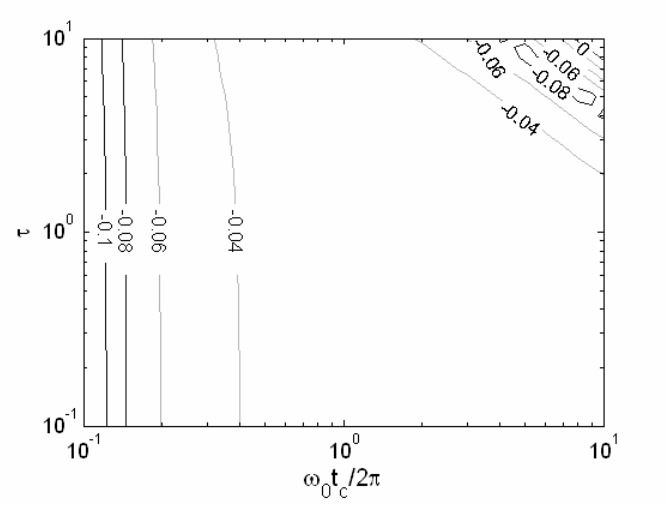

(b) Coherent energy flux

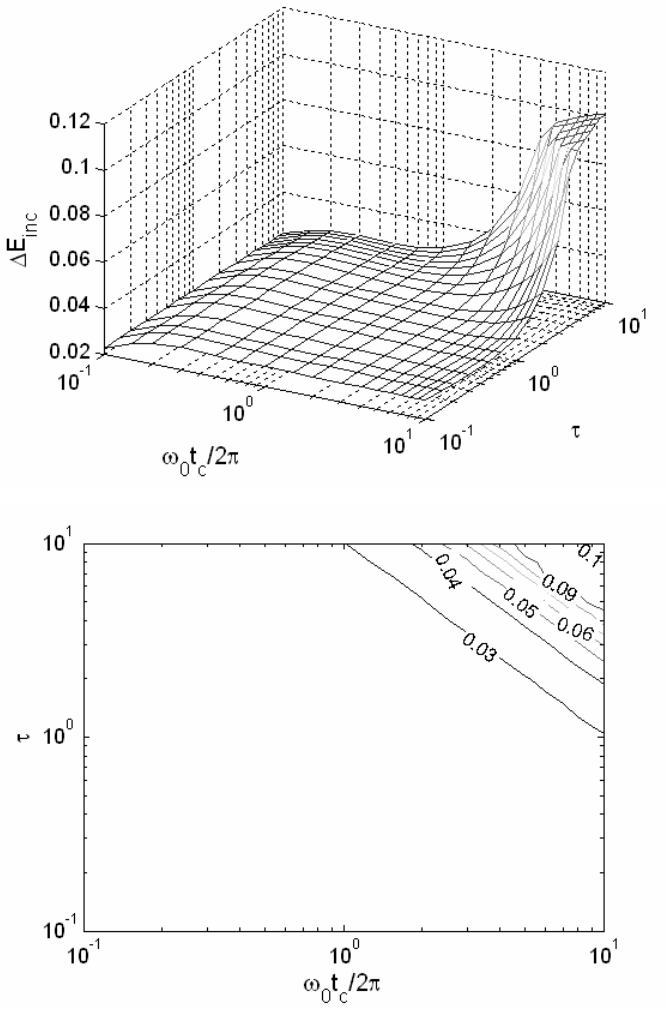

(c) Incoherent energy flux

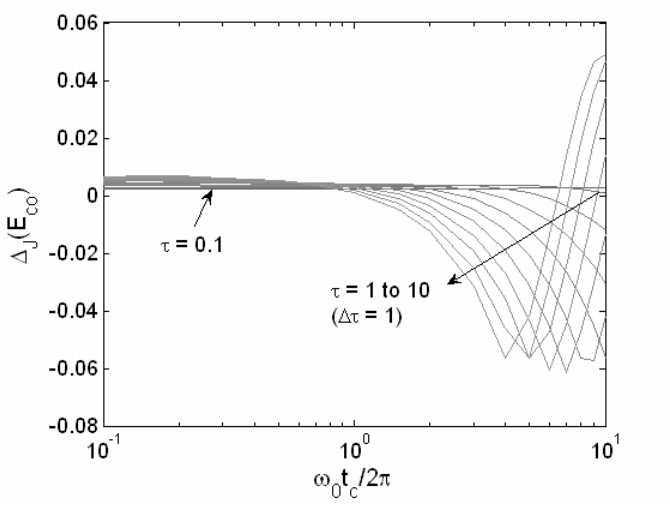

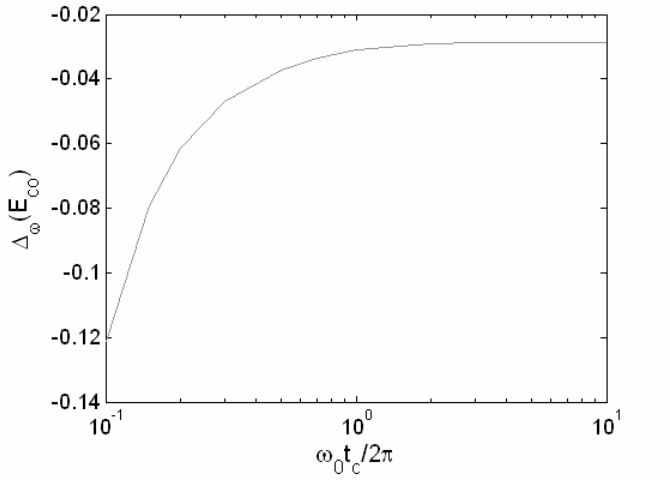

(d) Coherent energy flux (jump + wrinkling)

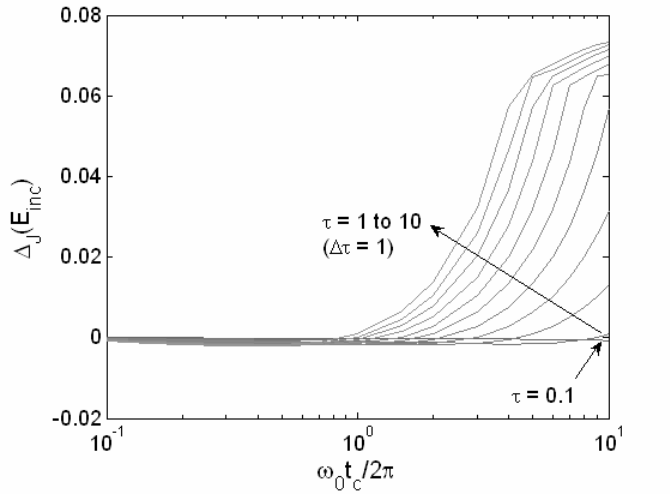

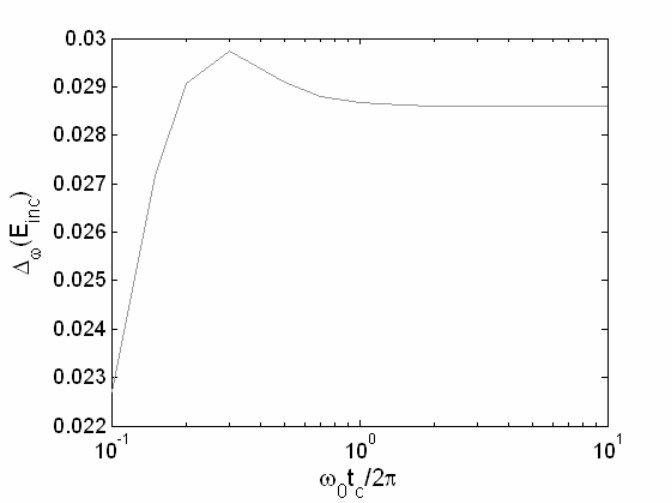

(e) Incoherent energy flux (jump + wrinkling)

Figure 22 Dependence of net energy flux upon $\tilde{f}_0$ and τ. ($\tilde{\sigma}$=0.3, $\tilde{l}_c$=1.5, ϕ_0=10 deg)

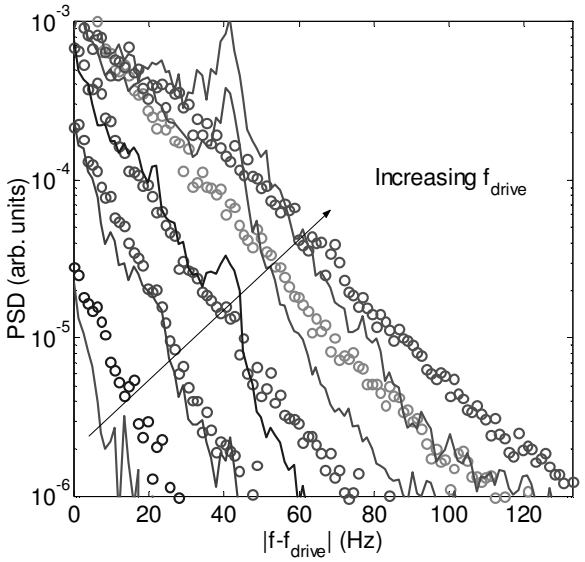

Figure 23 Characteristics of high (solid line) and low (symbol) frequency spectral sidebands at driving frequencies of f_{drive} = 5, 7.5, 10, 12.5, and 15 kHz and ϕ = 0.79. (courtesy of Lieuwen *et al*.[65])

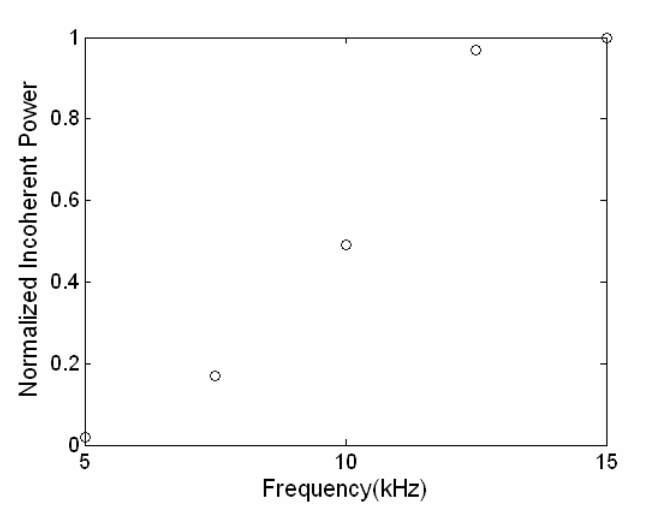

Figure 24 Dependence of power, normalized by value at f_{drive} = 15 kHz, in incoherent spectral sidebands upon driving frequency (ϕ = 0.93) (courtesy of Lieuwen *et al*.[65])

Figure 25 plots the variation of net energy flux with $\tilde{f}_0$ and τ for a supercritical incidence angle, 30 deg. Total net energy flux, as shown in (a), has a similar trend to the subcritical case in Figure 22(a), with maximum damping of 12 % at $\tilde{f}_0$ = 0.1 and maximum amplification of 10 % at $\tilde{f}_0 = \tau$ = 10. Coherent flux also has similar trends to the subcritical case, as in Figure 22(b), except for a larger coherent damping of 21 %, which is almost twice as large as the subcritical case at $\tilde{f}_0$ = 0.1. This coherent damping is attributed primarily to wrinkling effects, as shown in (d) and (e). The incoherent flux, however, exhibits quite a different trend from the subcritical case in Figure 22(c), in that remarkable production of incoherent flux occurs at $\tilde{f}_0$ = 0.1 and $\tilde{f}_0\tau$ ~20. Such net incoherent flux at $\tilde{f}_0$ = 0.1 is due primarily to the wrinkling effect. This wrinkling effect greatly diminishes with increasing $\tilde{f}_0$, as shown in (e), because a smaller f_c and larger $\tilde{f}_0$ implies slower movement of flame front and, subsequently, diminishes the flame's

unsteady wrinkling effect. Large incoherent production along $\tilde{f}_0\tau$ ~20 is, however, due almost equally to jump and wrinkling effects, as shown in (e).

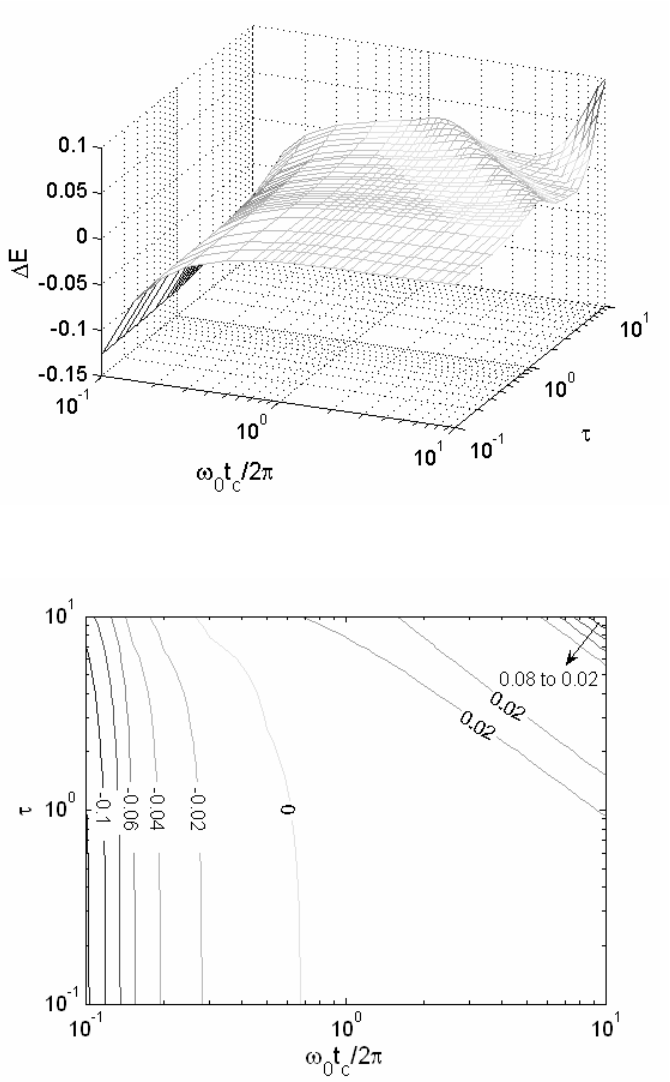

(a) Total net energy flux

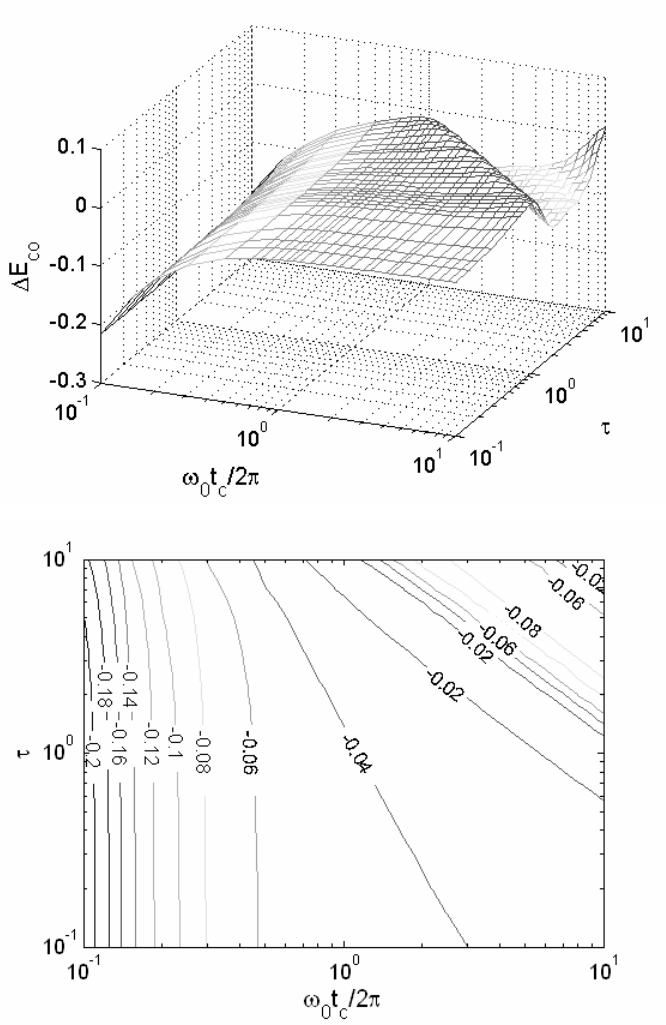

(b) Coherent energy flux

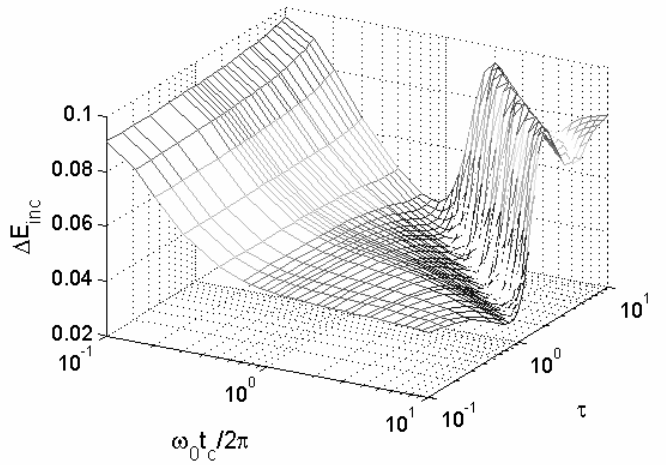

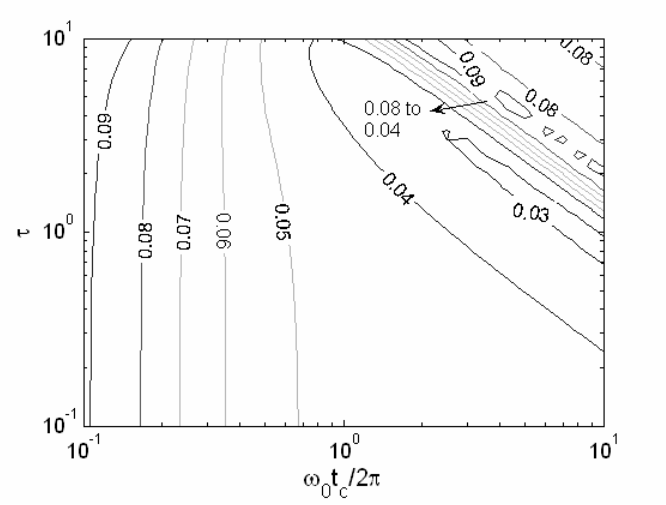

(c) Incoherent energy flux

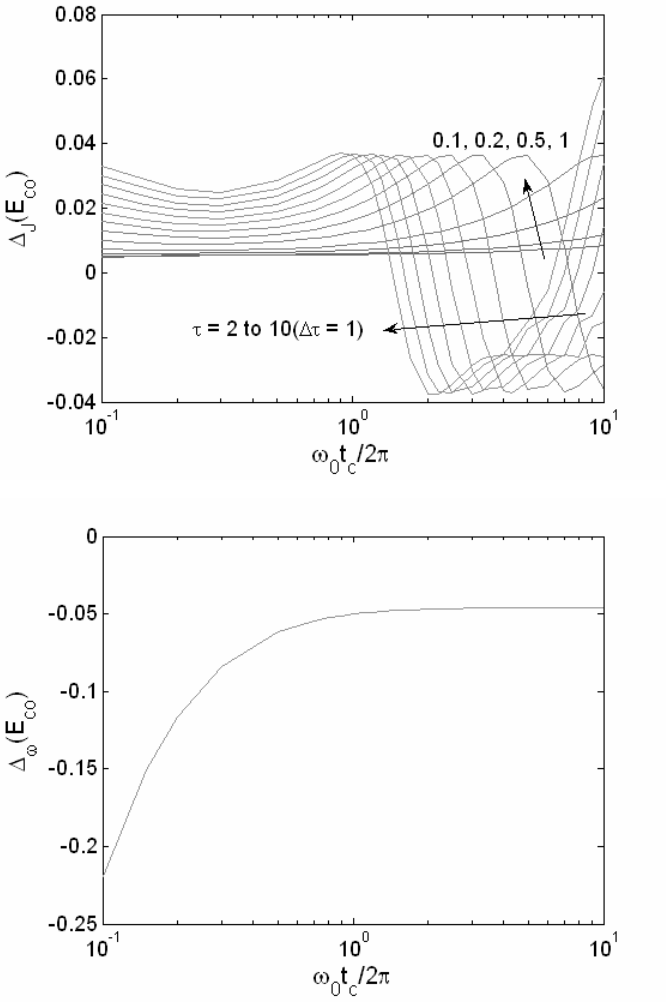

(d) Coherent energy flux (jump + wrinkling)

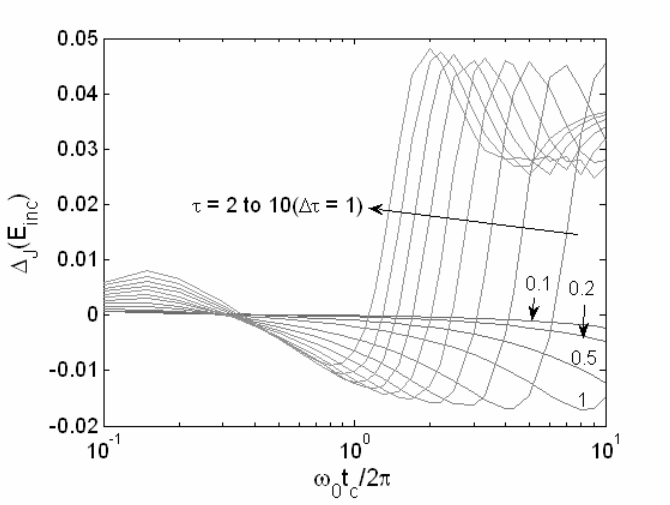

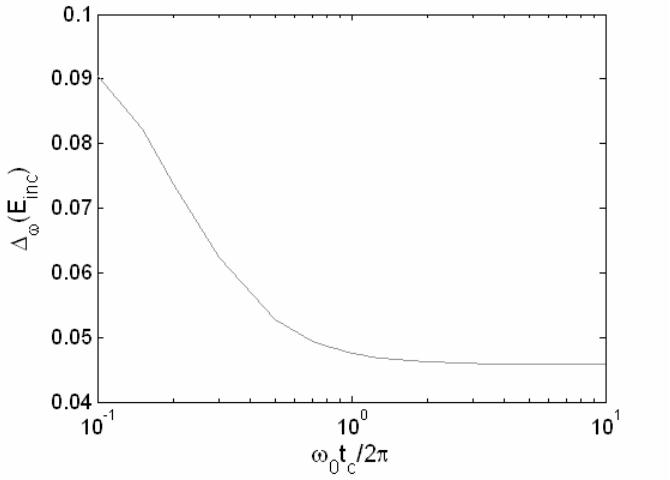

(e) Incoherent energy flux (jump + wrinkling)

Figure 25 Dependence of net energy flux upon $\tilde{f}_0 (= \omega_0 t_c/(2\pi))$ and τ ($\tilde{\sigma}$ = 0.3, $\tilde{l}_c$ =1.5, ϕ_0 =30 deg)

Figure 26 plots the variation of net energy flux with $\tilde{f}_0$ and τ for near-critical incidence angle (24°). Total energy flux, as shown in (a), is amplified for the entire range of $\tilde{f}_0$ (= $\omega_0 t_c/(2\pi)$) and τ. Note that (a) exhibits somewhat different trends from sub/supercritical cases in that noticeable total energy amplification is observed even at smaller values of $\tilde{f}_0$. This amplification results from production of incoherent flux, as

shown in (c), as coherent flux is damped slightly, as shown in (b). Such incoherent flux production is attributed primarily to wrinkling effects, not much to jump effects. The jump effect is less than 1 %, while the wrinkling effect is 7 %, see (e). Coherent energy is only slightly damped or amplified for $\tilde{f}_0\tau \leq 4$, as shown in (b), but it has a significant damping at $\tilde{f}_0\tau \sim 40$ due to the jump effect, as shown in (d), and recovers toward amplification for $\tilde{f}_0\tau > 40$.

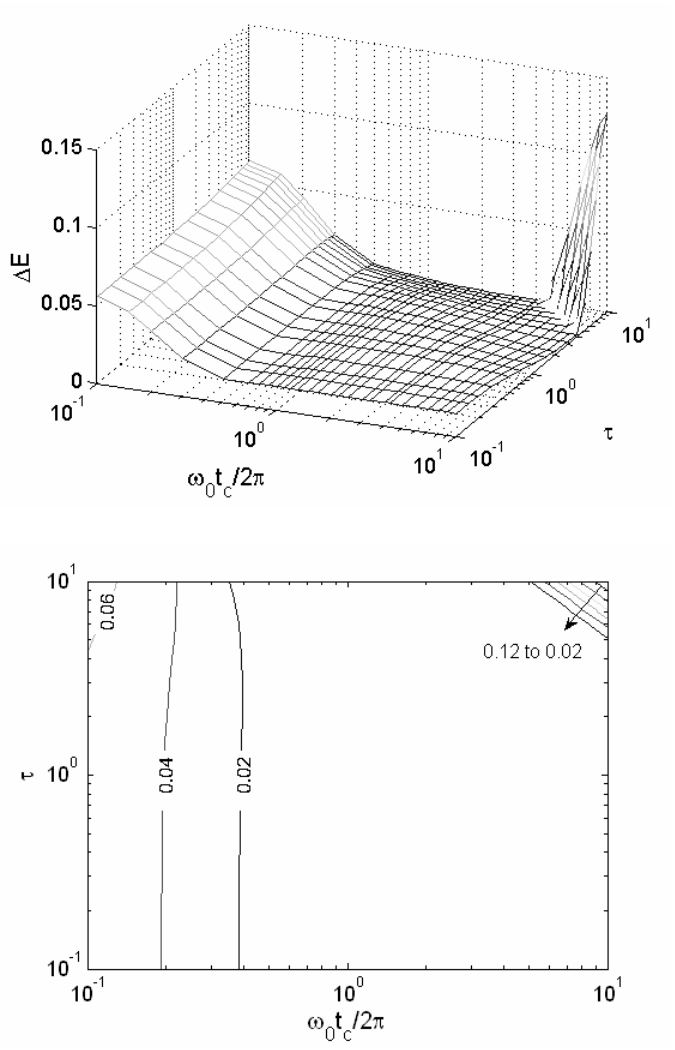

(a) Total net energy flux

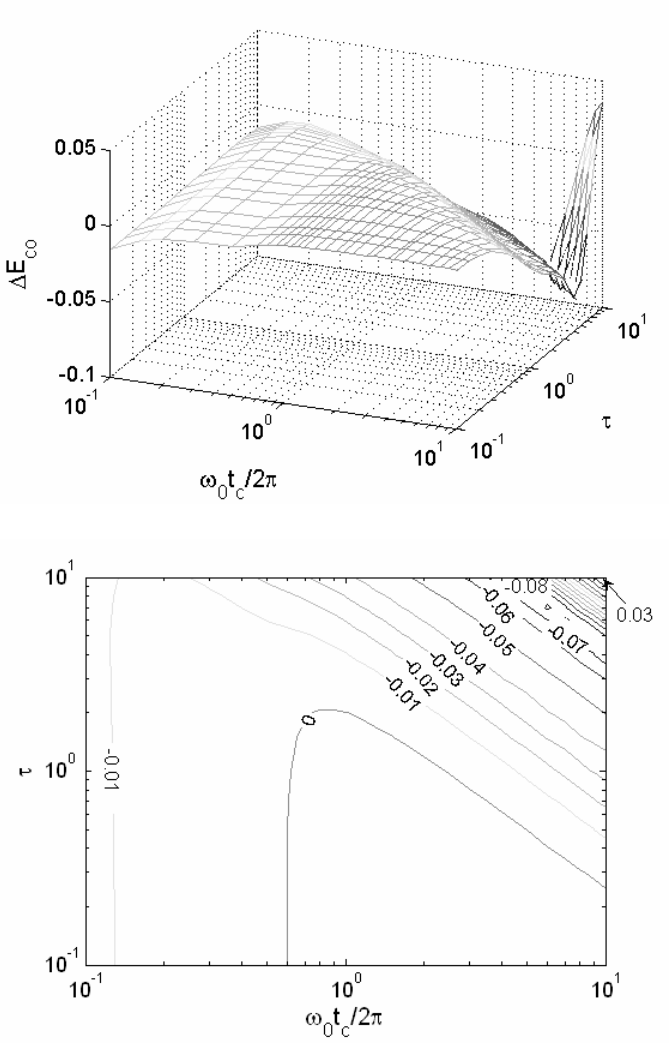

(b) Coherent energy flux

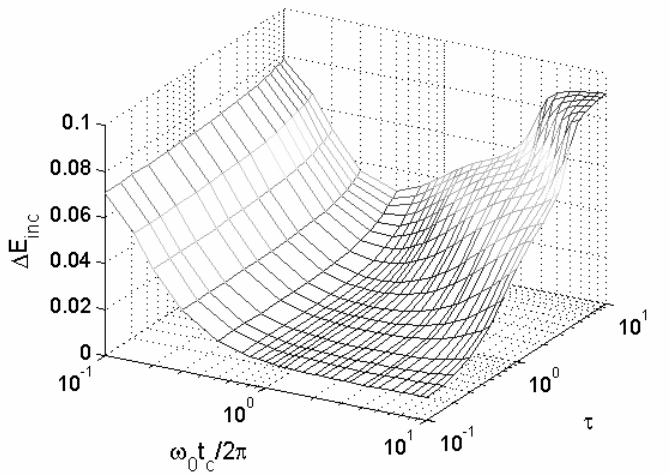

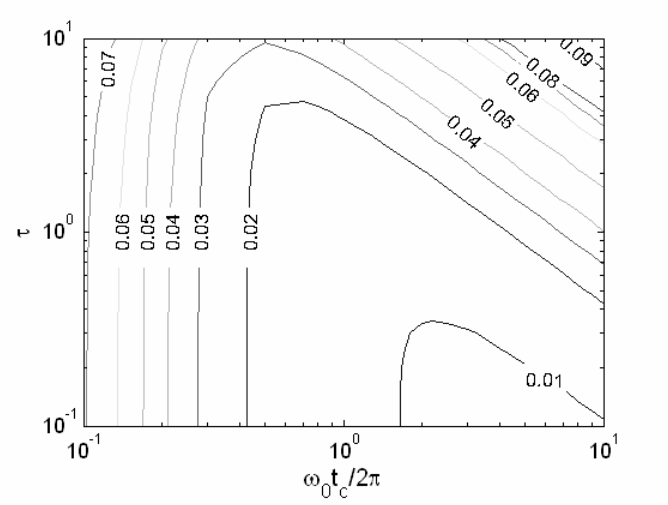

(c) Incoherent energy flux

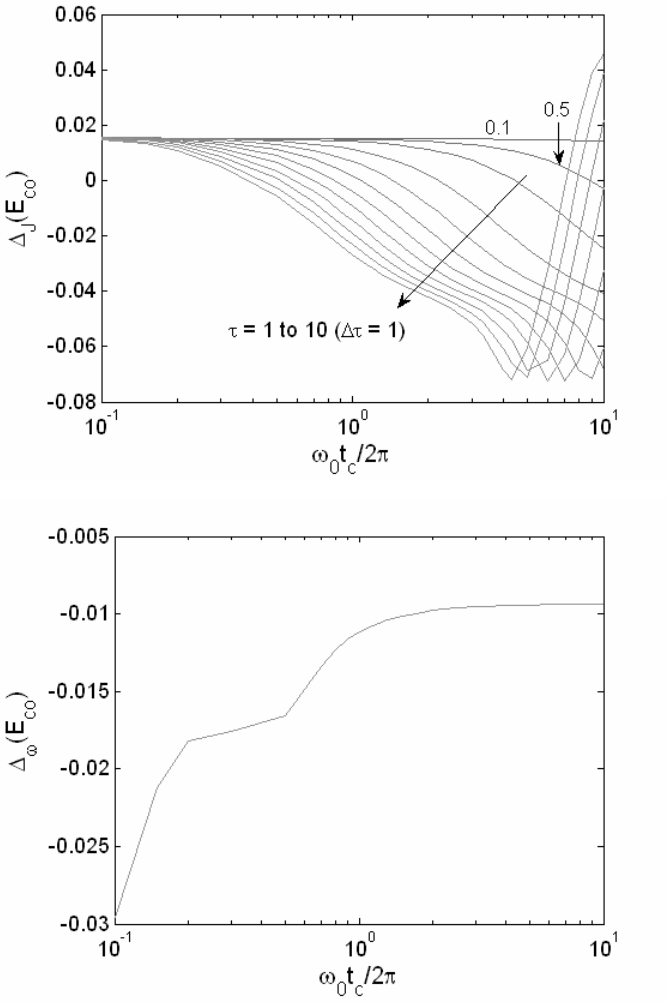

(d) Coherent energy flux (jump + wrinkling)

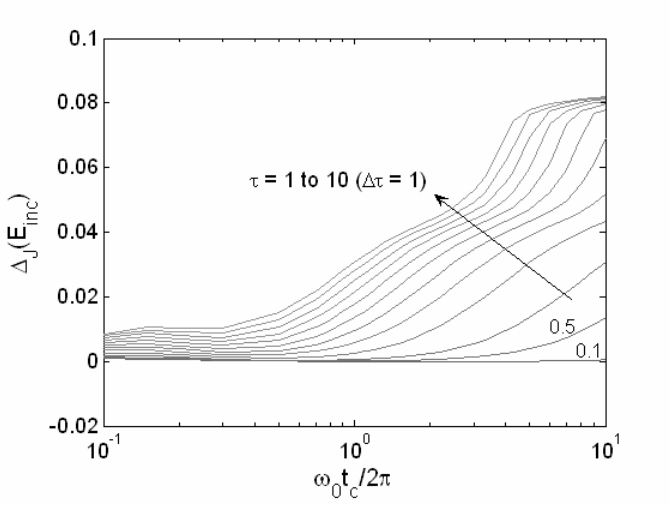

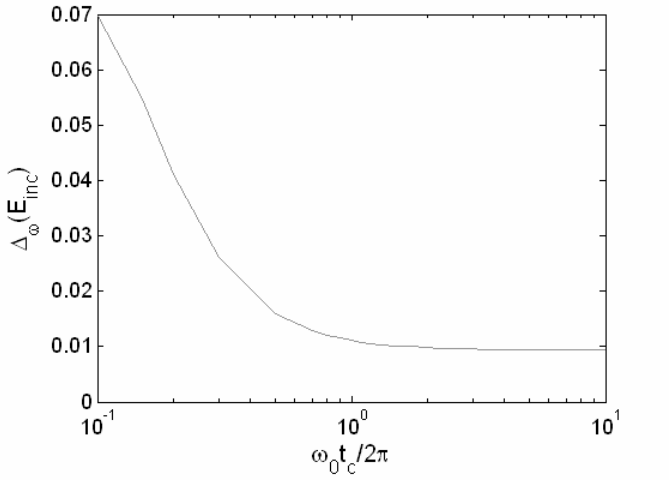

(e) Incoherent energy flux (jump + wrinkling)

Figure 26 Dependence of net energy flux upon $\tilde{f}_0$ and τ near the critical angle ($\tilde{\sigma}$ = 0.3, $\tilde{l}_c$ =1.5, ϕ_0 =24 deg)

Figure 27 shows the dependence of net energy flux upon $\tilde{l}_c$ and ϕ_0 for $\tilde{f}_0 = \tau =$ 0.1. Total energy flux, as shown in (a), is damped except for near-critical angle as explained for Figure 16. Figure 27(a) also shows that total net energy flux has little dependence upon $\tilde{l}_c$, as opposed to large dependencies upon the incidence angle. Coherent flux, as shown in (b), has a similar trend to the total energy flux, except that

coherent energy is damped for the entire range of $\tilde{l}_c$ and incidence angle, and most coherent damping occurs at supercritical angles, about 35°. Incoherent flux, as shown in (c), is always produced for the entire range of $\tilde{l}_c$ and incidence angle. The amount of incoherent production is nearly constant for sub- and supercritical angles, respectively, with a sudden jump across critical angle. Accordingly, more incoherent flux is produced for supercritical angles than for subcritical angles.

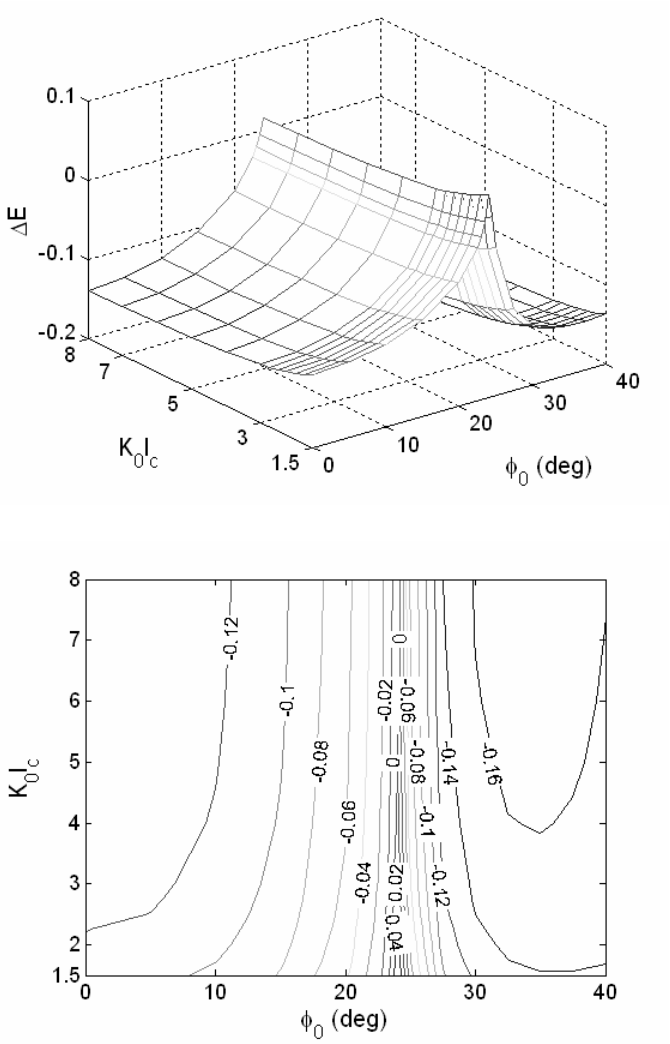

(a) Total net energy flux

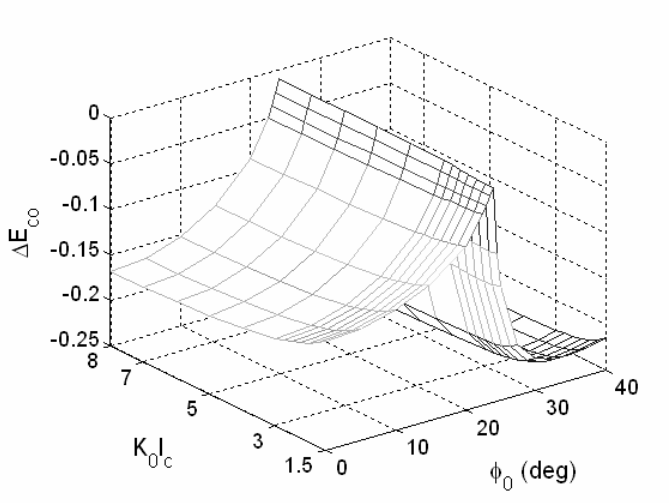

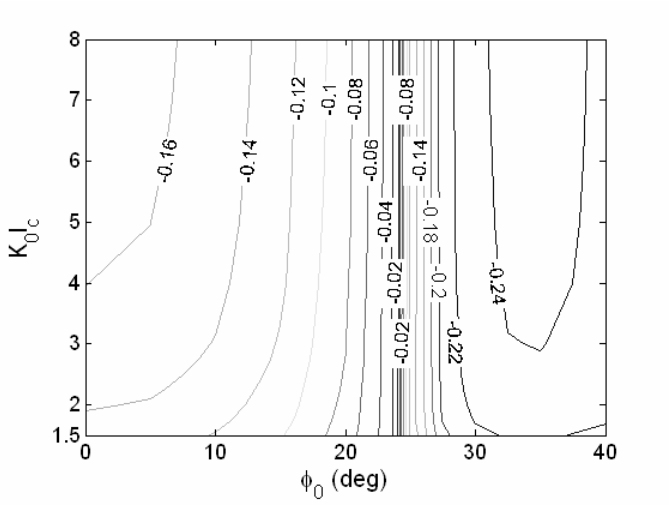

(b) Coherent energy flux

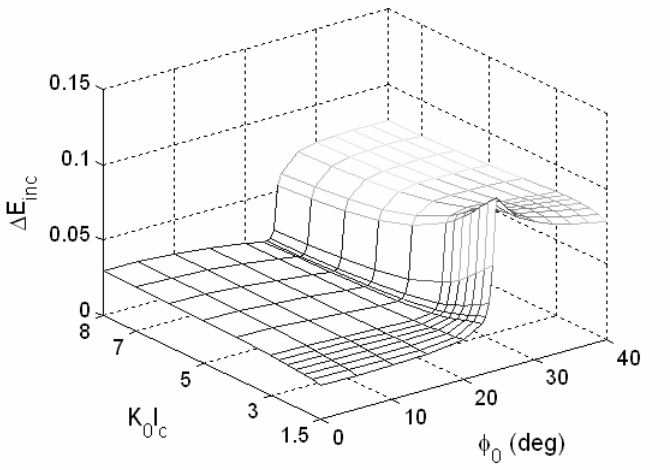

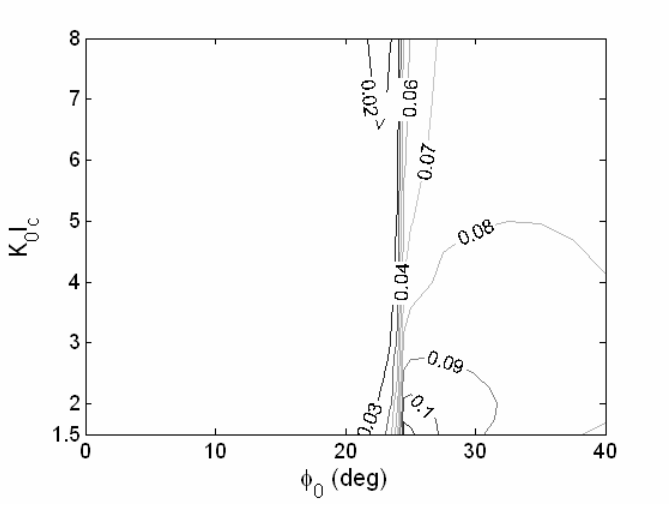

(c) Incoherent energy flux

Figure 27 Dependence of net energy flux upon $\tilde{l}_c$ and ϕ_0 ($\tilde{\sigma}$ = 0.3, $\tilde{f}_0$ = τ = 0.1)

Figure 28 shows the dependence of net energy flux upon $\tilde{l}_c$ and ϕ_0 for $\tilde{f}_0$=10 and τ = 0.1. Total energy flux, as shown in (a), is amplified in an entire range, which signifies the effect of $\tilde{f}_0$ in comparison with the case of $\tilde{f}_0$ = 0.1 in Figure 27, where total energy flux is damped over most of the range. Total net energy flux has little dependence upon $\tilde{l}_c$ and has maximum amplification by 2 % near critical angle. Coherent flux, as shown in (b), is damped for the entire range. Incoherent flux, as shown in (c), is produced almost as much as coherent flux is damped, which leads to only small amount of total net energy flux of about 2 %.

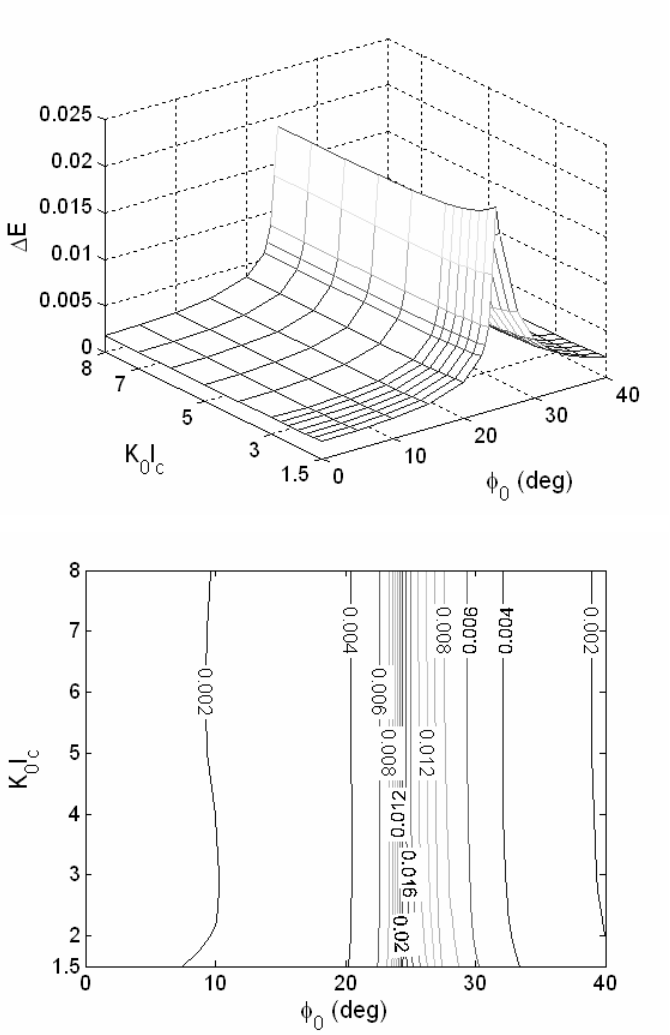

(a) Total energy flux

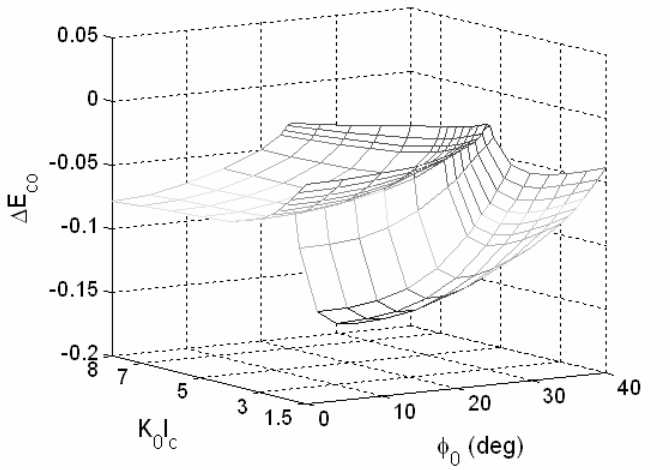

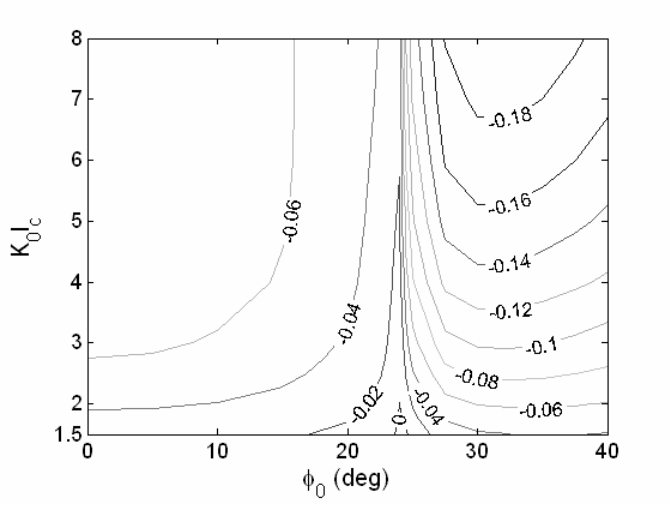

(b) Coherent energy flux

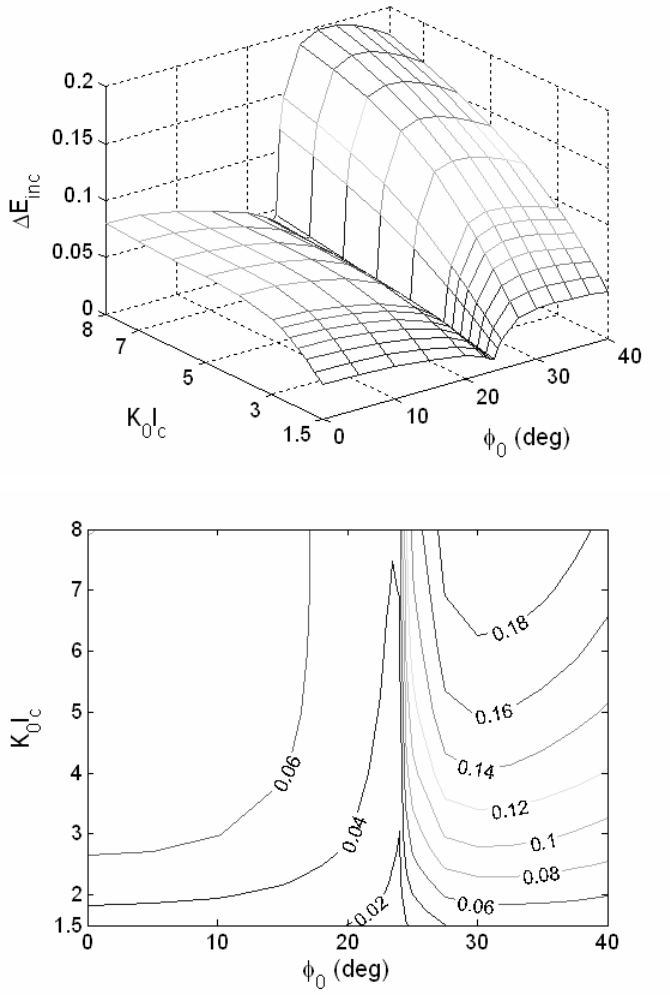

(c) Incoherent energy flux

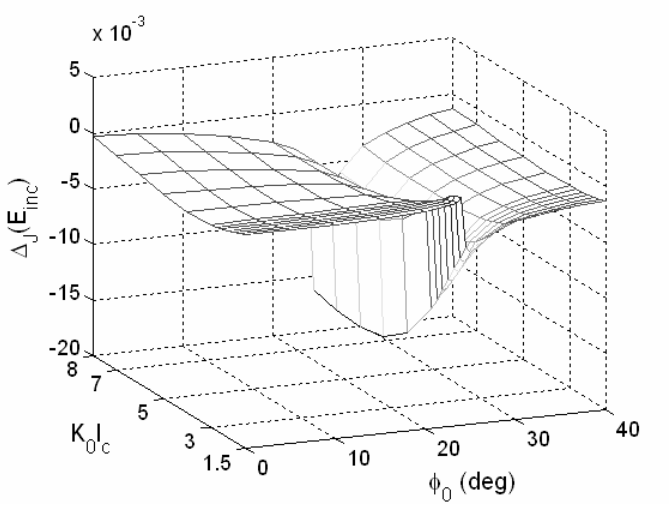

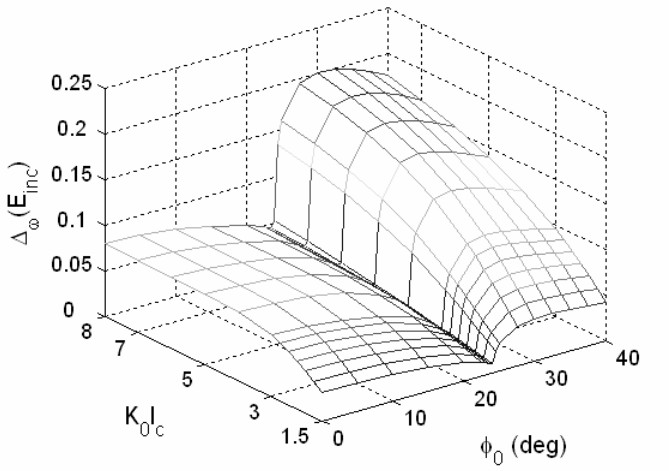

(d) Incoherent energy flux (jump + wrinkling)

Figure 28 Dependence of net energy flux upon $\tilde{l}_c$ and ϕ_0 ($\tilde{\sigma}$ = 0.3, $\tilde{f}_0$=10, τ = 0.1)

Note also in Figure 28(c) that incoherent flux increases more with increasing $\tilde{l}_c$, i.e., for a smoother surface. This appears to contradict the fact that a smoother surface produces less incoherent flux. (the jump effect has a very small contribution to the incoherent flux, as seen in (d), and is neglected here.) However, rms height $\tilde{\sigma}$ is still non-zero as 0.3, which implies that the surface is still in random motion and, hence, produces incoherent flux. A surface of the same rms height but of less wrinkle (larger correlation length) causes more correlated oscillation of wrinkled surface, which may

lead to more production of incoherent flux. Another way to explain this may be that smaller $\tilde{l}_c$ leads to more wrinkled surface which causes a more diffuse incoherent field. Such broader distributions of the incoherent field may induce more evanescent waves which make no contribution to net energy flux, as shown in Figure 29. The curves drawn are in the form of $\tilde{l}_c \exp[-(k\tilde{l}_c)^2/4]$ that appears in the expression of incoherent flux, e.g., in Eq. (4.82). The curve of $\tilde{l}_c = 4$ has a larger area, compared to the curve of $\tilde{l}_c = 1$, within the range of real q_k. (Note that this is only for demonstration of a simplified case, which may not be directly applied to Eq. (4.82) because of other factors like *C*'s and *I*'s in the integral.)

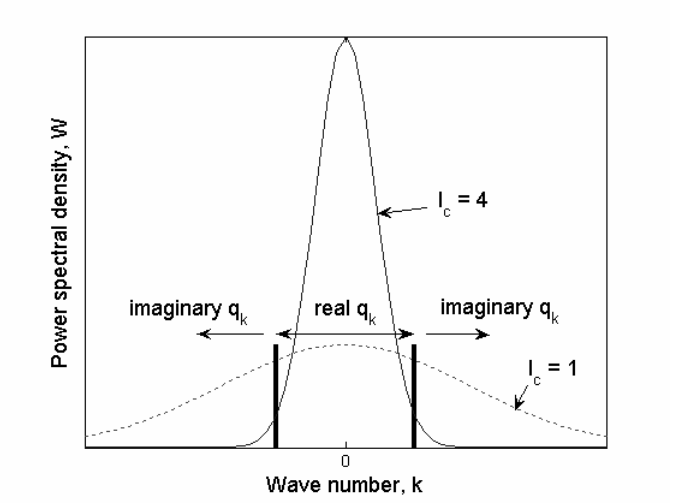

Figure 29 Illustration of the effect of $\tilde{l}_c$ upon power spectral density

Then, with increasing $\tilde{l}_c$ in Figure 28(d), does net incoherent flux increase indefinitely, or saturate to a certain limit, or vanish? The answer may be sought analytically in a simple case of a stationary wrinkled surface with normal incidence,

$\tilde{k}_0 = 0$. Substituting $\tilde{\beta} = 0$ and $\tilde{k}_0 = 0$ in Eq. (4.82) yields net incoherent reflection flux due to spatial wrinkling in the form

$$\begin{aligned}
\Delta_\omega(E_{R,inc})_{spatial} &= \iint\limits_{|\boldsymbol{k}|<\frac{\omega_0}{c_1}} \left|A(\boldsymbol{k},\boldsymbol{k_0},\omega_0,\omega_0)\right|^2 W(\boldsymbol{k}-\boldsymbol{k_0})d\boldsymbol{k} \\
&= \frac{2\tilde{\sigma}^2\tilde{l}_c^{\,2}}{\Lambda^{-1}(\Lambda^{-1/2}+1)^2}\int_0^1 k\,\tilde{C}_{20}(k,\tilde{\omega}_0)\Big|_{\tilde{\beta}=0}\,\mathrm{e}^{-(k\tilde{l}_c)^2/4}\,dk \qquad (5.6)\\
&= 2\tilde{\sigma}^2\tilde{l}_c^{\,2}(\Lambda^{-1/2}-1)^2\int_0^1 \frac{k(1-k^2)^{1/2}\,|\,\Lambda^{-1}-k^2\,|}{\left|\Lambda^{-1}(1-k^2)^{1/2}+(\Lambda^{-1}-k^2)^{1/2}\right|^2}\mathrm{e}^{-(k\tilde{l}_c)^2/4}\,dk
\end{aligned}$$

where terms including $\tilde{l}_c$ are $\tilde{l}_c^{\,2}$ and $\exp[-(k\tilde{l}_c)^2/4]$, whose product vanishes for a given k as $\tilde{l}_c \to \infty$. But the above equation is not such a case since k is an integral variable. Introducing a variable $u = (k\tilde{l}_c)^2$ leads Eq. (5.6) to the form

$$\begin{aligned}
&\Delta_\omega(E_{R,inc})_{spatial} \\
&= 2\tilde{\sigma}^2\tilde{l}_c^{\,2}(\Lambda^{-1/2}-1)^2\int_0^1 k\chi(k)\,\mathrm{e}^{-(k\tilde{l}_c)^2/4}\,dk = \tilde{\sigma}^2(\Lambda^{-1/2}-1)^2\int_0^{\tilde{l}_c^2}\chi(\tilde{l}_c^{-1}u^{1/2})\,\mathrm{e}^{-u/4}\,du \\
&\xrightarrow{\tilde{l}_c\to\infty} \tilde{\sigma}^2(\Lambda^{-1/2}-1)^2\int_0^\infty \chi(0)\,\mathrm{e}^{-u/4}\,du = 4\tilde{\sigma}^2(\Lambda^{-1/2}-1)^2(\Lambda^{-1/2}+1)^{-2} \qquad (5.7)\\
&= 4\tilde{\sigma}^2\left(\frac{\Lambda^{1/2}-1}{\Lambda^{1/2}+1}\right)^2
\end{aligned}$$

where $\chi(k) \equiv \dfrac{(1-k^2)^{1/2}\,|\,\Lambda^{-1}-k^2\,|}{\left|\Lambda^{-1}(1-k^2)^{1/2}+(\Lambda^{-1}-k^2)^{1/2}\right|^2}$

For instance, $\Delta_\omega(E_{R,inc})_{spatial} = 0.0636$ for $\Lambda = 6$ and $\tilde{\sigma} = 0.3$. Figure 30 shows a numerical result of net incoherent reflection flux due to spatial wrinkling from Eq. (4.82). The point 'X' denotes a limit value obtained from Eq. (5.7). Therefore net incoherent flux saturates

to a non-zero limit value with increasing $\tilde{l}_c$ for a given $\tilde{\sigma}$. In reality, however, there may be a certain dependence of $\tilde{\sigma}$ upon $\tilde{l}_c$ that alters the pattern of net incoherent flux.

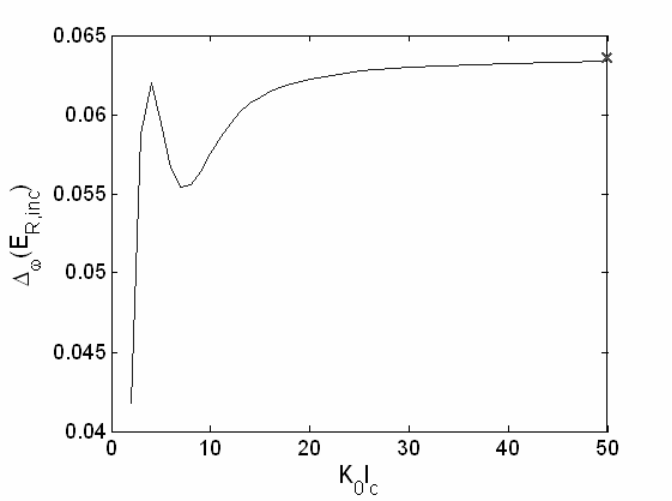

Figure 30 Variation of net incoherent reflection flux due to spatial wrinkling with $\tilde{l}_c$ (ϕ_0 = 0°, $\tilde{\sigma}$ = 0.3, $\tilde{\beta} = 0$)

Figure 31 shows the dependence of net energy flux upon $\tilde{l}_c$ and ϕ_0 for $\tilde{f}_0$ = 0.1, τ = 10. This figure is very similar to Figure 27 with $\tilde{f}_0$ = τ = 0.1, which implies that the effect of τ is negligible for small $\tilde{f}_0$.

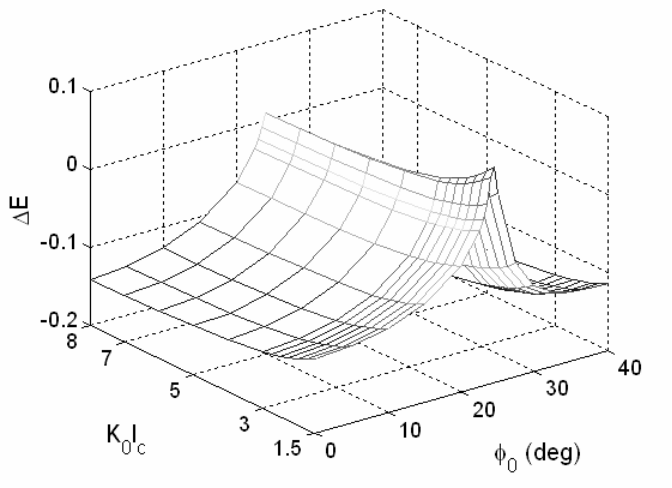

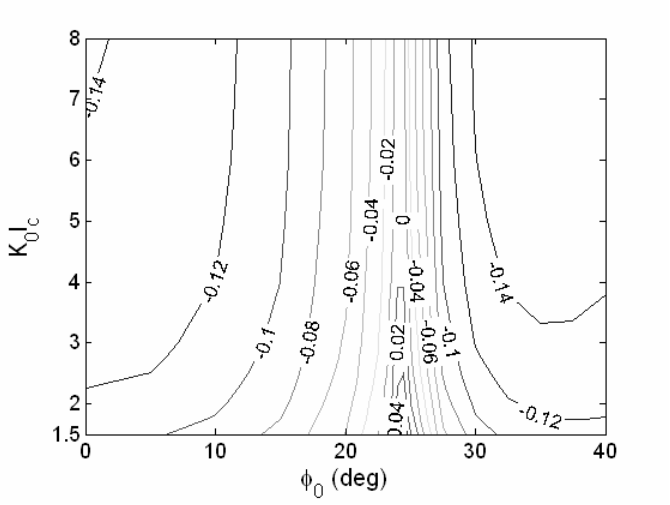

(a) Total energy flux

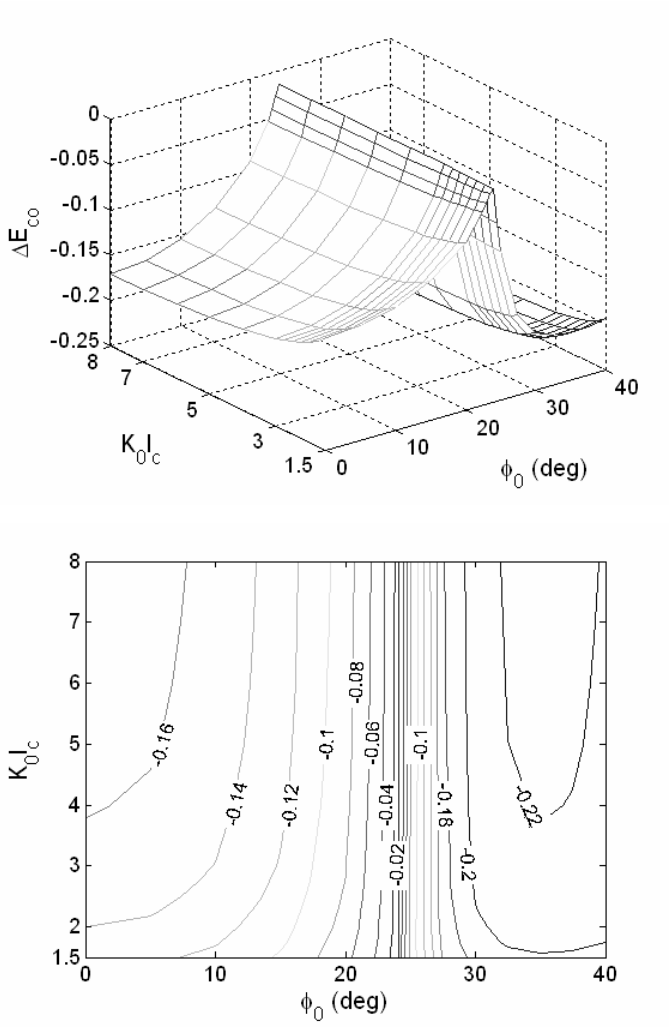

(b) Coherent energy flux

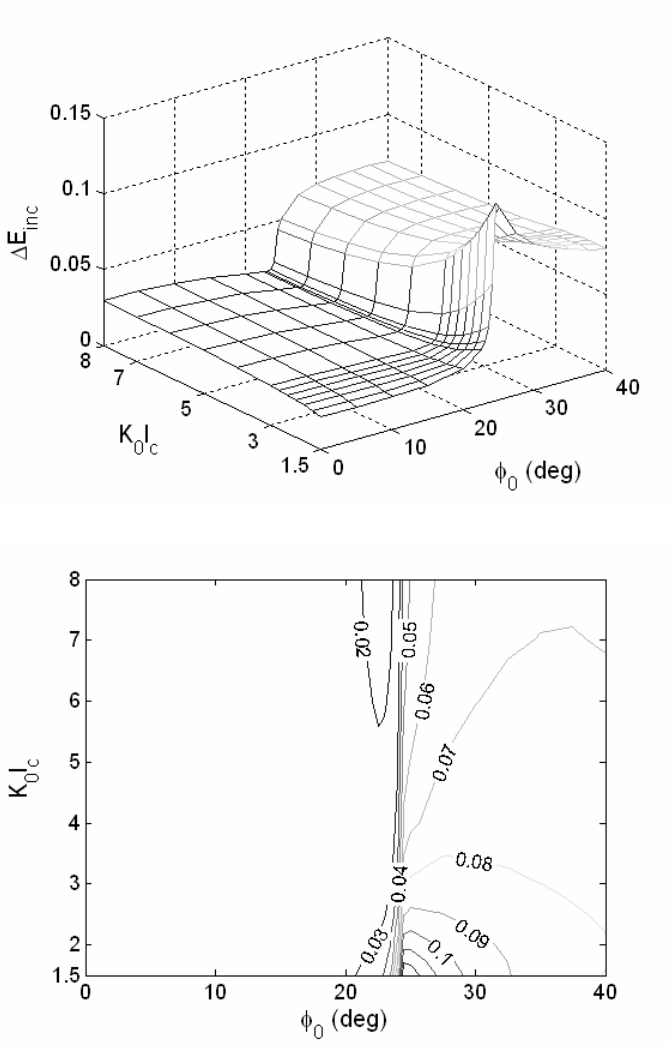

(c) Incoherent energy flux

Figure 31 Dependence of net energy flux upon $\tilde{l}_c$ and ϕ_0 ($\tilde{\sigma}$ = 0.3, $\tilde{f}_0$ = 0.1, τ = 10)

Figure 32 shows the dependence of the net energy flux upon $\tilde{l}_c$ and ϕ_0 for $\tilde{f}_0 = \tau$ = 10. This figure displays a different trend from previous cases, i.e., Figure 27, Figure 28, and Figure 31, in that the net energy flux has little dependence upon incidence angle, ϕ_0, and has significant dependence upon $\tilde{l}_c$. Figure 32(a) shows that total net energy flux is amplified in the entire range, as is the case for $\tilde{f}_0 = 10$, $\tau = 0.1$ in Figure 28. Total net

energy flux has maximum amplification of more than 10 % for smallest $\tilde{l}_c$ (= 1.5) and decreases dramatically with increasing $\tilde{l}_c$ to vanish for $\tilde{l}_c > 3$. Coherent flux, as shown in (b), is damped for nearly the entire range except for smallest value of $\tilde{l}_c$ (= 1.5) with little dependence upon ϕ_0. Coherent damping is enhanced with increasing $\tilde{l}_c$, as is the case for $\tilde{f}_0$=10 and τ = 0.1 in Figure 28. Incoherent flux, as shown in (c), is amplified for an entire range. Incoherent amplification is enhanced with increasing $\tilde{l}_c$ as much as coherent damping, which cancel to yield negligibly small amount of total net energy flux for $\tilde{l}_c > 3$.

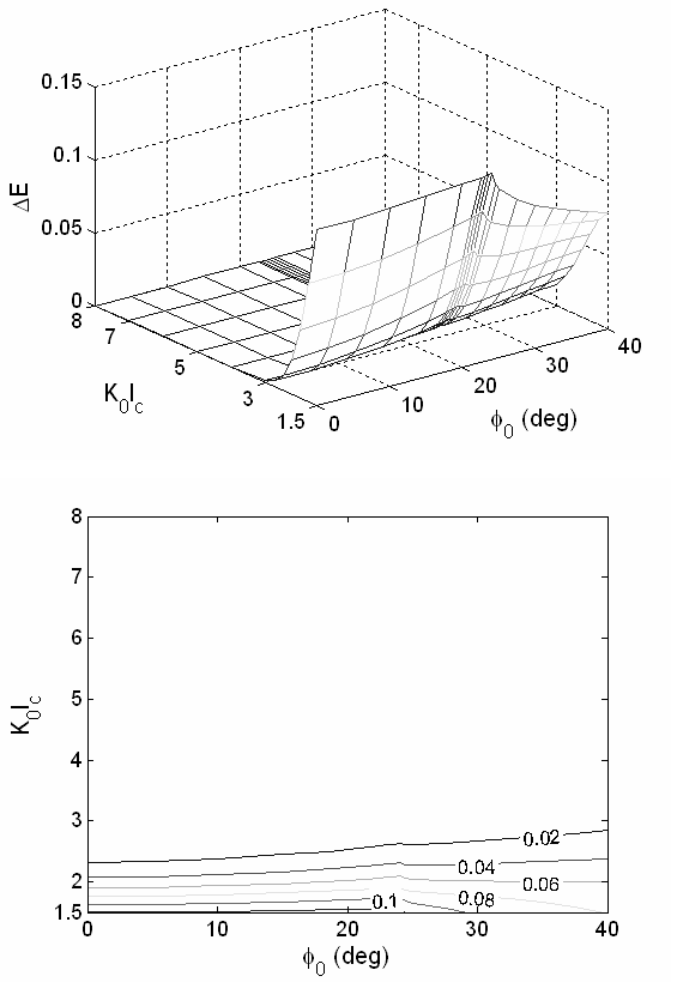

(a) Total energy flux

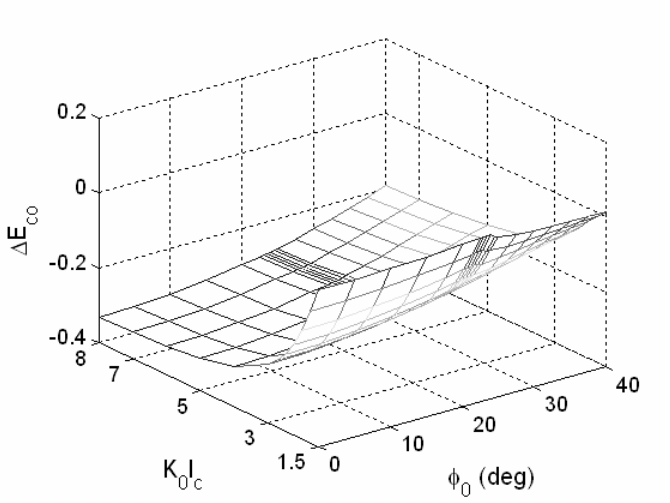

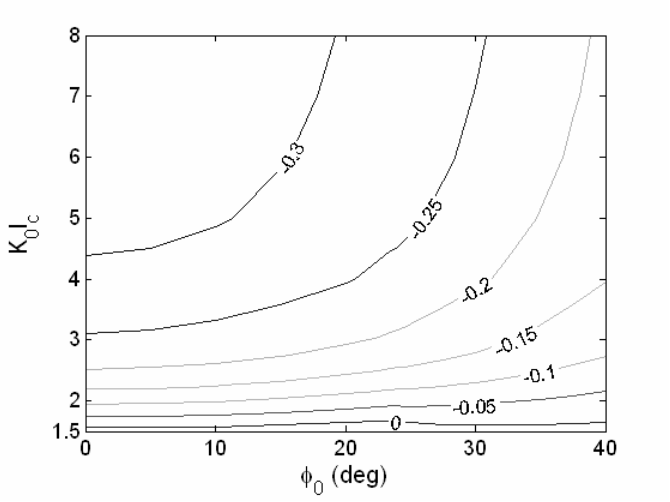

(b) Coherent energy flux

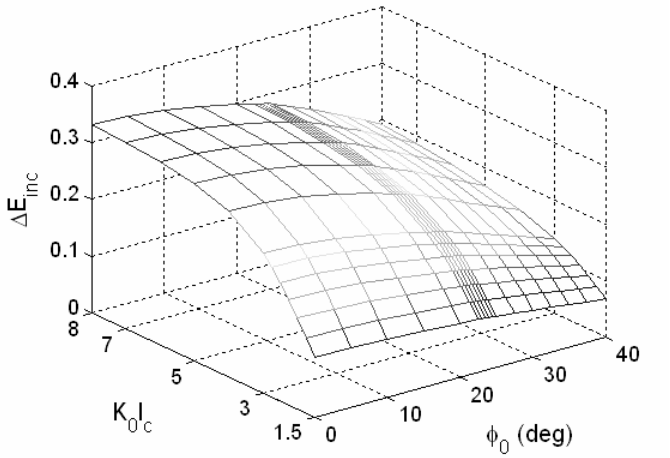

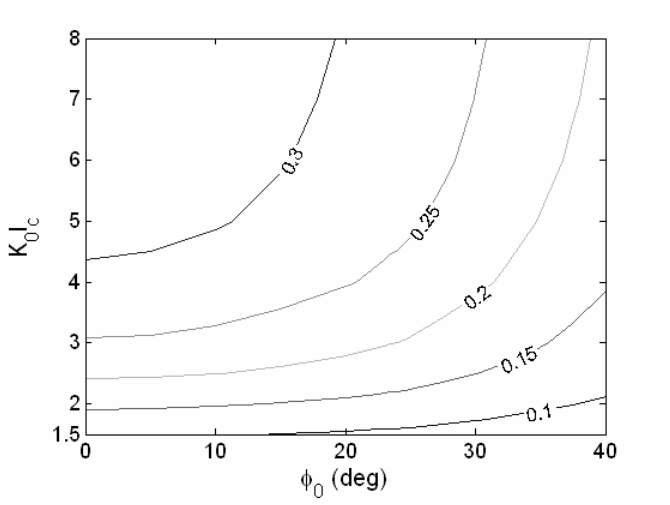

(c) Incoherent energy flux

Figure 32 Dependence of net energy flux upon $\tilde{l}_c$ and ϕ_0 ($\tilde{\sigma}$ = 0.3, $\tilde{f}_0 = \tau$ = 10)

Figure 33 illustrates correlation between net coherent and incoherent fluxes for various $\tilde{f}_0$ and τ. For subcritical angle (0, 10, 20^o) in (a), net coherent flux increases, i.e., coherent damping reduces, while net incoherent flux is nearly constant with increasing angle. However, for supercritical angle, net incoherent flux makes a jump from 2 % to 9 % when incidence angle goes beyond critical angle. (20 ^{o} → 30 ^{o}), see also Figure 27. Figure 33(c) shows a similar pattern to (a). The cases of $\tilde{f}_0$ = 10, as shown in (b) and (d) exhibit good correlation. (b), especially, shows a linear correlation with a slope of –1, which implies coherent damping goes directly to incoherent flux while total energy flux varies little, see also Figure 28 where net total energy flux is less than 1% except for near-critical angle. (d) shows almost linear correlation. Note that the lower right part of the curves has a slope of about –0.5 (> –1), which implies that total energy flux is damped with increasing $\tilde{l}_c$ because the rate of coherent damping is greater than that of incoherent amplification.

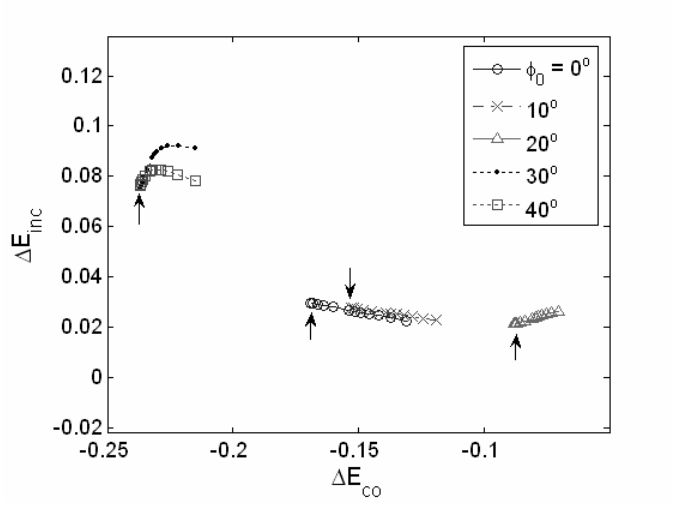

(a) $\tilde{f}_0 = \tau = 0.1$

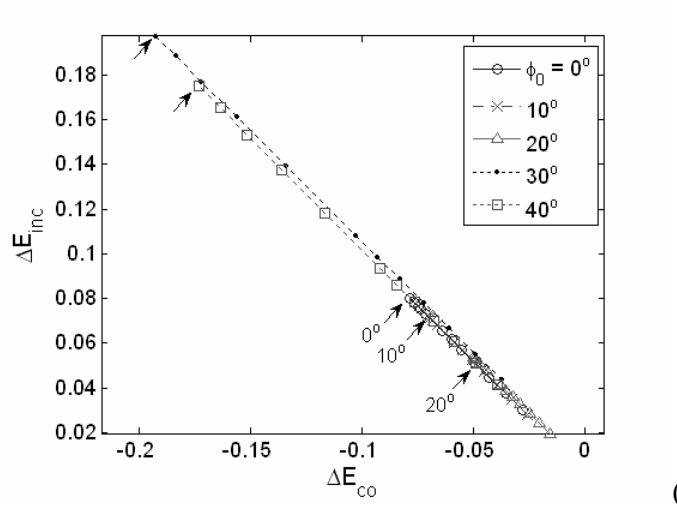

(b) $\tilde{f}_0 = 10,\ \tau = 0.1$

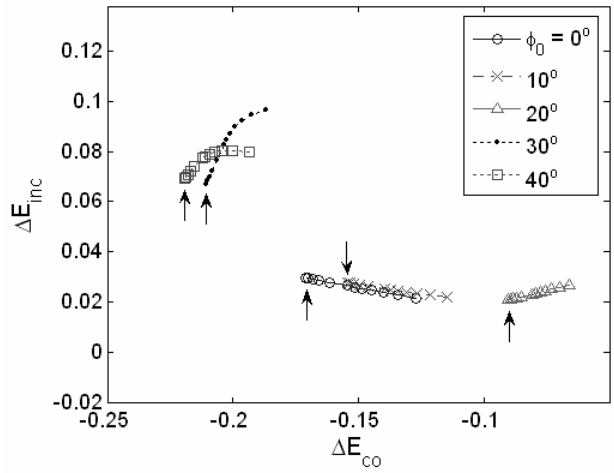

(c) $\tilde{f}_0 = 0.1,\ \tau = 10$

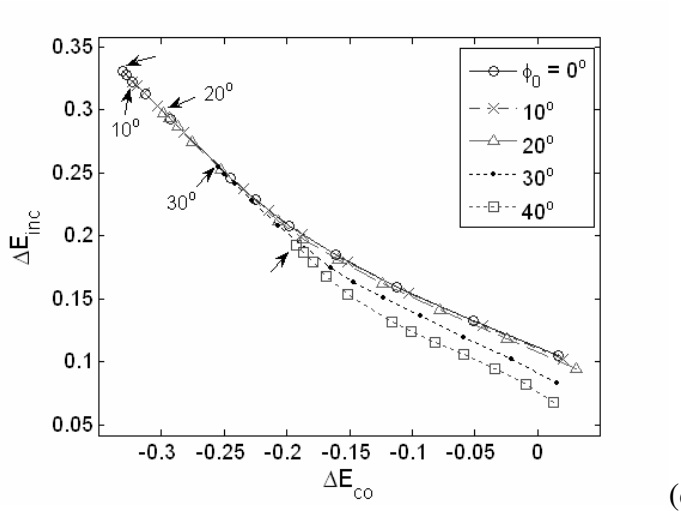

(d) $\tilde{f}_0 = \tau = 0.1$

Figure 33 Correlation between coherent and incoherent flux for various $\tilde{f}_0$ and τ ($\tilde{\sigma}$ = 0.3). Each curve for a given ϕ_0 is drawn for various $\tilde{l}_c$ from 1.5 to 8 ; arrows indicate points of $\tilde{l}_c$ = 8

Figure 34 shows outlined diagrams that illustrate amplification/ damping of the total energy. The size of (+) or (-) sign denotes the degree of amplification or damping. As shown in (a) and (b), the total energy is amplified when $\tilde{f}_0 \geq 1$. It is, however, amplified or damped when $\tilde{f}_0 < 1$, depending on whether the incidence angle is near the critical angle or not. Figure 34(c) shows that, for $\tilde{f}_0 < 1$, the energy damping increases as the incidence angle deviates from the critical angle. only when $\tilde{f}_0 < 1$. As shown in (d), however, the $\tilde{l}_c$ effect is more dominant than the incidence angle effect when $\tilde{f}_0 >> 1$.

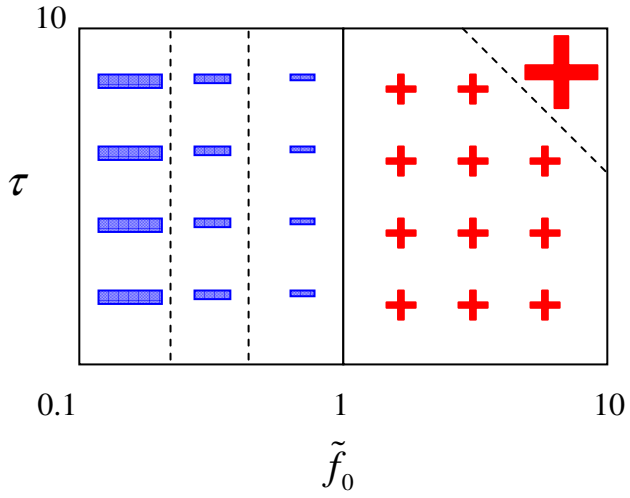

(a) Sub/supercritical angles

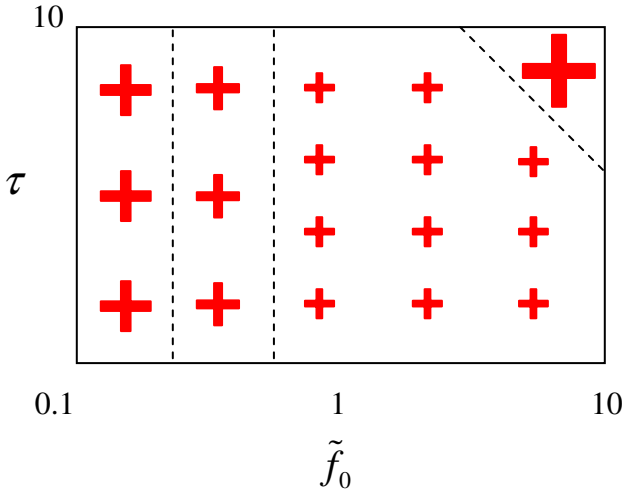

(b) Near-critical angle

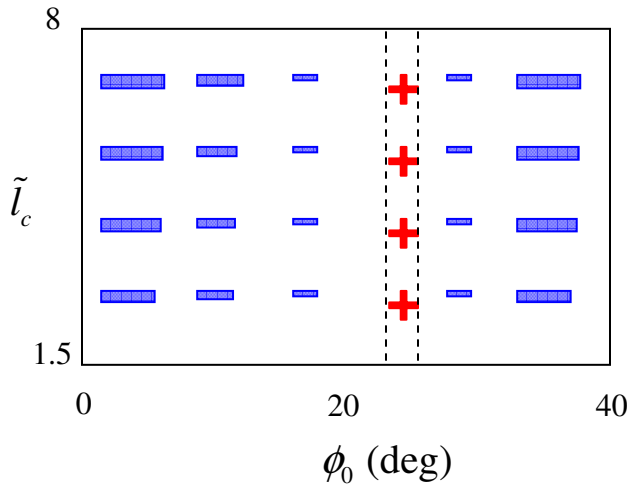

(c) $\tilde{f}_0 << 1$

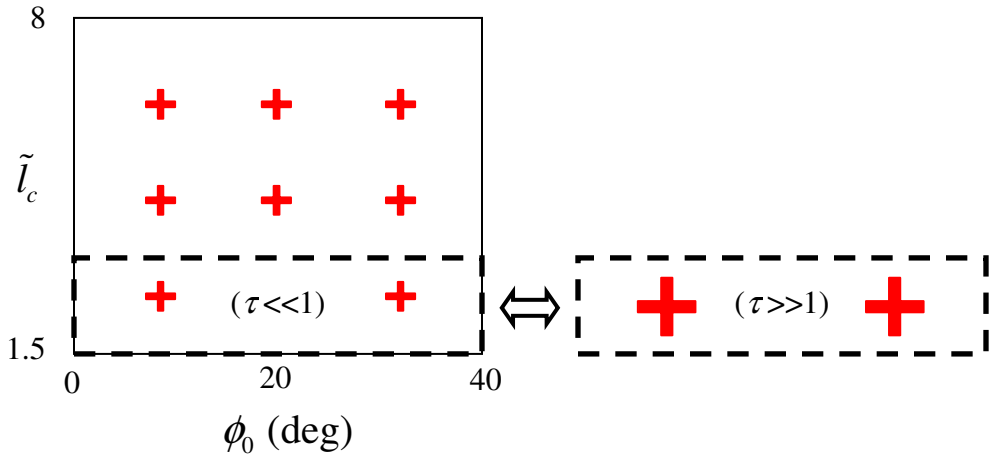

(d) $\tilde{f}_0 >> 1$

Figure 34 Outlined diagrams of the dependence of the total net energy upon key parameters

CHAPTER 6 FLAME'S KINEMATICS COUPLING WITH ACOUSTIC FIELDS

The instantaneous flame front position is described by the equation:

$$G(\vec{\boldsymbol{R}},t) = z - h(\boldsymbol{r},t) = 0 \tag{6.1}$$

The dynamics of the flame front is described by the G-equation, which represents a governing equation of a flame front position coupled with flow velocity and local flame speed.

$$\frac{DG(\vec{\boldsymbol{R}},t)}{Dt} = \frac{\partial G(\vec{\boldsymbol{R}},t)}{\partial t} + \vec{\boldsymbol{V}} \cdot \vec{\nabla} G - S_L \left| \vec{\nabla} G \right| = 0 \tag{6.2}$$

Substituting Eq. (6.1) and $\vec{\nabla} G = \vec{\boldsymbol{e}}_z - \nabla h$ into Eq. (6.2) yields:

$$-\frac{\partial h(\boldsymbol{r},t)}{\partial t} - \boldsymbol{V}_{\mathrm{H}} \cdot \nabla h + w - S_L \left(1 + \left|\nabla h\right|^2\right)^{1/2} = 0 \tag{6.3}$$

where $\boldsymbol{V}_{\mathrm{H}}$ is a horizontal component of $\vec{\boldsymbol{V}}$, i.e., $\boldsymbol{V}_{\mathrm{H}} = u\vec{\boldsymbol{e}}_x + v\vec{\boldsymbol{e}}_y$. Normalizing the variables in Eq. (6.3) leads to the following dimensionless form:

$$-\frac{\partial \tilde{h}(\tilde{\boldsymbol{r}},\tilde{t})}{\partial \tilde{t}} - \tilde{\boldsymbol{V}}_{\mathrm{H}}\Big|_{\tilde{h}} \cdot \tilde{\nabla}\tilde{h} + \tilde{w}\Big|_{\tilde{h}} - \tilde{S}_L \left(1 + \left|\tilde{\nabla}\tilde{h}\right|^2\right)^{1/2} = 0 \tag{6.4}$$

where $(\tilde{h},\tilde{\boldsymbol{r}}) = (h,\boldsymbol{r}) \times \omega_0 / c_1$, $\tilde{t} = t\omega_0$, $(\tilde{\boldsymbol{V}}_{\mathrm{H}}, \tilde{w}, \tilde{S}_L) = (\boldsymbol{V}_{\mathrm{H}}, w, S_L)/c_1$, $\tilde{\nabla} = \left(c_1/\omega_0\right)\nabla$ (6.5)

The variables in Eq. (6.4), e.g., horizontal velocity $\tilde{\boldsymbol{V}}_{\mathrm{H}}$, can be decomposed into mean velocity, $\tilde{\boldsymbol{V}}_{\mathrm{H},0}$, and perturbation velocity, $\tilde{\boldsymbol{V}}'_{\mathrm{H}}$. Note that these perturbation terms are caused by acoustic disturbance and, therefore, can be expanded in terms of the dimensionless incident pressure amplitude, ε ($\equiv \left|P_1\right| / (\rho_1 c_1^2)$), which is assumed to be small quantity. Therefore horizontal and vertical velocities have the form:

$$\tilde{\boldsymbol{V}}_H = \tilde{\boldsymbol{V}}_{H,0} + \tilde{\boldsymbol{V}}'_H = \tilde{\boldsymbol{V}}_{H,0} + \varepsilon\tilde{\boldsymbol{V}}_{H,1} + \varepsilon^2\tilde{\boldsymbol{V}}_{H,2} + \varepsilon^3\tilde{\boldsymbol{V}}_{H,3} + \cdots \tag{6.6}$$

$$\tilde{w} = \tilde{w}_0 + \varepsilon\tilde{w}_1 + \varepsilon^2\tilde{w}_2 + \varepsilon^3\tilde{w}_3 + \cdots$$

The velocity fields are also affected by the wrinkled flame surface when being reflected and transmitted through the flame surface, which implies that the coefficients of ε terms in Eq. (6.6), i.e., $\tilde{\boldsymbol{V}}_{H,1}$, $\tilde{\boldsymbol{V}}_{H,2}$, …, $\tilde{w}_1$, $\tilde{w}_2$, …, can subsequently be expanded in terms of flame front displacement $\tilde{h}$. For instance, the linearized velocity terms, $\tilde{\boldsymbol{V}}_{H,1}$ and $\tilde{w}_1$, were shown in section 2.3 to be expressed in terms of $\tilde{h}$ by means of scattering amplitudes being expanded in terms of power of $\tilde{h}$. Such analysis that utilizes two perturbation variables or more is also found in Culick [58].

$$\tilde{\boldsymbol{V}}_{H,1}\Big|_{\tilde{h}} = \tilde{\boldsymbol{V}}_{H,10} + \tilde{h}\tilde{\boldsymbol{V}}_{H,11} + \tilde{h}^2\tilde{\boldsymbol{V}}_{H,12} + \cdots \tag{6.7}$$

$$\tilde{\boldsymbol{V}}_{H,2}\Big|_{\tilde{h}} = \tilde{\boldsymbol{V}}_{H,20} + \tilde{h}\tilde{\boldsymbol{V}}_{H,21} + \tilde{h}^2\tilde{\boldsymbol{V}}_{H,22} + \cdots$$

$$\vdots$$

$$\tilde{w}_1\Big|_{\tilde{h}} = \tilde{w}_{10} + \tilde{h}\tilde{w}_{11} + \tilde{h}^2\tilde{w}_{12} + \cdots$$

$$\tilde{w}_2\Big|_{\tilde{h}} = \tilde{w}_{20} + \tilde{h}\tilde{w}_{21} + \tilde{h}^2\tilde{w}_{22} + \cdots$$

$$\vdots$$

Note that the resultant velocity fields are a function of both acoustic disturbance ε and flame front displacement $\tilde{h}$ through Eqs. (6.6) and (6.7), which can then be substituted into Eq. (6.4) to yield differential equation of $\tilde{h}$ as a function of ε. It is then followed from a perturbation method that the solution of $\tilde{h}$ can be expressed as the power series of ε.

$$\tilde{h} = \tilde{h}_0 + \tilde{h}' = \varepsilon\tilde{h}_1 + \varepsilon^2\tilde{h}_2 + \varepsilon^3\tilde{h}_3 + \cdots \tag{6.8}$$

where mean planar flame position is set to zero, i.e., $\tilde{h}_0 = 0$. Substituting Eqs. (6.6) - (6.8) into Eq. (6.4) yields the following form in terms of small perturbation ε:

$$
\begin{aligned}
&-\frac{\partial}{\partial \tilde{t}}(\varepsilon\tilde{h}_1 + \varepsilon^2\tilde{h}_2 + \varepsilon^3\tilde{h}_3 + \cdots) \\
&-\Big[\tilde{\boldsymbol{V}}_{H,0} + \varepsilon\left\{\tilde{\boldsymbol{V}}_{H,10} + \tilde{\boldsymbol{V}}_{H,11}(\varepsilon\tilde{h}_1 + \varepsilon^2\tilde{h}_2 + \varepsilon^3\tilde{h}_3 + \cdots) + \tilde{\boldsymbol{V}}_{H,12}(\varepsilon\tilde{h}_1 + \varepsilon^2\tilde{h}_2 + \varepsilon^3\tilde{h}_3 + \cdots)^2 + \cdots\right\} \\
&\quad + \varepsilon^2\left\{\tilde{\boldsymbol{V}}_{H,20} + \tilde{\boldsymbol{V}}_{H,21}(\varepsilon\tilde{h}_1 + \varepsilon^2\tilde{h}_2 + \varepsilon^3\tilde{h}_3 + \cdots) + \tilde{\boldsymbol{V}}_{H,22}(\varepsilon\tilde{h}_1 + \varepsilon^2\tilde{h}_2 + \varepsilon^3\tilde{h}_3 + \cdots)^2 + \cdots\right\} \\
&\quad + o(\varepsilon^2)\Big]\cdot\tilde{\nabla}(\varepsilon\tilde{h}_1 + \varepsilon^2\tilde{h}_2 + \varepsilon^3\tilde{h}_3 + \cdots) \\
&+\tilde{w}_0 + \varepsilon\left\{\tilde{w}_{10} + \tilde{w}_{11}(\varepsilon\tilde{h}_1 + \varepsilon^2\tilde{h}_2 + \varepsilon^3\tilde{h}_3 + \cdots) + \tilde{w}_{12}(\varepsilon\tilde{h}_1 + \varepsilon^2\tilde{h}_2 + \varepsilon^3\tilde{h}_3 + \cdots)^2 + \cdots\right\} \\
&+\varepsilon^2\left\{\tilde{w}_{20} + \tilde{w}_{21}(\varepsilon\tilde{h}_1 + \varepsilon^2\tilde{h}_2 + \varepsilon^3\tilde{h}_3 + \cdots) + \tilde{w}_{22}(\varepsilon\tilde{h}_1 + \varepsilon^2\tilde{h}_2 + \varepsilon^3\tilde{h}_3 + \cdots)^2 + \cdots\right\} + o(\varepsilon^2) \qquad (6.9) \\
&-\tilde{S}_L\left(1 + \frac{1}{2}\left|\tilde{\nabla}(\varepsilon\tilde{h}_1 + \varepsilon^2\tilde{h}_2 + \varepsilon^3\tilde{h}_3 + \cdots)\right|^2\right) = 0
\end{aligned}
$$

where flame speed, $\tilde{S}_L$, and mean flow velocities, $\tilde{\boldsymbol{V}}_{H,0}$ and $\tilde{w}_0$, are assumed to be constant. Collecting terms of like order of ε yields:

$$
\begin{aligned}
&\left[\tilde{w}_0 - \tilde{S}_L\right] + \varepsilon\left[-\frac{\partial\tilde{h}_1(\tilde{\boldsymbol{r}},\tilde{t})}{\partial\tilde{t}} - \tilde{\boldsymbol{V}}_{\mathrm{H},0}\cdot\tilde{\nabla}\tilde{h}_1 + \tilde{w}_{10}\right] + \\
&\varepsilon^2\left[-\frac{\partial\tilde{h}_2(\tilde{\boldsymbol{r}},\tilde{t})}{\partial\tilde{t}} - \tilde{\boldsymbol{V}}_{\mathrm{H},0}\cdot\tilde{\nabla}\tilde{h}_2 - \tilde{\boldsymbol{V}}_{\mathrm{H},10}\cdot\tilde{\nabla}\tilde{h}_1 + \tilde{w}_{11}\tilde{h}_1 + \tilde{w}_{20} - \frac{1}{2}\tilde{S}_L\left|\tilde{\nabla}\tilde{h}_1\right|^2\right] + O(\varepsilon^3) = 0
\end{aligned}
\qquad (6.10)
$$

where the terms in the bracket, [.], should vanish because the above equation holds for any small values of ε. The analysis in this study will deal only with the term of $O(\varepsilon)$ since the second term of $O(\varepsilon^2)$ includes a nonlinear acoustic velocity term, $\tilde{w}_{20}$, which is beyond the scope of the present study. The term of $O(\varepsilon)$ describes the first order approximation of the flame front response to velocity fields and reduces to the following form when the mean flow is vertical, i.e., perpendicular to mean flame surface, $\tilde{\boldsymbol{V}}_{\mathrm{H},0} = 0$:

$$
-\frac{\partial\tilde{h}_1(\tilde{\boldsymbol{r}},\tilde{t})}{\partial\tilde{t}} + \tilde{w}_{10} = 0 \qquad (6.11)
$$

where $\tilde{w}_{10}$ can be evaluated by expanding the vertical component of a linearized velocity, $\tilde{w}_1\big|_{\tilde{h}}$, in Eq. (6.7) in terms of $\tilde{h}$ and taking terms of $O(\tilde{h}^0 = 1)$. For instance, if an incident plane wave comes from upstream, or medium (1), the vertical component of a linearized velocity can be obtained from Eq. (3.136) by taking z-component of $\tilde{\vec{v}}^{(1)}$.

$$
\begin{aligned}
&\tilde{w}_1\big|_{\tilde{h}} = \tilde{\vec{v}}^{(1)}(\vec{R},t)\cdot\vec{e}_z\Big|_{z=h(\boldsymbol{r},t)} \\
&= \frac{\varepsilon c_1}{\omega_0}\mathrm{Re}\Big\{ iq_0^{(1)}\,\mathrm{e}^{i(\boldsymbol{k_0}\cdot\boldsymbol{r}+q_0^{(1)}z-\omega_0 t)} - iq_0^{(1)}R_J(\boldsymbol{k_0},\omega_0)\,\mathrm{e}^{i(\boldsymbol{k_0}\cdot\boldsymbol{r}-q_0^{(1)}z-\omega_0 t)} \\
&-i\int_{\omega}\iint_{\boldsymbol{k}}(q_0^{(1)}q_k^{(1)})^{1/2}A_J(\boldsymbol{k},\boldsymbol{k_0},\omega,\omega_0)h(\boldsymbol{k}-\boldsymbol{k_0},\omega-\omega_0)\,\mathrm{e}^{i(\boldsymbol{k}\cdot\boldsymbol{r}-q_k^{(1)}z-\omega t)}\,d\boldsymbol{k}d\omega \\
&-\frac{i}{2}\int_{\omega}\iint_{\boldsymbol{k}}(q_0^{(1)}q_k^{(1)})^{1/2}D_J(\boldsymbol{k},\omega)\,\mathrm{e}^{i(\boldsymbol{k}\cdot\boldsymbol{r}-q_k^{(1)}z-\omega t)}\times \\
&\qquad\Big[\int_{\omega'}\iint_{\boldsymbol{k}'}F_J(\boldsymbol{k}',\boldsymbol{k_0},\boldsymbol{k},\omega',\omega_0,\omega)h(\boldsymbol{k}-\boldsymbol{k}',\omega-\omega')h(\boldsymbol{k}'-\boldsymbol{k_0},\omega'-\omega_0)d\boldsymbol{k}'d\omega'\Big]d\boldsymbol{k}d\omega\Big\}_{z=h(\boldsymbol{r},t)} + O(h^3)
\end{aligned}
$$

$$
\begin{aligned}
&= \frac{\varepsilon c_1}{\omega_0}\mathrm{Re}\Big\{ iq_0^{(1)}\,\mathrm{e}^{i(\boldsymbol{k_0}\cdot\boldsymbol{r}-\omega_0 t)}\Big[\Big(1+iq_0^{(1)}h(\boldsymbol{r},t)+O(h^2)\Big)-R_J(\boldsymbol{k_0},\omega_0)\Big(1-iq_0^{(1)}h(\boldsymbol{r},t)+O(h^2)\Big)\Big] \\
&-i\int_{\omega}\iint_{\boldsymbol{k}}(q_0^{(1)}q_k^{(1)})^{1/2}A_J(\boldsymbol{k},\boldsymbol{k_0},\omega,\omega_0)h(\boldsymbol{k}-\boldsymbol{k_0},\omega-\omega_0)\,\mathrm{e}^{i(\boldsymbol{k}\cdot\boldsymbol{r}-\omega t)}\Big(1-iq_k^{(1)}h(\boldsymbol{r},t)+O(h^2)\Big)d\boldsymbol{k}d\omega \\
&-\frac{i}{2}\int_{\omega}\iint_{\boldsymbol{k}}(q_0^{(1)}q_k^{(1)})^{1/2}D_J(\boldsymbol{k},\omega)\,\mathrm{e}^{i(\boldsymbol{k}\cdot\boldsymbol{r}-\omega t)}\Big(1-iq_k^{(1)}h(\boldsymbol{r},t)+O(h^2)\Big)\times \\
&\qquad\Big[\int_{\omega'}\iint_{\boldsymbol{k}'}F_J(\boldsymbol{k}',\boldsymbol{k_0},\boldsymbol{k},\omega',\omega_0,\omega)h(\boldsymbol{k}-\boldsymbol{k}',\omega-\omega')h(\boldsymbol{k}'-\boldsymbol{k_0},\omega'-\omega_0)d\boldsymbol{k}'d\omega'\Big]d\boldsymbol{k}d\omega\Big\} \\
&+O(h^3)
\end{aligned}
\tag{6.12}
$$

Terms of $O(h^0 = 1)$ in the above equation correspond to $\tilde{w}_{10}$:

$$
\tilde{w}_{10} = \frac{\varepsilon c_1 q_0^{(1)}}{\omega_0}\mathrm{Re}\Big[i\big(1-R_J(\boldsymbol{k_0},\omega_0)\big)\,\mathrm{e}^{i(\boldsymbol{k_0}\cdot\boldsymbol{r}-\omega_0 t)}\Big] \tag{6.13}
$$

Substituting Eq. (6.13) into Eq. (6.11) and integrating with respect to time yields an explicit solution for the first order approximation of the flame front response to acoustic velocity fields.

$$\tilde{h}_1(\boldsymbol{r},t) = \varepsilon(\cos\phi_0^{(1)})\,\mathrm{Re}\left[\left(1-R_J(\boldsymbol{k_0},\omega_0)\right)\mathrm{e}^{i\boldsymbol{k_0}\cdot\boldsymbol{r}}(1-\mathrm{e}^{-i\omega_0 t})\right]+\tilde{h}_1(\boldsymbol{r},0) \tag{6.14}$$

with $\cos\phi_0^{(1)} = \dfrac{c_1 q_0^{(1)}}{\omega_0}$, $\boldsymbol{k_0} = \dfrac{\omega_0 \sin\phi_0^{(1)}}{c_1}\left(\cos\theta_0^{(1)}\,\vec{\boldsymbol{e}}_{\boldsymbol{x}} + \sin\theta_0^{(1)}\,\vec{\boldsymbol{e}}_{\boldsymbol{y}}\right)$

where $\phi_0^{(1)}$ is a polar angle of an incident wave which is measured from $-$z-axis in medium (1) and $\theta_0^{(1)}$ is an azimuth angle measured from +x-axis. Based on Eq. (6.14), Figure 35 depicts the time evolution of a flame front which is initially in an undisturbed condition. This figure shows that disturbed flame front propagates in the direction of the horizontal component of the incident wave vector, i.e., $\boldsymbol{k_0} \,//\, \cos(-60^\circ)\,\vec{\boldsymbol{e}}_{\boldsymbol{x}} + \sin(-60^\circ)\,\vec{\boldsymbol{e}}_{\boldsymbol{y}}$ $= 1/2\,\vec{\boldsymbol{e}}_{\boldsymbol{x}} - \sqrt{3}/2\,\vec{\boldsymbol{e}}_{\boldsymbol{y}}$. Note that the flame front disturbance is maximized at $\omega_0 t = \pi$ but vanishes at $\omega_0 t = 2\pi$ returning to an initial state. These processes are repeated with a period of $\omega_0 T = 2\pi$.

The envelope of the flame front can be obtained by the fact that the time rate of change of flame front height vanishes when the flame front reaches its envelope at $t = t_E$:

$$\frac{\partial \tilde{h}_1(\boldsymbol{r},t_E)}{\partial t} = \varepsilon(\cos\phi_0^{(1)})\,\mathrm{Re}\left[i\omega_0\left(1-R_J(\boldsymbol{k_0},\omega_0)\right)\mathrm{e}^{i(\boldsymbol{k_0}\cdot\boldsymbol{r}-\omega_0 t_E)}\right] = 0 \tag{6.15}$$

$\Rightarrow \left(1-R_J(\boldsymbol{k_0},\omega_0)\right)\mathrm{e}^{i(\boldsymbol{k_0}\cdot\boldsymbol{r}-\omega_0 t_E)}$ is real.

$\Rightarrow \left(1-R_J(\boldsymbol{k_0},\omega_0)\right)\mathrm{e}^{i(\boldsymbol{k_0}\cdot\boldsymbol{r}-\omega_0 t_E)} = \pm\left|1-R_J(\boldsymbol{k_0},\omega_0)\right|$

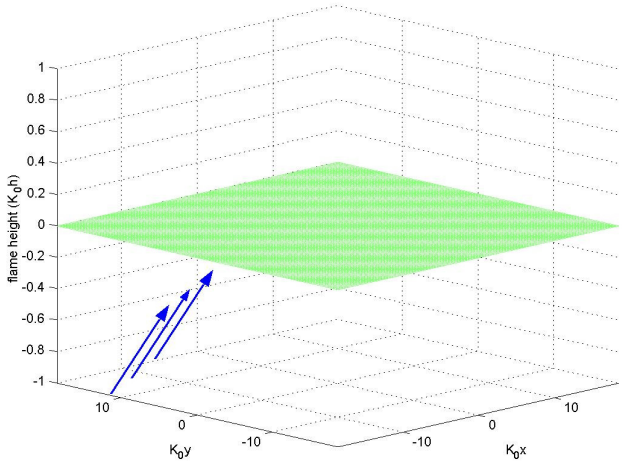

(a) $\omega_0 t = 0$

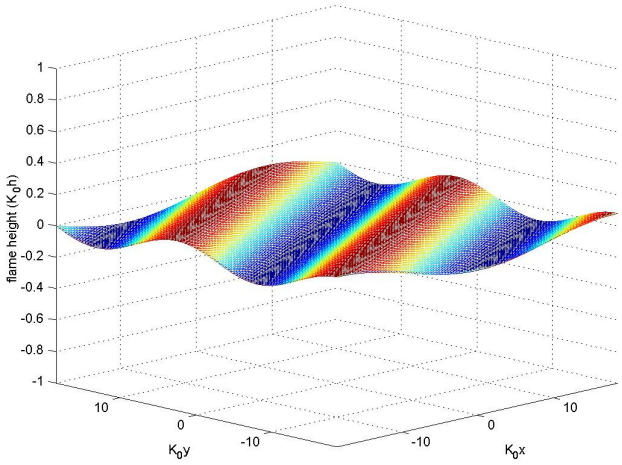

(b) $\omega_0 t = 0.5\pi$

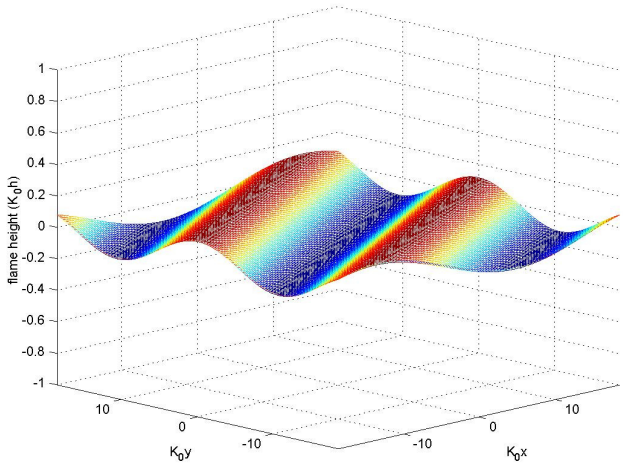

(c) $\omega_0 t = \pi$

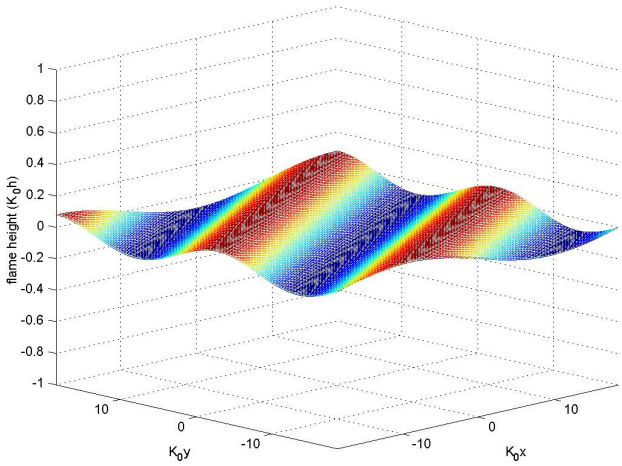

(d) $\omega_0 t = 1.5\pi$

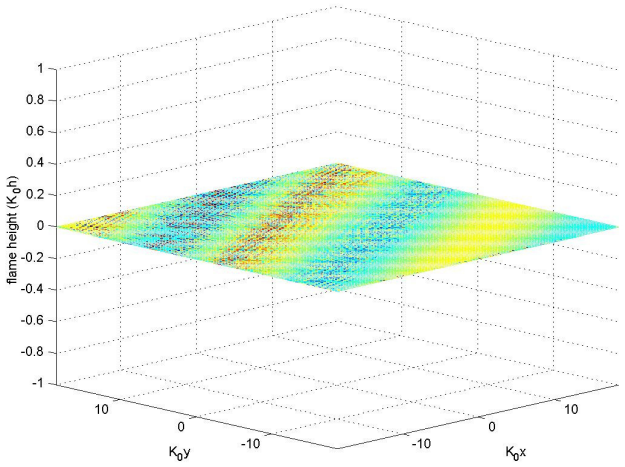

(e) $\omega_0 t = 2\pi$

Figure 35 Time evolution of the first-order approximation of flame front response to acoustic fields (ε = 0.05, R_J = -0.2, f_0 =100 Hz, $\phi_0^{(1)}$ = 20 °, $\theta_0^{(1)}$ = -60 °)

Therefore the envelope is of the form:

$$\tilde{h}_1(\boldsymbol{r}, t_E) = \varepsilon(\cos\phi_0^{(1)})\left\{\mathrm{Re}\left[\left(1 - R_J(\boldsymbol{k_0}, \omega_0)\right)\mathrm{e}^{i\boldsymbol{k_0}\cdot\boldsymbol{r}}\right] \pm \left|1 - R_J(\boldsymbol{k_0}, \omega_0)\right|\right\} + \tilde{h}_1(\boldsymbol{r}, 0) \qquad (6.16)$$

The flame envelope is of a sinusoidal form as shown in Figure 36. The reflection coefficient has the following form from Eq. (3.144).

$$R_J(\boldsymbol{k_0}, \omega_0) = \frac{\cos\phi_0^{(1)} - \Lambda^{1/2}\cos\phi_0^{(2)} + (\Lambda - 1)M_S(1 + 4i\omega_0 t_r)}{\cos\phi_0^{(1)} + \Lambda^{1/2}\cos\phi_0^{(2)} - (\Lambda - 1)M_S(1 + 4i\omega_0 t_r)}$$

where $\Lambda = T_2 / T_1$.

Figure 37 shows the dependence of flame shape upon the incident angle. The scale (or wavelength) of the flame shape increases as the impinging angle of an incident wave becomes more normal to the mean flame surface. This is due to increase in phase speed (or trace velocity) along the flame surface with decreasing (more vertical) incident angle.

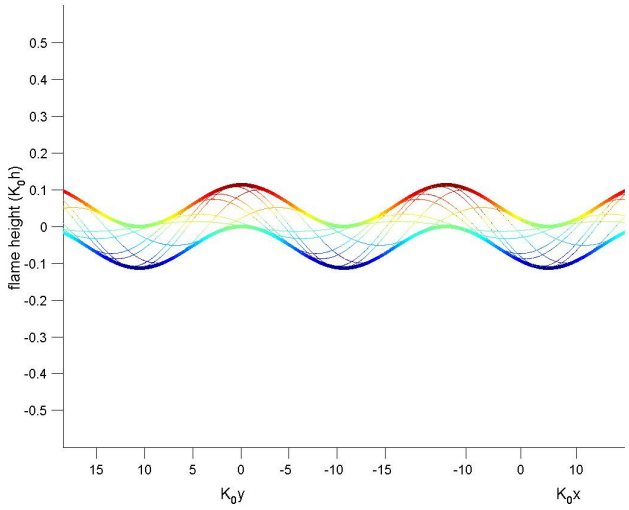

Figure 36 The envelope of transiently moving flame fronts (ε = 0.05, R_J = -0.2, f_0 =100 Hz, $\phi_0^{(1)}$ = 20 °, $\theta_0^{(1)}$ = -60 °)

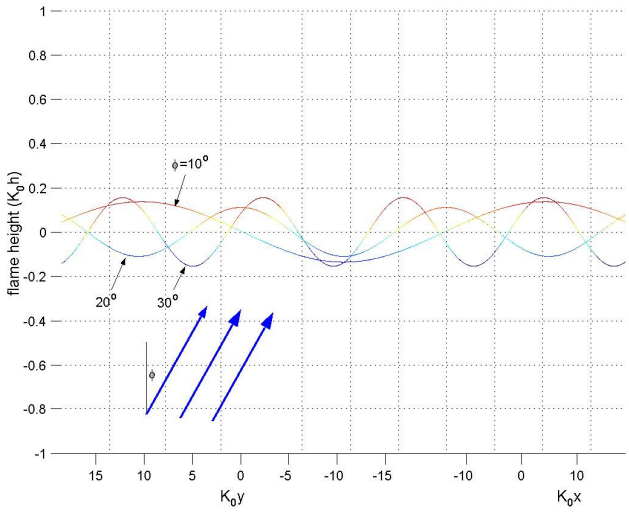

Figure 37 The dependence of flame shape upon the incident angle at $\omega t = \pi$

CHAPTER 7 LAMINAR PREMIXED FLAME RESPONSE TO EQUIVALENCE RATIO OSCILLATIONS

The effects of equivalence ratio oscillations upon laminar premixed flames are analyzed and discussed in this chapter. The analysis deals with the characteristics of the equivalence ratio-heat release transfer function and the role of the processes affecting the dynamics of the interaction.

7.1 Model for flame displacement perturbation

The analysis used here to model the flame's response is similar to that previously presented by Markstein [19], Fleifil *et al*. [4], Ducruix *et al*. [59], Baillot *et al*. [60], Dowling and Hubbard [6], Lee and Lieuwen [45], and others.

The combustor geometry is illustrated in Figure 38.

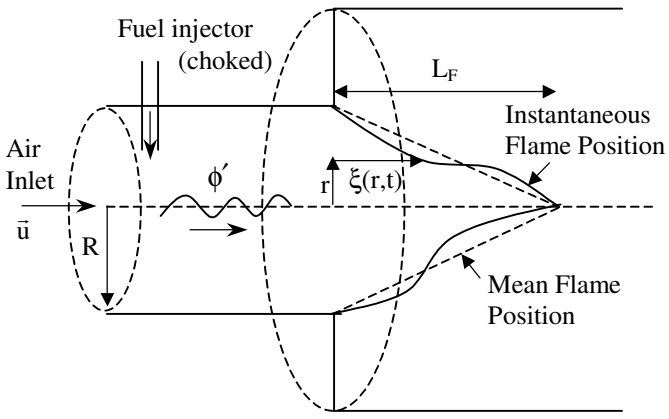

Figure 38 Schematic of investigated combustor geometry

The principle assumptions of the analysis are: 1) The flame is a thin sheet separating the cold reactants and hot products, 2) the flame is axi-symmetric, 3) the flame base remains anchored at its attachment point (i.e., its position does not fluctuate), 4)

flame displacement is described as a single valued function with respect to radial coordinate, 5) Mach number of the mean flow is very small (M << 1), 6) Flame speed dependence upon flame strain rate is neglected. As shown in Appendix D, Assumption (6) is satisfied at *all* points along the flame at frequencies where $\frac{\omega\delta}{\bar{S}_u}|Ma| \ll$ O(1), where δ and Ma denote the flame thickness and Markstein number. This inequality is quite conservative, however, as the effects of flame strain upon the overall heat release can be anticipated to be significant only at much higher frequencies where strain effects dominate equivalence ratio variation effects over an appreciable portion of the flame surface.

Following assumptions (1), (2), and (4), the instantaneous flame position is defined by the equation: (Note that notations used here are different from Eq. (6.1) in order to describe different geometry, i.e., horizontally aligned axisymmetric combustor.)

$$G(x,r,t) = x - \xi(r,t) = 0 \tag{7.1}$$

which leads to

$$\frac{\partial \xi}{\partial t} = u - v\frac{\partial \xi}{\partial r} - S_u\left[\left(\frac{\partial \xi}{\partial r}\right)^2 + 1\right]^{1/2} \tag{7.2}$$

The linear dynamics of the flame can be analyzed by decomposing the variables into their mean and fluctuating parts and retaining only the linear terms in fluctuations. Assuming harmonic oscillations (using the $\exp(-i\omega t)$ convention) for the fluctuating term yields:

$$-i\omega\xi'(r) = u'(r) - v'(r)\frac{d\bar{\xi}}{dr} - S_u'(r)\left[1+\left(\frac{d\bar{\xi}}{dr}\right)^2\right]^{1/2} - \bar{S}_u\left[\frac{\bar{v}}{\bar{S}_u} + \frac{d\bar{\xi}}{dr}\left\{1+\left(\frac{d\bar{\xi}}{dr}\right)^2\right\}^{-1/2}\right]\frac{d\xi'(r)}{dr} \tag{7.3}$$

Define the velocity fluctuation normal to the mean flame front, $u_n'(r)$ as:

$$u_n' = \vec{u}' \cdot \frac{\nabla \overline{G}}{\left|\nabla \overline{G}\right|} = \left(u'(r) - v'(r) \frac{d\overline{\xi}}{dr} \right) \Bigg/ \left[1 + \left(\frac{d\overline{\xi}}{dr} \right)^2 \right]^{1/2} \tag{7.4}$$

The variables are normalized (denoted by '^') as $(\hat{u}_n', \hat{S}_u', \hat{\overline{u}}, \hat{\overline{v}}, \hat{\overline{S}}_u) = (u_n', S_u', \overline{u}, \overline{v}, \overline{S}_u)/\overline{u}_0$, $(\hat{\xi}', \hat{\overline{\xi}}) = (\xi', \overline{\xi})/L_F$, and $\hat{r} = r/R$ where $L_F \equiv \max(\overline{\xi}(r))$ = mean flame length and $\overline{u}_0$ = mean flow speed at some reference point (e.g., at $r = 0$).

The normalized flame front equations are:

$$\hat{\overline{u}} = \frac{L_F}{R} \left[\hat{\overline{v}} \frac{d\hat{\overline{\xi}}}{d\hat{r}} + \beta(\hat{r}) \hat{\overline{S}}_u \right] \tag{7.5}$$

$$\frac{d\hat{\xi}'(\hat{r})}{d\hat{r}} + p(\hat{r}) \hat{\xi}'(\hat{r}) = q(\hat{r}) \tag{7.6}$$

where

$$\beta(\hat{r}) \equiv \left(\left(\frac{R}{L_F} \right)^2 + \left(\frac{d\hat{\overline{\xi}}}{d\hat{r}} \right)^2 \right)^{1/2}, \quad q(\hat{r}) \equiv \left(\frac{\hat{u}_n'(\hat{r}) - \hat{S}_u'(\hat{r})}{f(\hat{r}) \hat{\overline{S}}_u(\hat{r})} \right) \beta(\hat{r}) \tag{7.7}$$

$$p(\hat{r}) \equiv -\frac{i\omega R}{f(\hat{r}) \overline{S}_u(\hat{r})} = -i \ St \frac{\left|f\right|_m \hat{\overline{S}}_{u,0}}{f(\hat{r}) \hat{\overline{S}}_u(\hat{r})}, \quad f(\hat{r}) \equiv \frac{\hat{\overline{v}}(\hat{r})}{\hat{\overline{S}}_u(\hat{r})} + \frac{1}{\beta(\hat{r})} \frac{d\hat{\overline{\xi}}}{d\hat{r}}$$

The Strouhal number is defined as the normalized frequency:

$$St \equiv \frac{\omega R}{\left|f\right|_m \overline{S}_{u,0}} \tag{7.8}$$

where $|f|_m$ = max($|f(r)|$) and $\overline{S}_{u,0}$ = reference mean flame speed. Following assumption (3), the solution of Eq. (7.6) is given by:

$$\hat{\xi}'(\hat{r}) = \int_1^{\hat{r}} \frac{\beta(\eta)}{f(\eta)\hat{\bar{S}}_u(\eta)} \left(\hat{u}_n'(\eta) - \hat{S}_u'(\eta)\right) \exp\left(-i \quad St \int_{\hat{r}}^{\eta} \frac{\left|f\right|_m \hat{\bar{S}}_{u,0} d\rho}{f(\rho)\hat{\bar{S}}_u(\rho)} \right) d\eta \tag{7.9}$$

Following assumption (6), the flame speed perturbation is given by:

$$\hat{S}_u'(\eta) = \left. \frac{d\hat{S}_u}{d\phi} \right|_{\bar{\phi}} \phi'(\eta) \tag{7.10}$$

7.2 Flame transfer function calculation

We next consider the total heat release response of the flame. Following Fleifil *et al*. [4] and Ducruix *et al*. [59], its global heat release rate is written as:

$$Q(t) = \int_{A_f} \rho S_u \Delta h_R \, dA \tag{7.11}$$

where A_f denotes the instantaneous flame surface. Following assumption (5), the density of the reactive mixture is constant; i.e., *the equivalence ratio perturbation occurs at constant density*. Fluctuations in heat release can be decomposed into the separate contributions of heat of reaction, flame speed, and flame area fluctuations, i.e.,

$$Q' = Q'_{S_u} + Q'_{\Delta h_R} + Q'_{A_f} \tag{7.12}$$

Eq. (7.12) can then be written as:

$$\frac{Q'}{\bar{Q}} = \frac{Q'_{S_u}}{\bar{Q}} + \frac{Q'_{\Delta h_R}}{\bar{Q}} + \frac{Q'_{A_f}}{\bar{Q}} = \frac{\int_{R_{tip}}^{1} g(\hat{\bar{\xi}}(r), St) dr}{\int_{R_{tip}}^{1} r\beta(r) \quad \hat{\bar{S}}_u(r)\Delta\bar{h}_R(r) dr} \tag{7.13}$$

where

$$g(\hat{\bar{\xi}}(r), St) = \frac{r\Delta\bar{h}_R(r)}{f(r)} \left(\frac{d\hat{\bar{\xi}}}{dr} \right) \hat{u}_n'(r) + r \left[\beta(r) \left. \frac{d(\hat{S}_u \Delta h_R)}{d\phi} \right|_{\bar{\phi}} - \frac{\Delta\bar{h}_R(r)}{f(r)} \left(\frac{d\hat{\bar{\xi}}}{dr} \right) \left. \frac{d(\hat{S}_u)}{d\phi} \right|_{\bar{\phi}} \right] \phi'(r)$$

$$+i\ St\ r\frac{|f|_m}{f(r)}\frac{\hat{\bar{S}}_{u,0}\Delta\bar{h}_R(r)}{\beta(r)}\left(\frac{d\hat{\bar{\xi}}}{dr}\right)\hat{\xi}'(r) \tag{7.14}$$

In Eq. (7.13), the common factor $2\pi\rho\bar{u}_0 RL_F$ between Q' and $\bar{Q}$ was canceled for conciseness. The three terms in the right-hand side of Eq. (7.14) describe the heat release response to coupled perturbations in flow velocity, equivalence ratio, and flame displacement, respectively. The flame displacement perturbation is a function of flow velocity and equivalence ratio as shown in Eqs. (7.9) and (7.10). Note that Eq. (7.9) shows that a perturbation in velocity or flame speed exerts an identical effect upon the flame's displacement. As shown in Eq. (7.13), however, the overall effects of these perturbations upon the heat release are different, as the flame speed perturbation has an effect both on the flame front area and the local consumption rate, while the velocity perturbation primarily affects the former.

7.3 Sensitivity of flame transfer function to mean flame position

Having developed an analytical expression for the flame transfer function, this section derives upper bounds on the sensitivity of this function to small uncertainties in flame position. This issue is important for assessing the confidence that can be placed in an analytical prediction; i.e., if the sensitivity is high, inherent uncertainties in flame shape will render quantitative calculation difficult.

The heat release perturbation given in Eq. (7.13) can be expressed as:

$$Q' = \int_0^1 g(\hat{\bar{\xi}}(r), St)dr \tag{7.15}$$

Assume some uncertainty in the flame position, $\varepsilon Y(\hat{r})$, in the radial direction from its estimated position, $\hat{\bar{\xi}}$. This uncertainty is related to the uncertainty in the axial direction, $\Delta\hat{\bar{\xi}}$, as:

$$\Delta\hat{\bar{\xi}} \approx (-)\varepsilon Y(\hat{r}) \times \frac{d\hat{\bar{\xi}}(\hat{r})}{d\hat{r}} \left(1 + \varepsilon \frac{dY(\hat{r})}{d\hat{r}}\right)^{-1} \approx (-)\varepsilon Y(\hat{r}) \times \frac{d\hat{\bar{\xi}}(\hat{r})}{d\hat{r}} \quad (\varepsilon << 1) \tag{7.16}$$

where $Y(\hat{r})$ is an arbitrary real function which is bounded by a maximum variation Y_n. Its derivative is bounded by $\frac{dY(\hat{r})}{d\hat{r}} << \frac{1}{\varepsilon}$. Two maximum variation functions, given by Y_1 and Y_2, are considered, see Figure 39:

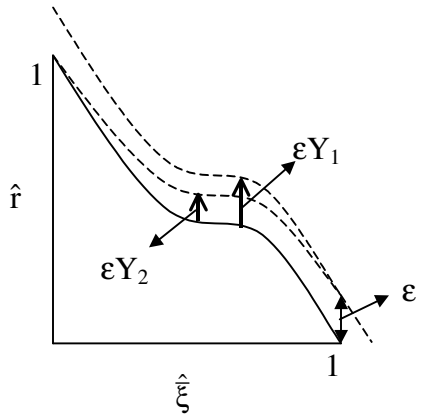

Figure 39 Functions defining uncertainties in estimated flame position

$$\left|Y(\hat{r})\right| \le 1 \equiv Y_1 \quad , \qquad \left|Y(\hat{r})\right| \le 1 - \hat{r} \equiv Y_2 \tag{7.17), (7.18}$$

where Y_2 is a slightly less general case than Y_1 because it assumes that the flame base always remains fixed and the uncertainty in flame position grows linearly with radial distance from the anchoring point.

Define a magnitude-sensitivity function, S_m, as the normalized uncertainty in unsteady heat release magnitude:

$$S_m \equiv \frac{1}{\varepsilon}\left|\frac{\Delta(Q')}{Q'}\right| \tag{7.19}$$

The uncertainty in unsteady heat release rate resulting from uncertainty in the estimated flame position is:

$$\Delta(Q') = Q'(\hat{\bar{\xi}} + \Delta\hat{\bar{\xi}}) - Q'(\hat{\bar{\xi}}) = \int_0^1 g(\hat{\bar{\xi}}(r) + \Delta\hat{\bar{\xi}}(r)) - g(\hat{\bar{\xi}}(r))dr \tag{7.20}$$

Assuming that $\varepsilon << 1$, expanding the equation in the integral by a Taylor series, and retaining only the first order term yields:

$$\Delta(Q') \approx \int_0^1 \Delta\hat{\bar{\xi}}(r) \times \frac{dg(r)}{d\hat{\bar{\xi}}}\, dr \tag{7.21}$$

An upper bound on the sensitivity, $S_1^{up}(Y_n)$, can be determined from the following integral inequality:

$$S_m = \frac{1}{|Q'|}\left|\int_0^1 Y(r)\frac{dg(r)}{dr}dr\right| \le \frac{1}{|Q'|}\int_0^1 \left|Y_n(r)\frac{dg(r)}{dr}\right|dr \equiv S_1^{up}(Y_n) \quad \text{for } n = 1,2 \tag{7.22}$$

where Eqs. (7.16), (7.19), and (7.21) are used. $S_1^{up}(Y_n)$ can be evaluated for a given estimated flame shape and Strouhal number. Note from Eq. (7.22) that the sensitivity is identically unity ($S_m = 1$) if $Y(\hat{r}) = \pm Y_2$, which refers to the case when the mean flame shape is simply elongated or contracted from its nominal mean flame shape:

$$S_m = \frac{1}{|Q'|}\left|\int_{r=0}^1 Y_2(r)\ dg\right| = \frac{1}{|Q'|}\left|\int_0^1 g(r)dr\right| = 1 \ \text{ for } Y(\hat{r}) = \pm Y_2 \quad (0 \le \hat{r} \le 1) \tag{7.23}$$

where we use $g(r=0) = Y_2(1) = 0$ and Eq. (7.15).

Note in Eq. (7.22) that the upper bound on the sensitivity, $S_1^{up}(Y_n)$, places no restrictions on the curvature of the variation $\varepsilon Y(\hat{r})$; i.e., the function can have arbitrary

large variations in flame curvature. As shown later, this leads to large uncertainties at high Strouhal numbers. As such, an additional sensitivity function can be defined that bounds $d^2Y/d\hat{r}^2$; i.e., $d^2Y/d\hat{r}^2 \le M$. For small slope of uncertainties, this is equivalent to bounding the smallest radius of flame curvature. Integrating Eq. (7.22) by parts yields:

$$S_m = \frac{1}{|Q'|}\left| \int_0^1 \frac{d^2Y}{dr^2} \int_0^r g(\eta)\, d\eta\, dr - Q' \left(\frac{dY}{dr}\right)_{r=1} \right|$$

$$\le 1 + \frac{M}{|Q'|} \int_0^1 \left| \int_0^r g(\eta)\, d\eta \right| dr \equiv S_2^{up} \qquad \text{for} \quad \frac{d^2Y(\hat{r})}{d\hat{r}^2} \le M \quad (0 \le \hat{r} \le 1) \tag{7.24}$$

where the use is made of $g(r=0) = Y(1) = 0$, $\left|dY(1)/d\hat{r}\right| \le \left|dY_2(1)/d\hat{r}\right| = 1$, and Eq. (7.15). Define also the phase-sensitivity of the transfer function, S_{phase}, as:

$$S_{phase} \equiv \frac{1}{\varepsilon} \max \left|\Delta\left(phase(Q')\right)\right| = \frac{1}{\varepsilon} \sin^{-1}\left(\left|\frac{\Delta Q'}{Q'}\right|\right) \approx S_m \,(\text{radian}) \quad \text{for } \varepsilon S_m << 1 \tag{7.25}$$

which indicates that $S_{phase} = S_m$.

7.4 Results and discussion

The prior section presented general results for the flame response, heat release, and sensitivity to equivalence ratio perturbations. This section presents explicit results for a conical flame front. It is assumed that $\overline{S}_u$ and $\overline{u}$ are spatially uniform and that $\overline{v}$ is negligible. In order to compare the transfer function characteristics of flames disturbed by velocity and equivalence ratio perturbations, the velocity term in Eq. (7.9) will be retained. The conical mean flame position is given by:

$$\hat{\overline{\xi}}(\hat{r}) = \frac{\overline{\xi}(\hat{r})}{L_F} = 1 - \hat{r} \quad (0 \le \hat{r} \le 1), \tag{7.26}$$

$$\beta = \left[\left(\frac{R}{L_F} \right)^2 + 1 \right]^{1/2}, \quad St = \frac{\beta \omega R}{\bar{S}_{u,0}} = \frac{\beta^2 \omega L_F}{\bar{u}}, \quad f = -\frac{1}{\beta} = -\left| f \right|_m \tag{7.27}$$

where Eqs. (7.5), (7.7), and (7.8) are used. Note that the Strouhal number in Eq. (7.27) is identical to the "reduced frequency", ω^*, defined by Ducruix *et al*. [59]. Substituting Eqs. (7.10) and (7.27) into Eq. (7.9) yields :

$$\hat{\xi}'(\hat{r}) = -\frac{\beta^2}{\hat{\bar{S}}_{u,0}} \int_1^{\hat{r}} \left(\hat{u}'_n(\eta) - \left. \frac{d\hat{S}_u}{d\phi} \right|_{\bar{\phi}} \phi'(\eta) \right) \times \exp\left[i\, St(\eta - \hat{r}) \right] d\eta \tag{7.28}$$

where it is assumed that the equivalence ratio disturbance is convected by the mean flow so that:

$$\phi'(\eta) = \phi'_b \exp\left[\frac{i\omega \bar{\xi}(\eta)}{\bar{u}(\eta)} \right] = \phi'_b \exp\left[\frac{i\, St}{\beta^2} (1 - \eta) \right] \tag{7.29}$$

where ϕ'_b denotes the value of the perturbation at the base of the flame.

It is assumed that the velocity perturbation consists of a uniform and an axially convected component. Both types of perturbations are retained to facilitate comparisons of their transfer functions with the equivalence ratio-heat release transfer function. The uniform and convected disturbances represent the disturbance of a flame by a long wavelength acoustic perturbation and a vortical disturbance, respectively, as in Fleifil *et al*. [4] and Ducruix *et al*.'s [59] analyses in the former case and Schuller *et al*.'s [61, 62] in the latter.

Using Eq. (7.29), Eq. (7.28) can be written as:

$$\hat{\xi}'(\hat{r}) = \frac{\beta^2}{\hat{\bar{S}}_{u,0}} \left[\hat{u}'_{n,uni} G_{u,uni}(St) + \hat{u}'_{n,cv} G_{u,cv}(St) + \left. \frac{d\hat{S}_u}{d\phi} \right|_{\bar{\phi}} \phi'_b G_\phi(St) \right] \tag{7.30}$$

with $G_{u,uni}(St) = \frac{i}{St}\left[1 - \exp\left\{i\ St\,(1-\hat{r})\right\}\right]$,

$$G_{u,cv}(St) = -G_{\phi}(St) = \frac{\beta^2}{\beta^2 - 1}\left(\frac{i}{St}\right)\left[\exp\left\{\frac{i\ St\,(1-\hat{r})}{\beta^2}\right\} - \exp\left\{i\ St\,(1-\hat{r})\right\}\right]$$

where $\hat{u}'_{n,uni}$ and $\hat{u}'_{n,cv}$ denote uniform and convected velocity perturbations, respectively. Substituting Eq. (7.30) into Eq. (7.14) yields the following expression for the flame transfer functions, F_u, $F_{u,cv}$, and F_{ϕ}, that describe its response to uniform/convected velocity and equivalence ratio perturbations, respectively.

$$F_u = \left(\frac{Q'_{u,uni}}{\overline{Q}}\right) \Bigg/ \left(\frac{\hat{u}'_{n,uni}}{\hat{\overline{S}}_u}\right) = \frac{2}{St^2}\left\{1 + i\ St - \exp(i\ St)\right\} \tag{7.31}$$

$$F_{u,cv} = \left(\frac{Q'_{u,cv}}{\overline{Q}}\right) \Bigg/ \left(\frac{\hat{u}'_{n,cv}}{\hat{\overline{S}}_u}\right) = \frac{-2\beta^4}{St^2(\beta^2 - 1)}\left\{1 - \frac{1}{\beta^2} + \frac{\exp(i\ St)}{\beta^2} - \exp(\frac{i\ St}{\beta^2})\right\} \tag{7.32}$$

$$F_{\phi} = \left(\frac{Q'_{\phi}}{\overline{Q}}\right) \Bigg/ \left(\frac{\phi'_b}{\overline{\phi}}\right) = F_H + F_S = F_H + \left(F_{S,dir} + F_A\right) \tag{7.33}$$

where

$$F_H = \left.\frac{d\left(\Delta h_R / \Delta \overline{h}_R\right)}{d\left(\phi/\overline{\phi}\right)}\right|_{\overline{\phi}} \frac{2\beta^4}{St^2}\left\{1 + \frac{i\ \ St}{\beta^2} - \exp(\frac{i\ \ St}{\beta^2})\right\},$$

$$F_{S,dir} = \left.\frac{d\left(S_u / \overline{S}_u\right)}{d\left(\phi/\overline{\phi}\right)}\right|_{\overline{\phi}} \frac{2\beta^4}{St^2}\left\{1 + \frac{i\ \ St}{\beta^2} - \exp(\frac{i\ \ St}{\beta^2})\right\},$$

$$F_A = \left.\frac{d\left(S_u / \overline{S}_u\right)}{d\left(\phi/\overline{\phi}\right)}\right|_{\overline{\phi}} \frac{2\beta^4}{St^2(\beta^2 - 1)}\left\{1 - \frac{1}{\beta^2} + \frac{\exp(i\ \ St)}{\beta^2} - \exp(\frac{i\ \ St}{\beta^2})\right\}$$

The above equations state that $F_{u,cv}$ and F_{ϕ} are functions of the Strouhal number and β. Note that $F_{u,cv}$ is identical to Eq. (7.26) in Schuller *et al.* [62] (F_{CCO} in their

notation). In contrast, F_u is only a function of the Strouhal number, due to the assumption of spatially uniform acoustic velocity perturbations. Figure 40 summarizes the manner through which Eq. (7.31) or (7.33) relates velocity or equivalence ratio perturbations to heat release perturbations. Velocity perturbations disturb the flame's position, thereby directly affecting its surface area, see Figure 40(a). Velocity perturbations may also cause flame speed perturbations by generating flame strain fluctuations, but this effect is not significant at low frequencies, see discussion below assumption (6). In contrast, equivalence ratio perturbations exert three comparable effects on the heat release, see Figure 40(b).

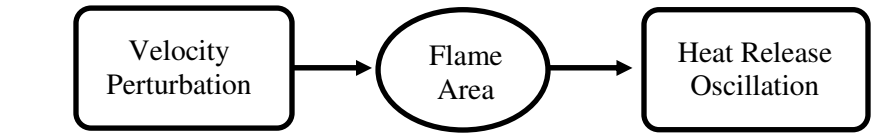

(a)

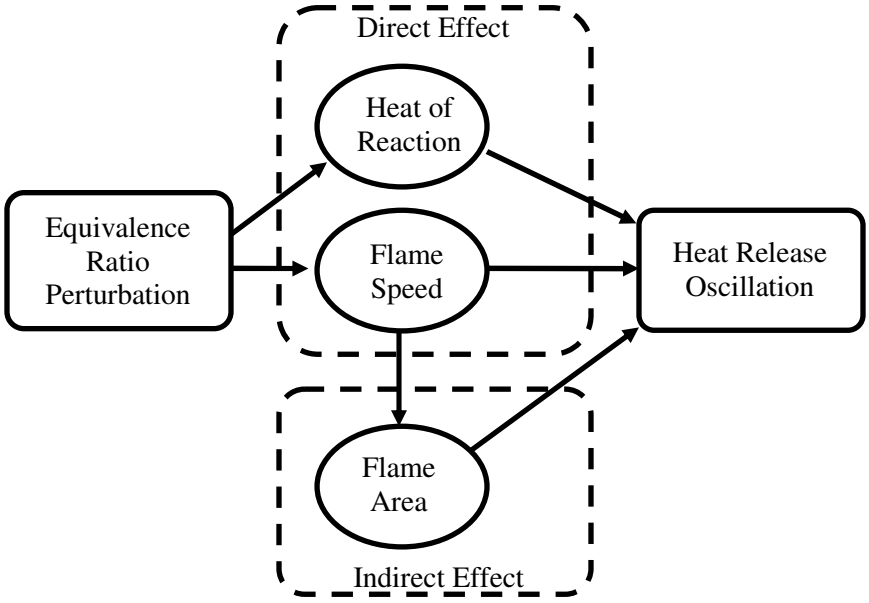

(b)

Figure 40 Dominant processes generating heat release oscillations caused by (a) acoustic velocity perturbation, *u'* (b) equivalence ratio perturbation, *ϕ'*

In Eq. (7.33), the first term, F_H, is due to perturbations in heat of reaction. The second term, F_S, is due to perturbations in flame speed. Note that perturbations in flame speed are further divided into two factors; one directly generates heat release fluctuations because of the flame speed sensitivity to equivalence ratio, $F_{S,dir}$, and the other by the subsequent fluctuation in flame surface area, F_A. In order to obtain explicit results, we assume below a quasi-steady relationship between equivalence ratio and flame speed (or heat of reaction); i.e., that $d(S_u / \bar{S}_u)/d(\phi/\bar{\phi})$ and $d(\Delta h_R / \Delta \bar{h}_R)/d(\phi/\bar{\phi})$ are independent of frequency. Incorporating additional dynamics into these relationships can be added in a straightforward manner, however. In cases where disturbances are not harmonic, the relationship between unsteady heat release rate and the velocity or equivalence ratio perturbations has a complex dynamic. A derivation of the time domain equations relating Q' to u' or ϕ' is presented in Appendix C. For $St << 1$ (i.e., a convectively compact flame), the Q'_u relationship can be put in terms of a simple n-τ model:

$$\hat{Q}'_u(t) = Q'_u(t)/\bar{Q} = n_u \hat{u}'_n(t-\tau_u) \tag{7.34}$$

where $n_u = 1/\hat{\bar{S}}_u$ and $\tau_u = \frac{\beta^2}{3}\frac{L_F}{\bar{u}}$.

The dynamics of Q'_ϕ cannot be generally described by an n-τ model, however, even in the $St << 1$ limit. This is due to the negative phase dependence of F_ϕ upon St when $St << 1$, which arises from the –90 degree phase F_S term, see Figure 41(b); i.e., the flame can not respond to ϕ' before being disturbed by it. The low St dynamics of Q'_ϕ are given by (See the second part of Appendix C):

$$\hat{Q}'_{\phi}(t) = n_H \phi'_b(t-\tau_H) + n_S \frac{d\ \phi'_b(t)}{dt} \tag{7.35}$$

where $n_H = \left.\frac{d\left(\Delta h_R / \Delta \bar{h}_R\right)}{d\phi}\right|_{\bar{\phi}}$, $\tau_H = \frac{L_F}{3\bar{u}}$, and $n_S = \frac{\beta^2}{3}\frac{L_F}{\bar{u}}\left.\frac{d\left(S_u/\bar{S}_u\right)}{d\phi}\right|_{\bar{\phi}}$

Therefore, the time domain transfer function in the *St* << 1 case is:

$$\hat{Q}'(t) = \hat{Q}'_u(t) + \hat{Q}'_{\phi}(t) = n_u \hat{u}'_n(t-\tau_u) + n_H \phi'_b(t-\tau_H) + n_S \frac{d\phi'_b(t)}{dt} \tag{7.36}$$

Equation (7.34) indicates that the time-response of the heat release rate to perturbations in acoustic velocity, $Q'_u(t)$, is delayed by a retarded time, τ_u. For a long flame ($\beta \approx 1$), τ_u represents the time taken by the mean flow to convect a distance of 1/3 of the flame length, which can be regarded as the effective position of concentrated heat release; i.e., $L_{eff} \approx L_F / 3$. However, the heat release response to equivalence ratio perturbations, $Q'_{\phi}(t)$, in Eq. (7.35) is delayed or advanced depending on the combined effect of the delayed time and temporal rate of change of the equivalence ratio perturbations. A number of studies have attempted to account for distributed flame effects by replacing the flame with a concentrated source at some "average" axial location between the base and the tip of the flame; e.g., see Ref. [15]. This analysis suggests that this approximate treatment may be quite wrong at low Strouhal numbers; in fact, it suggests that such a fictitious concentrated source may actually be located upstream of the flame.

In order to quantify the dependence of heat of reaction and flame speed upon equivalence ratio, the following correlation is used for methane [63]:

$$S_u(\phi) = A\phi^B e^{-C(\phi-D)^2} \quad \text{(m/s)} \tag{7.37}$$

where A = 0.6079, B = -2.554, C = 7.31, D = 1.230 and

$$\Delta h_R(\phi) = \frac{2.9125\times10^6 \min(1,\phi)}{1+0.05825\phi} \quad \text{(J/kg)} \tag{7.38}$$

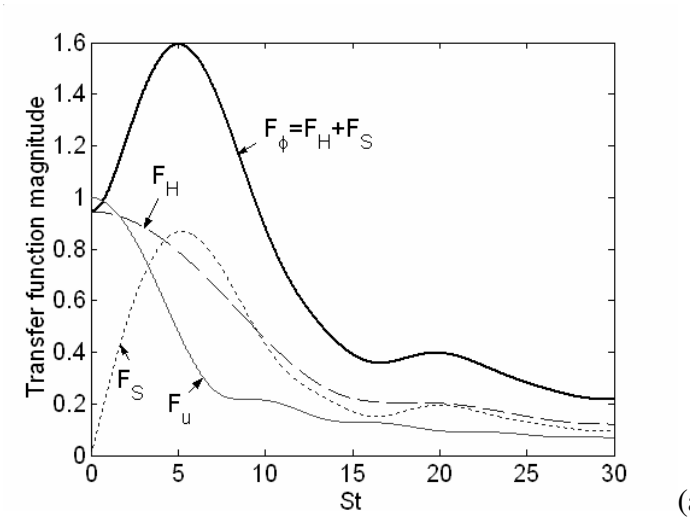

(a)

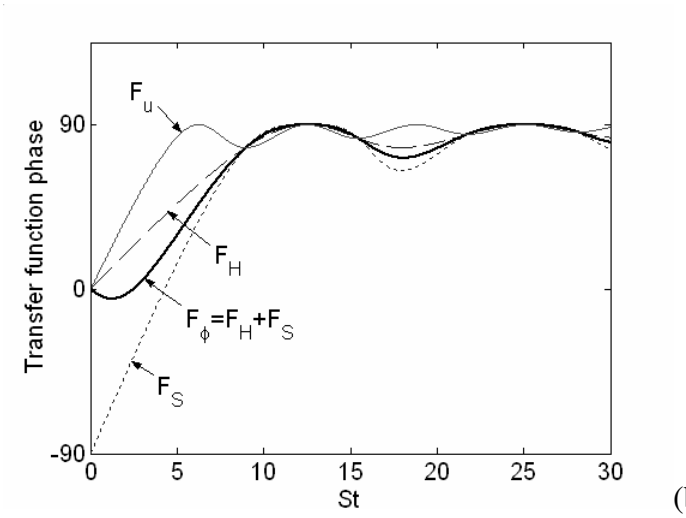

(b)

Figure 41 Dependence of the flame transfer functions upon Strouhal number for L_F/R = 1 ($\beta = \sqrt{2}$) and $\bar{\phi} = 1$

Figure 41 plots the dependence of the flame transfer function upon Strouhal number. Figure 41(a) shows the amplitude of the velocity, F_u, and the equivalence ratio, F_ϕ, transfer functions. F_ϕ is further decomposed into the effects of heat of reaction, F_H, and flame speed, F_S, respectively. F_u and F_H have similar characteristics, except that F_H

is elongated in the *St*-direction by a β^2 factor. They become identical for long flames ($L_F/R >> 1$) where $\beta \approx 1$. F_H decreases monotonically from its maximum response at St = 0. In contrast, the heat release response to flame speed perturbation, F_S, vanishes at St = 0. This is due to the exact cancellation of the direct flame speed and flame area perturbation terms which have equal magnitudes, but opposite phases at St = 0 (See Figure 42); i.e., the flame area and flame speed fluctuate with exactly the opposite phase (-180^o). This zero response at St = 0 can be understood from quasi-steady arguments: note that the flame speed and area perturbation terms account for the flame's response to a mixture with constant heat of reaction. For example, two sub-stoichiometric flames with the same fuel flow, but differing amounts of air, release the same amount of heat, although the flames have different areas. In the same way, slow time scale perturbations may affect the flame's local consumption rate, but the resultant heat release perturbation must be exactly balanced by the resultant variations in flame area.

The flame speed transfer function, F_S, increases with Strouhal number from zero because the phase difference between the terms $F_{S,dir}$ and F_A decreases with Strouhal number until these two terms equate at $St \sim 10$, see Figure 42(b). As such, these two terms add constructively to enhance the combined flame speed term, F_S. Note that this increasing F_S occurs even as both terms $F_{S,dir}$ and F_A decrease in magnitude with Strouhal number, as shown in Figure 42(a). F_S reaches a global maximum at $St \sim 5$ where the two terms $F_{S,dir}$ and F_A add in the most constructive manner. As the Strouhal number increases further, F_S decreases in an oscillatory pattern due to the alternating phase difference between $F_{S,dir}$ and F_A and their decreasing magnitudes. The magnitude of the total heat release response, F_ϕ, in Figure 41(a) also increases until $St \sim 5$ and decreases in

an oscillatory manner with further increasing *St* due to the alternating magnitudes of F_H and F_S.

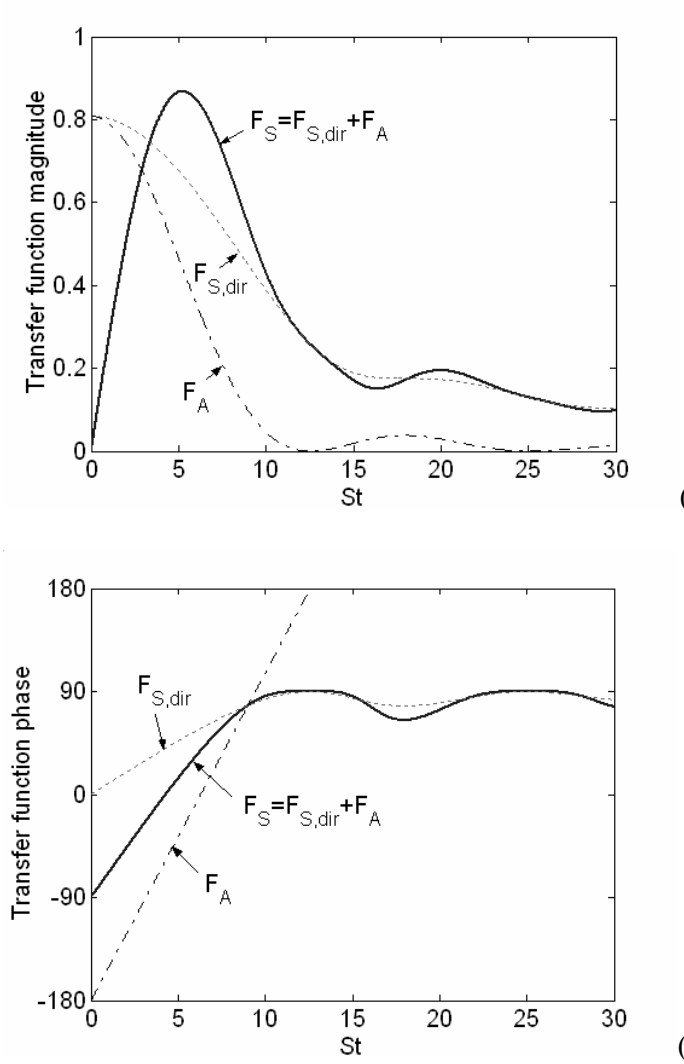

Figure 42 Dependence of the transfer functions due to direct flame speed, $F_{S,dir}$, and flame area fluctuation, F_A, upon Strouhal number for $L_F/R = 1$ ($\beta = \sqrt{2}$) and $\bar{\phi} = 1$

Figure 41(b) plots the dependence of the phase of the transfer functions upon Strouhal number. As in the magnitude results, F_u and F_H have a similar Strouhal number dependence, except for the stretching of F_H in the *St*-direction by the β^2 factor. The heat of reaction term, F_H, starts with zero-phase at $St = 0$ and increases monotonically to and

oscillates around 90^o. On the other hand, the flame speed term starts with -90^o phase. This is the average of the direct flame speed term, $F_{S,dir}$, and the flame area perturbation term, F_A, which have phases of 0^o and -180^o, respectively. The phase of F_ϕ lies between F_H and F_S. Note that the phase of F_ϕ initially decreases slightly toward F_S as discussed earlier. As discussed in the context of Eqs. (34)-(36), this negative slope of the phase of F_ϕ at low Strouhal number implies that the flame's response to equivalence ratio perturbation cannot be described by a pure n-τ model, in contrast to the velocity transfer function.

Figure 43 plots the effects of the ratio of flame length to base radius, L_F/R, upon the flame transfer function. Plots are shown for L_F/R values of 0.3, 1, 3, and 20, corresponding to β values of ~3.5, 1.4, 1.1, 1.0, respectively. Figure 43(a) shows that the transfer function is independent of this ratio for $St \ll 1$. This occurs because the flame's spatial distribution is unimportant when the flame is convectively compact. As the Strouhal number increases, the flame transfer function increases until it reaches its maximum of about 3 to 4 at $St \sim 5$. Note that this maximum value is higher for a shorter flame (smaller L_F/R). This results from the definition of Strouhal number and the fact that, for a shorter flame, the flame is more likely to be convectively-compact at lower St values and, therefore, the local heat release is more likely to be simply added along the flame to generate a higher value of maximum transfer function. Long flames ($L_F/R \geq 3$ in this case) exhibit a highly oscillating pattern in amplitude of transfer function that vanishes for higher Strouhal number. The phase dependence in Figure 43(b) also exhibits a more oscillatory pattern for longer flames. The phases of all the flames, however, approach and oscillate around 90^o for high Strouhal numbers.

Figure 44 plots these transfer functions in the complex domain, where the Strouhal number varies.

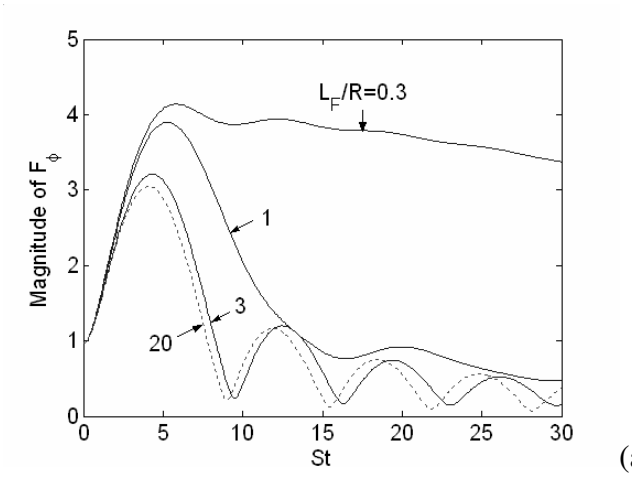

(a)

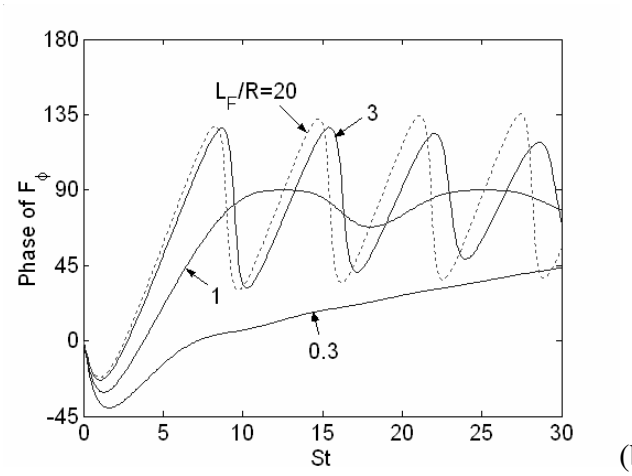

(b)

Figure 43 Dependence of the flame transfer function, F_ϕ, upon Strouhal number for several values of L_F/R with $\bar{\phi} = 0.6$

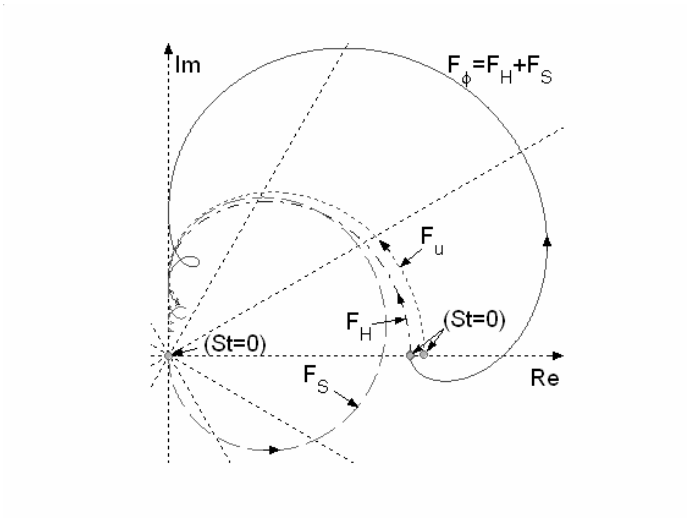

Figure 44 Polar plot of the flame transfer functions for L_F/R = 1, $\bar{\phi}=1$; arrows point in direction of increasing Strouhal number

Figure 45 plots the dependence of $F_{u,cv}$ upon St for several L_F/R values. The magnitude and phase of $F_{u,cv}$ and F_u are nearly identical for low L_F/R values. Note that $F_{u,cv}$ becomes identical to F_u in Eq. (7.31) for a very short flame (β >>1). With increasing L_F/R values the phase characteristics of $F_{u,cv}$ diverges. Figure 46 plots the effect of the mean equivalence ratio upon the flame transfer function, using the correlations in Eqs. (7.37) and (7.38). Figure 46(a) shows that mixture stoichiometry exhibits little effect upon the flame transfer function, F_ϕ, for St << 1. This is because the flame speed transfer function, F_S, makes little contribution to F_ϕ for St << 1; note that heat of reaction is much less sensitive to mixture ratio than the flame speed. For St ~ $O(1)$, the flame response increases with decreasing mean equivalence ratio. This is due to the increased sensitivity of the flame speed to equivalence ratio for leaner mixtures. Note that the point of maximum flame response, St ~ 5, remains essentially independent of the mean equivalence ratio.

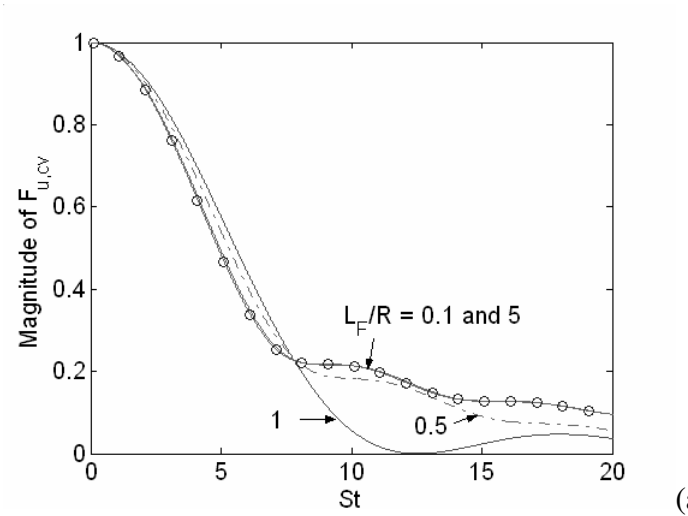

(a)

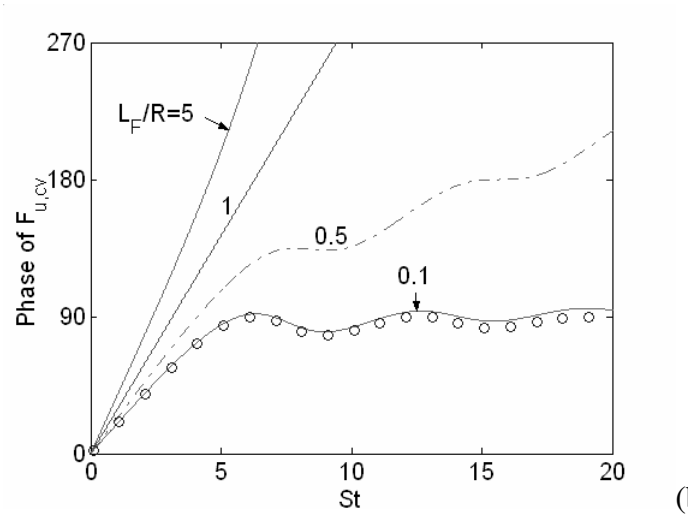

(b)

Figure 45 Dependence of the flame transfer functions, $F_{u,cv}$ (-) and **F_u** (o), **upon Strouhal number for several values of L_F/R with $\bar{\phi} = 1$**

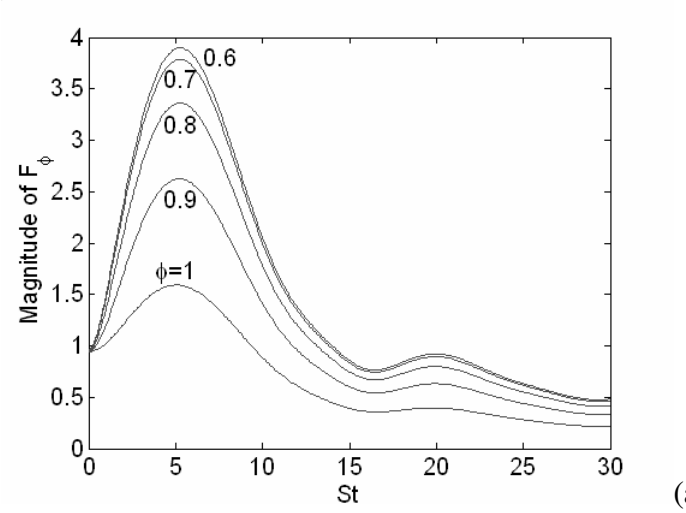

(a)

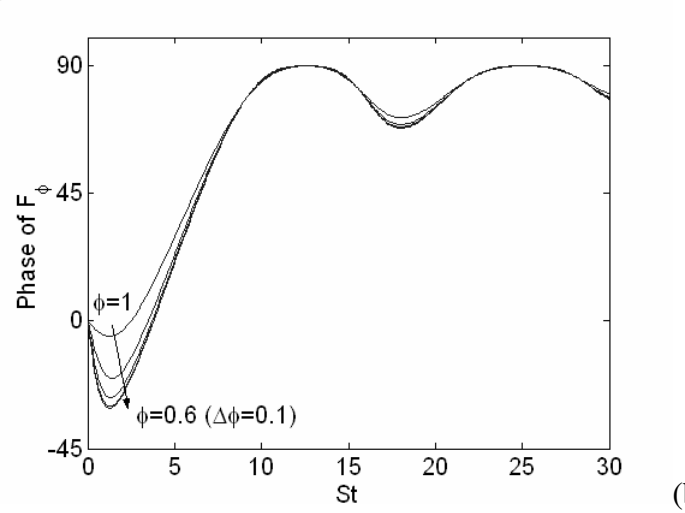

(b)

Figure 46 Dependence of the flame transfer function, F_ϕ, upon mean equivalence ratio, $\bar{\phi}$, for $L_F/R = 1$

Figure 46(b) shows the phase dependence upon the mean equivalence ratio. It shows that the primary equivalence ratio effect exists in the $St < 5$ region, where the initial rate of phase dip increases with reduced equivalence ratio. The deviation, however, vanishes when the phase reaches its maximum of 90^{o}. These results modify the conclusions of a related analysis of Lieuwen and Zinn [13], who predicted that the flame response to equivalence ratio oscillations has much larger values for leaner flames

compared to near stoichiometric flames. The present calculations suggest that this result is only correct when $St > 1$. Consider next the sensitivities of the transfer functions to small uncertainties in mean flame position. The function *dg/dr* is obtained from Eq. (7.14) for a conical mean flame front:

$$\frac{dg}{dr} = C_1\left(1 - i\ \ St\ \ r/\beta^2\right)\exp\left\{i\ \ St(1-r)/\beta^2\right\} + C_2\left(1 - i\ \ St\ \ r\right)\exp\left\{i\ \ St(1-r)\right\} \tag{7.39}$$

where $C_1 = \beta\left[\left.\frac{d(\hat{S}_u \Delta h_R)}{d\phi}\right|_{\bar{\phi}} + \frac{\Delta\bar{h}_R}{\beta^2 - 1}\left.\frac{d\hat{S}_u}{d\phi}\right|_{\bar{\phi}}\right]\phi_b' - \frac{\beta\,\Delta\bar{h}_R}{\beta^2 - 1}\hat{u}_{n,cv}'$,

$$C_2 = \beta\left[\hat{u}_{n,uni}' + \frac{\beta^2}{\beta^2 - 1}\left(\hat{u}_{n,cv}' - \left.\frac{d\hat{S}_u}{d\phi}\right|_{\bar{\phi}}\phi_b'\right)\right]\Delta\bar{h}_R$$

Substituting Eq. (7.39) into Eq. (7.22) and integrating leads to $S_1^{up}(Y_2)$, which is associated with the restrictions on the magnitude of mean flame variations. The sensitivity, S_2^{up}, associated with the restrictions on the degree of wrinkling of mean flame variations, was estimated by numerical integration of Eq. (7.24). These results are shown in Figure 47 to Figure 50. Figure 47 shows that the sensitivity S_1^{up} of equivalence ratio transfer function, F_ϕ, associated with Y_1 is almost twice as high as that with Y_2. This result arises from the fact that Y_1 allows a larger variation in flame position than Y_2 for a given ε. Note that, for $St << 1$, the upper bound of sensitivity for Y_2 is unity. The sensitivity S_1^{up} increases rapidly with increasing Strouhal number.

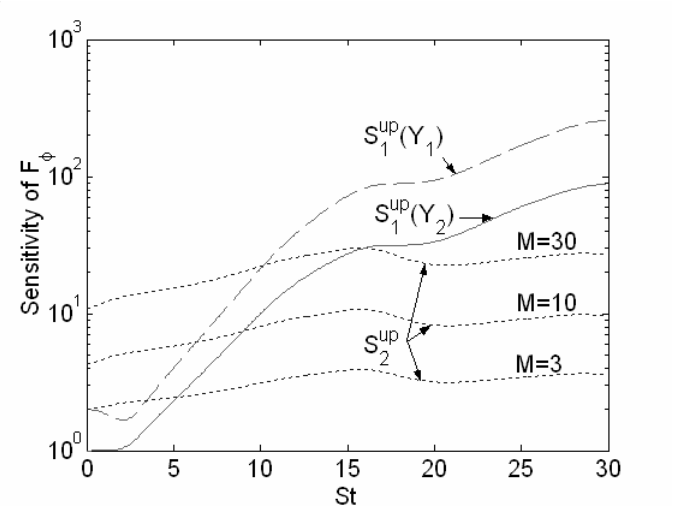

Figure 47 Dependence of the upper bound of sensitivities of the flame transfer function, F_ϕ, upon Strouhal number for $L_F/R=1$, $\bar{\phi}=1$

Figure 47 also shows the dependence of the sensitivity S_2^{up} upon Strouhal number. S_2^{up} increases with increasing *M* since higher *M* allows smaller scale wrinkles in the variations in mean flame position, leading to higher sensitivity. S_1^{up} is lower than S_2^{up} for lower *St* where the restrictions on the magnitude of mean flame variations, i.e., $|Y| \le Y_2$, is more dominant in reducing the sensitivity than the restrictions on the degree of wrinkling (note that S_2^{up} does not restrict the magnitude of mean flame variations.) However, S_1^{up} is higher than S_2^{up} for higher *St* where the restrictions on the degree of wrinkling are more consequential than the magnitude of mean flame variations. Although not shown, similar results are obtained for the sensitivity of the velocity transfer function, $F_{u,cv}$.

Figure 48(a) plots the effects of mean flame shape upon the sensitivity $S_1^{up}(Y_2)$ of F_ϕ. While all sensitivities increase with Strouhal number, the longer flames have higher sensitivities and more oscillatory characteristics.

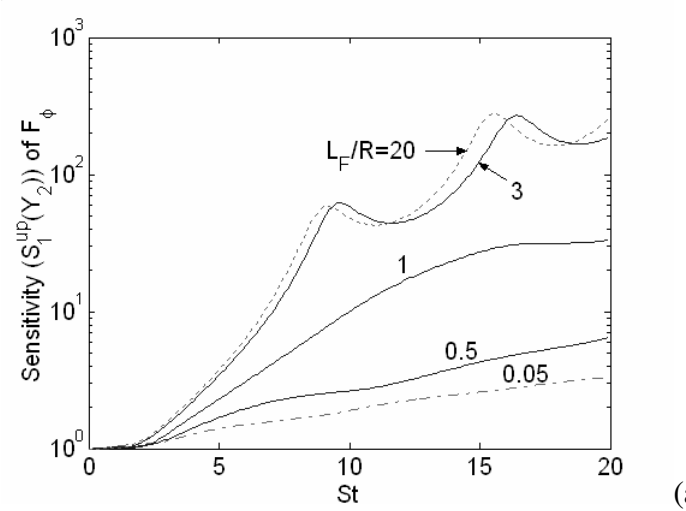

(a)

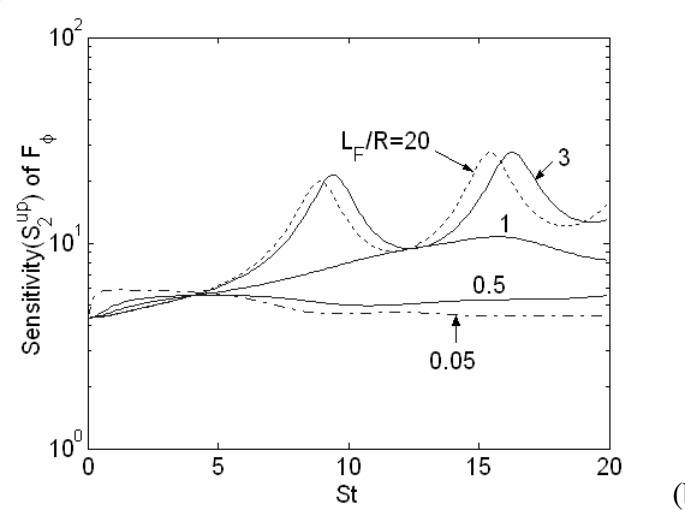

(b)

Figure 48 Dependence of the upper bound of sensitivities of the flame transfer function, F_ϕ, upon Strouhal number for several values of L_F/R with $\bar{\phi} = 1$

This result can be understood from Figure 43(a), which shows that the amplitude of the transfer function is smaller and has a more oscillatory pattern for the longer flames (the sensitivity maxima correspond to the local transfer function minima). Figure 48(b) plots the effects of mean flame shape upon the sensitivity S_2^{up} of F_ϕ. For $St > 5$, S_2^{up} increases with the longer flames, but is not as much affected by mean flame shape as $S_1^{up}(Y_2)$ from Figure 48(a). Figure 49 plots the dependence of these sensitivities at

several mean equivalence ratios. Although the sensitivities are higher at lower mean equivalence ratios, their quantitative values are quite comparable over the range 0.6 < ϕ < 0.9.

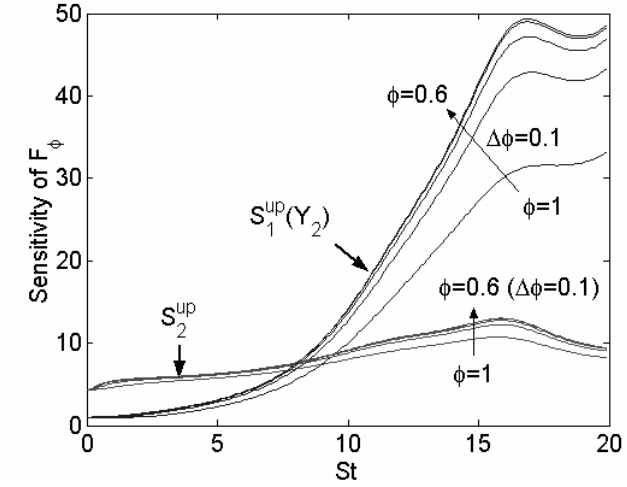

Figure 49 Dependence of the upper bound of sensitivities of the flame transfer function, F_ϕ, upon mean equivalence ratio, $\bar{\phi}$, for L_F/R = 1; M = 10 for S_2^{up}

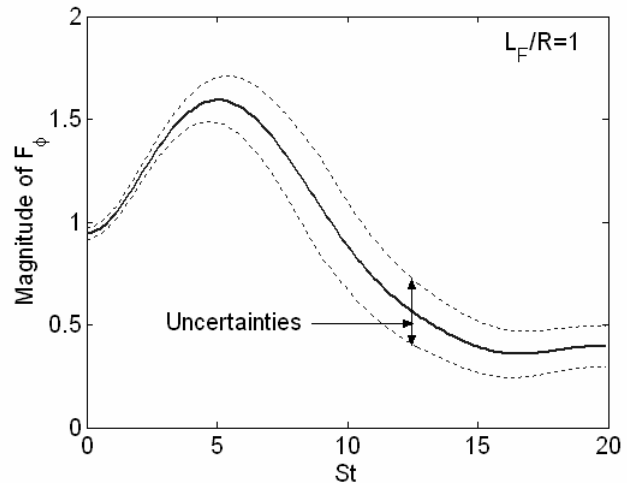

Figure 50 Uncertainties in the flame transfer function, F_ϕ, due to the sensitivity, min(S^{up}) $\equiv \min\left(S_1^{up}(Y_2),\ S_2^{up}\big|_{M=10}\right)$, for ε = 0.03, $\bar{\phi}=1$, and L_F/R = 1

The impact of these sensitivities upon the transfer function is illustrated in Figure 50, which bounds the uncertainties in flame transfer functions due to a 3% variation in mean flame position and $M = 10$. The dashed bounds plot the uncertainties due to the minimum of the sensitivities obtained by bounding the flame position and curvature. The figure indicates that flame transfer functions can be calculated with reasonable levels of uncertainty over the entire Strouhal number range, assuming low levels of uncertainty in mean flame position.

CHAPTER 8 CONCLUSIONS AND RECOMMENDATIONS

8.1 Conclusions of present work

Acoustic wave-flame interactions were analyzed in the long wavelength regime using the small perturbation method (SPM) to second order. This allowed for an explicit evaluation of the reflected /transmitted scattering fields as a result of the wave interaction with a randomly moving turbulent flame. Coherent and incoherent acoustic energy amplification /damping were formulated and simulated using stochastic analysis of the net acoustic energy flux. Net acoustic energy flux is caused by two factors: (1) the acoustic velocity jump due to the flame's unsteady burning rate. (2) the flame's unsteady motion. Acoustic energy is conserved in the case of neither jump nor unsteady motion. The reciprocity theorem also holds for a locally reacting, stationary wrinkling surface. There are five (5) dimensionless parameters that govern the net energy flux: rms height of flame front, $\tilde{\sigma} = K_0\sigma$, correlation length, $\tilde{l}_c = K_0 l_c$, incident wave frequency, $\tilde{f}_0 = f_0 / f_c$, the ratio of flame's diffusion time to correlation time, $\tau = t_r / t_c$, and incidence angle, ϕ_0. Numerical simulations for Gaussian flame statistics showed that:

1. The major factors that determine amplification /damping of total net energy flux, ΔE, are $\tilde{f}_0$ and incidence angle; Amplification occurs when $\tilde{f}_0 \geq 1$ or $\phi_0 \approx \phi_{\text{critical}}$, see Figure 34.
2. τ has a significant effect on ΔE only for a large value (>>1) of $\tilde{f}_0$.
3. $\tilde{l}_c$ has a significant effect on ΔE only for large values (>>1) of τ and $\tilde{f}_0$.
4. Smaller $\tilde{f}_0$ makes the wrinkling effect larger and the jump effect smaller.

5. Coherent (incoherent) net energy flux damps (amplifies) with the squre of rms height, $\tilde{\sigma}^2$.

The flame transfer function due to perturbations in equivalence ratio was derived and investigated for an axi-symmetric flame. The heat of reaction contribution to this transfer function dominates at low Strouhal numbers because of the cancellation between the two flame speed contributions (i.e., oscillations in local consumption rate and flame surface area). However, the heat of reaction and the flame speed effects play equal roles at Strouhal numbers of order unity. The heat release response increases with decrease in mean equivalence ratio and has a maximum value at $St \sim 5$. The transfer function has an oscillatory pattern for higher Strouhal numbers because a flame becomes more "distributed" along the flame with locally varying phases, leading to successive reinforcement and cancellation of local heat release rate. Two types of upper bound of sensitivities are defined. The sensitivity S_1^{up}, associated with bounds on the magnitude of mean flame variations, increases substantially with Strouhal number. The sensitivity S_2^{up}, associated with bounds on the radius of flame wrinkling, increases much more slowly than S_1^{up} and gives lower value of sensitivity for higher Strouhal number.

8.2 Recommendations for future studies

Suggestion for experimental analysis of acoustic wave-flame interaction:

This section provides suggested experiments to compare with the results of the present analysis. Generation of a turbulent flame with a mean flat surface is one of the key factors that the analysis is based on. Two configurations are suggested here; One is from Lawn *et al*. [64], as in Figure 51(a). The other uses a slot burner, as in (b). Lawn *et*

al. utilized the settling chamber with wall-jet injection annulus and a quarts diffuser, as illustrated in (a). Turbulent flame is generated by a perforated plate (wire-mesh) and stabilized in the diffuser. The 'flattish' flame, i.e., an approximately flat flame, can be generated by controlling the moments of wall-jet injection. The 'flattish' flame base was shown to extend over about two-thirds of the diameter of the diffuser. However, this configuration seems to be limited to normal acoustic excitation. Figure 51(b) illustrates another configuration, which is being used by our colleagues. This allows oblique angles of incidence. Once laser sheet images of flame fronts are gathered, then rms height, s, correlation length and time, l_c and t_c, can be obtained by evaluating a correlation function of flame height, $\left\langle h(\boldsymbol{r}_1,t_1)h(\boldsymbol{r}_2,t_2)\right\rangle = \sigma^2 e^{-|\boldsymbol{\xi}|^2/l_c^2-\eta^2/t_c^2}$, as in Eq. (4.64). Power spectral density (PSD) is then obtained by taking Fourier transform of measured signals, as shown in Figure 52 for instance. A peak at 7.5 kHz corresponds to coherent part while broadband signals correspond to incoherent part. Note that aoucstic energy flux, or intensity, of scattered fields can be obtained by calculating the area under a curve of PSD since

$$\text{Area of PSD} = \int PSD\, df = \frac{1}{2\pi}\int F(Corr)(\omega)e^{-i\omega\cdot(\tau=0)}d\omega$$

$$= \frac{Corr(\tau=0)}{2\pi} = \frac{\left\langle p(t)v(t)\right\rangle}{2\pi} = I/(2\pi)$$

where F(corr) denotes Fourier transform of correlation function. Discrepancy between analytical results and experimental data may result from several causes including finite dimensionality, multiple scattering, second-order approximation, temperature /density gradient, inclusion of evanescent waves.

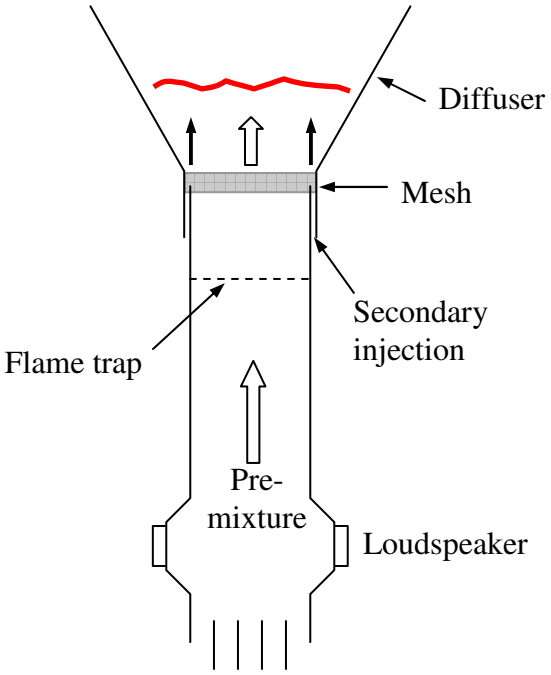

(a)

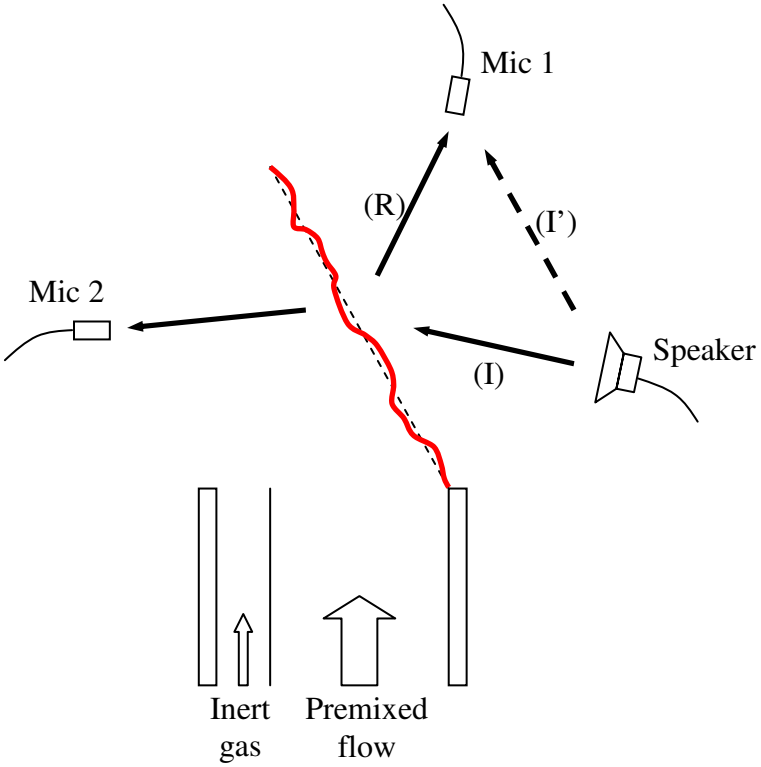

(b)

Figure 51 Example of experimental set ups for acoustic wave-flame interaction

As shown in Figure 51(b), microphone 1 gathers mixed signals, i.e., reflected signal, denoted by (R), and a signal directly from the source, denoted by (I'). There may be some difficulty to separate the reflected signal from mixed one. However, if there is any way to keep trace of incident signal only, then it is possible to separate it by subtracting incident signal from mixed one, as in Figure 53.

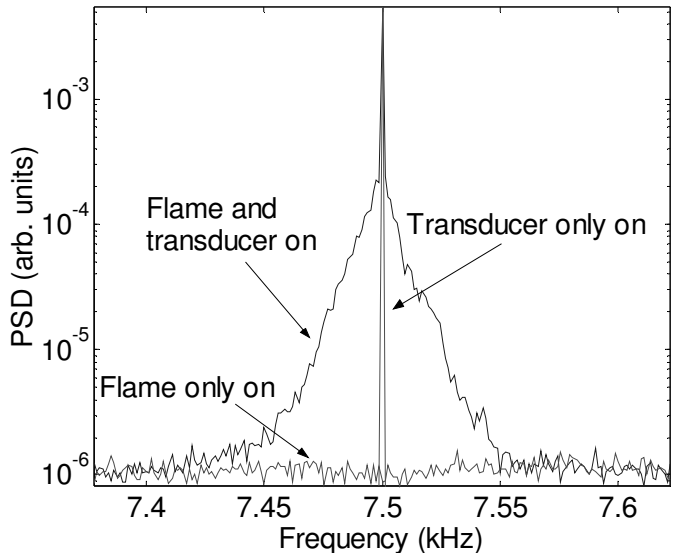

Figure 52 Detail of measured power spectrum of acoustic data, f_{drive} =7.5 kHz. (courtesy of Lieuwen *et al*. [65])

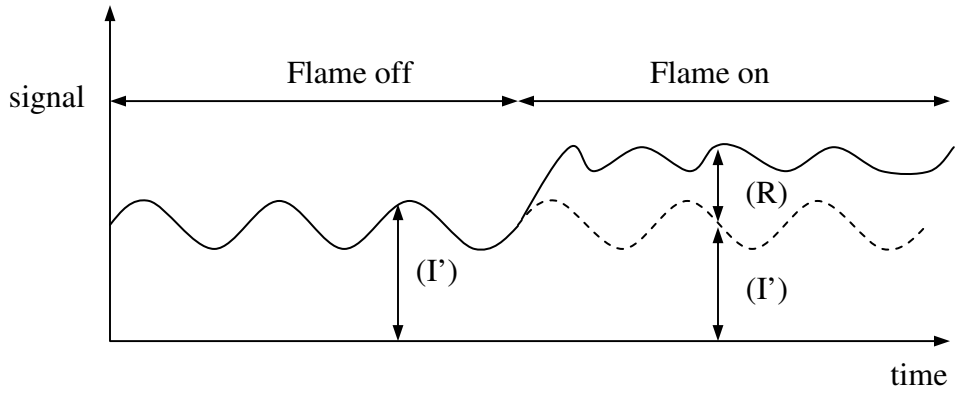

Figure 53 Separation of reflected signal from incident signal

APPENDIX A RECIPROCITY THEOREM

The reciprocity theorem basically refers to situations for which the interchange between source and receiver does not alter the ratio of receiver's signal strength to source strength. For instance, pressure amplitude p_a at $\vec{\boldsymbol{x}}_2$ caused by a point source at $\vec{\boldsymbol{x}}_1$ with strength amplitude Q_a is related to pressure amplitude p_b at $\vec{\boldsymbol{x}}_1$ caused by a point source at $\vec{\boldsymbol{x}}_2$ with strength amplitude Q_b by $p_a(\vec{\boldsymbol{x}}_2)/Q_a(\vec{\boldsymbol{x}}_1) = p_b(\vec{\boldsymbol{x}}_1)/Q_b(\vec{\boldsymbol{x}}_2)$. ([54], p.198)

In the present study, source is regarded as an incident plane wave and receiver as an individual scattering plane wave. In what follows, reciprocity relation with respect to wave number vector for a single frequency will be drived in the case where there is a jump condition in acoustic velocity to show

$$S^{N_1N_2}(-\boldsymbol{k}_2, \boldsymbol{k}_1) = S^{N_2N_1}(-\boldsymbol{k}_1, \boldsymbol{k}_2) \qquad \{(N_1, N_2)\} = \{(1,1),(1,2),(2,2)\} \tag{A.1}$$

The derivation starts with a reduced wave equation, or Helmholtz equation, which describes acoustic fields with constant frequency, $\omega = \omega_0$, in medium (1) and (2).

$$(\Delta + K_1^2)\psi^{(1)} = 0 \qquad \text{with} \quad K_1 = \omega_0 / c_1 \tag{A.2}$$

$$(\Delta + K_2^2)\psi^{(2)} = 0 \qquad \text{with} \quad K_2 = \omega_0 / c_2 \tag{A.3}$$

together with two boundary conditions from Eqs. (3.1) and (3.101) with $\partial / \partial t$ being replaced by $-i\omega_0$.

$$\rho_1 \psi^{(1)}(\vec{\boldsymbol{R}})\Big|_{z=h(\boldsymbol{r})} = \rho_2 \psi^{(2)}(\vec{\boldsymbol{R}})\Big|_{z=h(\boldsymbol{r})} \tag{A.4}$$

$$\frac{\partial \psi^{(1)}(\vec{\boldsymbol{R}})}{\partial n}\bigg|_{z=h(\boldsymbol{r})} = \left(\frac{\partial \psi^{(2)}(\vec{\boldsymbol{R}})}{\partial n} - i\beta(\omega_0)\psi^{(2)}(\vec{\boldsymbol{R}})\right)_{z=h(\boldsymbol{r})} ; \beta(\omega_0) = \beta_X \omega_0 - i\beta_Y \omega_0^2 \tag{A.5}$$

The following relation, which will be used to derive the final forms of reciprocity, is based on Voronovich's approach ([50], p. 97). Note, however, that the expression derived below extends to the situations where acoustic velocity jump condition across flame front is applied. Two sets of solutions $(\psi_1^{(1)},\psi_1^{(2)})$, $(\psi_2^{(1)},\psi_2^{(2)})$ satisfying Eqs. (A.2) and (A.3) fulfill the following identity in the first equality.

$$0=\rho_1\int\limits_{z_1<z<h(\boldsymbol{r})}(\psi_2^{(1)}\Delta\psi_1^{(1)}-\psi_1^{(1)}\Delta\psi_2^{(1)})d\boldsymbol{R}+\rho_2\int\limits_{h(\boldsymbol{r})<z<z_2}(\psi_2^{(2)}\Delta\psi_1^{(2)}-\psi_1^{(2)}\Delta\psi_2^{(2)})d\boldsymbol{R}$$

$$=\rho_1\int\limits_{z_1<z<h(\boldsymbol{r})}\nabla\cdot(\psi_2^{(1)}\nabla\psi_1^{(1)}-\psi_1^{(1)}\nabla\psi_2^{(1)})d\boldsymbol{R}+\rho_2\int\limits_{h(\boldsymbol{r})<z<z_2}\nabla\cdot(\psi_2^{(2)}\nabla\psi_1^{(2)}-\psi_1^{(2)}\nabla\psi_2^{(2)})d\boldsymbol{R}$$

$$=-\rho_1\iint\limits_{z=z_1}\left(\psi_2^{(1)}\frac{\partial\psi_1^{(1)}}{\partial z}-\psi_1^{(1)}\frac{\partial\psi_2^{(1)}}{\partial z}\right)d\boldsymbol{r}+\rho_1\iint\limits_{z=h(\boldsymbol{r})}\left(\psi_2^{(1)}\frac{\partial\psi_1^{(1)}}{\partial n}-\psi_1^{(1)}\frac{\partial\psi_2^{(1)}}{\partial n}\right)d\Sigma$$
$$+\rho_2\iint\limits_{z=z_2}\left(\psi_2^{(2)}\frac{\partial\psi_1^{(2)}}{\partial z}-\psi_1^{(2)}\frac{\partial\psi_2^{(2)}}{\partial z}\right)d\boldsymbol{r}-\rho_2\iint\limits_{z=h(\boldsymbol{r})}\left(\psi_2^{(2)}\frac{\partial\psi_1^{(2)}}{\partial n}-\psi_1^{(2)}\frac{\partial\psi_2^{(2)}}{\partial n}\right)d\Sigma$$

where the last equality results from applying the Divergence theorem, which takes the following form by applying boundary conditions of Eqs. (A.4) and (A.5) to the second term

$$=-\rho_1\iint\limits_{z=z_1}\left(\psi_2^{(1)}\frac{\partial\psi_1^{(1)}}{\partial z}-\psi_1^{(1)}\frac{\partial\psi_2^{(1)}}{\partial z}\right)d\boldsymbol{r}+\rho_2\iint\limits_{z=z_2}\left(\psi_2^{(2)}\frac{\partial\psi_1^{(2)}}{\partial z}-\psi_1^{(2)}\frac{\partial\psi_2^{(2)}}{\partial z}\right)d\boldsymbol{r}$$
$$+\rho_2\iint\limits_{z=h(\boldsymbol{r})}\left[\psi_2^{(2)}\left(\frac{\partial\psi_1^{(2)}}{\partial n}-i\beta(\omega_0)\psi_1^{(2)}\right)-\psi_1^{(2)}\left(\frac{\partial\psi_2^{(2)}}{\partial n}-i\beta(\omega_0)\psi_2^{(2)}\right)\right]d\Sigma$$
$$-\rho_2\iint\limits_{z=h(\boldsymbol{r})}\left(\psi_2^{(2)}\frac{\partial\psi_1^{(2)}}{\partial n}-\psi_1^{(2)}\frac{\partial\psi_2^{(2)}}{\partial n}\right)d\Sigma$$

$$=-\rho_1\iint\limits_{z=z_1}\left(\psi_2^{(1)}\frac{\partial\psi_1^{(1)}}{\partial z}-\psi_1^{(1)}\frac{\partial\psi_2^{(1)}}{\partial z}\right)d\boldsymbol{r}+\rho_2\iint\limits_{z=z_2}\left(\psi_2^{(2)}\frac{\partial\psi_1^{(2)}}{\partial z}-\psi_1^{(2)}\frac{\partial\psi_2^{(2)}}{\partial z}\right)d\boldsymbol{r}\qquad(A.6)$$

which is identical to the expression in p. 97 in ref.[50].

$$\rho_1 \iint_{z=z_1<\min h(\boldsymbol{r})} \left(\psi_2^{(1)} \frac{\partial \psi_1^{(1)}}{\partial z} - \psi_1^{(1)} \frac{\partial \psi_2^{(1)}}{\partial z} \right) d\boldsymbol{r} = \rho_2 \iint_{z=z_2>\max h(\boldsymbol{r})} \left(\psi_2^{(2)} \frac{\partial \psi_1^{(2)}}{\partial z} - \psi_1^{(2)} \frac{\partial \psi_2^{(2)}}{\partial z} \right) d\boldsymbol{r} \quad \text{(A.7)}$$

Note that Eq. (A.7) does not contain a jump boundary condition. The solution set $(\psi^{(1)}, \psi^{(2)})$ satisfying Eqs. (A.2) and (A.3), respectively, has a similar form to velocity potentials in (18) and (20) by setting $S(\boldsymbol{k}, \boldsymbol{k_0}, \omega, \omega_0) = S(\boldsymbol{k}, \boldsymbol{k_0})\delta(\omega - \omega_0)$ and suppressing A_1 and $e^{-i\omega_0 t}$ terms. Two sets of solutions $(\psi_1^{(1)}, \psi_1^{(2)})$, $(\psi_2^{(1)}, \psi_2^{(2)})$ can be considered depending on the propagating direction of an incident wave as follows.

Case (1): An incident wave propagates in the direction of $(\boldsymbol{k_1}, q_1^{(1)})$ in medium (1)

$$\psi_1^{(1)} = (\rho_1 q_1^{(1)})^{-1/2} e^{i(\boldsymbol{k_1}\cdot\boldsymbol{r} + q_1^{(1)} z)} + \iint_{\boldsymbol{k}} S^{11}(\boldsymbol{k}, \boldsymbol{k_1})(\rho_1 q_k^{(1)})^{-1/2} e^{i(\boldsymbol{k}\cdot\boldsymbol{r} - q_k^{(1)} z)} \, d\boldsymbol{k} \quad \text{(A.8)}$$

$$\psi_1^{(2)} = \iint_{\boldsymbol{k}} S^{21}(\boldsymbol{k}, \boldsymbol{k_1})(\rho_2 q_k^{(2)})^{-1/2} e^{i(\boldsymbol{k}\cdot\boldsymbol{r} + q_k^{(2)} z)} \, d\boldsymbol{k} \quad \text{(A.9)}$$

Case (2): An incident wave propagates in the direction of $(\boldsymbol{k_2}, q_2^{(1)})$ in medium (1)

$$\psi_2^{(1)} = (\rho_1 q_2^{(1)})^{-1/2} e^{i(\boldsymbol{k_2}\cdot\boldsymbol{r} + q_2^{(1)} z)} + \iint_{\boldsymbol{k}} S^{11}(\boldsymbol{k}, \boldsymbol{k_2})(\rho_1 q_k^{(1)})^{-1/2} e^{i(\boldsymbol{k}\cdot\boldsymbol{r} - q_k^{(1)} z)} \, d\boldsymbol{k} \quad \text{(A.10)}$$

$$\psi_2^{(2)} = \iint_{\boldsymbol{k}} S^{21}(\boldsymbol{k}, \boldsymbol{k_2})(\rho_2 q_k^{(2)})^{-1/2} e^{i(\boldsymbol{k}\cdot\boldsymbol{r} + q_k^{(2)} z)} \, d\boldsymbol{k} \quad \text{(A.11)}$$

where $q_1^{(1)} = [(\omega_0 / c_1)^2 - k_1^2]^{1/2}$, $\quad q_2^{(1)} = [(\omega_0 / c_1)^2 - k_2^2]^{1/2}$

$q_k^{(1)} = [(\omega_0 / c_1)^2 - k^2]^{1/2}$, $\quad q_k^{(2)} = [(\omega_0 / c_2)^2 - k^2]^{1/2}$, $k = |\boldsymbol{k}|$.

Substituting Eqs. (A.8) and (A.10) into Eq. (A.7) yields the form

1st term of L.H.S. of Eq. (A.7) = $\iint_{z=z_1<\min h(\boldsymbol{r})} \psi_2^{(1)} \frac{\partial \psi_1^{(1)}}{\partial z} d\boldsymbol{r}$

$$= \iint_{z=z_1} \left[(\rho_1 q_2^{(1)})^{-1/2} \, \mathrm{e}^{i(\boldsymbol{k}_2 \cdot \boldsymbol{r} + q_2^{(1)} z)} + \iint_{\boldsymbol{k}} S^{11}(\boldsymbol{k}, \boldsymbol{k}_2)(\rho_1 q_k^{(1)})^{-1/2} \, \mathrm{e}^{i(\boldsymbol{k} \cdot \boldsymbol{r} - q_k^{(1)} z)} \, d\boldsymbol{k} \right] \times$$

$$i \left[q_1^{(1)} (\rho_1 q_1^{(1)})^{-1/2} \, \mathrm{e}^{i(\boldsymbol{k}_1 \cdot \boldsymbol{r} + q_1^{(1)} z)} + \iint_{\boldsymbol{k}} (-q_k^{(1)}) S^{11}(\boldsymbol{k}, \boldsymbol{k}_1)(\rho_1 q_k^{(1)})^{-1/2} \, \mathrm{e}^{i(\boldsymbol{k} \cdot \boldsymbol{r} - q_k^{(1)} z)} \, d\boldsymbol{k} \right] d\boldsymbol{r}$$

$$= (2\pi)^2 (i/\rho_1) \begin{bmatrix} (q_1^{(1)} / q_2^{(1)})^{1/2} \, \mathrm{e}^{i(q_1^{(1)} + q_2^{(1)}) z_1} \, \delta(\boldsymbol{k}_1 + \boldsymbol{k}_2) \\ -S^{11}(-\boldsymbol{k}_2, \boldsymbol{k}_1) + S^{11}(-\boldsymbol{k}_1, \boldsymbol{k}_2) \\ -\iint_{\boldsymbol{k}} S^{11}(\boldsymbol{k}, \boldsymbol{k}_2) S^{11}(-\boldsymbol{k}, \boldsymbol{k}_1) \, \mathrm{e}^{-2i q_k^{(1)} z_1} \, d\boldsymbol{k} \end{bmatrix} \tag{A.12}$$

2^{nd} term of L.H.S. $= \iint_{z=z_1 < \min h(\boldsymbol{r})} \psi_1^{(1)} \frac{\partial \psi_2^{(1)}}{\partial z} \, d\boldsymbol{r} = \iint_{z=z_1 < \min h(\boldsymbol{r})} \psi_2^{(1)} \frac{\partial \psi_1^{(1)}}{\partial z} \, d\boldsymbol{r} \Big|_{\substack{\boldsymbol{k}_1 \leftrightarrow \boldsymbol{k}_2 \\ q_1^{(1)} \leftrightarrow q_2^{(1)}}}$

$$= (2\pi)^2 (i/\rho_1) \begin{bmatrix} (q_2^{(1)} / q_1^{(1)})^{1/2} \, \mathrm{e}^{i(q_1^{(1)} + q_2^{(1)}) z_1} \, \delta(\boldsymbol{k}_1 + \boldsymbol{k}_2) \\ +S^{11}(-\boldsymbol{k}_2, \boldsymbol{k}_1) - S^{11}(-\boldsymbol{k}_1, \boldsymbol{k}_2) \\ -\iint_{\boldsymbol{k}} S^{11}(\boldsymbol{k}, \boldsymbol{k}_1) S^{11}(-\boldsymbol{k}, \boldsymbol{k}_2) \, \mathrm{e}^{-2i q_k^{(1)} z_1} \, d\boldsymbol{k} \end{bmatrix}$$

$$= (2\pi)^2 (i/\rho_1) \begin{bmatrix} (q_2^{(1)} / q_1^{(1)})^{1/2} \, \mathrm{e}^{i(q_1^{(1)} + q_2^{(1)}) z_1} \, \delta(\boldsymbol{k}_1 + \boldsymbol{k}_2) \\ +S^{11}(-\boldsymbol{k}_2, \boldsymbol{k}_1) - S^{11}(-\boldsymbol{k}_1, \boldsymbol{k}_2) \\ -\int_{\boldsymbol{k}'=-\infty}^{\infty} S^{11}(-\boldsymbol{k}', \boldsymbol{k}_1) S^{11}(\boldsymbol{k}', \boldsymbol{k}_2) \, \mathrm{e}^{-2i q_{k'}^{(1)} z_1} \, d\boldsymbol{k}' \end{bmatrix} \quad \text{by } \boldsymbol{k}' = -\boldsymbol{k} \tag{A.13}$$

Hence, L.H.S. of Eq. (A.7) = $\rho_1 \times$[Eq. (A.12) – Eq. (A.13)]

$$= (2\pi)^2 i \begin{bmatrix} \left[(q_1^{(1)} / q_2^{(1)})^{1/2} - (q_2^{(1)} / q_1^{(1)})^{1/2} \right] \mathrm{e}^{i(q_1^{(1)} + q_2^{(1)}) z_1} \, \delta(\boldsymbol{k}_1 + \boldsymbol{k}_2) \\ -2S^{11}(-\boldsymbol{k}_2, \boldsymbol{k}_1) + 2S^{11}(-\boldsymbol{k}_1, \boldsymbol{k}_2) \end{bmatrix}$$

$$= 2(2\pi)^2 i \left[-S^{11}(-\boldsymbol{k}_2, \boldsymbol{k}_1) + S^{11}(-\boldsymbol{k}_1, \boldsymbol{k}_2) \right] \tag{A.14}$$

R.H.S. of Eq. (A.7) has the form using Eqs. (A.9) and (A.11).

R.H.S. of Eq. (A.7) $= \rho_2 \iint_{z=z_2 > \max h(\boldsymbol{r})} \left(\psi_2^{(2)} \frac{\partial \psi_1^{(2)}}{\partial z} - \psi_1^{(2)} \frac{\partial \psi_2^{(2)}}{\partial z} \right) d\boldsymbol{r}$

$$= (2\pi)^2 i \left[\iint_{\boldsymbol{k}} S^{21}(\boldsymbol{k},\boldsymbol{k_1}) S^{21}(-\boldsymbol{k},\boldsymbol{k_2}) \mathrm{e}^{2iq_k^{(2)} z_2} \, d\boldsymbol{k} - \iint_{\boldsymbol{k}} S^{21}(\boldsymbol{k},\boldsymbol{k_2}) S^{21}(-\boldsymbol{k},\boldsymbol{k_1}) \mathrm{e}^{2iq_k^{(2)} z_2} \, d\boldsymbol{k} \right]$$

$$= (2\pi)^2 i \left[\iint_{\boldsymbol{k}} S^{21}(\boldsymbol{k},\boldsymbol{k_1}) S^{21}(-\boldsymbol{k},\boldsymbol{k_2}) \mathrm{e}^{2iq_k^{(2)} z_2} \, d\boldsymbol{k} - \int_{-\infty}^{\infty} \int_{-\infty}^{\infty} S^{21}(-\boldsymbol{k}',\boldsymbol{k_2}) S^{21}(\boldsymbol{k}',\boldsymbol{k_1}) \mathrm{e}^{2iq_{k'}^{(2)} z_2} \, d\boldsymbol{k}' \right] \quad \text{(A.15)}$$

$$= 0$$

Equating Eq. (A.14) to Eq. (A.15) leads to reciprocity $S^{11}(-\boldsymbol{k_2},\boldsymbol{k_1}) = S^{11}(-\boldsymbol{k_1},\boldsymbol{k_2})$ in case of $(N_1, N_2) = (1,1)$ in Eq. (A.1). The reciprocity with $(N_1, N_2) = (1,2)$ can be derived by changing the incident wave direction in Case (2), i.e., replacing the incident wave direction $(\boldsymbol{k_2}, q_2^{(1)})$ from medium (1) by $(\boldsymbol{k_2}, -q_2^{(2)})$ from medium (2) in Eqs. (A.10) and (A.11) to yield the form

$$\psi_2^{(1)} = \iint_{\boldsymbol{k}} S^{12}(\boldsymbol{k},\boldsymbol{k_2}) (\rho_1 q_k^{(1)})^{-1/2} \mathrm{e}^{i(\boldsymbol{k}\cdot\boldsymbol{r} - q_k^{(1)} z)} \, d\boldsymbol{k} \quad \text{(A.16)}$$

$$\psi_2^{(2)} = (\rho_2 q_2^{(2)})^{-1/2} \mathrm{e}^{i(\boldsymbol{k_2}\cdot\boldsymbol{r} - q_2^{(2)} z)} + \iint_{\boldsymbol{k}} S^{22}(\boldsymbol{k},\boldsymbol{k_2}) (\rho_2 q_k^{(2)})^{-1/2} \mathrm{e}^{i(\boldsymbol{k}\cdot\boldsymbol{r} + q_k^{(2)} z)} \, d\boldsymbol{k} \quad \text{(A.17)}$$

where $q_2^{(2)} = [(\omega_0 / c_2)^2 - k_2^2]^{1/2}$

Using Eqs. (A.8), (A.9), (A.16), and (A.17) leads to

$$\text{L.H.S. of Eq. (A.7)} = \rho_1 \iint_{z=z_1 < \min h(\boldsymbol{r})} \left(\psi_2^{(1)} \frac{\partial \psi_1^{(1)}}{\partial z} - \psi_1^{(1)} \frac{\partial \psi_2^{(1)}}{\partial z} \right) d\boldsymbol{r}$$

$$= \rho_1 \iint_{z=z_1} \left[\iint_{\boldsymbol{k}} S^{12}(\boldsymbol{k},\boldsymbol{k_2}) (\rho_1 q_k^{(1)})^{-1/2} \mathrm{e}^{i(\boldsymbol{k}\cdot\boldsymbol{r} - q_k^{(1)} z)} \, d\boldsymbol{k} \right] \times$$

$$i \left[q_1^{(1)} (\rho_1 q_1^{(1)})^{-1/2} \mathrm{e}^{i(\boldsymbol{k_1}\cdot\boldsymbol{r} + q_1^{(1)} z)} + \iint_{\boldsymbol{k}} (-q_k^{(1)}) S^{11}(\boldsymbol{k},\boldsymbol{k_1}) (\rho_1 q_k^{(1)})^{-1/2} \mathrm{e}^{i(\boldsymbol{k}\cdot\boldsymbol{r} - q_k^{(1)} z)} \, d\boldsymbol{k} \right] d\boldsymbol{r}$$

$$- \rho_1 \iint_{z=z_1} \left[(\rho_1 q_1^{(1)})^{-1/2} \mathrm{e}^{i(\boldsymbol{k_1}\cdot\boldsymbol{r} + q_1^{(1)} z)} + \iint_{\boldsymbol{k}} S^{11}(\boldsymbol{k},\boldsymbol{k_1}) (\rho_1 q_k^{(1)})^{-1/2} \mathrm{e}^{i(\boldsymbol{k}\cdot\boldsymbol{r} - q_k^{(1)} z)} \, d\boldsymbol{k} \right] \times$$

$$i \left[\iint_{\boldsymbol{k}} (-q_k^{(1)}) S^{12}(\boldsymbol{k},\boldsymbol{k_2}) (\rho_1 q_k^{(1)})^{-1/2} \mathrm{e}^{i(\boldsymbol{k}\cdot\boldsymbol{r} - q_k^{(1)} z)} \, d\boldsymbol{k} \right] d\boldsymbol{r}$$

$$= (2\pi)^2 i \left[S^{12}(-\boldsymbol{k}_1, \boldsymbol{k}_2) - \iint_{\boldsymbol{k}} S^{12}(\boldsymbol{k}, \boldsymbol{k}_2) S^{11}(-\boldsymbol{k}, \boldsymbol{k}_1) \mathrm{e}^{-2iq_k^{(1)} z_1} \, d\boldsymbol{k} \right]$$
$$-(2\pi)^2 i \left[-S^{12}(-\boldsymbol{k}_1, \boldsymbol{k}_2) - \iint_{\boldsymbol{k}} S^{12}(\boldsymbol{k}, \boldsymbol{k}_2) S^{11}(-\boldsymbol{k}, \boldsymbol{k}_1) \mathrm{e}^{-2iq_k^{(1)} z_1} \, d\boldsymbol{k} \right] \qquad \text{(A.18)}$$
$$= 8\pi^2 i S^{12}(-\boldsymbol{k}_1, \boldsymbol{k}_2)$$

It follows from comparison between Eqs. (A.8) and (A.17) and between Eqs. (A.9) and (A.16) that $\psi_1^{(2)}$ and $\psi_2^{(2)}$ becomes $\psi_2^{(1)}$ and $\psi_1^{(1)}$, respectively, by interchanging $1 \leftrightarrow 2$ and changing $z \to -z (\equiv z')$.

$$\psi_1^{(2)} = \psi_2^{(1)}\Big|_{\substack{1 \leftrightarrow 2 \\ z \to z'}} \qquad \psi_2^{(2)} = \psi_1^{(1)}\Big|_{\substack{1 \leftrightarrow 2 \\ z \to z'}} \qquad \text{with } z' = -z \qquad \text{(A.19)}$$

Hence

$$\frac{\partial \psi_1^{(2)}}{\partial z} = -\frac{\partial}{\partial z'}\left(\psi_2^{(1)}\Big|_{\substack{1 \leftrightarrow 2 \\ z \to z'}} \right) = -\left(\frac{\partial \psi_2^{(1)}}{\partial z} \right)_{1 \leftrightarrow 2}, \qquad \frac{\partial \psi_2^{(2)}}{\partial z} = -\frac{\partial}{\partial z'}\left(\psi_1^{(1)}\Big|_{\substack{1 \leftrightarrow 2 \\ z \to z'}} \right) = -\left(\frac{\partial \psi_1^{(1)}}{\partial z} \right)_{1 \leftrightarrow 2}$$

from which it is found that

$$\text{R.H.S. of Eq. (A.7)} = \rho_2 \iint_{z = z_2 > \max h(\boldsymbol{r})} \left(\psi_2^{(2)} \frac{\partial \psi_1^{(2)}}{\partial z} - \psi_1^{(2)} \frac{\partial \psi_2^{(2)}}{\partial z} \right) d\boldsymbol{r}$$

$$= \rho_2 \iint_{z = -z_2 < \min h(\boldsymbol{r})} \left(-\psi_1^{(1)} \frac{\partial \psi_2^{(1)}}{\partial z} + \psi_2^{(1)} \frac{\partial \psi_1^{(1)}}{\partial z} \right)_{1 \leftrightarrow 2} d\boldsymbol{r}$$

$$= \left[\rho_1 \iint_{z = constant < \min h(\boldsymbol{r})} \left(\psi_2^{(1)} \frac{\partial \psi_1^{(1)}}{\partial z} - \psi_1^{(1)} \frac{\partial \psi_2^{(1)}}{\partial z} \right) d\boldsymbol{r} \right]_{1 \leftrightarrow 2}$$

$$= 8\pi^2 i S^{12}(-\boldsymbol{k}_1, \boldsymbol{k}_2)\Big|_{1 \leftrightarrow 2} \qquad \text{(from Eq. (A.18))}$$

$$= 8\pi^2 i S^{21}(-\boldsymbol{k}_2, \boldsymbol{k}_1) \qquad \text{(A.20)}$$

where z_2 can be chosen as $z_2 > -\min h(\boldsymbol{r})$. Equating Eq. (A.18) to Eq. (A.20) leads to reciprocity $S^{12}(-\boldsymbol{k}_1, \boldsymbol{k}_2) = S^{21}(-\boldsymbol{k}_2, \boldsymbol{k}_1)$ in case of $(N_1, N_2) = (1, 2)$.

$S^{22}(-\boldsymbol{k_1}, \boldsymbol{k_2}) = S^{22}(-\boldsymbol{k_2}, \boldsymbol{k_1})$ in case of $(N_1, N_2) = (2, 2)$ can be proved in a similar manner by changing the incident wave direction $(\boldsymbol{k_2}, -q_2^{(2)})$ in Eqs. (A.16) and (A.17) to $(\boldsymbol{k_1}, -q_1^{(2)})$ for $(\psi_1^{(1)}, \psi_1^{(2)})$, and using the same $(\psi_2^{(1)}, \psi_2^{(2)})$ as Eqs. (A.16) and (A.17).

APPENDIX B ACOUSTIC VELOCITY JUMP INCORPORATING FLAME AREA FLUCTUATION

This section incorporates unsteady heat release due to flame area fluctuation effect, into the acoustic velocity jump condition. This makes it possible to describe the effect of area variation of a wrinkled flame surface upon the net acoustic energy flux.

The velocity jump condition at the flame front can be obtained from the energy equation. The energy equation has the following form [34, 66] neglecting heat diffusion and viscous terms.

$$\frac{\partial p}{\partial t} + \vec{v} \cdot \nabla p = -\gamma p \nabla \cdot \vec{v} + (\gamma - 1) q \tag{B.1}$$

where q is heat release rate per unit volume due to chemical reaction. The above equation can be linearized as

$$\frac{\partial p_1}{\partial t} = -\vec{v}_0 \cdot \nabla p_1 - \gamma p_0 \nabla \cdot \vec{v}_1 + (\gamma - 1) q_1 = -\nabla \cdot (p_1 \vec{v}_0 + \gamma p_0 \vec{v}_1) + (\gamma - 1) q_1 \tag{B.2}$$

where mean quantities, p_0 and $\vec{v}_0$, are uniform. Integrating over a control volume taken around a curved flame surface, as shown in Figure 54, gives the form after applying divergence theorem.

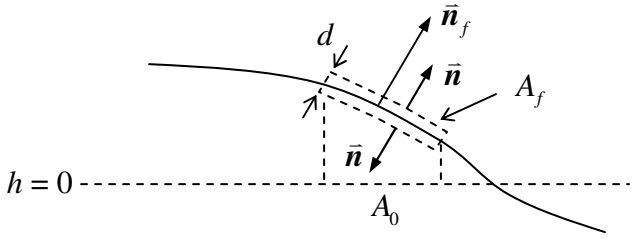

Figure 54 Control volume around a flame surface

$$\iiint_{V_f} \frac{\partial p_1}{\partial t} dV = -\iint_{A_f} (p_1 \vec{v}_0 + \gamma p_0 \vec{v}_1) \cdot \vec{n} ds + (\gamma - 1) Q_1 \tag{B.3}$$

where $Q_1 = \iiint_{V_f} q_1 dV = (m_1 A_0 + m_0 A_1)\Delta h_R = m_0 A_0 \left(\frac{m_1}{m_0} + \frac{A_f - A_0}{A_0} \right) \Delta h_R$

$$m_0 = \rho_0^{(1)} S_{L,0}^{(1)}, \qquad \frac{m_1}{m_0} = \frac{\rho_1^{(1)}}{\rho_0^{(1)}} + \frac{S_{L,1}^{(1)}}{S_{L,0}^{(1)}}, \qquad A_f / A_0 = |\cos\phi_f|^{-1} = \left(1 + |\nabla h(\boldsymbol{r},t)|^2\right)^{1/2}$$

Note that mixture ratio (equivalence ratio) is assumed to be constant and so is heat of reaction. Eq. (B.3) then has the form after divided by A_f.

$$\begin{aligned} &\frac{\partial p_1}{\partial t} d = [(p_1 \vec{\boldsymbol{v}}_0 + \gamma p_0 \vec{\boldsymbol{v}}_1)^{(1)} - (p_1 \vec{\boldsymbol{v}}_0 + \gamma p_0 \vec{\boldsymbol{v}}_1)^{(2)}] \cdot \vec{\boldsymbol{n}}_f \\ &+ (\gamma - 1) m_0 \left[(m_1 / m_0 - 1)(1 + |\nabla h(\boldsymbol{r},t)|^2)^{-1/2} + 1 \right] \Delta h_R \end{aligned} \tag{B.4}$$

where the left hand side is of the order of a flame thickness, *d*, and will be neglected. Total enthalpy conservation reads

$$[C_p T + \Delta h_f + \vec{\boldsymbol{v}}_0 \cdot \vec{\boldsymbol{v}}_0 / 2]^{(1)} = [C_p T + \Delta h_f + \vec{\boldsymbol{v}}_0 \cdot \vec{\boldsymbol{v}}_0 / 2]^{(2)}$$

which yields

$$\begin{aligned} &\Delta h_R = \Delta h_f^{(1)} - \Delta h_f^{(2)} = C_p (T^{(2)} - T^{(1)}) + [(S_{L,0}^{(2)})^2 - (S_{L,0}^{(1)})^2] / 2 \\ &= C_p T^{(1)} (\Lambda - 1) + (\Lambda^2 - 1)(S_{L,0}^{(1)})^2 / 2 \end{aligned} \tag{B.5}$$

where $S_{L,0}^{(2)} = (\rho_0^{(1)} / \rho_0^{(2)}) S_{L,0}^{(1)} = \Lambda S_{L,0}^{(1)}$ are used.

For a case of vertical mean flow field, i.e., $\vec{\boldsymbol{v}}_0 = v_0 \vec{\boldsymbol{e}}_z$,

$$\vec{\boldsymbol{v}}_0^{(m)} \cdot \vec{\boldsymbol{n}}_f = \left| v_0^{(m)} \right| \left(1 + |\nabla h(\boldsymbol{r},t)|^2\right)^{-1/2} = S_{L,0}^{(m)} \left(1 + |\nabla h(\boldsymbol{r},t)|^2\right)^{-1/2} \qquad \text{m} = \{1,2\}$$

from which Eq. (B.4) has the form using Eq. (B.5) and pressure continuity of the first order of M_S, i.e., $p_1^{(1)} = p_1^{(2)} = p_1$.

$$\frac{v_{1,n}^{(2)}-v_{1,n}^{(1)}}{c^{(1)}}=(1-\Lambda)\frac{p_1}{\gamma p_0}\frac{S_{L,0}^{(1)}}{c^{(1)}}\left(1+|\nabla h(\boldsymbol{r},t)|^2\right)^{-1/2}$$

$$+\frac{(\gamma-1)}{\gamma p_0}\frac{\rho_0^{(1)}S_{L,0}^{(1)}}{c^{(1)}}\left[(m_1/m_0-1)(1+|\nabla h(\boldsymbol{r},t)|^2)^{-1/2}+1\right][C_pT^{(1)}(\Lambda-1)+(\Lambda^2-1)(S_{L,0}^{(1)})^2/2]$$

$$=(1-\Lambda)\frac{p_1}{\gamma p_0}M_S(1+|\nabla h(\boldsymbol{r},t)|^2)^{-1/2}$$

$$+(\Lambda-1)M_S\left[(m_1/m_0-1)(1+|\nabla h(\boldsymbol{r},t)|^2)^{-1/2}+1\right][1+(\gamma-1)(\Lambda+1)M_S^2/2]$$

$$=(\Lambda-1)M_S\left[\left(\frac{m_1}{m_0}-\frac{p_1}{\gamma p_0}-1\right)(1+|\nabla h(\boldsymbol{r},t)|^2)^{-1/2}+1\right]+O(M_S^3)$$

$$=(\Lambda-1)M_S\left[\left(S_{L,1}^{(1)}/S_{L,0}^{(1)}-1\right)(1+|\nabla h(\boldsymbol{r},t)|^2)^{-1/2}+1\right]+O(M_S^3)$$

$$=(\Lambda-1)M_S\left[S_{L,1}^{(1)}/S_{L,0}^{(1)}+\frac{(1-S_{L,1}^{(1)}/S_{L,0}^{(1)})}{2}|\nabla h(\boldsymbol{r},t)|^2+O(h^4)\right]+O(M_S^3) \qquad \text{(B.6)}$$

where $p_0=\rho_0^{(1)}RT^{(1)}$, $\frac{m_1}{m_0}=\frac{\rho_1^{(1)}}{\rho_0^{(1)}}+\frac{S_{L,1}^{(1)}}{S_{L,0}^{(1)}}$, $\rho_1^{(1)}/\rho_0^{(1)}=p_1/(\gamma p_0)$ are used. Eq. (B.6) has a $|\nabla h|^2$ term, which implies that flame area fluctuation has a second-order contribution to the acoustic velocity jump, compared to Eq. (3.82).

APPENDIX C TIME DOMAIN ANALYSIS OF THE FLAME TRANSFER FUNCTION

Time domain analysis of F_u for a conical flame

The unsteady heat release response to velocity perturbation in Eq. (7.31) is given by:

$$\frac{Q'_u(\omega)}{\bar{Q}} = \frac{u'_n(\omega)}{\bar{S}_u}\frac{2}{St^2}\left[1 + i\,St - \exp(i\,St)\right] \tag{C.1}$$

where $St = \tau_c\,\omega$ and $\tau_c = \beta^2\frac{L_F}{\bar{u}} = \beta\frac{R}{\bar{S}_{u,0}}$ ($\beta = 1/\cos\theta$). Note that τ_c equals the time taken by the mean flow to convect a disturbance along the flame front, βL_F, at the speed of the tangential mean flow component, $\bar{u}_t = \bar{u}\cos\theta$, as depicted in Figure 55. Taking the inverse Fourier transform of Eq. (C.1) yields:

$$\frac{d^2}{dt^2}\left(\frac{Q'_u(t)}{\bar{Q}}\right) = \frac{2}{\bar{S}_u}\frac{1}{\tau_c}\left[\frac{du'_n(t)}{dt} - \frac{u'_n(t) - u'_n(t-\tau_c)}{\tau_c}\right] \tag{C.2}$$

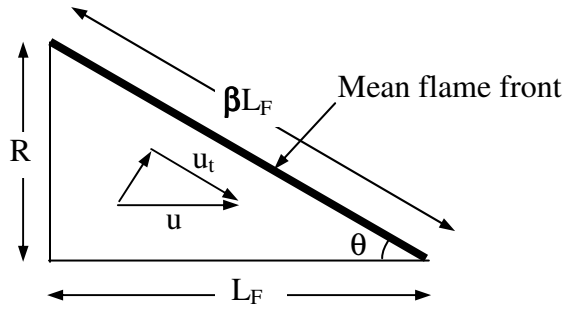

Figure 55 Convective time, τ_c (= $\beta L_F / u_t$), along the flame front

Note that τ_c is minimized when the flame is long; i.e., $\min(\tau_c) = R/\bar{S}_{u,0} (= L_F/\bar{u})$ as $\beta \to 1$. Equation (C.2) indicates that a second-order temporal derivative of heat

release response to acoustic velocity is associated with the difference between the exact value of the velocity derivative and a first order approximation of this derivative over a time interval τ_c. For low frequency disturbances ($St << 1$), the acoustic period T_a is much greater than the convective time τ_c because $St = \omega\tau_c \sim \tau_c/T_a << 1$, which makes it reasonable to assume a slow change in acoustic velocity perturbation over the time τ_c. Then, expanding the right-hand side of Eq. (C.2) in a Taylor series and integrating twice yields:

$$\frac{Q'_u(t)}{\overline{Q}} \approx \frac{1}{\overline{S}_u} u'_n(t - \tau_c/3) \tag{C.3}$$

Time domain analysis of F_ϕ for a conical flame

A similar approach to the previous section is utilized to obtain the time domain expression for the unsteady heat release response to equivalence ratio perturbation:

$$\frac{d^2}{dt^2}\left(\frac{Q'_\phi(t)}{\overline{Q}}\right) = \frac{2C}{\tau_{c1}}\left[\frac{d\hat{\phi}'_b(t)}{dt} - \frac{\hat{\phi}'_b(t) - \hat{\phi}'_b(t-\tau_{c1})}{\tau_{c1}}\right]$$

$$+ \frac{2D}{\tau_{c1}\cdot\tau_{c2}}\left[\tau_c\left(\frac{d\hat{\phi}'_b(t)}{dt} - \frac{\hat{\phi}'_b(t) - \hat{\phi}'_b(t-\tau_{c1})}{\tau_{c1}}\right) - \tau_{c1}\left(\frac{d\hat{\phi}'_b(t)}{dt} - \frac{\hat{\phi}'_b(t) - \hat{\phi}'_b(t-\tau_c)}{\tau_c}\right)\right] \tag{C.4}$$

where $C \equiv \dfrac{d(\Delta h_R/\Delta\overline{h}_R)}{d(\phi/\overline{\phi})}$, $\quad D \equiv \dfrac{d(S_u/\overline{S}_u)}{d(\phi/\overline{\phi})}$,

$$\tau_{c1} = L_F/\overline{u} = \tau_c/\beta^2,\ \tau_{c2} = \tau_c - \tau_{c1}, \qquad \hat{\phi}'_b(t) = \phi'_b(t)/\overline{\phi}$$

Equation (C.4) quantifies the time-response of the heat release rate to perturbations in equivalence ratio of arbitrary time dependence. The first term on the right-hand side of Eq. (C.4) represents the contribution from perturbations in heat of reaction, which exhibits the same form as the contribution from acoustic velocity in Eq.

(C.2) except for a different convective time τ_{c1}, which equals the time taken by the mean flow to convect a disturbance of the flame length, L_F, at the axial flow velocity, $\bar{u}$. The heat of reaction term mentioned above can be reduced, for low *St*(<<1), to the first term on the right-hand side of Eq. (7.35) with a retarded time $\tau_H = \tau_{c1}/3 = L_F/3\bar{u}$. The second term on the right-hand side of Eq. (C.4) represents the contribution from perturbations in flame speed, which depends upon both τ_c and τ_{c1}. In the low Strouhal number limit, this term becomes:

$$\hat{Q}'_{\phi}(t)\Big|_{S_u} \approx \frac{\tau_c}{3}\frac{d(S_u/\bar{S}_u)}{d(\phi/\bar{\phi})}\Bigg|_{\bar{\phi}}\frac{d\hat{\phi}'_b(t)}{dt} \tag{C.5}$$

which is identical to the second term on the right hand side of Eq. (7.35).

APPENDIX D FLAME SPEED DEPENDENCE UPON FLAME STRAIN RATE

The flame speed depends upon both the local equivalence ratio and local stretch rate:

$$\breve{S}_u(\kappa,\phi) = S_u(\phi)\left(1-\kappa L_M\right) \tag{D.1}$$

where $\breve{S}_u(\kappa,\phi)$ is the local flame speed, $S_u(\phi)$ is the unstretched flame speed, κ is the local flame front curvature, and L_M is the Markstein length.

Decomposing the flame speed into mean and fluctuating terms in Eq. (D.1) yields:

$$\breve{S}'_u(\kappa,\phi) = S'_u(\phi)(1-\bar{\kappa}\bar{L}_M) - \kappa'\bar{L}_M\,\bar{S}_u(\bar{\phi}) \tag{D.2}$$

The linearized expression for flame front curvature perturbation for a conical mean flame ($\bar{\kappa}=0$) is expressed as:

$$\kappa' = \frac{\dfrac{d^2\xi'}{dr^2}}{\left[1+\left(\dfrac{d\bar{\xi}}{dr}\right)^2\right]^{3/2}} = \left(\frac{R}{L_F\beta}\right)^3 \mathrm{Re}\left\{\frac{d^2\xi'(r)}{dr^2}e^{-i\omega t}\right\} \tag{D.3}$$

where the second derivative of $\xi'(r)$ (due to ϕ fluctuations) is estimated from Eq. (7.30):

$$\frac{d^2\xi'(r)}{dr^2} = -i\,St\,\frac{L_F}{R^2}\left.\frac{dS_u}{d\phi}\right|_{\bar{\phi}}\frac{\phi_b'}{\bar{S}_{u,0}}\frac{\left\{\beta^4 e^{i\,St(1-\hat{r})} - e^{i\,St(1-\hat{r})/\beta^2}\right\}}{\beta^2-1} \tag{D.4}$$

The conditions of interest are ones under which the strain contribution is negligible; i.e.,

$$\max_{0\le\hat{r}\le1}(\kappa') \quad \left|\bar{L}_M\right|\frac{\bar{S}_u(\bar{\phi})}{S_u'(\phi)} \ll 1 \tag{D.5}$$

Combining Eqs. (D.3)-(D.5) yields (note also that $\bar{S}_u = \bar{S}_{u,0}$ and the exponential term in the brace in Eq. (D.4) is bounded by β^4+1):

$$(\beta^2+\beta^{-2})\left|Ma\right|\frac{\omega\delta}{\bar{S}_u} << 1 \tag{D.6}$$

where $Ma \equiv L_M/\delta$ is Markstein number. However, the relative area of the flame front whose curvature is comparable to the maximum curvature is a small portion of the entire flame front; i.e., less than 20 % of the flame front has its curvature of more than 95% of the maximum curvature. Moreover, alternating signs of flame curvature along the flame front significantly attenuate the overall strain effects. These arguments lead to the conclusion that the overall flame strain effects may be reasonably neglected up to much higher frequencies than those predicted by Eq. (D.6).

REFERENCES

1. Putnam, A.A., *Combustion Driven Oscillations in Industry*, American Elsevier, New York (1971).

2. Lieuwen, T. and Yang, V., *Combustion Instabilities in Gas Turbine Engines*, AIAA, Inc., Reston (2005).

3. McManus, K.R., Poinsot, T.J. and Candel, S.M., "A Review of Active Control of Combustion Instabilities," *Prog. Energy Combust. Sci.* 19 (1993), pp. 1-29.

4. Fleifil, M., Annaswamy, A.M., Ghoniem, Z.A. and Ghoniem, A.F., "Response of a Laminar Premixed Flame to Flow Oscillations: A Kinematics Model and Thermoacoustic Instability Results," *Combust. Flame* 106 (1996), pp. 487-510.

5. Hubbard, S. and Dowling, A.P., "Acoustic Instabilities in Premix Burners," *AIAA* # 98-2272 (1998).

6. Dowling, A.P. and Hubbard, S., "Instability in Lean Premixed Combustors," *Proc. Instn. Mech. Engrs.* 214(A) (2000), pp. 317-332.

7. Hubbard, S. and Dowling, A.P., "Acoustic Resonances of an Industrial Gas Turbine Combustion System," *J. Engr. Gas Turb. Power* 123 (2001), pp. 766-773.

8. Dowling, A.P. and Stow, S.R., "Acoustic Analysis of Gas Turbine Combustors," *J. Prop. Power* 19(5) (2003), pp. 751-764.

9. Lipatnikov, A.N. and Sathiah, P., "Effects of Turbulent Flame Development on Thermoacoustic Oscillations," *Combust. Flame* 142 (2005), pp. 130-139.

10. Schadow, K.C., Gutmark, E.J., Parr, T.P., Parr, D.M., Wilson, K.J. and Crump, J.E., "Large-Scale Coherent Structures as Drivers of Combustion Instability," *Comb. Sci. Tech.* 64 (1989), pp. 167-186.

11. Broda, J.C., Seo, S., Santoro, R.J., Shirhattikar, G. and Yang, V., "An Experimental Study of Combustion Dynamics of a Premixed Swirl Injector," *Proc. Comb. Inst.* 27 (1998), pp. 1849-1856.

12. Schuller, T., Durox, D. and Candel, S., "Dynamics of and Noise Radiated by a Perturbed Impinging Premixed Jet Flame," *Combust. Flame* 128 (2002), pp. 88-110.

13. Lieuwen, T. and Zinn, B.T., "The Role of Equivalence Ratio Oscillations in Driving Combustion Instabilities in Low NO_x Gas Turbines," *Proc. Comb. Inst.* 27 (1998), pp. 1809-1816.

14. Straub, D.L. and Richards, G.A., "Effect of Fuel Nozzle Configuration on Premix Combustion Dynamics," *ASME* # 98-GT-492 (1998).

15. Lieuwen, T., Torres, H., Johnson, C. and Zinn, B.T., "A Mechanism of Combustion Instability in Lean Premixed gas Turbine Combustors," *J. Engr. Gas Turb. Power* 123 (2001), pp. 182-189.

16. Richards, G.A. and Janus, M.C., "Characterization of Oscillations During Premix Gas Turbine Combustion," *J. Engr. Gas Turb. Power* 120 (1998), pp. 294-302.

17. Kendrick, D.W., Anderson, T.J., Sowa, W.A. and Snyder, T.S., "Acoustic Sensitivities of Lean Premixed Fuel Injectors in a Single Nozzle Rig," *J. Engr. Gas Turb. Power* 121 (1999), pp. 429-436.

18. Chu, B.T., "On the Generation of Pressure Waves at a Plane Flame Front," *Proc. Comb. Inst.* 4 (1952), pp. 603-612.

19. Mark stein, G.H., *Nonsteady Flame Propagation*, Pergamon Press, Oxford (1964)

20. McIntosh, A.C., "Pressure Disturbances of Different Length Scales Interacting with Conventional Flames," *Comb. Sci. Tech.* 75 (1991), pp. 287-309.

21. McIntosh, A.C., "Deflagration Fronts and Compressibility," *Phil. Trans. Royal Soc. London* 357 (1999), pp. 3523-3538.

22. McIntosh, A.C. and Wilce, S.A., "High Frequency Pressure Wave Interaction with Premixed Flames," *Comb. Sci. Tech.* 79 (1991), pp. 141-155.

23. McIntosh, A.C., "Combustion-Acoustic Interaction of a Flat Flame Burner System Enclosed within an Open Tube," *Comb. Sci. Tech.* 54 (1987), pp. 217-236.

24. Peters, N. and Ludford, G.S.S., "The Effect of Pressure Variations on Premixed Flames," *Comb. Sci. Tech.* 34 (1983), pp.331-344.

25. Ledder, G. and Kapila, A.K., "The Response of Premixed Flames to Pressure Perturbations," *Comb. Sci. Tech.* 76 (1991), pp.21-44.

26. Lieuwen, T., "Theoretical Investigation of Unsteady Flow Interactions with a Premixed Planar Flame," *J. Fluid Mech.* 435 (2001), pp. 289-303.

27. Clavin, P., Pelce, P. and He, L., "One-Dimensional Vibratory Instability of Planar Flames Propagating in Tubes," *J. Fluid Mech.* 216 (1990), pp. 299-322.

28. Poinsot, T.J. and Candel, S.M., "A Nonlinear Model for Ducted Flame Combustion Instabilities," *Comb. Sci. Tech.* 61 (1988), pp.121-153.

29. Searby, G. and Rochwerger, D., "A Parametric Acoustic Instability in Premixed Flames," *J. Fluid Mech*. 231 (1991), pp. 529-543.

30. Fleifil, M., Annaswamy, A.M., Ghoniem, Z.A. and Ghoniem, A.F., "Response of a Laminar Premixed Flame to Flow Oscillations: A Kinematic Model and Thermoacoustic Instability Results," *Combust. Flame* 106 (1996), pp. 487-510.

31. Chu, B.T. and Kovasznay, L.S.G., "Nonlinear Interactions in a Viscous Heat-Conducting Compressible Gas," *J. Fluid Mech.* 3 (1958), pp.494-514.

32. Bloxsidge, G.J., Dowling, A.P., Hooper, N. and Langhorne, P.J., "Active Control of Reheat Buzz," *AIAA J.* 26 (7) (1988), pp. 783-790.

33. Poinsot, T.J., Trouve, A.C., Veynante, D.P., Candel, S.M. and Esposito, E.J., "Vortex-Driven Acoustically Coupled Combustion Instabilities," *J. Fluid Mech.* 177 (1987), pp. 265-292.

34. Nicoud, F. and Poinsot, T., "Thermoacoustic Instabilities: Should the Rayleigh Criterion be Extended to Include Entropy Changes?," *Combust. Flame* 142 (2005), pp. 153-159.

35. Searby, G. and Clavin, P., "Weakly Turbulent, Wrinkled Flames in Premixed Gases," *Comb. Sci. Tech.* 46 (1986), pp.167-193.

36. Lieuwen, T., "Theory of High Frequency Acoustic Wave Scattering by Turbulent Flames," *Combust. Flame* 126 (1-2) (2001), pp. 1489-1505.

37. Lieuwen, T., "Analysis of Acoustic Wave Interactions with Turbulent Premixed Flames," *Proc. Comb. Inst.* 29 (2002), pp. 1817-1824.

38. Lieuwen, T. and Cho, J.H., "Coherent Acoustic Wave Amplification/Damping by Wrinkled Flames," *J. Sound and Vib.*, 279 (2004), pp. 669-686.

39. Lieuwen, T., "Explicit Results for Wave Scattering and Transmission through a Rough Fluid-Fluid Interface," *Applied acoustics*, 63 (2002), pp. 1031-1050.

40. Mongia, R., Dibble, R. and Lovett, J., "Measurement of Air-Fuel Ratio Fluctuations Caused by Combustor Driven Oscillations," *ASME* # 98-GT-304 (1998).

41. Lee, D.S. and Anderson, T.J., "Measurements of Fuel/Air Acoustic Coupling in Lean Premixed Combustion Systems," *AIAA* # 99-0450 (1999).

42. Straub, D. and Richards, G., "Importance of Axial Swirl Vane Location of Combustion Dynamic for Premix Fuel Injectors," *AIAA* # 98-3909 (1998).

43. Krebs, W., Flohr, P., Prade, B. and Hoffman, S., "Thermoacoustic Stability Chart for High-Intensity Gas Turbine Combustion Systems," *Comb. Sci. Tech.* 174(7) (2002), pp. 99-128.

44. Prasanth, R.K., Annaswamy, A.M., Hathout, J.P. and Ghoniem, A.F., **"**When Do Open-Loop Strategies for Combustion Control Work?**,"** *J. Prop. Power* 18(3) (2002) pp. 658-668.

45. Lee, D.H. and Lieuwen, T., "Premixed Flame Kinematics in a Longitudinal Acoustic Field**,"** *J. Prop. Power*:19 (5) (2003), pp. 837-846.

46. Jones, D.S., *The Theory of Electromagnetism*, Pergamon Press, London (1964).

47. Kevorkian, J., *Partial Differential Equations: Analytical Solution Techniques*, 2nd Ed., Springer-Verlag, New York (2000).

48. Crighton, D.G., Dowling, A.P., Ffowcs Williams, J.E., Heckl, M., Leppington, F.G., *Modern Methods in Analytical Acoustics*, Springer-Verlag (1992).

49. Skelton, E.A. and James, J.H., *Theoretical Acoustics of Underwater Structures*, Imperial College Press (1997).

50. Voronovich, A.G., *Wave Scattering from Rough Surfaces*, Springer-Verlag, 2nd Ed. (1999).

51. Ogilvy, J. A., *Theory of Wave Scattering from Random Rough Surfaces*, IOP Publishing Ltd. (1991).

52. Peters, N., Ludford, G.S.S., "The Effect of Pressure Variations on Premixed Flames," *Comb. Sci. Tech.* 34 (1983), pp. 331-344.

53. Wunenburger, R., Mujica, N. and Fauve, S., "Experimental Study of the Doppler Shift Generated by a Vibrating Scatterer," *J. Acoust. Soc. Am.*, 115(2) (2004), pp. 507 – 514.

54. Pierce, A.D., *Acoustics: An Introduction to Its Physical Principles and Applications*, the Acoustical Society of America (1991).

55. Meirovitch, L., *Analytical Methods in Vibrations*, the Macmillan Company, London (1971).

56. Abramowitz, M. and Stegun, I.A., *Handbook of Mathematical Functions with Formulas, Graphs, and mathematical Tables*, Dover publications, Inc., New York (1970)

57. Modest, M.F., *Radiative Heat Transfer*, McGraw-Hill, Inc. (1993).

58. Culick, F.E.C., "A Note on Ordering Perturbations and the Insignificance of Linear Coupling in Combustion Instabilities," *Comb. Sci. Tech.* 126 (1997), pp. 359-379.

59. Ducruix, S., Durox, D. and Candel, S., "Theoretical and Experimental Determinations of the Transfer Function of a Laminar Premixed Flame," *Proc. Comb. Inst.* 28 (2000), pp. 765-773.

60. Baillot, F., Durox, D. and Prud'homme, R., "Experimental and Theoretical Study of a Premixed Vibrating Flame," *Combust. Flame* 88 (1992), pp. 149-168.

61. Schuller, T., Ducruix, S., and Durox, D. and Candel, S., "Modeling Tools for the Prediction of Premixed Flame Transfer Functions," *Proc. Comb. Inst.* 29 (2002), pp. 107-113.

62. Schuller, T., Durox, D. and Candel, S., "A unified model for the prediction of laminar flame transfer functions: comparisons between conical and V-flame dynamics," *Combust. Flame* 134 (2003), pp. 21-34.

63. Abu-Off, G.M. and Cant, R.S., "Reaction Rate Modeling for Premixed Turbulent Methane-air Flames", *Proceedings of the Joint Meeting of Spanish, Portuguese, Swedish and British Sections of the Combustion Institute, Madeira*, 1996.

64. Lawn, C.J., Williams, T.C. and Schefer, R.W., "The Response of Turbulent Premixed Flames to Normal Acoustic Excitation", *Proc. Comb. Inst.* 30 (2005), pp. 1749-1756.

65. Lieuwen, T., Rajaram, R., Neumeier, Y. and Nair, S., "Measurements of Incoherent Acoustic Wave Scattering from Turbulent Premixed Flames", *Proc. Comb. Inst.* 29 (2002), pp. 1809-1815.

66. Poinsot, T. and Veynante, D., *Theoretical and Numerical Combustion*, R.T. Edwards (2001).